Dry degradation processes at solid surfaces

Ohesiek, Susanne Maria

DRY DEGRADATION PROCESSES AT SOLID SURFACES

Susanne Maria Ohsiek

PhD Thesis

University of Durham

Department of Chemistry

December 1998

Meinen stets geduldigen Eltern in Dankbarkeit

Abstract

Polymer surfaces were modified by exposure to a silent discharge plasma, by exposure to UV radiation and by chemical functionalisation. Additionally, the silent discharge treatment of alkali halide disks was investigated.

Employing XPS and IR, the silent discharge treatment of poly (phenylmethylsilane) and poly (cyclohexylmethylsilane) thin films was found to result in the formation of a carbonaceous SiO_x layer. Oxidation occurred faster and to a larger degree in the case of the aromatic polysilane.

A XPS study of the UV irradiation of poly (phenylmethylsilane) thin films in the presence of CCl_4 vapour revealed the formation of a chlorinated silicon species. The analysis of aged samples showed that this initially formed product was unstable in moist air.

The silent discharge treatment of alkali halide disks (KCl, KBr, KI) was studied in ambient air, as well as in dried and humidified gases (artificial air, He, N_2, O_2). IR and XPS were used as analytical methods. In most cases nitrate and halogenate were formed upon treatment in air. Depending on the reaction conditions treated KI disks sometimes showed the presence of nitrite as an additional or as the main product. In oxygen atmospheres halogenate was formed as the exclusive product. Treatments in the remaining atmospheres did not lead to product formation. The presence of water vapour in the feed gas increased the amount of product. Changes in the IR spectra of the nitrate species upon storage in a desiccator and after exposure to heat were found and monitored.

Pentafluoropropionic anhydride was tested for its suitability as a vapour phase labelling reagent for hydroxyl groups on polymer surfaces. Derivatised films were analysed by XPS and IR. Using Polyvinyl alcohol as a model polymer the reaction proceeded fast and quantitative. Moreover, the cross-reaction with a number of polymers containing functionalities other than hydroxyl was studied. The reaction with nylon 6,6 was investigated in detail.

The vacuum photodegradation of polyethersulfone upon irradiation with the full and a selected part of a Hg (Xe) lamp spectrum was studied. The volatile products were identified with in-situ quadrupole mass spectrometry. Monitoring the intensities of some products in subsequent irradiation phases provided evidence for a crosslinking process. In samples irradiated with the complete lamp spectrum crosslinking occurred faster. Additionally, the XP spectra of the corresponding samples revealed a stronger modification which became most obvious in the presence of a reduced sulfur species.

Declaration

The work described in this thesis was carried out in the Chemistry Department at the University of Durham between October 1993 and December 1996. All the work is my own unless stated to the contrary and has not been submitted previously for a degree at this or any other University.

Statement of Copyright

Acknowledgements

Many thanks to:

all members of staff who spent time and effort to sort my supervision out.

Prof. D. Parker for acting as my academic mentor from February 1996.

all members of the technical staff for skilfully manufacturing and patiently maintaining equipment used in this work and to Dr. R.F. Matthews for recording the ^{19}F-NMR spectra of the anhydrides used in chapter 6.

Prof. Dr. H. Esrom, Fachhochschule Mannheim; Dr. U. Kogelschatz, Brown Boveri Reasearch Center, Baden, Switzerland; Prof. Dr. K. Schank, Universität Saarbrücken, and Dr. R. Vogt, Ford Research Center Aachen, for helpful discussions on silent discharges, organosulfur chemistry and halide aerosols, respectively.

Dr. Karen Peat and Tim West for the proofreading of the chapters as well as for helpful and encouraging comments.

my colleagues in lab 98 for chats and E-mails and for favours during the write-up phase.

the members of the Rotary Club St. Ingbert for their spontaneous interest in my studies abroad and for paying two of the tuition fees.

the University Hardship Fund for financial support from October until December 1996 and to the Graduate Society for not charging me rent during that time.

all those who provided the much needed moral support.

my parents - simply for everything !

Contents

Chapter 6: Investigation of the suitability of pentafluoropropionic anhyride as a reagent for chemical derivatisation of hydroxyl groups on polymer surfaces

Chapter 7: In-situ mass spectrometric study on the vacuum photodegradation of Polyethersulfone

Chapter 1: An introduction to silent discharges

1.1 Introduction

This chapter will provide a short introduction into plasmas in general and will then focus on the discussion of silent discharges, a special type of electrical discharges relevant for the present work. In the text the terms plasma and discharge will be used as equivalents.

1.2 Definition of plasma and other important terms

A *plasma* can be defined as a gaseous complex that may be composed of a multitude of constituents. These include electrons, ions of either polarity, gas atoms and molecules in various excited states as well as light quanta [1]. This state can be generated by the application of energy to matter, where the latter is most often present as a gas. The energy required has to be larger than the ionisation energy of the matter under consideration [2] and can be provided in the form of thermal or electrical energy, as shockwaves or as laser pulses [3].

Each volume element of a plasma contains an almost equal number of positive and negative charge carriers such that the plasma as a whole appears neutral and is therefore referred to as *quasi-neutral.* This term is still valid in the case of a local excess of one type of charge carrier leading to the development of a space charge because the amount of excess charge carriers is small compared to the total amount of charged particles. Quasi-neutrality is the prerequisite for the build-up of high charge carrier densities within the plasma which would otherwise be prevented because of mutual repulsion [4].

The amount of charge carriers n_i with respect to the amount of neutral particles n contained in a plasma is called the *degree of ionisation* ($\alpha = n_i/n$) [2].

All plasma constituents have an individual kinetic energy distribution. Applying statistical thermodynamics the average energy value of each plasma particle can be expressed in terms of a temperature [4]. If the temperatures of all the plasma constituents are approximately the same the plasma is called an *equilibrium plasma.*

This type of plasma is often observed at high temperatures and is therefore also referred to as a *hot plasma.*

A complete thermodynamic equilibrium can, however, only be established when the energy exchange processes prevail over processes which consume or supply energy [4]. These conditions can be met in extended volumes of a hot gas like in a fixed star. On earth, these conditions cannot be realised because the dimensions of laboratory plasmas are relatively small. As a consequence of the small plasma volume radiation of the plasma can escape without being absorbed. This energy loss has to be compensated from external sources. These conditions only allow the development of a local thermodynamic equilibrium and plasmas of this type are therefore called Local Thermodynamic Equilibrium (LTE) plasmas [4].

In plasmas which are not in local thermal equilibrium (non-LTE plasmas), the electrons have a much higher kinetic energy or temperature than the heavy constituents. In most electrical discharges, for example, plasma formation is due to external electric fields acting upon both electrons and ions. Due to their small weight electrons are accelerated faster acquiring higher energies than the heavy ions [5]. As a consequence electrons undergo frequent collisions with the other plasma constituents thereby transferring most of the energy from the external field to the particles. Only a small amount of heat is transferred in the collisions between electrons and gas particles or solids in contact with the plasma. Additionally, the electron densities in such plasmas are usually low. Due to these reasons, non-LTE plasmas are also called cold plasmas [2].

1.3 Plasma chemistry [6,7]

In a plasma a row of elementary reactions occurs simultaneously during which the plasma constituents are created, destroyed or transformed into other species. Each process requires a minimum amount of energy which is dependent on the nature of the gas(es) involved. Moreover, a reaction and its rate are determined by the probability or cross-section of the particular process at a given energy. Finally, the form of energy used to generate the plasma state exerts an important influence on both type and frequency of elementary reactions. In electrical discharges for example electron collisions are the preferential method of energy transfer. The combination of

all elementary reactions represents the overall mechanism of the plasma process. The knowledge of the single processes and their characteristics are important for the theoretical modelling and the control of the whole plasma process.

1a	Ionisation	$A + e \rightarrow A^+ + 2e$ $A_2 + e \rightarrow A_2^+ + 2e$
1b	Dissociative Ionisation	$AB + e \rightarrow A^+ + B + 2e$
2 2b	Excitation	$A + e \rightarrow A^* + e$ $AB + e \rightarrow AB^* + e$ $e + AB \rightarrow e + (AB)^* \rightarrow e + A + B$
3a	Radiative Recombination	$A^+ + e \rightarrow A + h\nu$
3b	Dissociative Recombination	$e + AB^+ \rightarrow (AB)^* \rightarrow A^* + B$
3c		$e + AB^+ \rightarrow (AB)^* + M \rightarrow AB + M_{kin}$
3d		$A^+ + B^- \rightarrow AB + h\nu$
3e		$A^+ + B^- + M \rightarrow AB + M_{kin}$
3f		$A^+ + B^- \rightarrow A + B$
4a	Electron Attachment	$e + A \rightarrow A^- + h\nu$
4b	Dissociative Attachment	$AB + e \rightarrow A + B^-$
		$e + AB \rightarrow (AB)^{-*} + M \rightarrow AB^- + M_{kin}$
5a	Penning Dissociation	$S^* + AB \rightarrow A + B + S$
5b	Penning Ionisation	$S^* + AB \rightarrow AB^+ + e + S$
6a	Charge Transfer	$S^+ + A \rightarrow S + A^+$ $S^+ + AB \rightarrow S + AB^+$
6b	Dissociative Charge Transfer	$S^+ + AB \rightarrow S + A + B^+$
6c	Symmetric Charge Transfer	$A + A^+ \rightarrow A^+ + A$

Tab. 1 Important elementary reactions in plasmas

Elastic and inelastic collisions are distinguished; both types of particle interaction are important for the development and the maintenance of the plasma state. *Elastic collisions* are characterised by an exchange of kinetic energy between the collision partners whilst the sum of the kinetic energy remains the same; an

excitation of the target does not take place. In *inelastic collisions*, however, a part of the kinetic energy transferred to the target is used to increase its internal energy resulting in an excitation of the particle. This can lead to dissociation, ionisation, and the formation of metastables or radicals. Table 1 summarises the most important elementary reactions.

Ionisation (1a) which corresponds to the complete removal of a bound electron from an atom, requires electron energies higher than the ionisation energy of the gas in question. This is why only the high energy electrons of the electron energy distribution can cause this reaction to occur. Ionisation potentials for different gases have values in the range of 8-25 eV. For a particular molecule or atom the cross-section for ionisation passes through a maximum at energies corresponding to three to five times the ionisation energy value. Ionised molecules can additionally be rotationally and vibrationally excited, the latter of which can lead to their dissociation (1b). Product ions formed with sufficiently high vibrational energy can again dissociate further.

Excitation is the result of a collision process with an energy transfer corresponding to the difference between the ground and an excited state of the target molecule or atom. A comparison of excitation and ionisation shows that excitation processes do not only have a lower appearance potential but also a steeper excitation curve (plot of cross-section versus electron energy). Therefore, the "fast" plasma electrons cause excitation rather than ionisation of neutral particles.

Contrary to its photochemical equivalent, plasma excitation is not restricted by quantum-mechanical selection rules such that "forbidden" transitions occur in plasmas. Particles excited to allowed states can return to their ground state by spontaneous emission of light quanta in the UV and VIS region, the latter of which accounts for the plasma glow. Since the lifetime of those excited species is very short (10^{-7} - 10^{-8} s) their participation in additional chemical reactions is very unlikely. Radiative decay is not a possible relaxation route for particles excited to forbidden states. Due to their increased lifetime the exact value of which is dependent on parameters like the pressure and the nature of the gas, those states are termed "metastable". The deexcitation of particles in metastable states is possible following a second collision which causes a transfer to an allowed state for spontaneous

emission. A second pathway involves the transfer of energy to a molecule which can then dissociate (Penning dissociation, 5a) or be ionised (Penning ionisation, 5b).

Molecules can be excited electronically, rotationally and vibrationally. Vibrational excitation is especially important for plasma chemistry because it can lead to dissociation which is a source of reactive atoms or radicals (2b). In comparison to radiative decay the dissociation of an excited molecule into neutral fragments proceeds very fast (10^{-13} s) and is therefore the more probable reaction to occur.

Recombinations (3a-f) are reactions which result in the neutralisation of positive charge carriers either by the uptake of an electron or the combination with a negative ion. The different types of recombination depend on the nature of the collision partners, the velocity of the particles and the pressure of the neutral gas.

Recombinations of atomic ions and electrons are accompanied by the emission of electromagnetic radiation (3a). Dissociative recombination of molecules (3b) occurs preferably at low charge carrier density. In this case the neutral particles produced in the reaction can ensure the conservation of energy and momentum. Increased pressure and /or higher charge carrier densities are the favoured conditions for three-body collisions according to (3c). The additional collision partner M can be an atom or a molecule which carries away the excess energy of the process in form of kinetic energy, thereby heating up the plasma.

Similar observations are made in the recombination of oppositely charged ions (3d-f). At very low pressures, the process occurs as a two-body reaction (3d) whereas at pressures > 0.1 mtorr a three-body reaction occurs (3e). Recombinations of ions can also occur as a charge transfer process (3f).

Although the formation of positive ions is prevalent in most cold plasmas, *negative ions* can also be formed. This occurs by the attachment of low energy electrons of a few electron volts to neutral particles. The amount of energy released during this process is called electron affinity (EA). It is a measure of the stability of a negative ion and therefore its lifetime in the plasma. Electron attachment reactions can be expected for plasmas ignited in gases with high EA values, for example gases containing electronegative elements like oxygen or halogens. The importance of negative ions for a plasmachemical process increases with increasing electronegative character of the gas and increasing pressure.

Attachment can occur according to different mechanisms which are influenced by the way in which the energy developed in the process is carried away (4a-c). In the first case which is especially observed in atoms, the reaction energy corresponding to the sum of the EA and the kinetic energy of the electron is emitted in the form of radiation. Due to the energy distribution of the electrons it appears as a continuum (4a). Electron attachment to molecules is often followed by dissociation (dissociative attachment, 4b). The excess energy is distributed as kinetic energy between the two fragments. The cross-sections for this process have maxima at electron energies between 0 and 1 eV and in the energy range between a few eV and the ionisation potential, respectively. At higher pressures where the collision frequency is increased and three-body reactions are more probable, the large vibrational energy of the molecules can be transferred to a third collision partner and the molecules do not dissociate (4c).

Some *collisions between heavy particles* in multicomponent systems involve a direct transfer of internal energy from one collision partner to the other with none or only a small amount of the original internal energy being transformed into kinetic energy. These processes represent a possibility to activate non-reactive atomic or molecular plasma particles. In *Penning processes* metastables dissociate or ionise molecules according to (5a) and (5b). These reactions occur under the condition that the excited states of the activating particle S* are energetically higher than the dissociation and ionisation potential of the target, respectively.

Reactions can also be activated by a charge transfer process between particles differing in their ionisation potentials (6a). Asymmetric processes involving atoms are less frequent. In contrast, those involving molecules often have high cross-sections especially at low electron energies. Depending on the difference between the internal energy of the activating particle and the ionisation potential of the substrate, a charge transfer can be accompanied by other processes like the excitation of the product ion which can cause its dissociation (6b). Charge transfer can also take place between an ion and a neutral particle of an identical type. Although equation (6c) shows no obvious difference in the particles before and after this symmetrical charge transfer, the collision results in a slower ion and a faster neutral.

1.4 Silent discharge plasmas

1.4.1 Definition and characteristics

A silent discharge (also called dielectric barrier discharge or barrier discharge) is a quasi-neutral, non-equilibrium plasma with a low degree of ionisation which is usually run at high pressures [5]. Its characteristics are summarized in table 2.

Pressure range	0.1 - 10 bar
Electric fields	0.1 - 100 kV/cm
Average electron energy	1 - 10 eV
Electron density	10^{14} cm^{-3}
Degree of ionisation	10^{-4}

Tab. 2 Characteristics of silent discharges [5,8]

1.4.2 Set-up

A silent discharge set-up consists of two electrodes which are separated by a gap and in between which there is at least one dielectric layer [5,8-10]. Depending on the application, several geometrical arrangements have been used employing different types of dielectric materials such as glass, quartz, ceramics, polymers or enamel [5,11]. Preferred configurations are planar or annular discharge gaps [9,11]. Figure 1 shows possible arrangements of the dielectric for the example of plane-parallel electrodes [10].

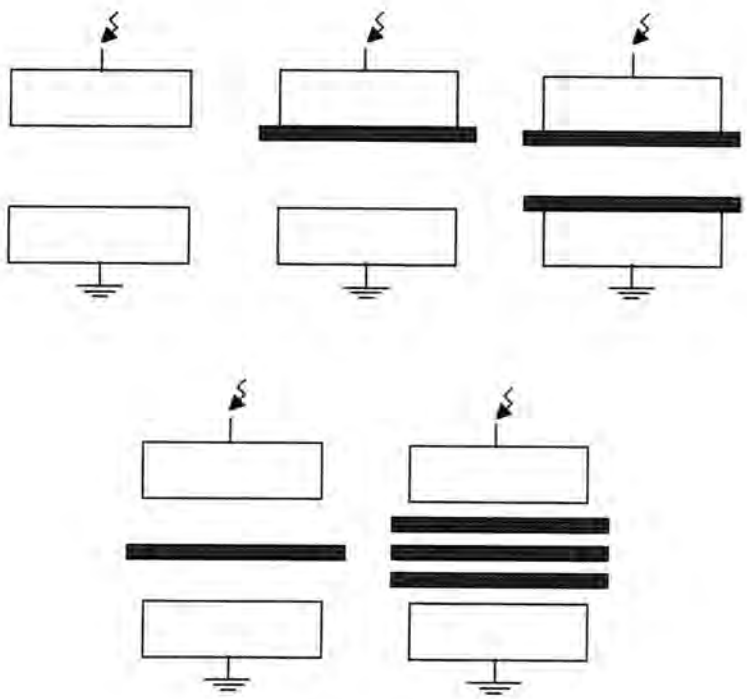

Fig. 1 Possible arrangements of the dielectric in a silent discharge set-up [10]

1.4.3 Properties of the silent discharge

The application of a suitable voltage to a silent discharge set-up results in the electrical breakdown of the gas filling the gap. The gas between the electrodes is no longer an insulator and charge transport takes place. Due to the presence of the dielectric the discharge is composed of many cylindrical microdischarges or filaments of nanosecond duration [5,13-15]. The discharge as a whole is therefore inhomogeneous in nature. In practice, the discharge conditions are often chosen such that most of the charge transport occurs via electrons. At the dielectric the discharge channels spread into surface discharges which have a larger diameter than the original filaments [8,12,16]. The exact dimensions of the surface discharges depend on the experimental conditions. Each microdischarge charges up a small segment of the barrier area where the charge is not distributed evenly over the affected area but decreases with increasing distance from the discharge centre [12]. Depending on the polarity of the set-up two types of surface processes can be distinguished [9,10,12,15] which are schematically shown in figure 2.

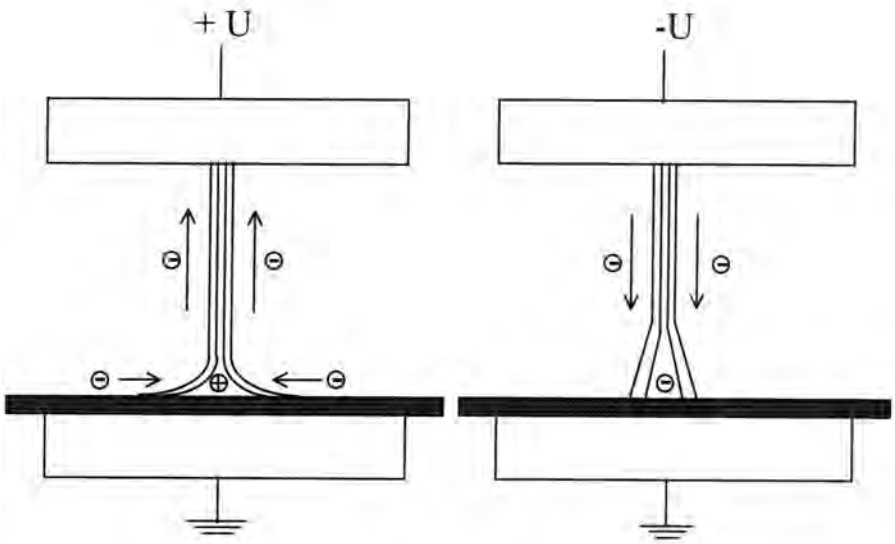

Fig. 2 Development of a microdischarge in dependence of the polarity of the set-up [10]

If the barrier is the anode of the set-up (figure 2, right) electrons travel towards the dielectric through the microdischarge channels. Each filament builds up a negative charge on the dielectric segment which it strikes. Electrons subsequently passing through the same channel are deflected towards the side such that the microdischarge is broadened into a funnel shape in the vicinity of the barrier. Photographs of such discharges taken through transparent dielectric materials show diffuse spots [9]. The negative charge accumulating on the dielectric area affected by a microdischarge creates an electric field which locally reduces the applied field and finally causes the microdischarge to terminate [10,12].

In cases where the dielectric is the cathode of the set-up (figure 2, left) electrons in the microdischarges are accelerated towards the powered electrode by the influence of the applied field. The positive charge each filament leaves behind on the dielectric causes a potential difference with respect to the regions of the dielectric which are not affected by a microdischarge. The difference finally becomes large enough to ignite discharges along the dielectric surface through which electrons are fed into the microdischarge while a further positive charge is built up on the dielectric. Optically, the surface discharges appear as strongly branched channels which meet in a centre [9,12,15]. Their diameter is larger than that of the surface discharges developed when the dielectric represents the anode [9,12]. As in the first case, the charge accumulating on the dielectric increasingly weakens the applied field

until the microdischarge cannot longer be sustained and is extinguished [10,12]. The characteristics of the surface discharges in dependence of the polarity can be observed both in single microdischarges and in set-ups continuously operated with voltages comprised of successive positive and negative half cycles [17].

During their passage through the microdischarge channels the electrons accelerated in the electrical field initiate plasmachemical processes in collisions with gas particles. The properties of the microdischarges determine which of the multitude of simultaneous elementary reactions take place in a gas or a gas mixture. Therefore, the experimental conditions for a particular silent discharge application have to be optimised such that the desired reaction is favoured and undesired reactions are reduced to a minimum. The term "discharge strength" often used in this context refers to the amount of charge transferred through a discharge channel, a strong microdischarge being a filament through which a large charge is transported.

The properties of the filaments can be influenced by experimental factors like the characteristics of the feeding circuit, the nature and the thickness of the dielectric, the gas pressure, the gas composition and the gap spacing [13].

The *rise time of the applied voltage* influences the temporal and local distribution of the microdischarges. If the voltage increases slowly with respect to the lifetime of the microdischarge, filaments are ignited and extinguished randomly with respect to time and location as long as the voltage is increased and the field is sufficiently high to cause breakdown [11]. Under these conditions the dielectric is not charged up simultaneously and pronounced surface discharges can develop. Each microdischarge gives rise to a short current pulse which can be measured as a needle like signal [10]. The opposing field built up by the charge deposition on the dielectric finally terminates the microdischarge. Since a remaining charge on the barrier weakens the field strength on the location where the microdischarge had taken place, the ignition of another filament at the same place is prevented until the charge has been reduced. Subsequent microdischarges therefore strike other locations on the dielectric such that the filaments are distributed over the whole discharge area over a certain amount of time [7,10,13].

If steep voltages (kV/ns range) are applied, the breakdown of the gas results in the simultaneous formation of many parallel microdischarges. The charge transport during the whole discharge phase takes place via the microdischarge

channels initially developed; subsequent microdischarges are not ignited [10,16]. Depending on the characteristics of the applied voltage pulse the duration of a discharge phase is in the range of tens to hundreds of nanoseconds [10]. Due to the more homogeneous nature of the discharge approximately all segments of the dielectric are charged up simultaneously. Thereby the occurrence of extended surface discharges is prevented [18]. The measured current is the sum of the currents of all the microdischarges and therefore a lot larger than in the former case [18].

The *properties of the dielectric* determine the amount of charge that can be deposited on the barrier. The amount of charge transferred through a microdischarge channel is proportional to the dielectric constant of the dielectric material and inversely proportional to the dielectric thickness [8,12].

A decrease in *pressure* leads to more numerous filaments with increasingly large diameter [8]. At the same time the overall appearance of the discharge becomes more and more diffuse until at sufficiently low pressures the filamentary structure is replaced by a glow discharge [11].

The *gas properties* determine which elementary reactions take place at a certain electrical field value and have therefore an influence on the characteristics of the respective microdischarges. Microdischarges in electronegative gases have a much shorter lifetime transferring a smaller charge than those ignited in inert gases [9,19]. This is due to the tendency of electronegative gases to undergo electron attachment which represents a powerful electron loss pathway in addition to recombination processes which prevail in inert gases.

An increase of the *gap width* results in the concentration of the discharge to a few bright microdischarge channels with pronounced surface discharges [10,18]. The optical appearance [10,18], charge measurements [12] and mathematical simulations [8] show that the charge transported over a single filament increases with increasing gap width. In cases where slowly increasing voltages are applied the concentration of the discharge can already be observed at small gap widths [12] whereas the use of fast rising voltages allows the discharge to be kept more homogeneous over larger gap spacings [16,18].

1.5 Applications of silent discharge processes

1.5.1 Ozone generation

The oldest but still most important application of silent discharges is ozone production for fresh and waste water treatment as well as for industrial bleaching and oxidation purposes [8,11,13]. Both dry oxygen and dry air can be used as feed gases for large ozoniser installations [5,8]. Numerous possible elementary reactions contribute to the overall plasma process in both gases [8]. In comparison with pure oxygen, air as a mixture of gases represents, however, the more complex system. Only the key reactions will be considered in the following description. Excited molecules will appear in the respective equations marked with an asterisk.

1.5.1.1 Ozone generation from oxygen

Two reaction phases can be distinguished in the context of ozone formation in oxygen-fed silent discharges [18]. The first phase occurs during the charge transport of the microdischarge and hence lasts only a few nanoseconds [14]. Electron impact processes are dominant during this period. The following reactions are regarded as the most important ones in oxygen:

$$e + O_2 \rightarrow e + O_2(A^3\Sigma_u^+) \rightarrow e + 2\,O(^3P) \qquad (1)$$

$$e + O_2 \rightarrow e + O_2(B^3\Sigma_u^-) \rightarrow e + O(^3P) + O(^1D) \qquad (2)$$

$$e + O_3 \rightarrow e + O_2 + O \qquad (3)$$

Oxygen dissociation can proceed via two reaction pathways. These involve oxygen molecules in two different excited states as shown in equations (1) and (2). Since the energy thresholds for the first step of eq. (1) and (2) are 6.0 and 8.4 eV, respectively [13,14], the ideal electron energy for obtaining oxygen atoms is in the range of 6-9 eV [5,8]. If ozone molecules are already present in the gas volume subjected to

the discharge treatment, they can dissociate according to pathway (3) upon electron impact.

During the subsequent reaction phase the intermediates created in the microdischarge form stable products within microseconds [5,8,9]. These are for oxygen:

$$O_2 + O + M \leftrightarrow O_3^* + M \leftrightarrow O_3 + M_{kin} \quad (4)$$

$$O + O + M \rightarrow O_2 + M_{kin} \quad (5)$$

$$O + O_3^* \rightarrow 2\,O_2 \quad (6)$$

Ozone molecules are formed in a three-body collision according to (4). M is a third collision partner carrying away the excess energy of the product molecule which is initially formed in a vibrationally excited state [8,11,12,14]. After their formation in the extinguished microdischarge channels the ozone molecules diffuse until they are evenly distributed in the gas volume.

In order to obtain an optimum ozone yield the microdischarges have to be adjusted such that their strength is neither too strong nor too weak. The medium discharge strength represents a compromise between conflicting requirements concerning the efficiency of the conversion of oxygen atoms and oxygen molecules to ozone on the one hand and the efficiency of oxygen molecule dissociation on the other [15]. Too strong microdischarges result in the formation of too many oxygen atoms with respect to oxygen molecules present. In this case the efficiency of the conversion of oxygen atoms to ozone is reduced by oxygen atoms taking part in the undesired side reactions (5) and (6). In weak microdischarges those side reactions are negligible but these conditions favour an increased proportion of the energy to be transported by ions. Since ions do not take part in oxygen molecule dissociation and thus do not contribute to ozone formation, an energy transport via ions represents a loss which reduces the efficiency of oxygen molecule dissociation and consequently the overall efficiency of ozone formation.

In a volume of feed gas which is exposed to many successive microdischarges, the efficiency of the individual microdischarges with respect to product formation is gradually reduced as the gas is enriched with ozone [14], because

ozone destruction processes described in equations (3) and (6) gain importance. Finally, a saturation concentration is reached where ozone producing and loss processes initiated by a microdischarge are balanced [13,14].

The saturation concentration drops with increasing temperature. This behaviour can be explained with the fact that reaction constants of (4) and (6) and to a lower extent the constant of reaction (5) are dependent on temperature. With increasing gas temperature the equilibrium of reaction (4) is shifted towards the left side ("thermal ozone destruction") and ozone destruction according to (6) is increased [9]. It is therefore important to prevent the gas from heating up during silent discharge treatment. This can be achieved by efficient external cooling of the ozoniser [15] and the choice of the appropriate discharge conditions. Feeding the energy into the gas via many parallel microdischarges is more favourable than allowing the discharge to concentrate on a few strong filaments with large surface discharges. The latter conditions lead to the development of local temperature maxima which give rise to a high rate of thermal ozone destruction [16].

1.5.1.2 Ozone generation from air

In air, the energy of the discharge electrons is distributed among nitrogen and oxygen. The discharge chemistry therefore involves both oxygen and nitrogen species [20,21]. Apart from oxygen (1,2) and ozone (3), nitrogen molecules are subject to electron impact during the microdischarge phase. The following additional elementary reactions have to be considered:

$$e + N_2 \rightarrow e + 2\,N \qquad (7)$$

$$e + N_2 \rightarrow e + N_2^* \qquad (8)$$

A large part of the input energy is initially stored in excited states of nitrogen molecules (8) [9,14]. Several metastable states are possible with threshold energies between 6.17 and 11.9 eV [22]. In the subsequent reaction phase the following processes involving nitrogen compounds occur in addition to reactions (4) to (6):

reactions of metastable nitrogen molecules:

$$N_2^* + O_2 \rightarrow N_2 + 2\,O \quad (9)$$

$$N_2^* + O_2 \rightarrow N_2O + O \quad (10)$$

$$N_2^* + O_2 \rightarrow 2\,NO \quad (11)$$

reactions of nitrogen atoms:

$$N + O_2 \rightarrow NO + O \quad (12)$$

$$N + O_3 \rightarrow NO + O_2 \quad (13)$$

$$N + NO \rightarrow N_2 + O \quad (14)$$

$$N + NO_2 \rightarrow N_2 + O_2 \quad (15)$$

nitrogen oxide transformation reactions:

$$O + NO + M \rightarrow NO_2 + M \quad (16)$$

$$O + NO_2 \rightarrow NO + O_2 \quad (17)$$

$$NO + O_3 \rightarrow NO_2 + O_2 \quad (18)$$

$$NO_2 + O_3 \rightarrow NO_3 + O_2 \quad (19)$$

$$NO_2 + O + M \rightarrow NO_3 + M_{kin} \quad (20)$$

$$NO + NO_3 \rightarrow 2\,NO_2 \quad (21)$$

$$NO_2 + NO_3 \rightarrow NO_2 + O_2 \quad (22)$$

$$O + NO_3 \rightarrow NO_2 + O_2 \quad (23)$$

$$NO_2 + NO_3 + M \leftrightarrow 2\,N_2O_5 + M_{kin} \quad (24)$$

$$O + N_2O_5 \rightarrow 2\,NO_2 + O_2 \quad (25)$$

In air the two reaction steps of ozone formation cannot be linked as strictly to the discharge and the reaction phase as in the case of oxygen. Oxygen atoms are not only produced directly by electron impact dissociation of oxygen molecules during the current flow of the microdischarge but there are also substantial indirect sources of atomic oxygen in the reaction phase. Those involve nitrogen atoms (12,14) and nitrogen metastables (9,10) of sufficient energy [23]. These processes are also the reason why in air the ozone yield obtained is larger than can be expected from its oxygen mole fraction [8,13]. A further difference of ozone production in oxygen and air consists in the time scale of ozone formation. Mathematical simulations of a microdischarge in air and in oxygen revealed that ozone production proceeds faster in oxygen where the maximum ozone concentration is reached after approximately 10^{-5} seconds. The maximum ozone concentration in air is reached after 10^{-4} seconds. The differences were attributed to the small partial pressure of oxygen in air [8,9].

Beside ozone, nitrogen oxides are formed as stable products of the discharge treatment of air. Due to their different formation pathways and their different influence on the overall plasma chemistry, N_2O and the other nitrogen oxides which will be referred to as NO_x in the following discussion (NO_x = NO, NO_2, NO_3, N_2O_5 and under certain experimental conditions HNO_3) can be distinguished.

N_2O is almost exclusively formed via nitrogen metastables (10) [24]. At the temperatures usually present in ozonisers it is inert and exerts no influence on ozone formation [21,22]. In contrast, NO_x formation proceeds under consumption of ozone and atomic oxygen. The discharge conditions determine which chemical reactions are favoured and therefore which products are obtained. Those can be either both nitrogen oxides and ozone or only nitrogen oxides ("ozoneless mode, discharge poisoning").

NO_x production starts with atomic nitrogen which forms at first nitrogen oxide, NO, in reactions with oxygen (12) or ozone molecules already present in the gas (13). In the presence of sufficient ozone, pathway (13) is dominant [22]. NO is then further oxidised to higher nitrogen oxides in the transformation reactions. Within the transformation cycle, the sum concentration of the nitrogen oxides remains unchanged since reactions (14) and (15), the only possible destruction pathways in the reaction phase, only gain importance in the absence of ozone; otherwise NO and NO_2 preferably react with ozone according to reactions (18) and (19).

Under normal operation conditions (presence of ozone, moderate temperature and microdischarge strength) all nitrogen atoms are finally converted to N_2O_5 because the equilibrium of reaction (24) is shifted to the right hand side and thus provides an effective removal of NO, NO_2 and NO_3 [21]. In this case, N_2O_5 and N_2O are the only nitrogen oxides detected in considerable amounts in addition to ozone [8,13,22]. Their proportion corresponds to about 1% of the respective ozone yield [13,21]. Reaction (24) is important because even small concentrations of the low nitrogen oxides can have a strongly detrimental effect on ozone yield since they take part in catalytic chains leading to ozone destruction and atomic oxygen recombination, respectively. These chains consist of combinations of nitrogen oxide transformation reactions as can be seen below:

$$O + NO_2 \rightarrow NO + O_2 \qquad (17)$$

$$NO + O_3 \rightarrow NO_2 + O_2 \qquad (18)$$

sum [8,9,20,22]: $O + O_3 \rightarrow 2\,O_2$

$$NO_2 + O_3 \rightarrow NO_3 + O_2 \qquad (19)$$

$$O + NO_3 \rightarrow NO_2 + O_2 \qquad (23)$$

sum [22]: $O + O_3 \rightarrow 2\,O_2$

$$O + NO + M \rightarrow NO_2 + M \qquad (16)$$

$$O + NO_2 \rightarrow NO + O_2 \qquad (17)$$

sum [8,9]: $O + O \rightarrow O_2$

$$NO_2 + O + M \rightarrow NO_3 + M_{kin} \qquad (20)$$

$$O + NO_3 \rightarrow NO_2 + O_2 \qquad (23)$$

sum [22]: $O + O \rightarrow O_2$

An increase in temperature changes the discharge chemistry as follows [9]: The amount of NO produced according to reaction (12) increases, the ozone destruction processes according to (3), (6), (18) and (19) are favoured and the equilibria (4) and (24) are shifted to the left side. This means that at the same time less ozone is formed and a higher proportion of ozone is consumed by the respective destruction reactions. By the shift of reaction (24) the gas volume is enriched with NO, NO_2 and NO_3 and the catalytic cycles gain more importance. The more often these cycles are passed through the more ozone is lost. In the most extreme case all ozone molecules are consumed and N_2O_5 disappears such that the lower nitrogen oxides together with N_2O are the only product of the discharge [5,8,13]. This phenomenon is referred to as discharge poisoning and can be recognized by a colour change of the processed gas from colourless to brown (NO_2) [12].

1.5.1.3 The influence of humidity

Several authors have observed a reduction in ozone yield when the feed gas (oxygen or air) contained moisture [8,12,16]. Both changes in the discharge physics and in the discharge chemistry have been discussed as possible reasons for this phenomenon.

Studies carried out in moist air [12,19] revealed that under these conditions the discharge is composed of fewer but more intense microdischarges. The discharge channels appeared brighter, burnt continuously and transferred a larger charge than the corresponding microdischarges in dried feed gas. Furthermore, an increase in the diameter of the surface discharge was found for microdischarges ignited in the presence of water vapour [19]. These observations were taken as evidence for a fundamental change of the discharge mechanism. Hirth assumed that a conducting aqueous layer was formed on the dielectric in which ions from the glass (which

served as the dielectric in the study) and nitric acid produced in the discharge (see below) are dissolved. Permanent discharges were thought to be developed because the charge is distributed by charge conduction in the conductive layer thus preventing the self termination of the microdischarge by charge build - up [12]. The lower ozone yield was explained by the reduction of the volume affected by the reactive plasma within the system [19] and the thermal ozone loss due to the temperature increase in the few remaining strong discharge channels [12].

Comparing the behaviour of moist and dried oxygen, Labrenz [16] could only partly confirm the findings described above. Irrespective of whether a slowly increasing or a steeply increasing voltage was applied to the ozoniser, a lower ozone yield was found following the treatment of the humid feed gas. Measuring the absorbance across the gap, an increase in the ozone concentration in direction of the dielectric was found. This observation was made both when dried and moist feed gas was used. The drop in ozone concentration in the vicinity of the dielectric which could have been expected in the case of the moist feed gas as a consequence of the surface conductivity suggested by Hirth could not be observed. This led to the conclusion that in this system the increase in surface conductivity is at least not the only reason leading to the decrease in ozone yield. The author [16] considers the change of plasma chemistry in the presence of humidity as the major factor.

The presence of water vapour as a further gaseous component of the feed gas increases the number of possible elementary reactions contributing to the plasma chemistry. A simplified numerical calculation of the temporal evolution of various neutral species in humid oxygen [25,26] and humid air [27] has been reported. Due to the assumptions made in their calculations the authors consider their model to be applicable up to a relative humidity of 35 %. Like nitrogen and oxygen molecules water molecules dissociate upon electron impact, the latter forming hydrogen and hydroxyl radicals as a primary product. HO_2 radicals and H_2O_2 are products of the reactions between the primary radicals formed in the dissociation step or of the reactions between those radicals and secondary products [26]. Of the products mentioned, only H_2O_2 is stable. In oxygen, an increasing water content is assumed to lead to the formation of a larger proportion of hydrogen peroxide with respect to ozone [25]. In humid air, the formation of the water related species was found to be delayed in comparison to the corresponding reactions in humid oxygen. Quantitative

statements concerning these products are not given [27]. H_2O_2 is, however, assumed to be formed in non - negligible amounts both in moist air and moist oxygen.

In air, the presence of humidity also affects the formation of the nitrogen oxides. It was found that while NO_x production does not change with rising moisture content, the N_2O production decreases slowly with increasing humidity [21,22]. Depending on the humidity, a mixture of N_2O_5 and HNO_3 (water content 10 - 300 ppm) or exclusively HNO_3 (water content > 300 ppm) was detected. Nitric acid is formed according to:

$$N_2O_5 + H_2O \rightarrow 2\,HNO_3 \qquad (26)$$

Since N_2O_5 is continuously removed by this elementary reaction, the equilibrium of reaction (24) has to be re-established by producing further N_2O_5. This, in turn, reduces the concentration of NO_2 and NO_3 and thereby prevents discharge poisoning. This beneficial effect of water vapour does, however, not outweigh the loss in ozone yield [21].

1.5.2 Excimer lamps

The operation of barrier discharges under suitable conditions in rare gases, halogens or rare gas-halogen mixtures [28] as well as in mercury vapour and mercury vapour-rare gas mixtures [29], gives rise to the formation of excimers, excited molecular complexes which do not possess a stable ground state [5]. Due to their inherent instability excimers dissociate within nanoseconds and emit their excitation energy as a narrow band radiation in the VIS / UV or VUV region. The emitted radiation is dependent on the properties of the particular molecule and the radiation for the wide range of known excimers covers wavelengths between 50 and 600 nm [28].

On the basis of this principle novel high intensity VUV and UV radiation sources have been designed which can be used complementary or as an alternative to existing sources depending on their respective wavelength. The flexibility in the geometrical configuration of the barrier discharge and the variety of wavelengths available due to different filling gases and gas mixtures allows the construction of large area and high spectral purity lamps which are tailored for a specific

photochemical application [30]. Excimer lamps have been tested for purposes of polymer photooxidation and etching [31,32], the photodissociation of organometallic precursors [28,33] and photoassisted chemical vapour deposition [34-36].

1.5.3 Flue gas treatment

Since barrier discharges offer the possibility of processing large amounts of gases at atmospheric pressure they have been tested as a means of waste gas treatment. The toxins undergo reactions with the species created in the discharge. Removal proceeds most often via oxidative pathways involving atomic oxygen and hydroxyl radicals formed from the moist air or moist oxygen background. Examples include the processing of SO_2/NO_x mixtures produced in coal combustion plants [37,38] (ultraviolet radiation exerts an additional beneficial effect) as well as the treatment of volatile organic compounds like C_2HCl_3 [39] and CH_2O [40]. Both oxidation and reduction processes are involved in the remediation of nitrogen oxides from diesel exhaust [41]. Optimum efficiency of the respective processes can be achieved by choosing the appropriate plasma conditions. The treatment results in mixtures of new stable products some of which are non-toxic and can be released into the atmosphere. Others can be washed out and possibly isolated as byproducts of economical interest. Harmful products, however, require additional processing steps which may be so complicated that they limit the scope of the treatment as has been found in the case of formaldehyde [40].

1.6 References

1) Yasuda, H. *J. Pol. Sci Macromolecular Reviews* **1981**, *16*, 199
2) Grill, A. *Cold Plasma in Materials Fabrication*, IEEE Press-The Institute of Electrical Engineers Inc. : New York, 1994, pp.1-22
3) Kirk-Othmer *Encyclopedia of Chemical Technology* 4th edition, Kroschwitz, J. Ed., J. Wiley and Sons : New York, 1996, Vol.19, pp.226-258
4) Drost, H. *Plasmachemie*, Akademie-Verlag : Berlin, 1978, pp.20-26
5) Eliasson, B.; Kogelschatz, U. *IEEE Transactions on Plasma Science* **1991**, *19 (6)* 1063

6) Grill, pp.46-62

7) Drost, pp.38-56

8) Eliasson, B.; Kogelschatz, U. *IEEE Transactions on Plasma Science* **1991**, *19 (2),* 309

9) Heuser, C. *Zur Ozonerzeugung in elektrischen Gasentladungen*, PhD Thesis: RWTH Aachen, 1985

10) Reitz, U. *Barrierenentladungen zur plasmagestützten Oberflächenbehandlung*, Berichte des Forschungszentrums Jülich 2613, 1992

11) Eliasson, B.; Egli, W.; Kogelschatz, U. *Pure & Appl.Chem.* **1994**, *66(6)*, 1275

12) Hirth, M.; *Teilprozesse bei der Ozonerzeugung mittels stiller elektrischer Entladung*, PhD Thesis: TH Karlsruhe, 1979

13) Kogelschatz, U. in: *Process Technologies for Water Treatment*, Brown Boveri Symposium on Process Technologies for Water Treatment, Stucki, S. Ed., Plenum Press: New York, 1987, pp.87-118

14) Eliasson, B.; Hirth, M.; Kogelschatz, U. *J. Phys. D: Appl. Phys.* **1987**, *20*, 1421

15) Braun, D.; Küchler, U.; Pietsch, G. *J Phys. D: Appl. Phys.* **1991**, *24*, 564

16) Labrenz, M. *Elektrische Gasentladungen zur Ozonerzeugung*, PhD Thesis: TU Braunschweig, 1983

17) Kogelschatz, U. personal communication

18) Braumann, P. *Über die Erzeugung von Gasentladungen zur Herstellung von Ozon*, PhD Thesis: TU Braunschweig,1981

19) Falkenstein, Z.; Coogan, J.J *J. Phys. D : Appl. Phys.* **1997**, *30*, 817

20) Yagi, S.; Tanaka, M. *J. Phys D: Appl. Phys.* **1979**, *12*, 1509

21) Braun, D.; Küchler, U.; Pietsch, G. *Pure & Appl.Chem.* **1988**, *60 (5)*, 741

22) Küchler U. *Zur Optimierung luftbetriebener Ozonerzeuger*, PhD Thesis: RWTH Aachen, 1990

23) Eliasson, B.; Kogelschatz, U.; Baessler, P *J. Phys. B: At. Mol. Phys.* **1984**, *17*, L797

24) Eliasson, B.; Kogelschatz, U. *Journal de chimie physique*, **1986**, *83(4)*, 279

25) Peyrous, R.; Pignolet, P.; Held, B. *J. Phys. D : Appl. Phys.* **1989**, *22*, 1658

26) Peyrous, R. *Ozone Science & Engineering* **1990**, *12*, 19

27) Peyrous, R. *Ozone Science & Engineering* **1990**, *12*, 41

28) Kogelschatz, U. *Appl. Surf. Sci.* **1992**, *54*, 410

29) Eliasson, B.; Gellert, J. *J. Appl. Phys.* **1990**, *68 (5)*, 2026

30) Kogelschatz, U. *Pure & Appl. Chem* **1990**, *62*, 1667

31) Esrom, H.; Kogelschatz, U. *Thin Solid Films* **1992**, *218*, 231

32) Zhang, J.Y.; Esrom, H.; Kogelschatz, U.; Emig, G. *Appl. Surf. Sci.* **1993**, *69*, 299

33) Esrom, H.; Kogelschatz, U. *Appl. Surf. Sci.* **1992**, *54*, 440

34) Bergonzo, P.; Kogelschatz, U.; Boyd, I.W. *Appl. Surf. Sci.* **1993**, *69*, 393

35) Bergonzo, P.; Patel, P.; Boyd, I.W.; Kogelschatz, U. *Appl. Surf. Sci.* **1992**, *54*, 424

36) Yokotani, A.; Takezoe, N.; Kurosawa, K.; Igarashi, T.; Matsuno, H. *Appl. Phys. Lett.* **1996**, *69(10)* 1399

37) Dhali, S.K.; Sardja, I. *J. Appl. Phys.* **1991**, *69*, 6319

38) Chang, M.B.; Balbach, J.H.; Rood, M.J.; Kushner, M.J. *J. Appl. Phys.*, **1991**, *69 (8)* 4409

39) Evans, D.; Rosocha, L.A.; Anderson, G. K.; Coogan, J.J.; Kushner, M.J. *J. Appl. Phys.* **1993**, *74 (9)*, 5378

40) Storch, D.G.; Kushner, M.J. *J. Appl. Phys.* **1993**, *73(1)* ,51

41) Gentile, A.C.; Kushner, M.J. *J. Appl. Phys.* **1995**, *78 (3)*, 2074

Chapter 2: Fundamentals of the experimental techniques

2.1 Introduction

This chapter gives a brief introduction to the analysis techniques used in this work. Those include bulk (Transmission Infrared Spectroscopy), surface sensitive (Attenuated Total Reflection Infrared Spectroscopy) and surface specific (X-Ray Photoelectron Spectroscopy) techniques for the analysis of solids (chapters 3-6) as well as Mass Spectrometry for the monitoring of the volatile species evolved during the photodecomposition studies (chapter 7).

2.2 Infrared Spectroscopy

2.2.1 General

The infrared (IR) region comprises the wavelengths between 7.8×10^{-5} and 10^{-1} cm (12800-10 cm^{-1}) in the electromagnetic spectrum [1]. Upon absorption of radiation in this energy range molecules can reach vibrational levels of higher energy. Gases show a fine structure caused by rotational transitions whereas in solids the free rotation of the molecules is restricted. An appropriate model which describes the vibrational behaviour of molecules is that of the anharmonic oscillator. Most of the signals observed in IR spectra are due to transitions to the first excited vibrational level and are referred to as fundamental vibrations. Transitions to higher levels, so called overtones can occur as well but their probability is small such that they usually appear in the spectra as signals of low intensity. The same applies to combination bands which are caused by the coupling of two or sometimes three fundamental vibrations [2].

Apart from the quantum conditions which define the location of the resonance energies the occurrence and intensity of absorption bands is dependent on the dipole moment of the molecules: Only those vibrations which involve a simultaneous change in the dipole moment are IR active since the changing charge distribution accompanying the vibration creates an alternating electric field which can interact with the electric field component of the incident radiation [3]. The larger the change in

the dipole moment the more effective the energy transfer from the IR photon to the molecule and the larger the signal intensity [1].

Molecular vibrations can either lead to a movement along the bond axis (stretching) or to a change in the bond angle between bonds with a common atom (bending). The latter can again be differentiated into in-plane (scissoring, rocking) and out-of-plane (wagging, twisting) vibrations [2,3,4]. For a particular group, the stretching signal appears at a higher wavenumber than the bending band because the forces which try to conserve the bond angle are smaller than the forces which act against changes in the interatomic distance [4]. The spectra show band shaped signals; interactions of the molecules in the liquid or solid state can play a role in both band broadening and peak position.

The region in which the most important fundamental vibrations occur and thus most informations about the structure of molecules can be obtained is limited to a wavenumber range of 4000 - 400 cm^{-1} [2,3,4]. This area falls into two regimes. At wavenumbers between 4000 and 1250 cm^{-1} localized vibrations take place in which the shift of a certain group of atoms is much bigger than the shift of all the other atoms [4]. Characteristic absorption bands of functional groups and of double and triple bonds are situated in this area. Each bond has its own frequency. The vibrations, however, are not completely uncoupled from the neighbouring atoms, the resonance frequency is dependent to a certain extent on the chemical environment which on the other hand can help to assign bands [3]. In the region from 1250 to 400 cm^{-1} molecule vibrations occur, all atoms have the same shift and informations which are characteristic of the molecule as a whole can be obtained ("fingerprint region") [2,3,4].

2.2.2 Attenuated Total Reflection (ATR)

Attenuated Total Reflection (ATR) which is also termed Internal Reflection Spectroscopy (IRS) is a technique which is based on the phenomenon of total internal reflection. In the measurements a sample of refractive index n_s is brought into close contact with a prism or an internal reflectance crystal of refractive index n_c where $n_c > n_s$. A beam of light passing through the reflectance element such that it arrives at the element-sample interface at an angle θ which is higher than the critical angle θ_c is totally reflected back into the reflection element. Some radiation of the totally

reflected beam penetrates a small distance into the sample where absorption at the characteristic frequencies of the sample takes place. The totally internal reflected beam is therefore attenuated in the wavelength regions which correspond to the respective absorption bands. The penetration depth depends on the wavelength of the radiation in the refractive element λ_r, the angle of incidence θ and the refractive indices of the sample and the crystal, n_s and n_c, repectively according to [5,7]:

$$d_p = \frac{\lambda_r}{\{ 2\pi [\sin^2 \theta - (n_s/n_c)^2] \}^{0.5}}$$

Due to this wavelength dependence sampling depth varies through the spectrum. Typical values for d_p are between 0.25 and 4 μm [6] such that ATR is a surface sensitive technique whereas transmission spectra provide information about the bulk of a sample. ATR and transmission IR spectra are similar with respect to the positions of the characteristic bands and the same correlation charts can be used for their interpretation. The wavelength dependence of d_p leads, however, to differences in the relative intensities of the signals. In ATR spectra the signals at longer wavelengths appear more intense than in the corresponding transmission spectra [7].

A variety of experimental set-ups are possible; both single and multiple reflections can be employed. In the latter case, attenuation takes place at each reflection resulting in an amplification of absorption [1]. There are a number of chemically inert infrared transmitting materials with high refractive index which can be used as reflecting elements [5,6]. The method is applicable to the study of a large variety of samples including nontransparent materials like fabrics, fibers and opaque materials [5,7].

2.3 Mass Spectrometry

Mass Spectrometry involves the separation and subsequent detection of ions according to their mass-to-charge ratio. Mass spectrometers are operated under UHV conditions and consist in principle of three parts: an ion source, a mass separation unit and a detector. There are several methods by which molecules can be ionised, separated and detected. The respective method of choice depends on the particular

system to be studied. Only the techniques relevant for this work which are electron impact ionisation and separation of ions in a quadrupole mass filter will be described below.

2.3.1 The Quadrupole Mass Filter [8-11]

In a quadrupole mass filter, 4 rods of either circular or hyperbolical cross-section are arranged in parallel. Opposing rods are electrically connected together. The voltage applied to the two pairs of rods consists of an alternating component of radiofrequency (rf) V ($V = V_0 \cos \omega t$) which is superimposed on a direct component U. Upon application of the voltage, neighbouring rods are oppositely charged, the voltage on the positive electrodes being $+ (U + V_0 \cos \omega t)$ and the voltage of the negative electrodes $- (U + V_0 \cos \omega t)$. Thereby, a high frequency field is created which causes ions entering the assembly to vibrate. By choosing the appropriate values for U and V only ions of a certain mass-to-charge ratio have a stable trajectory with small amplitude and can reach the detector, usually an electron multiplier. Other ions follow unstable paths and are finally lost by either collision with the rods or by escaping through the spaces between them. A mass scan is taken by simultaneously varying U and V such that both the ratio U/V and the frequency stay constant.

Quadrupoles are popular because they are compact, robust and reasonably priced. Their main disadvantage consists in the loss of sensitivity with increasing mass and generally their low mass resolution. Mass resolution and sensitivity in quadrupole instruments are roughly inversely proportional [8].

2.3.2 Electron Impact Ionisation

Electron Impact Ionisation is the most widespread ionisation method for samples which can be introduced into the mass spectrometer in gaseous form. Ions are generated by exposing the vapourised sample molecules at a reduced pressure to a beam of thermally emitted electrons from a filament like that schematically shown in figure 1.

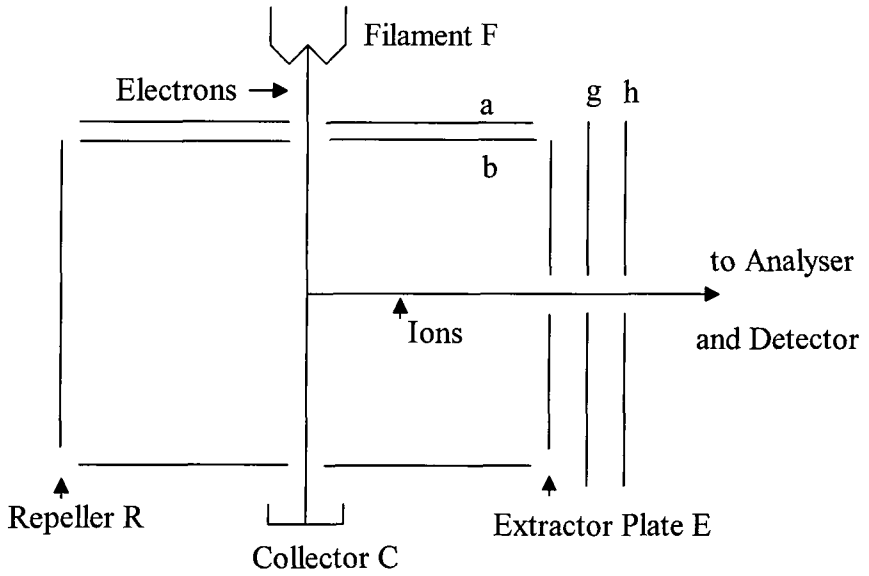

Fig. 1 Schematic of an Electron Impact ion source according to [12] (sample molecules entering the assembly perpendicular to the electron beam are omitted for clarity)

Electrons thermally emitted from filament F pass through narrow slits in plates a and b. A is held at a small positive potential in order to attract the electrons. The electrons are then accelerated towards the ionisation chamber by a large potential drop between F and b where the magnitude of the potential drop determines the electron energy. The small dimensions of the slits in plates a and b serve the purpose of collimating the electron beam. A further focussing of the beam can be achieved by applying a magnetic field in direction of the beam [12,13,14].

Inelastic collision processes between electrons and sample molecules lead to the formation of mostly singly charged positive ions. These are extracted from the ionisation chamber by a small potential difference between the repeller R and extractor plate E and subsequently focussed to the entrance of the analyser after passing a strong electric field between g and h [14]. Negatively charged ions are removed by the repeller. The electrons finally reach a collector C which is also called a trap. The stability of the ionising current is ensured by an electronic feedback system between the trap current and the heating current of the filament [14].

Ions striking the detector after passing the separation unit give rise to a signal, the so called ion current. The signal intensity is proportional to the number of incident ions. The ion current is dependent on the sample pressure in the ionisation

chamber, the electron current, the ionisation cross section of the molecules, the effective pathlength of the electrons in the chamber and the efficiency of the extraction of ions [15]. In a spectrum ion currents are plotted versus the mass - to charge ratios.

The appearance of a spectrum for which electron impact is employed as the ionisation method depends on the energy of the bombarding electrons. Below a certain threshold value, the ionisation energy, which is typically between 7 and 15 eV, no ionisation occurs [16]. As the energy is increased, the formation of the parent molecular ion (pmi) according to :

$$M + e \rightarrow M^+ + 2e$$

is observed. Negative and doubly charged positive ions are formed as well but usually to a lower extent. The probability of parent molecular ion formation and therefore the observed signal intensity increases at first with increasing electron energy. In collisions with electrons of even higher energy content sufficient energy is transferred to the sample molecules that bond dissociation becomes possible and fragment ions are formed. In some cases the appearance of fragment ions is accompanied by a concurrent loss in pmi intensity or even the complete disappearance of this signal. The frequency of fragmentation processes again increases with electron energy until at energy values over 40-50 eV the relative intensities of the fragments are not further affected by small changes in energy. Mass spectra are, therefore, often recorded above this threshold, usually at electron energies of 70 eV, to ensure good reproducibility and optimum ion yield at this energy [16].

2.4 X-Ray Photoelectron Spectroscopy (XPS)

2.4.1 Principle

XPS (also called Electron Spectroscopy for Chemical Analysis, ESCA) is a surface specific analysis technique which is based on measuring the energy of photoelectrons emitted from a sample when it is irradiated with soft x-rays. Knowing

the radiation wavelength of the x-ray source, hν, and measuring the kinetic energy, E_{kin}, of the emitted electrons, the binding energy BE of the states, from which the electrons are detached can be calculated according to [17] :

$$E_{kin} = h\nu - BE - \phi_{sp} (- S) \qquad (1)$$

ϕ_{sp} is the spectrometer work function. In the case of non-conducting samples the additional term S has to be introduced to equation (1). It represents a correction for the binding energy shift to higher values caused by the build-up of positive charge in the specimen following photoelectron loss. Since the shift is unpredictable and varies from sample to sample corrections are carried out relative to a binding energy standard. The hydrocarbon signal arising either from carbon present in the sample or from adventitious hydrocarbon is often used for this purpose [18,19].

2.4.2 Surface sensitivity

Contrary to the fairly high penetration depth of the exciting x-radiation, the photoelectrons can travel only short distances in solid samples before losing part or all of their energy in inelastic scattering processes. Only electrons originating in the top few atomic layers of the solid can escape with their original kinetic energy and contribute to the photoelectron peak. Electrons from deeper layers contribute to the background after having suffered ineleastic collisions. This phenomenon is the reason for the surface sensitivity of the technique [20]. Inelastic scattering is dependent on the matrix through which the electrons travel and the kinetic energy of the electrons and can be described according to [21]:

$$I(x) = I_0 \, e^{- x / \cos\theta \times \lambda (Ek, Z)} \qquad (2)$$

where I_0 is the original photoelectron intensity, I(x) the intensity after travelling through a material of thickness x, θ the angle of emission with respect to the surface normal and λ the so called inelastic mean free path (IMFP), a material and energy dependent factor which describes the average distance that an electron can travel in a material before inelastic scattering takes place [22]. The dependence of the IMFP on

the kinetic energy has been empirically determined to show following proportionality for $E_{kin} > 50$ eV:

$$\lambda \sim (E_{kin})^{1/2} \qquad (3)$$

Theoretical calculations [23] suggested an energy dependence close to $(E_{kin})^{3/4}$. 95% of the intensity measured in a photoelectron peak is due to the contribution of electrons detached from within a distance of 3λ within the sample [21]. It can be seen from equation (3) that the sampled depth varies for photoelectrons detached from different energy levels of the same atom. Equation (2) on the other hand shows that the sampled depth of a particular core level varies with the angle of emission θ [24,25]. Both phenomena can be used for non-destructive depth profiling within the limits of a few monolayers [21].

2.4.3 Instrumentation

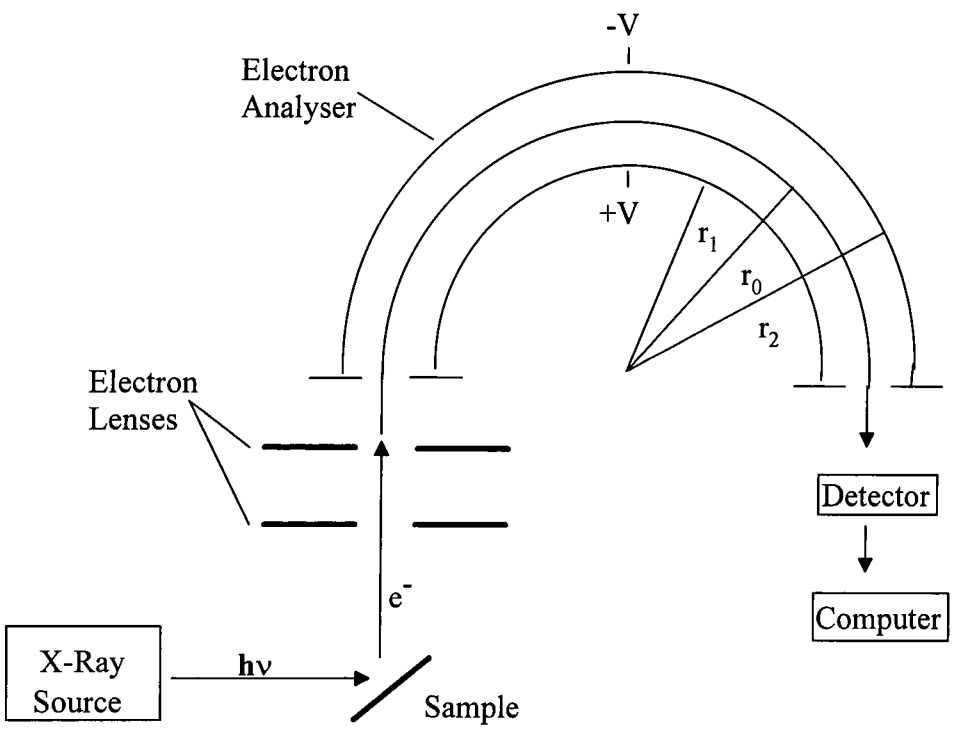

Fig. 2 Schematic of XPS set-up after [20] (UHV environment omitted for clarity)

Figure 2 shows the schematic set-up of a XPS instrument. The whole system is operated in an ultra high vacuum (UHV) environment in order to avoid surface contamination of the sample and energy loss of the photoelectrons by collisions with gas molecules on their way to the analyser [17,24,26,27]. The x-radiation is produced by the bombardment of the anode with thermally emitted electrons from a filament giving rise to a source spectrum in which the principal x-ray line appears together with less intense x-ray lines (satellites) on a broad continuum called Bremsstrahlung [17,24]. The choice of the anode material is guided by its stability under prolonged electron bombardment, its thermal conductivity which assures effective cooling and both the energy and the linewidth of its characteristic radiation. The energy of the characteristic radiation should be high enough to detach photoelectrons from most core levels in order to provide sufficient information and the linewidth of the characteristic radiation should be small because it contributes to the linewidth of the observed photoelectron peak. The most common anode materials which fulfil those criteria are Mg (1253.6 eV, FWHM: 0.7 eV) and Al (1486.6 eV; FWHM: 0.85eV) [21,28].

An aluminium window which attenuates the low energy Bremsstrahlung whilst transmitting the characteristic x-ray lines is placed between the source and the sample. Additionally, the window prevents the sample from being changed by stray electrons, heating effects and by any contamination originating in the source region [21,24,28].

Energy analysis of the emitted photoelectrons is achieved by an analyser. The most popular analyser type for XPS instruments is the Concentric Hemispherical Analyser (CHA) which consists of two hemispheres of radius r_1 and r_2 arranged in parallel. Electrons can enter and leave the analyser through input and exit slits of width w_1 and w_2. Application of a voltage to the plates results in the build-up of an electrical field in which the electrons are deflected. For a given voltage, only electrons with a certain energy content can travel through the analyser in a path close to the mean radius r_0 and pass the exit slit to reach an electron multiplier. The energy resolution of such a set-up can be described by the following equation [26]:

$$(\Delta E / E) = [(w_1+w_2)/2r_0] + \alpha^2$$

with α = angle at which the electrons enter the analyser with respect to the axis. It can be seen from the equation above that the resolution ΔE is improved if the electron energy E is low. Therefore, electrons are retarded prior to their entrance to the analyser. This is usually achieved by an electron optical lens. Its design depends on which of two possible recording modes is employed. In the first one, called Fixed or Constant Analyser Transmission (FAT/CAT) a scan is taken by varying the lens potential. At each step of the scan only electrons of a certain initial kinetic energy are focussed to the analyser which is held at one particular pass energy. In the second mode, Fixed or Constant Retard Ratio (FRR/CRR) the lens potential is fixed and therefore retards the incoming electrons by a certain percentage such that they are focussed to the analyser entrance with a spread of energy. Continuous variation of the analyser voltage allows the recording of a spectrum [17,24,26].

Energy resolution can be given in terms of absolute resolution ΔE and the relative resolution $\Delta E / E_0$ where ΔE is the full width at half maximum (FWHM) of the peak and E_0 is the kinetic energy at the peak position. The absolute resolution is therefore independent of the location of the peak in the spectrum whereas the relative resolution is always related to a particular kinetic energy. Spectra recorded in FAT mode have constant absolute resolution whereas those obtained in FRR mode have constant relative resolution [28].

2.4.4 Spectral Interpretation

2.4.4.1 Main features in the spectra

In an XPS spectrum, the photoelectron intensities or counts are plotted versus kinetic or binding energy [17]. For each element the principal x-ray line of the source produces a unique set of photoelectron signals with approximately constant line positions. The spectrum reflects the number and the approximate energy of the occupied orbitals in an atom under consideration [22,29]. Both loosely bound valence and tightly bound core electrons can be detached. Ionisation, however, can only occur in energy levels with a lower binding energy than the energy of the incident radiation [20]. The characteristic line positions are the basis for qualitative elemental analysis. All elements apart from hydrogen and helium can be detected [20].

Most of the photoelectron lines associated with one energy level appear as a doublet. This can be explained with the coupling of the spin angular momentum s of the unpaired electron left behind after electron removal from a completely filled orbital with the orbital angular momentum l to the total angular momentum j (j = l + s). Since there are two possible values for s (± ½), two values for j corresponding to two different energies are obtained in cases where l > 0 (p,d,f levels) [20,25,27]. Therefore, all levels except s-levels show a doublet structure. The relative intensities of the doublet components corresponds to the ratio of the degeneracies (2j + 1) of the states [25].

The linewidth of the photoelectron peak (expressed as FWHM) is determined by the width of the exciting x-ray line ΔE_p, the natural width of the core hole ΔE_n and the analyser resolution ΔE_a and can be expressed by the following equation [25]:

$$\Delta E = (\Delta E_n^{\,2} + \Delta E_p^{\,2} + \Delta E_a^{\,2})^{1/2}$$

ΔE_a is an instrumental constant when the analyser is operated in CAT mode but varies across the spectrum when FRR mode is employed. The natural line width of the core hole depends on the core hole's lifetime before it is filled in a relaxation process (see 2.3.4.3). This lifetime τ has no fixed value but is related to the energy by the uncertainty principle according to $\Delta E = h/\tau$ where h is Planck's constant [25].

2.4.4.2 Chemical shifts

Non-equivalent atoms of the same element in a solid give rise to core level peaks which differ in their binding energies. These variations in the binding energies are called chemical shifts. Atoms can be non-equivalent with respect to their chemical environment, their formal oxidation state or their lattice site. As a general rule, the BE of a particular core level increases with increasing oxidation state of the element under consideration. In cases where the formal oxidation state is the same the core level BEs of the central atom increase with the electronegativity of the attached groups or atoms [25]. The more electronegative substituents are attached to an atom under consideration the larger is the observed shift. Therefore, chemical shifts not only depend on the nature but also on the number of the substituents [30]. In a

simple model these shifts are ascribed to the electrostatic screening of the core electrons by the valence electrons which increases as a bond to electron withdrawing substituents is formed and decreases upon attachment of electron donating substituents. Photoelectron ejection is therefore hindered in the former case and requires more energy causing the signal to appear at high BE while the situation is opposite in the latter case. Strongly electronegative substituents cause secondary shifts in atoms adjacent to the primary shifted atom. Those are smaller than the primary shifts [22]. Chemical shifts therefore provide information about the chemical state(s) in which an element is present on a sample surface. The overall energy range covered by the shifts varies from element to element.

Core level shifts are not always very specific, that means, different groups give rise to a similar chemical shift. This may lead to broad unresolved signals especially in the case of multifunctional surfaces which in turn renders the identification of the chemical species difficult. To overcome those difficulties mathematical procedures have been developed to resolve the spectral envelopes into the individual contributions [27]. Another approach consists of the chemical derivatisation of functional groups on a sample surface prior to XPS measurements. A range of reagents can be employed to label the most common chemical functionalities. Most of them contain several halogen atoms per reacting molecule which allows a sensitive and unambiguous identification of a functional group [31].

2.4.4.3 Additional features in the spectra

In addition to the principal photoelectron lines a number of additional features can be observed in XPS spectra.

Apart from the principal x-ray line the weaker x-ray lines ("satellites") contained in the spectrum of an unmonochromatized source give rise to photoelectron peaks as well. Those *satellite lines* are separated from the main photoelectron peak by a characteristic amount of energy and their intensity corresponds to a defined fraction of the principal feature's intensity [20,24].

A de-excitation process following ionisation leads to the occurrence of *Auger peaks*. The core hole remaining in a sample atom after photoemission can be filled by an electron from a higher orbital. The excess energy can either be emitted as x-ray

fluorescence or be used to remove a second electron giving rise to a signal in the XP spectrum (Auger process). The two relaxation processes compete. In the case of K shell vacancies the preferred decay mechanism depends on the atomic number of the element. For heavier elements x-ray fluorescence is the major de-excitation route whereas lighter elements (especially those with atomic number <12) [29] tend to relax by the Auger process [27,29]. Irrespective of the atomic number of the element, the emission of an Auger electron is the preferred decay mechanism for vacancies in the L, M, N etc. shell [25].

Shake-up satellites are a result of a reorganisation process of the valence electrons during photoemission. While core level ionisation occurs there can be a simultaneous excitation of a valence electron to a higher unfilled energy level. The amount of energy required for this transition is not available for the core electron leaving the target atom resulting in a signal at the high binding energy side of the main photoelectron peak [25]. The spacing between main signal and satellite offers information about the valence energy states of the system under consideration [29]. Shake-up features are often observed in the spectra of transition element compounds and in some organic substances [29]. In the analysis of polymers they have a qualitative analytical importance because they generally appear in systems containing unsaturation but are especially pronounced in the C (1s) spectra of aromatic polymers. This allows saturated and unsaturated polymers which only contain carbon and hydrogen to be distinguished [31].

It is possible that the valence electron is completely removed during the reorganisation process. This process is referred to as *shake-off*. Unlike shake-up it does not lead to sharp features but to rarely discernible broad shoulders on the background on the high BE side of the parent photoelectron peak [25,29].

2.5 Quantification

The intensities of XPS signals can be used to derive quantitative information about a sample surface. A rigorous treatment shows that the peak intensity of a photoelectron signal is dependent on a multitude of factors some of which are instrument related while others are characteristic of the sample. Those factors are: the characteristic x-ray flux on the sample surface, the surface roughness, the

photoelectric cross-section for the ionisation of the respective core level by a photon of energy hν, the analyser transmission and detector efficiency for the photoelectron of E_{kin}, the asymmetry factor for emission from the particular core level at photon energy hν (this factor describes the dependency of the photoelectron cross-section on the relative directions of photon incidence and photoelectron emission [21]), the distribution of atoms of the type of interest in the matrix with depth z, the IMFP of the photoelectron from the particular element with E_{kin} in a matrix M and the angle of emission θ [32].

Practically, the use of sensitivity factors has proved to be a simple and useful approach for quantification although it involves crude assumptions. Sensitivity factors ensure the normalisation of core level intensities with respect to the intensity of a chosen reference level. The quantification is based on the comparison of the relative intensities thus obtained. Sensitivity factors can either be calculated theoretically from known values of the factors listed above or be experimentally determined by measuring appropriate standards. In the latter case the peak area obtained for a particular core level is related to the area of a reference core level contained in the same sample. The sensitivity factor is the number with which the peak area of the core level of interest has to be multiplied in order to obtain the correct stoichiometry with respect to the reference level area [17,21].

2.6 References

1) Colthup, N.B.; Daly, L.H.; Wiberley, S.E. *Introduction to Infrared and Raman Spectroscopy*, 3rd edition, Academic Press : Boston, 1990, p.2

2) Hesse, M.; Meyer, H.; Zeeh, B. *Spektroskopische Methoden in der Organischen Chemie, Thieme* : Stuttgart, 1987, pp.27-34

3) Silverstein, R.M.; Bassler, G.C.; Morrill, T.C. *Spectrometric Identification of Organic Compounds*, 5th edition, John Wiley : Chichester, 1991

4) Christen, H.R. *Grundlagen der Organischen Chemie*, Salle-Sauerländer, Frankfurt, 1985, pp.301-308

5) Siesler, H.W.; Holland-Moritz, K. *Infrared and Raman Spectroscopy of Polymers,* Marcel Dekker Inc. : NewYork, 1980, pp.118-126

6) Belton, P.S.; Wilson, R.H. in *Perspectives in Modern Chemical Spectroscopy*; Andrews, D.L. Ed.; Springer : Berlin, 1990, pp.77-80

7) Ingle, J.D.jr. ; Crouch, S.R. *Spectrochemical Analysis,* Prentice Hall : London, 1988, pp.432-434

8) Rivière, J.C. *Surface Analytical Techniques*, Clarendon Press : Oxford, 1990, pp.64-65

9) Beynon, J.H.; Brenton, A.G. *An Introduction to Mass Spectrometry*, University of Wales Press : Cardiff, 1982, pp.30-32

10) Litzow, M.R.; Spalding, T.R. *Mass Spectrometry of Inorganic and Organometallic Compounds*, Elsevier : Amsterdam, 1973, pp.13-14

11) Creaser, C.S.; Mellon, F.A. in: *Perspectives in Modern Chemical Spectroscopy*, Andrews, D.L., Ed., Springer : Berlin, 1990, pp.274-276

12) Litzow, Spalding, pp.4-6

13) Constantin, E.; Schnell, A. *Mass Spectrometry*, Ellis Horwood : New York, 1990, pp.4-6

14) Beynon, Brenton, pp.16-18

15) Constantin, Schnell, p.16

16) Litzow, Spalding, pp.24-25

17) Desimoni, E.; Zambonin, P.G. in: *Surface Characterisation of Advanced Polymers*, Sabbatini, L.; Zambonin, P.G., Eds.; VCH : Weinheim, 1993, pp.6-19

18) Johansson, G.; Hedman, J.; Berndtsson, A.; Klasson, M.; Nilsson, R. *J. El. Spectr. Rel. Phenom.* **1973**, *2*, 295

19) Barr, T.L.; Seal, S. *J.Vac. Sci. Technol.* **1995**, *A 13 (3)*, 1239

20) Brundle, C.R. in: *Encyclopedia of Materials Characterisation*; Brundle, C.R.; Evans, C.A. Jr.; Wilson, S., Eds.; Butterworth - Heinemann: Boston, 1992, pp.282-299

21) Christie, A.B. in: *Methods of Surface Analysis, Techniques and Applications*, Walls, J.M., Ed.; Cambridge University Press : Cambridge, 1989, pp.127-168

22) Smith, G.C. *Surface Analysis by Electron Spectroscopy - Measurement and Interpretation*, Plenum Press : NewYork, 1994, pp.3-14

23) Powell, C.J. *Surface Science* **1994,** *299/300*, 34

24) Rivière, *Surface Analytical Techniques*, pp.27-80

25) Briggs, D.; Rivière, J.C. in: *Practical Surface Analysis by Auger and X-Ray Photoelectron Spectroscopy*, Briggs, D.; Seah, M.P.,Eds.; John Wiley and Sons: Chichester, 1983, pp.87-139

26) Smith, pp.15-40

27) *Spectroscopy* Vol. 3, Straughan, B.P.; Walker, S., Eds.; Chapman and Hall : London, 1976, pp.240-296

28) Rivière, J.C. in: *Practical Surface Analysis by Auger and X-Ray Photoelectron Spectroscopy*, Briggs, D.; Seah, M.P.,Eds.; John Wiley and Sons: Chichester, 1983, pp.17-85

29) Baker, A.D.; Brundle, C.R. in: *Electron Spectroscopy: Theory, Techniques and Applications*, Vol. 1, Brundle, C.R.; Baker, A.D., Eds.; Academic Press : London, 1977, pp.2-73

30) Kloepffer, W. *Introduction to Polymer Spectroscopy, Polymers / Properties and Applications 7*, Springer Verlag : Heidelberg, 1984, pp.11-13

31) Briggs, D. in: *Practical Surface Analysis by Auger and X-Ray Photoelectron Spectroscopy*, Briggs, D.; Seah, M.P.,Eds.; John Wiley and Sons: Chichester, 1983, pp.358-396

32) Rivière, J.C., *Surface Analytical Techniques*, pp.274-278

Chapter 3:
Silent discharge oxidation of Poly (cyclohexylmethylsilane) and Poly (phenylmethylsilane) thin films

3.1 Introduction

Polysilanes are polymers in which organic substituents are attached to an inorganic linear backbone composed exclusively of silicon atoms. Since soluble polysilane homopolymers and copolymers have become available they were found to have interesting properties both from the theoretical and from the practical point of view [1,2]. Their general properties include inertness towards oxygen at normal temperatures, only mild susceptibility towards hydrolysis and good thermal stability [2,3]. In contrast, they show a high lability towards UV light as well as sensitivity towards electron beams, γ and x-radiation [4]. A summary about the photochemistry of polysilanes will be given in chapter 4.2.

Depending on their particular properties polysilanes find practical use as radical initiators for organic polymerisation reactions, resist and contrast enhancement materials for the microelectronics industry, nonlinear optical materials, charge conductors, photoconductors and precursors for silicon carbide ceramics [2,4,5].

In the present chapter the reaction behaviour of two model polysilanes in an atmospheric pressure air plasma will be investigated.

3.2 Background

Reports about air plasma treatments of polysilanes are not known. The studies on polysilane behaviour in pure oxygen plasmas described in the following paragraphs are the most closely related investigations.

Contrary to carbon based materials which are continuously attacked and finally form volatile products upon exposure to an oxygen plasma, organosilicon polymers form an involatile silicon dioxide-like "SiO_x" layer [6]. It is inert against chemical etching and can only be eroded by physical sputtering. Once this layer is formed it protects any underlying material from being etched [6]. The formation of the layer is independent of whether the silicon atoms are integrated into the polymer

backbone or present in the pendant groups [7]. A minimum silicon percentage is, however, required in order to obtain a continuous coating [8], a silicon content of 8-10 weight % in a polymer is regarded to be adequate for the formation of a suitable layer [9]. The formation mechanism of SiO_x layers is not understood so far [10]. As could be expected the treatment of polysilanes in low pressure oxygen plasmas has been reported to result in the formation of a SiO_x layer [1,2,4,9,11,12]. The plasmas were operated under RIE (Reactive Ion Etching) conditions.

Depending on the operating conditions an oxygen plasma has different characteristics and involves different etch mechanisms. Pressures lower than 100 mtorr, typically even below 20 mtorr [10] are representative for Reactive Ion Etching (RIE) conditions. In this case chemical etching by the activated species generated in the plasma and physical sputtering of high energy ions occur simultaneously enhanced by the synergistic effect between these two factors [10,13]. While chemical etching is an isotropic process, sputtering introduces a directional component to the process. The low pressures are required for the ions to gain sufficient energy while passing through the high potential of the plasma sheath without colliding with other gas particles. Such ions strike the surface with normal incidence and cause a material removal in vertical direction. At higher pressures ion bombardment is less important and chemical etching prevails.

Oxygen plasmas operated under RIE conditions are employed for pattern transfer in multilayer lithography. Polysilanes are especially suited for a positive bilayer process because they combine two advantageous properties - photosensitivity and etch resistance [4,11]. In the process a thin layer of polysilane is spincoated on top of a thick carbon based planarizing layer which in turn covers the substrate. Irradiation, mostly through a mask, causes chain scission of the polysilane in the exposed areas. The low M_w material thus formed can either be washed away with a suitable solvent in a wet development step or in some cases be directly volatilized using the appropriate polymer and irradiation conditions. In the RIE step the exposed carbon containing material is transformed into volatile compounds. Ion bombardment supports the product desorption in vertical direction and ensures the undistorted replication of the pattern into the substrate. At the same time the polysilane left on the surface forms a SiO_x layer, the etch rate of which is

considerably smaller than that of the planarizing layer. This etch resistant layer prevents the covered carbon material from being removed.

Since the interest of the studies was focussed on the suitability of polysilanes for a bilayer process, the experiments were mostly evaluated using the SEM data of the patterns obtained. Miller et al. [9] report qualitative results of the XPS analysis of the oxidised surface of poly (di-n-pentylsilane). Apart from a significant decrease in the C (1s) signal intensity and a corresponding increase in the O (1s) signal intensity the Si (2s) environment of those films appeared shifted towards higher binding energy by about 3 eV.

A detailed investigation on the oxidation of poly (cyclohexylmethylsilane) and poly (phenylmethylsilane) in a rf oxygen glow discharge at varying discharge powers was reported [12]. A plateau in the elemental concentrations was reached already at powers lower than 5 W. The aromatic polysilane reached its limiting elemental percentages at lower discharge powers and was oxidized to a lower degree compared to the aliphatic polymer. Depth profiling of treated films with Ar^+ ions revealed that the aromatic polysilane forms a thicker oxidized layer than the aliphatic polysilane. This finding was further supported by the appearance of siloxane species in the FTIR spectra of treated poly (phenylmethylsilane) films while in the case of poly (cyclohexylmethylsilane) no difference in the corresponding spectra of treated and untreated polymer samples was found [12].

In the following chapter the susceptibility of an aromatic substituted and an aliphatic substituted polysilane towards oxidation in a silent discharge operated in air is investigated. The properties of this type of atmospheric pressure discharge have already been described in chapter 1.4. The structures of the two model polymers chosen for the study, poly (cyclohexylmethylsilane), PCHMS, and poly (phenylmethylsilane), PPMS, are given in figure 1. Both polysilanes are structurally identical apart from the former containing a saturated 6-membered ring whereas the latter has a phenyl substituent. Studying the two polymers therefore allows the influence of the polymeric structure in the reactions to be compared and contrasted. It has been pointed out that the silicon content is the determining property governing SiO_x build-up in oxygen plasmas under RIE conditions whereas the polymer structure is irrelevant. The structure of the polymer to be etched is thought to gain more

importance at higher pressures [7]. Differences in the reaction behaviour of the two model polysilanes can therefore be expected.

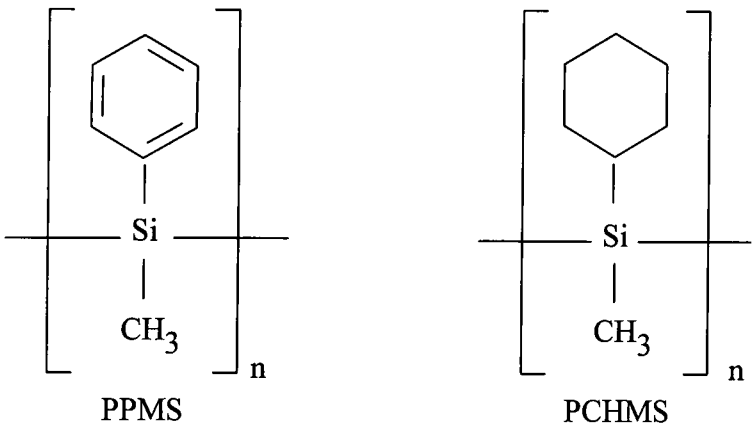

Fig. 1 Structures of the two model polysilanes

Modified films were analyzed immediately after silent discharge treatment by X-Ray Photoelectron Spectroscopy (XPS) as well as by Transmission and Attenuated Total Reflection (ATR) Infrared Spectroscopy.

3.3 Experimental

3.3.1 Silent discharge set-up

The silent discharge treatment of the samples was carried out in a dielectric barrier discharge cell a schematic of which is shown in figure 2. In the present study it was operated at 3 kHz and 7.7 kV with an electrode gap of 3 ± 0.05 mm. A double layer of polyethylene served as the dielectric material to cover the lower electrode. Both electrodes were made of aluminium (top diameter 4.5 cm, bottom diameter 3.5 cm). They were chemically polished and then degreased using isopropanol prior to use.

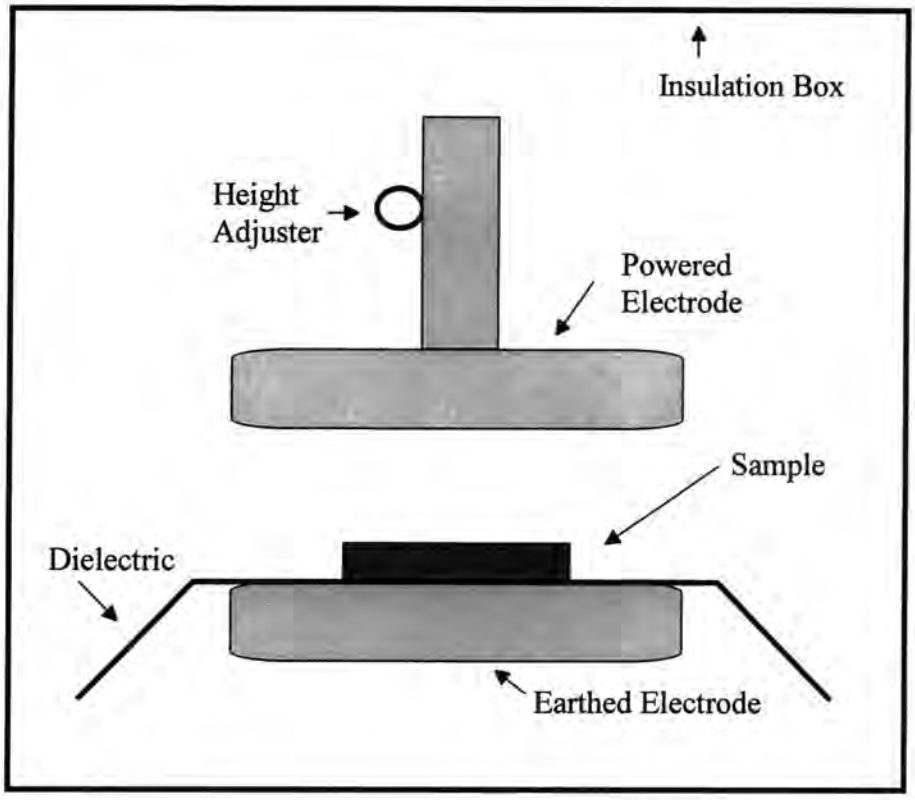

Fig. 2 Schematic of the silent discharge set-up

PCHMS and PPMS (ABCR) films were spincoated onto PET substrates (12μm PET, Hoechst) from 2% weight per volume solutions in toluene. The samples were then placed on the dielectric and treated for treatment times varying between 5 and 120 seconds. The discharge in the gap appeared as a homogeneous, faint purple glow.

3.3.2 Analysis

X-Ray photoelectron spectroscopy (XPS) characterization was carried out on a Kratos ES300 X-ray Photoelectron Spectrometer equipped with an unmonochromatized Mg K_α X-Ray source and a cylindric hemispherical analyzer (CHA) operating in the fixed retarding ratio (FRR, 22:1) mode. Photo-emitted electrons were collected at a take-off angle of 30° from the substrate normal. Data accumulation and analysis were carried out employing in-house software. All

binding energies were referenced to the adventitious hydrocarbon component [14] the binding energy of which was taken to be 285.0 eV [15].

For the measurements the samples were mounted on a degreased stainless steel sample holder using double sided sticky tape. The probe to which the sample holder was attached was wiped with isopropanol prior to insertion into the spectrometer. Instrumentally determined sensitivity factors for unit stoichiometry were taken as being C (1s) : Si (2p) : O (1s) = 1 : 1.02 : 0.62.

Infrared spectra were collected on a FTIR Mattson Polaris instrument. Thin polysilane films were spin coated from 2% weight per volume solutions in toluene either onto KBr discs (transmission measurements) or onto strips of polyethylene film (ATR measurements). Both types of samples were exposed to the silent discharge for 30 seconds. After the treatment the ATR samples were mounted into a KRS-5 crystal sample holder. An incident beam angle of 45° was used which resulted in 14 internal reflections. Typically, 100 scans were acquired at a resolution of 4 cm^{-1}.

3.4 Results

3.4.1 XPS

Within the limits of the instrument's sensitivity no other elements than silicon, oxygen and carbon could be detected either in treated or untreated films. Since XPS excludes any hydrogen content analysis [16] both polysilanes give rise to identical stoichiometries in the untreated coating, table 1.

	%C	%Si	%O
Theoretical PPMS / PCHMS	87.5%	12.5%	0%
Experimental PPMS	85.2 ± 0.6%	13.3 ± 0.4%	1.6 ± 0.3%
Experimental PCHMS	85.6 ± 0.3%	12.6 ± 0.2%	1.8 ± 0.3%

Tab. 1 Elemental composition of the untreated PPMS and PCHMS films

In both untreated polysilanes shown in figures 3 and 4 the main C (1s) peak is centred at a binding energy of 285.0 eV and can be assigned to C-H, C-C and C-Si environments [17,18]. In the case of PPMS, an additional C (1s) component around 291.9 eV having an area of 6.1 ± 0.6 % of the main C (1s) peak and exhibiting a Gaussian profile of different FWHM can be observed. This feature can be attributed to π-π^* shake-up transitions accompanying core level ionization of the aromatic rings [19]. The predominant type of Si (2p) core level environment appears at 100.4 eV for PCHMS and at 100.6 eV for PPMS, which is characteristic of the $-[(R^1)Si(R^2)]_n-$ structure [20], figures 5 and 6. A shoulder at 102.1 eV in the case of PCHMS and at 102.5 eV in the case of PPMS is discernible (about 12% of total Si (2p) peak area), which can be attributed to siloxane moieties. These can originate from the polysilane production process by Wurtz Coupling [21] or slight surface oxidation of the films during their preparation. The binding energy of the corresponding O (1s) signal located at 532.8 eV for PPMS and 532.5 eV for PCHMS supports the assumption of the presence of siloxane linkages, figures 7 and 8.

The change of elemental composition of the PPMS and PCHMS films as a function of exposure time to the silent discharge is shown in figures 9 and 10. It can be seen that oxygen is incorporated into the sample surfaces. At the same time, the silicon content increases while the carbon content decreases suggesting that a SiO_x layer is built up on the sample surfaces. The treatment very rapidly reaches the depths accessible by XPS; a plateau in the respective elemental concentrations is reached after approximately 60 seconds. The aromatic polysilane oxidizes at a faster rate to yield a higher silicon content at the surface compared to its aliphatic counterpart. Table 2 compares the elemental compositions of both polymers at the maximum treatment time of the present study, 120 seconds.

	% C	% Si	% O
treated PPMS	19.8 ± 1.7 %	21.7 ± 1.0%	58.4 ± 1.3%
treated PCHMS	25.6 ± 1.0 %	18.1 ± 1.0 %	56.2 ± 0.4 %

Tab. 2 Elemental composition of PPMS and PCHMS films after 120s silent discharge treatment

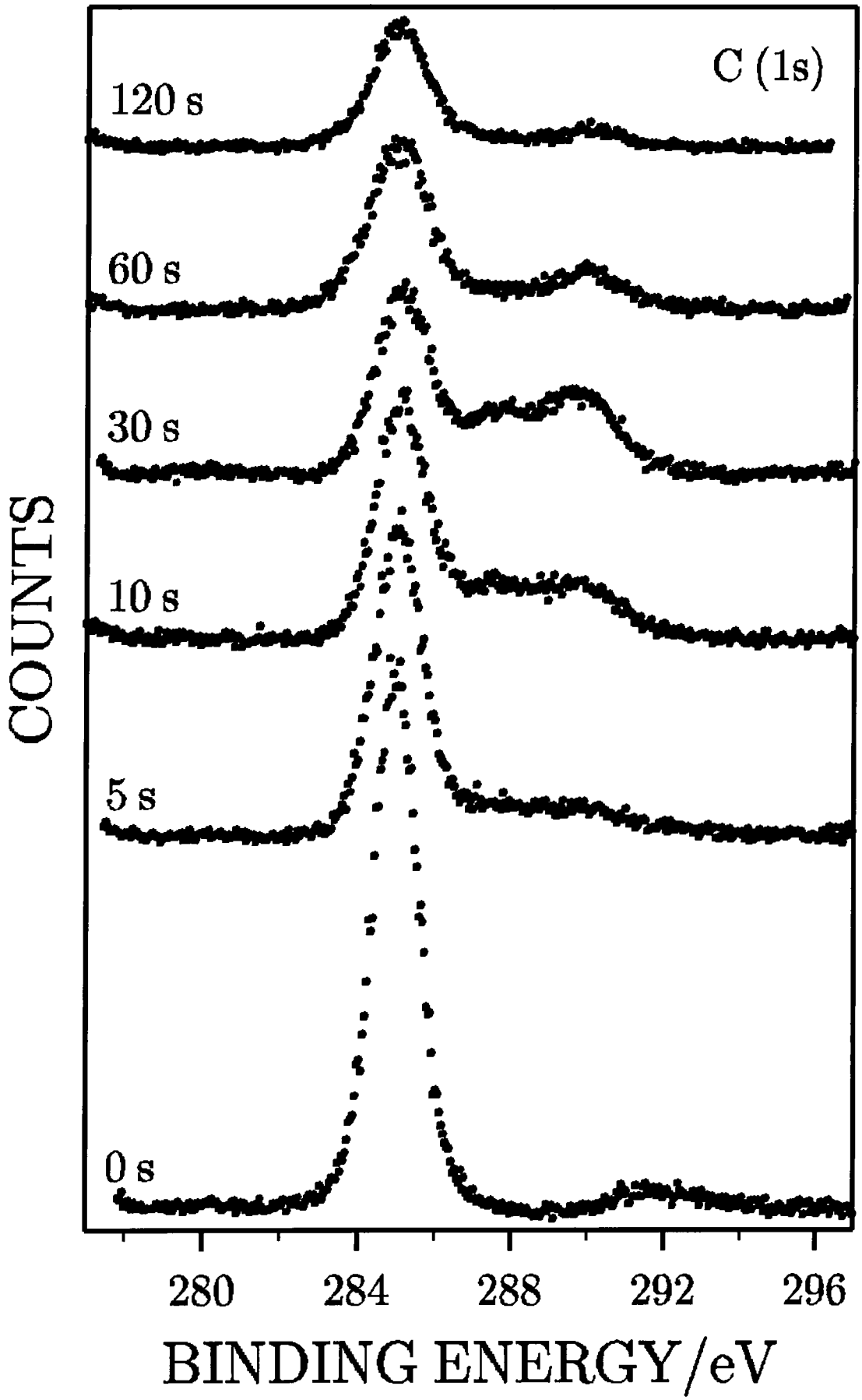

Fig. 3 C (1s) XP spectra of PPMS films as a function of silent discharge treatment time

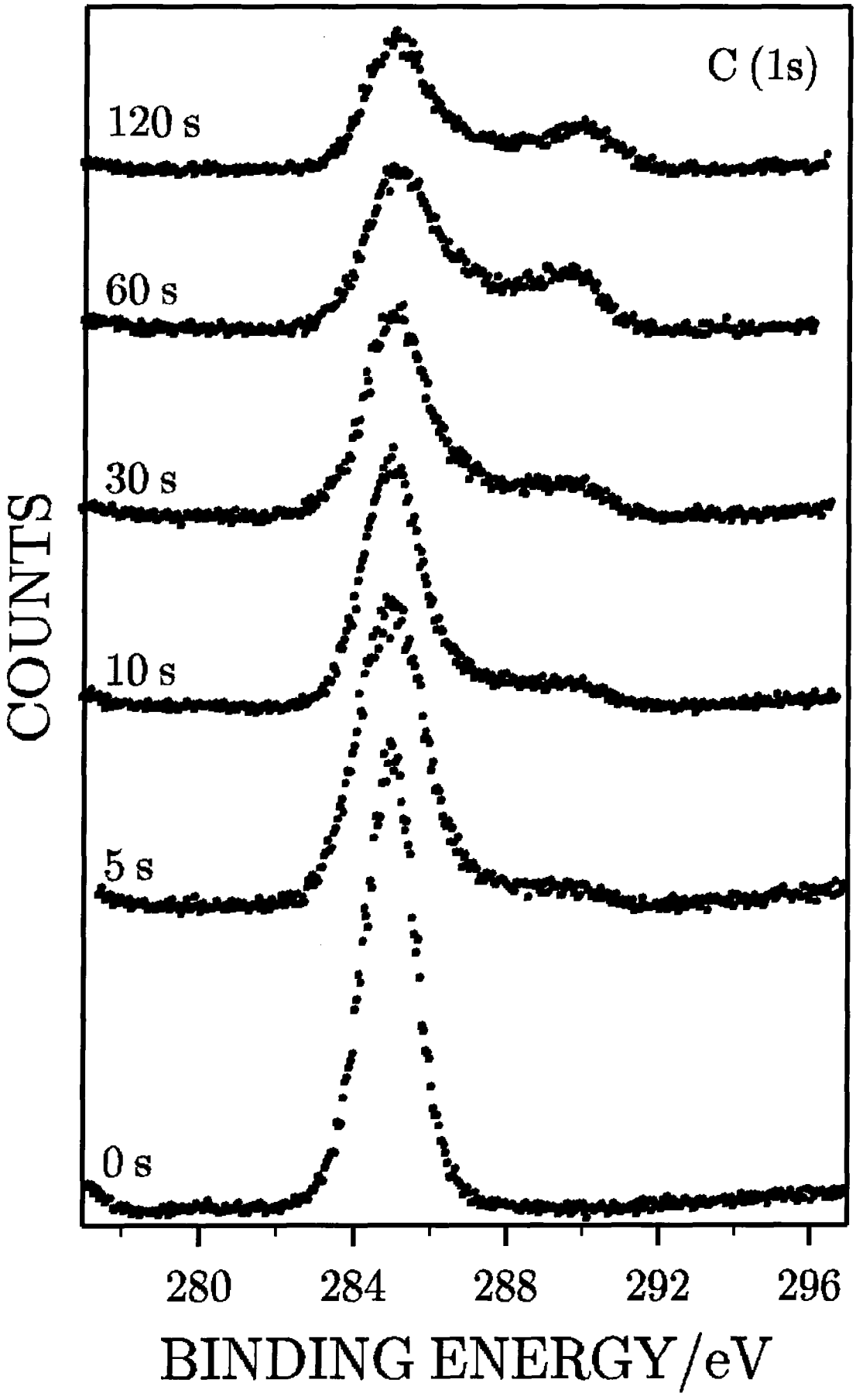

Fig. 4 C (1s) XP spectra of PCHMS films as a function of silent discharge treatment time

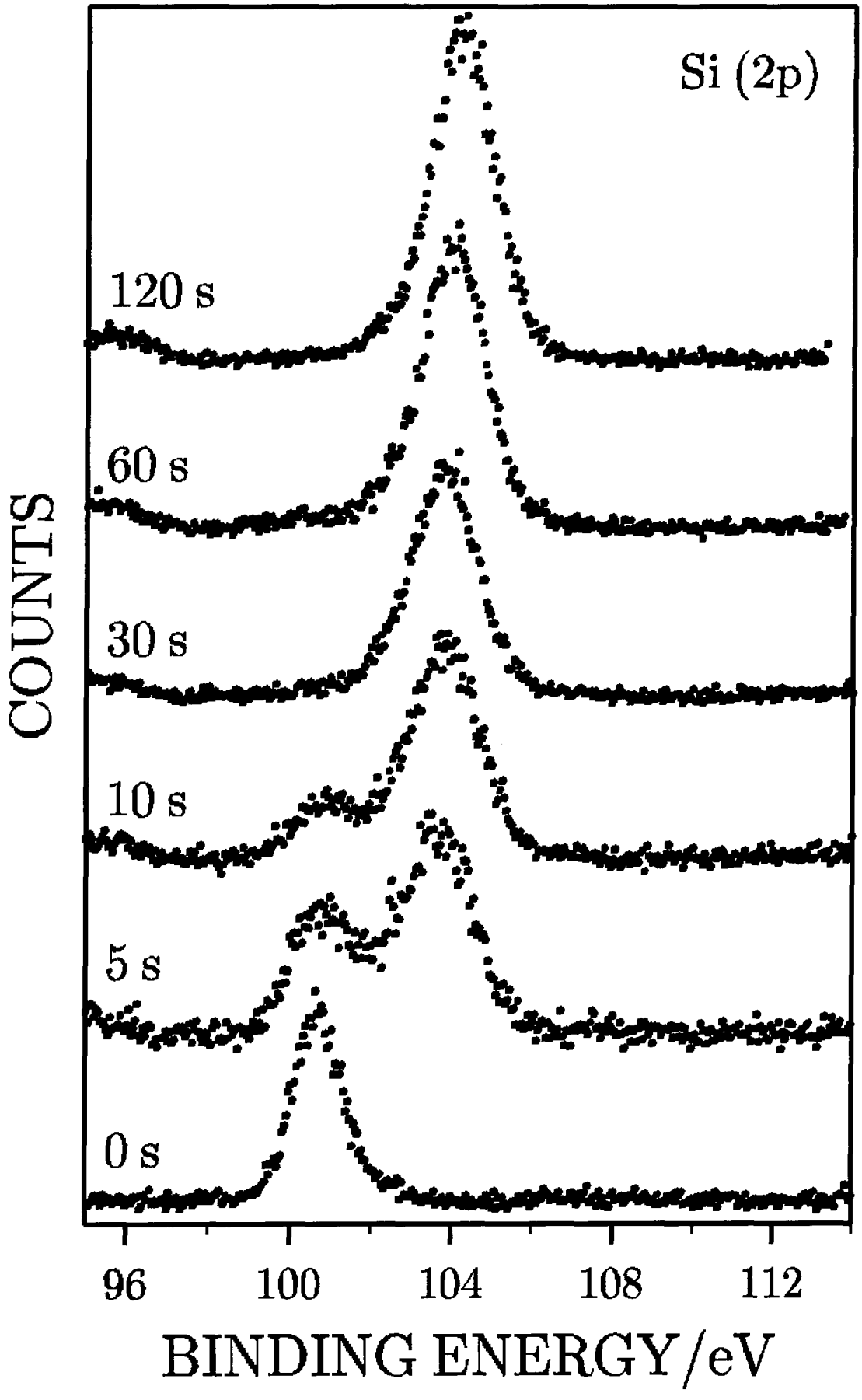

Fig. 5 Si (2p) XP spectra of PPMS films as a function of silent discharge treatment time

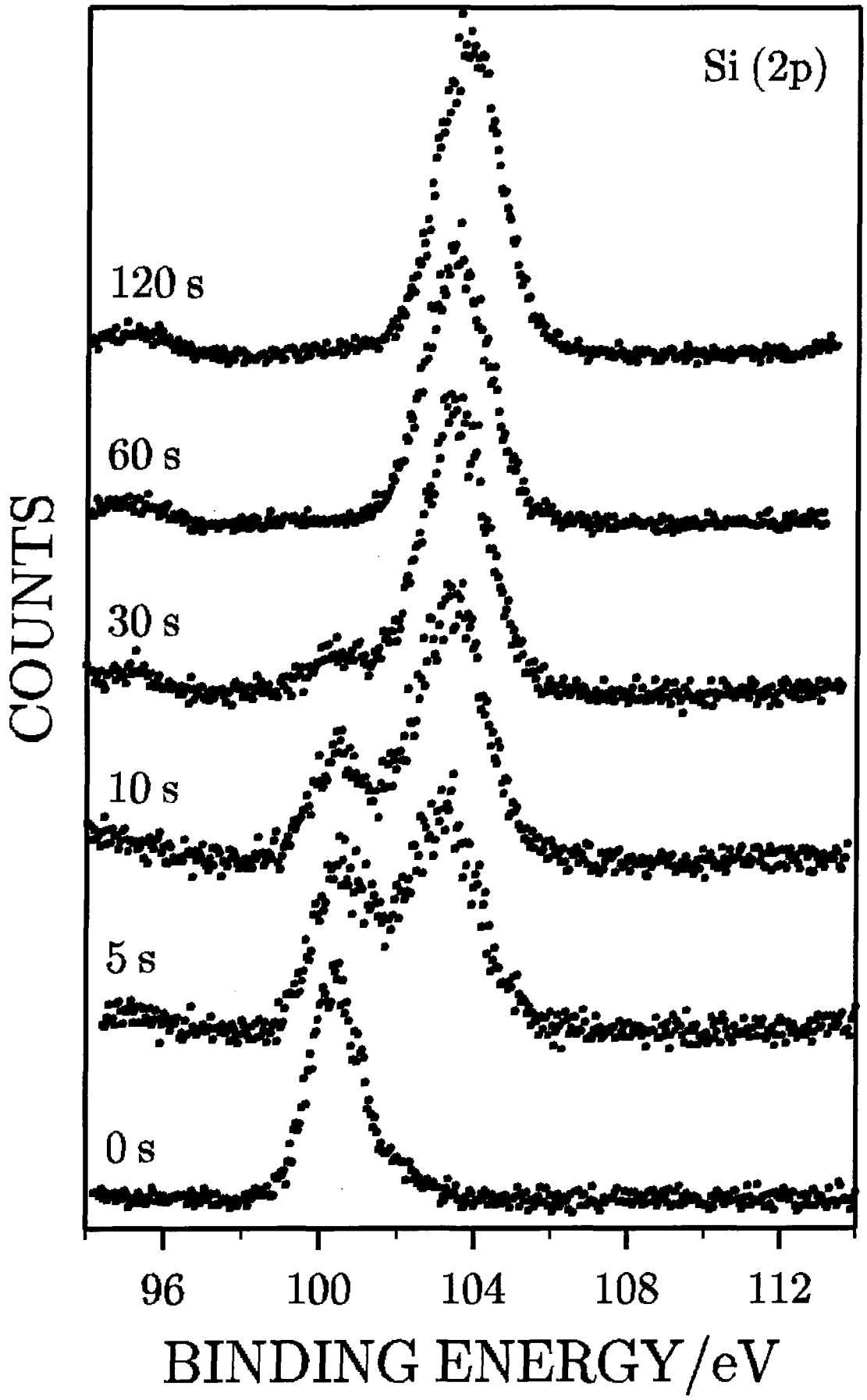

Fig. 6 Si (2p) XP spectra of PCHMS films as a function of silent discharge treatment time

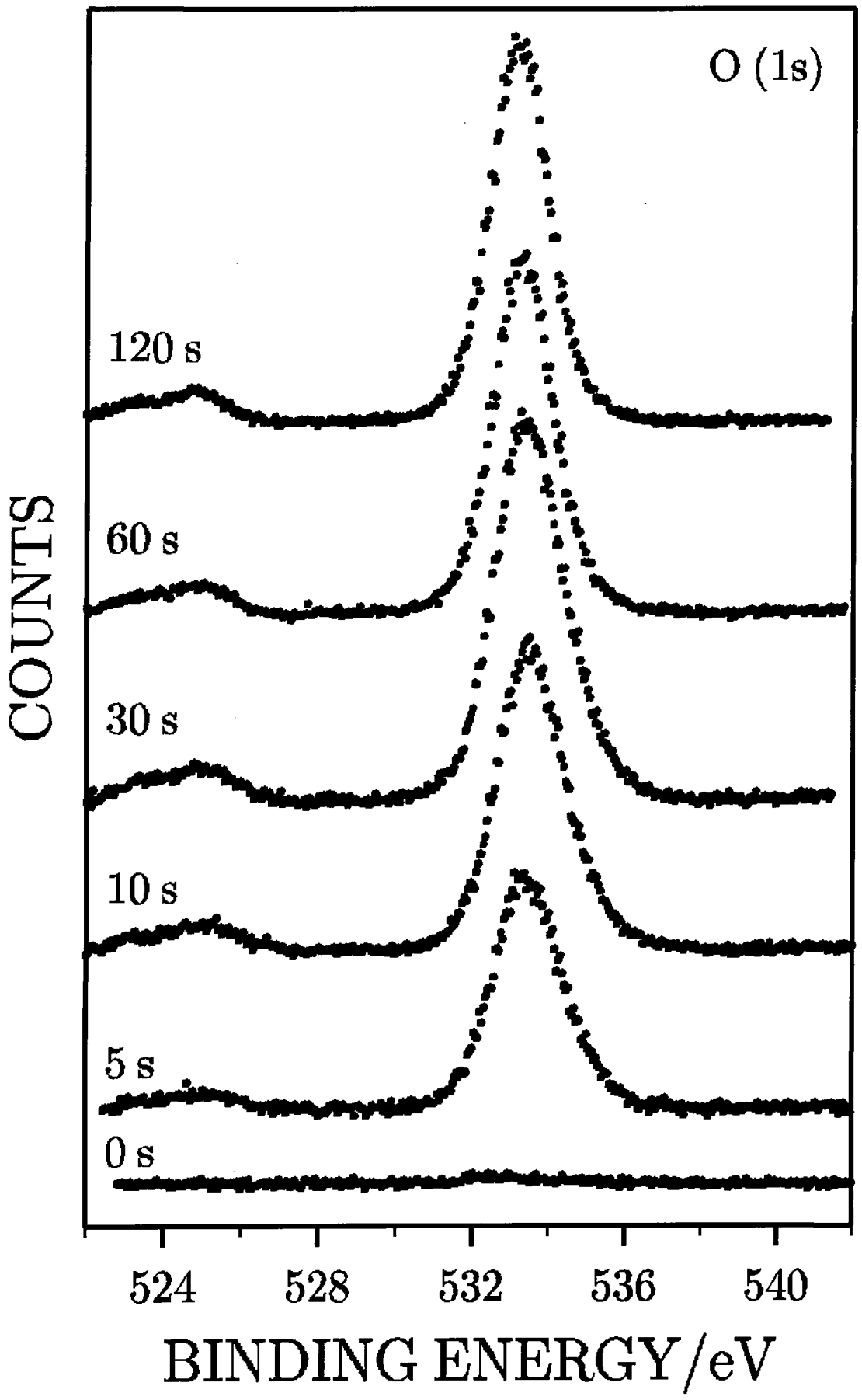

Fig. 7 O (1s) XP spectra of PPMS films as a function of silent discharge treatment time

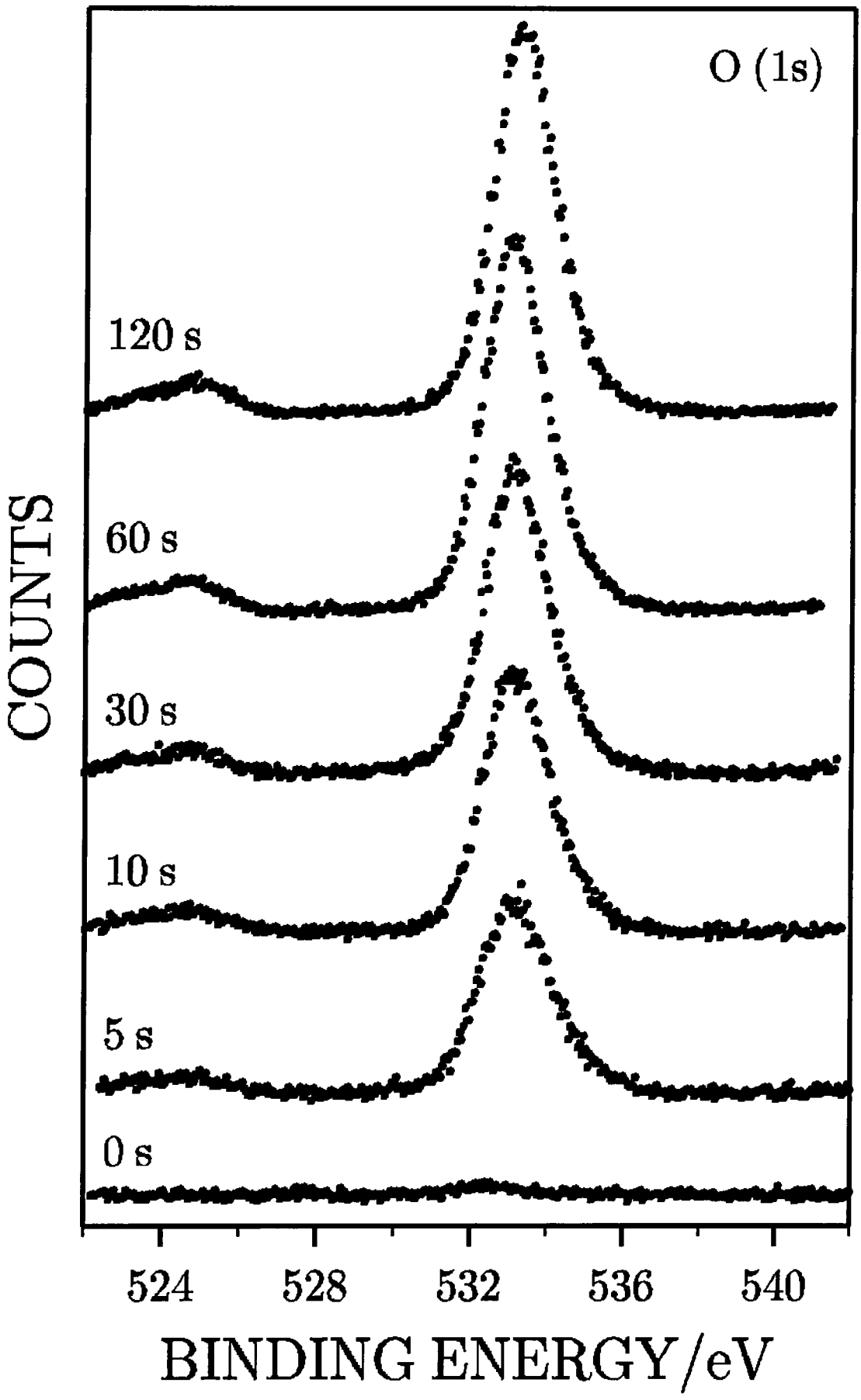

Fig. 8 O (1s) XP spectra of PCHMS films as a function of silent discharge treatment time

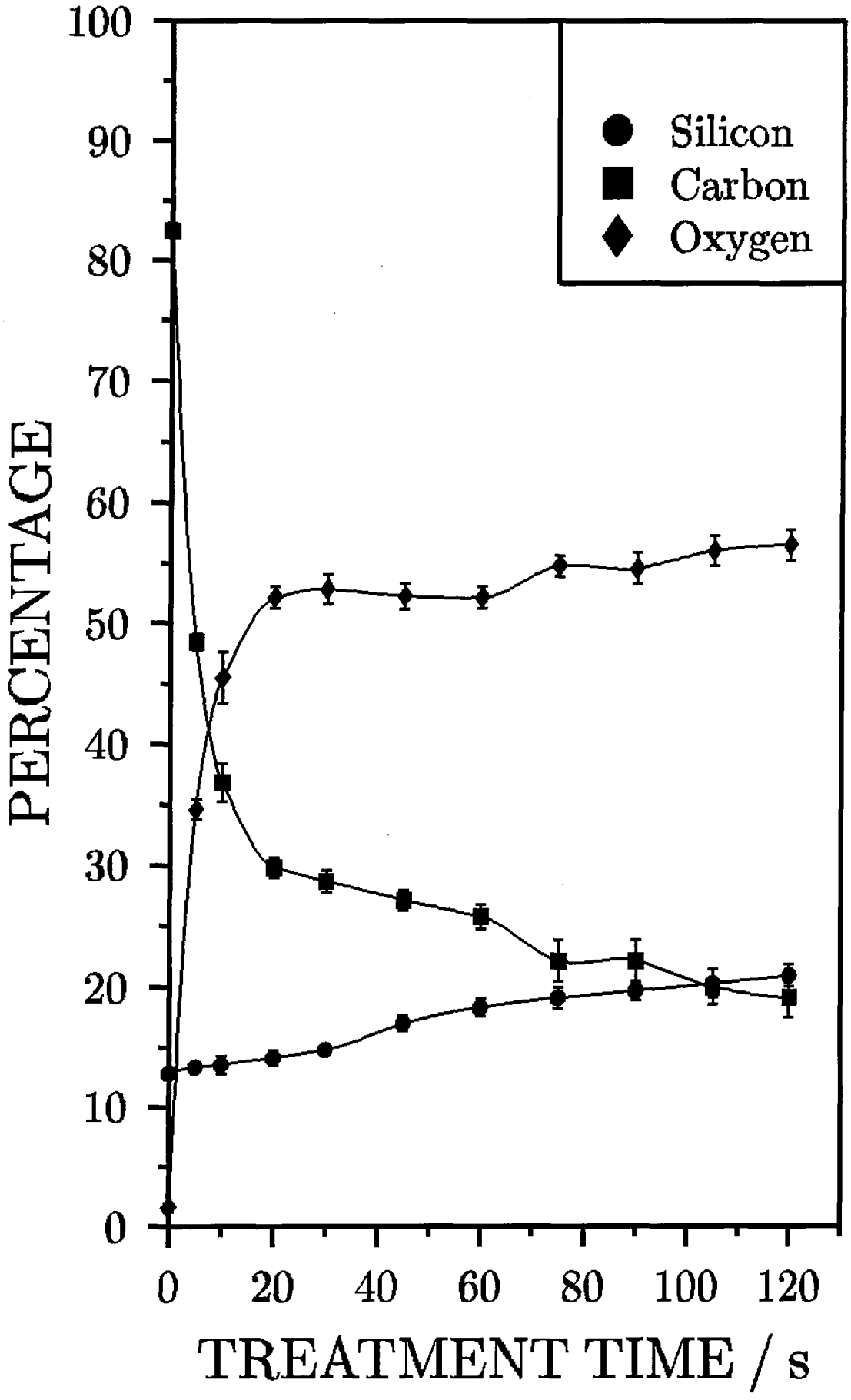

Fig. 9 Elemental composition of PPMS films as a function of silent discharge treatment time

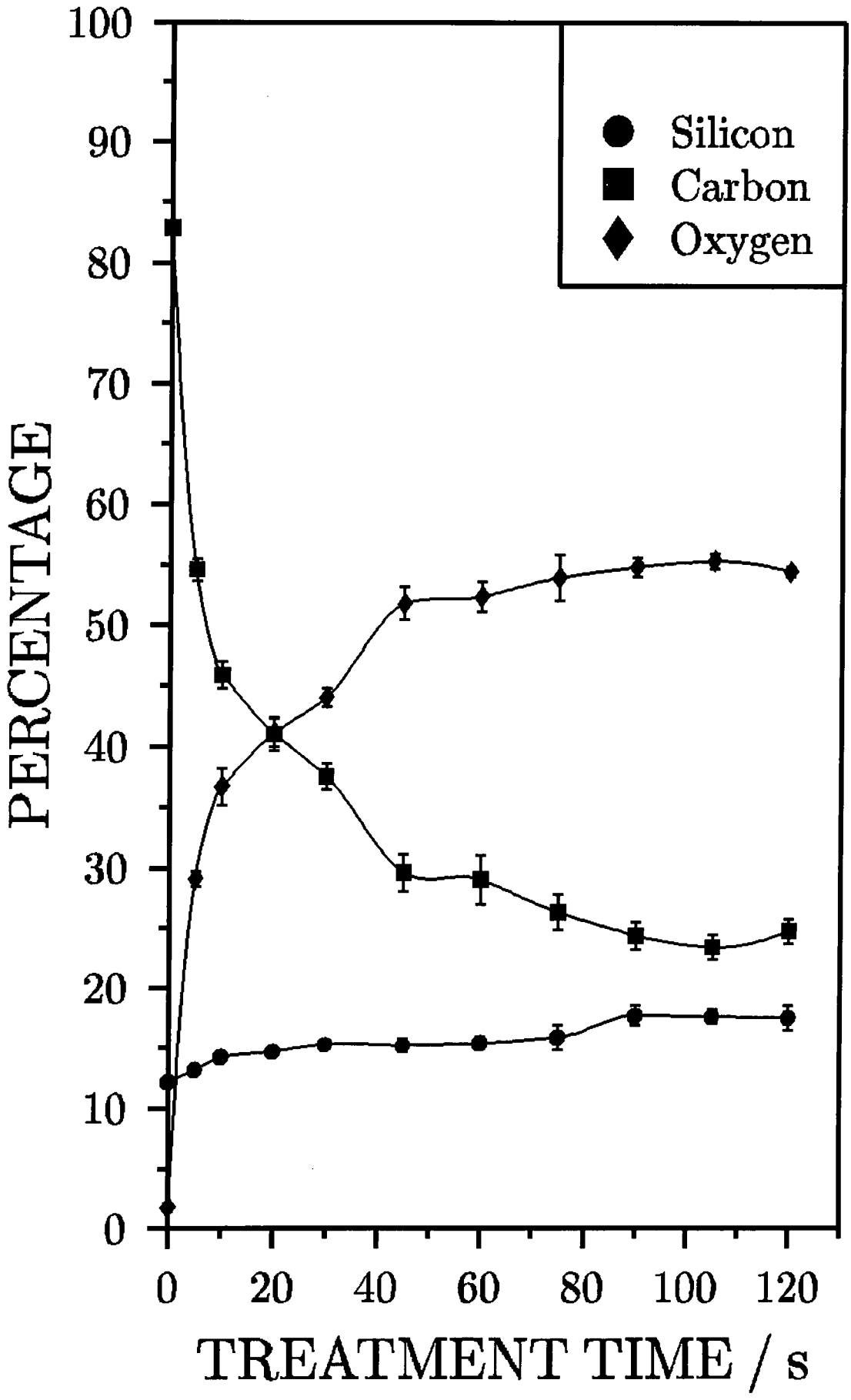

Fig. 10 Elemental composition of PCHMS films as a function of silent discharge treatment time

The envelopes of the spectra of the elements (figures 3-8) provide more details about the chemical changes occurring during the silent discharge treatment. Attenuation in the C (1s) peak is observed in conjunction with the emergence of an oxidized component at higher binding energy, which can be taken as a convolution of >C-CO_2- (285.7 eV), >C-O- (286.6 eV), >C=O / -O-C-O- (287.9 eV), -O-C=O (289.0 eV), and -O-CO-O- (290.4 eV) functionalities [22]. This oxidized shoulder passes through a maximum at 30s treatment time for PPMS. Since the aliphatic polymer does not show this behaviour the maximum in the oxidized components could be due to reactions of the aromatic rings. A possible explanation could be the initial formation of an aromatic ozonide [23] followed by subsequent further oxidation.

At the same time the Si (2p) peak gains intensity and shifts by approximately 3.4 eV for PCHMS and 3.5 eV for PPMS towards higher binding energy. The shift reflects the transition of the Si atoms into a new chemical environment, the Si (2p) binding energy of which corresponds well to those reported for SiO_2 and SiO_x thin films [24-26]. The shape of the silicon envelope of the aromatic polysilane changes more quickly than that of its aliphatic counterpart signifying faster oxidation.

The binding energy of the O (1s) signal in the treated samples is centred at about 533.3 eV in agreement with the BEs of oxygen in SiO_2 [24,25] and remains nearly constant with increasing treatment time. A simultaneous reduction in FWHM signifies, however, that the oxygen environments are becoming more homogeneous. This observation holds for both polymers.

3.4.2 Infrared Spectra

In figure 11 the ATR-IR spectra of untreated and 30 s silent discharge treated PPMS are compared. Figure 12 shows the corresponding spectra of PCHMS films. Since changes upon treatment are observed at lower wavenumbers only the wavelength region beween 400 and 2500 cm^{-1} is shown in the figures for reasons of clarity. The absorbances of the polymers at the higher wavenumbers are, however, included in tables 3, 4 and 5. Apart from being surface sensitive, the ATR technique was chosen because an additional, intense signal at about 1370 cm^{-1} appeared in the transmission IR spectra of silent discharge treated polysilane samples spin coated onto a KBr disc. This absorbance is not related to a modification of the polysilane

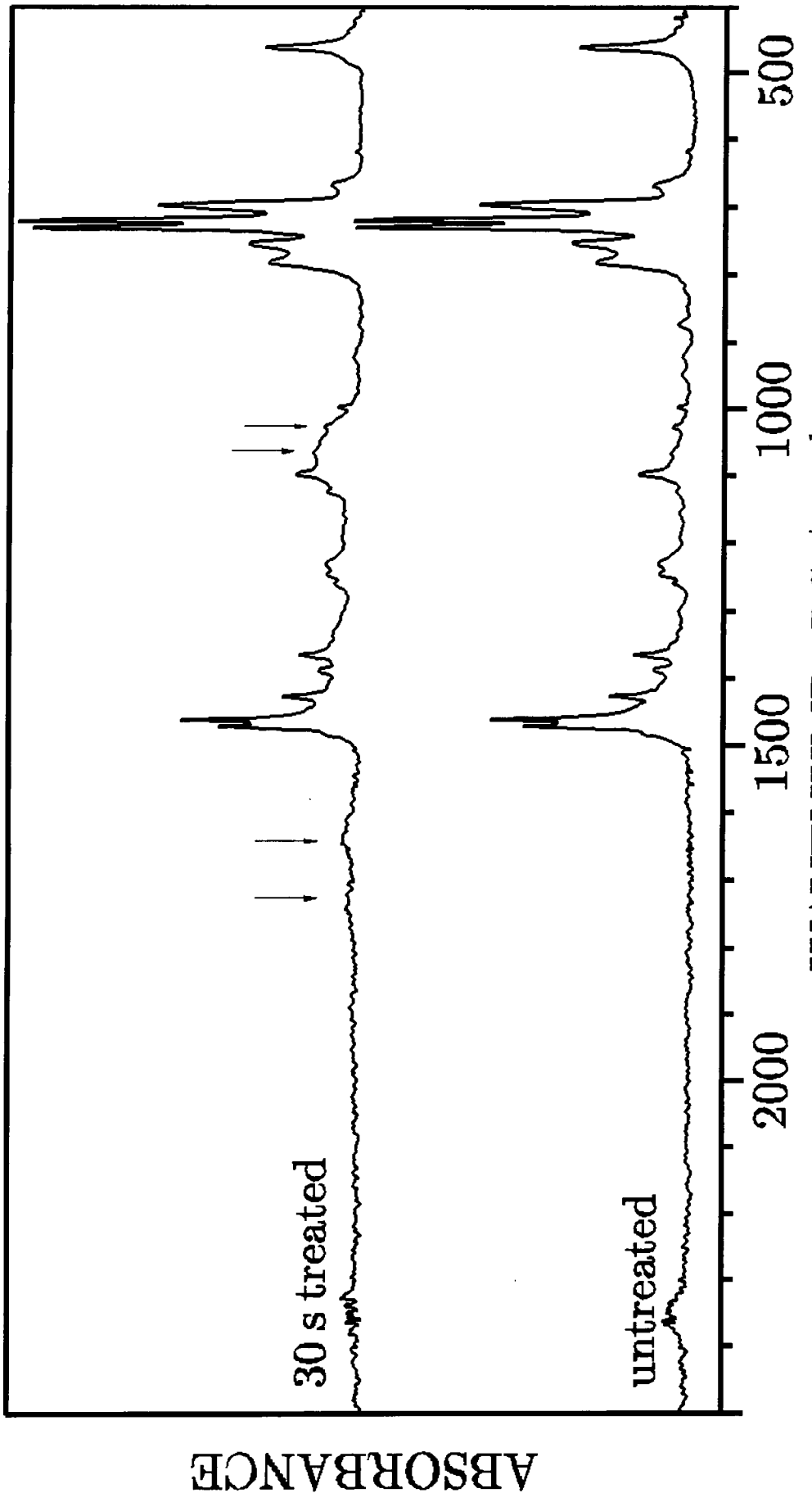

Fig. 11 ATR-IR spectra of untreated (bottom) and 30 seconds silent discharge treated (top) PPMS films

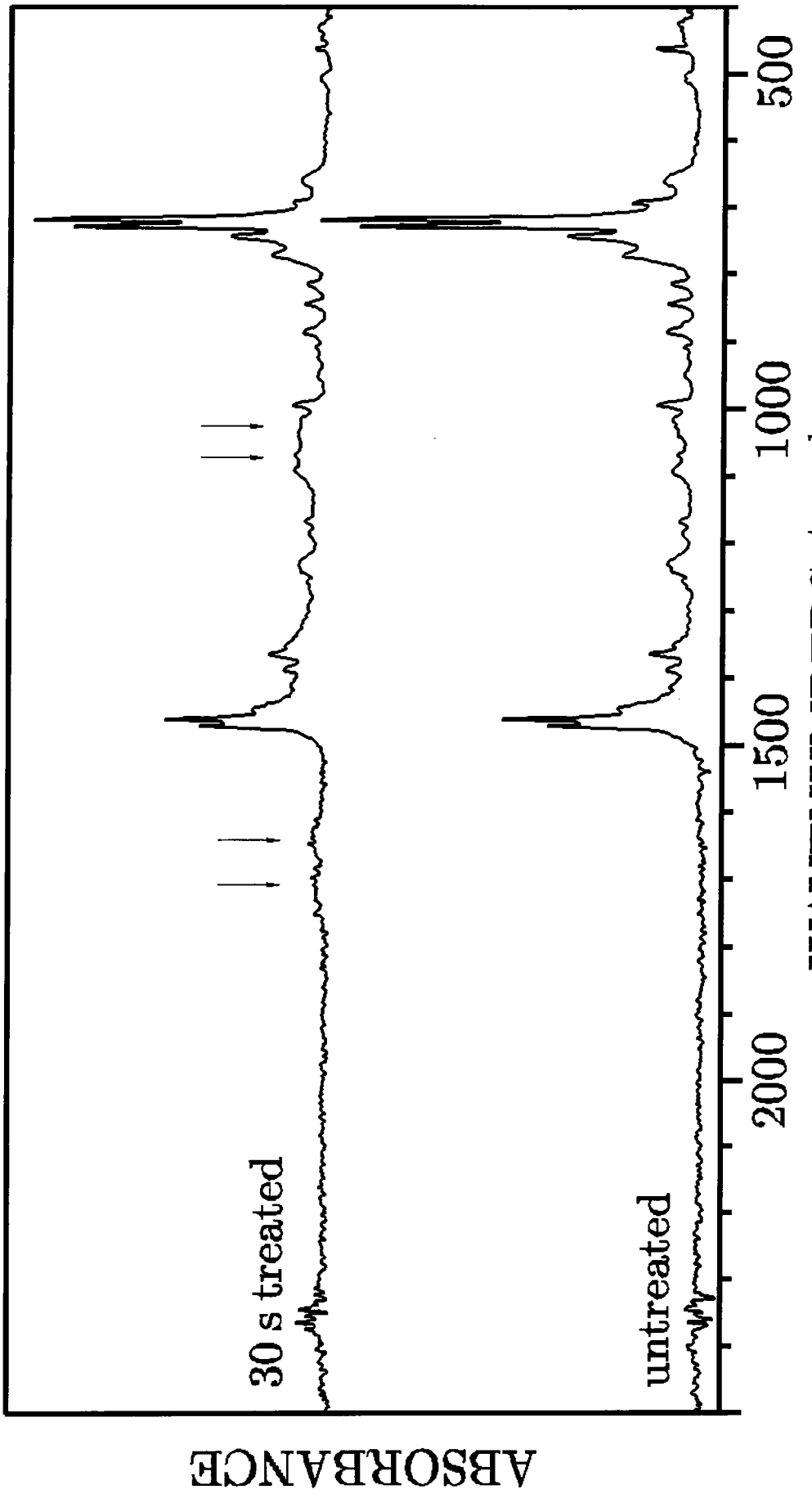

Fig. 12 ATR-IR spectra of untreated (bottom) and 30 seconds silent discharge treated (top) PCHMS films

but is due to a nitrate species formed as the product in the reaction of the KBr disc with the nitrogen containing gaseous components generated in the silent discharge. This and other reactions of alkali halide discs in silent discharges will be described in detail in chapter 5.

The ATR-IR spectra of both polysilanes contain contributions from the underlying polyethylene substrate [27,28] which are summarized in table 3. This is a result of the greater sampling depth of the ATR method compared to XPS [29,30]. The absorbances of untreated PPMS [31,32] and PCHMS [33,34] are compiled in tables 4 and 5.

Frequency [cm^{-1}]	Assignment
2916.6	CH_2 asymmetric stretching
2849.0	CH_2 symmetric stretching
1474 / 1464	CH_2 bending
1365	CH_2 wagging
731 / 719	CH_2 rocking

Tab. 3 Important absorbances of Polyethylene [27,28]

Frequency [cm^{-1}]	Assignment
3067, 3048, 3024, 3011	aromatic C-H stretches
2958	asymmetric stretch in Si-CH_3
2895	symmetric stretch in Si-CH_3
1426	C-C- ring stretch and C-H bending
1246	CH_3 bending in Si-CH_3
1098	in plane deformation of the ring and Si-C stretch
781	CH_3 rocking in Si-CH_3
754	out of plane bending of the ring C-H bonds
696	ring C-C bending
669	Si-C stretching
463	out of plane C-C ring bending

Tab. 4 Characteristic IR signals of PPMS [31,32]

Frequency [cm^{-1}]	Assignment
2921	asymmetric CH_2 stretching
2846	symmetric CH_2 stretching
1447	CH_2 bending
1244	CH_3 bending in Si-CH_3
995	C-C stretching
771	C-C rocking in Si-CH_3
745	CH_2 rocking
694	asymmetric Si-C stretching
662	symmetric Si-C stretching

Tab. 5 Characteristic IR signals of PCHMS [33,34]

Silent discharge treatment of PPMS samples caused an enhancement in the absorbances between 999 and 1067 cm^{-1} whereas the treatment of PCHMS produced an increase in signal intensity in the 1017- 1094 cm^{-1} region. These signals can be attributed to Si-O-Si stretches in siloxanes and / or Si-O-R (aliphatic) stretches [34]. Furthermore, the absorbances in this wavenumber range correspond to those reported for the structural components (certain types of rings or molecular complexes) in substoichiometric SiO_x films [35]. Weak absorbances at 1728 cm^{-1} and 1645 cm^{-1} (PPMS) and 1736 cm^{-1} and 1639 cm^{-1} (PCHMS) were also observed which are due to carbonyl functionalities and water or >C=C< stretching frequencies respectively [34].

3.5 Discussion

It has been mentioned in chapter 1.5.1 that numerous chemical processes are taking place simultaneously within a silent discharge in air such that it represents a complex oxidizing medium. In addition, there is still not a good understanding of the reactions of species created in the discharge with the sample surface. Since no nitrogen signal could be detected in the treated films nitrogen species do not seem to play an important role in the reactions on the polysilane surface. There are three oxygen species with pronounced oxidising properties which are likely to play a role in the oxidation of the films:

1) atomic oxygen, the precursor in ozone formation
2) ozone, the main and longest lived product of the silent discharge
3) hydroxyl radicals formed from the moisture of the ambient air

It is possible that all three factors contribute to product formation but is difficult to separate them. Additionally, an influence of other factors like the radiation emitted in the discharge on the modification process is conceivable but it is difficult to estimate their extent.

The reaction with ozone can be an important pathway although it is not an exclusive reaction route. It has been reported that most of the ozone is formed in the vicinity of the dielectric [36]. Therefore the position of the sample on the dielectric ensures that the film is exposed to a maximum concentration of ozone. No experimental data have been reported yet on the reactions of polysilanes with ozone. Since the reaction behaviour of polysilanes has been often deduced from the behaviour of small silane compounds it is likely that the silane reactions with ozone can serve as a model for the polymer. Generally, silanes have been found to be more reactive towards ozone than their carbon analogues. Si-Si and Si-phenyl bonds in small silanes react readily upon contact with ozone while the corresponding reaction of the Si-alkyl bond proceeds considerably slower. The reaction products are monomeric and oligomeric siloxanes [37]. Assuming that the polysilanes undergo similar reactions, ozone insertion into Si-Si bonds under formation of siloxane linkages occurs in both model polymers. The faster reaction of the aromatic polymer would correspond to the rapid reaction behaviour observed in the small silanes. This reaction ultimately results in the loss of the phenyl ring. It is assumed that the ring is oxidised but it has not been established whether the ring is first oxidised and subsequently split off or vice versa [37]. The observation of the highly oxidised shoulder in PPMS at 30s treatment time would support the former pathway.

The process cannot stop at this stage because the observed final silicon environment appears at a higher BE than a siloxane. The siloxanes thus formed can therefore only be an intermediate which is subsequently further oxidized by the reactive species in the plasma.

Since transmission IR reveals Si-O moieties in both treated films, it appears that in the present study the thickness of the oxidized layers is larger than those in reference 12 where the oxidized PCHMS layer did not give rise to additional signals.

Presumably the films in the low pressure plasma are densified by some degree of ion bombardment.

3.6 Conclusions

Silent discharge treatment of PPMS and PCHMS thin films results in the rapid formation of a carbonaceous SiO_x surface layer. The oxidation proceeds faster and more completely in the case of the aromatic polysilane.

3.7 References

1) West, R. *J. Organometallic Chem.* **1986**, *300*, 327

2) Miller, R.D.; Michl, J. *Chem. Rev.* **1989**, *89*, 1359

3) Mark, J.E.; Allcock, H.R.; West, R. *Inorganic Polymers*, Prentice Hall : New Jersey, 1992, pp.186-235

4) Miller, R.D. In : *Silicon - Based Polymer Science , A Comprehensive Resource*; Zeigler, J.M.; Fearon, F.W.G. Eds.; Advances in Chemistry Series 224; American Chemical Society : Washington, DC, 1990, pp.413-458

5) Miller, R.D. *Adv. Mater.* **1989**, *1(12)*, 433

6) Taylor, G.N.; Wolf, T.M. *Pol. Engin. and Sci.* **1980**, *20(16)*, 1087

7) Reichmanis, E.; Novembre, A.E.; Tarascon, R.G.; Shugard, A.; Thompson, L.F. In : *Silicon - Based Polymer Science , A Comprehensive Resource*; Zeigler, J.M.; Fearon, F.W.G. Eds.; Advances in Chemistry Series 224; American Chemical Society : Washington, DC, 1990, pp.265-281

8) Watanabe, F.; Ohnishi, Y. *J. Vac. Sci. Technol. B* **1986**, *4*, 422

9) Miller, R.D.; Hofer, D.; Rabolt, J.; Sooriyakumaran, R.; Willson, C.G.; Fickes, G.N.; Guillet, J.E.; Moore, J. In: *Polymers for High Technology - Electronics and Photonics*; Bowden, M.J.; Turner, S.R., Eds.; ACS Symposium Series 346; American Chemical Society : Washington, DC, 1987, pp.170-187

10) Hartney, M.A.; Hess, D.W.; Soane, D.S. *J. Vac. Sci. Technol.* **1989**, *B7 (1)*, 1

11) Miller, R.D.; Hofer, D.; McKean, D.R.; Willson, C.G.; West, R.; Trefonas III, P.T. In: *Materials for Microlithography*; Thompson, L.F.; Willson, C.G.; Frechet,

J.M.J. Eds.; ACS Symposium Series 266; American Chemical Society : Washington, DC, 1984, pp.293-310

12) Fonseca, J.L.C; Barker, C.P.; Badyal, J.P.S. *Macromolecules* **1995**, *28*, 6112

13) Coburn, J.W. *IEEE Transactions on Plasma Science* **1991**, *19(6)*, 1048

14) Barr, T.L.; Seal, S. *J. Vac. Sci. Technol.* **1995**, *A 13 (3)*, 1239

15) Johansson, G.; Hedman, J.; Berndtsson, A.; Klasson, M.; Nilsson, R. *J. El. Spectr. Rel. Phenom.* **1973**, *2*, 295

16) *Encyclopedia of Materials Characterisation*; Brundle, C.R.; Evans, C.A. Jr.; Wilson, S.,Eds.; Butterworth - Heinemann: Boston, 1992, p.285

17) Inagaki, N.; Katsuoka, *J. Memb. Sci.* **1987**, *34*, 297

18) Gray, R.C.; Carver, J.C.; Hercules, D.M. J. *El. Spectr. Rel Phenom.* **1976**, *8*, 14

19) Clark, D.T.; Dilks, A. *J. Pol. Sci. A - Pol. Chem. Ed.* **1977**, *15*, 15

20) Ban, H.; Sukegawa, K. *J. Appl. Pol. Sci.* **1987**, *33*, 2787

21) Jones, R.G.; Benfield, R.E.; Cragg, R.H.; Swain, A.C.; Webb, S.J. *Macromolecules* **1993**, *26*, 4878

22) Clark, D.T.; Dilks, A. *J. Pol. Sci. A - Pol. Chem. Ed.* **1979**, 957

23) Razumovskii, S.D.; Kefeli, A.A.; Zaikov, G.E. *European Polymer Journal* **1971**, *7*, 275

24) Carriere, B.; Deville, J.P.; Brion, D.; Escard, J. *J. El. Spectr. Rel. Phenom.* **1977**, *10*, 85

25) Barr, T. *Appl. Surf. Sci.* **1983**, *15*, 1

26) Alfonsetti, R.; Lozzi, L.; Passacantando, M.; Picozzi, P.; Santucci, S. *Appl. Surf. Sci.* **1993**, *70/71*, 222

27) Krimm, S.; Liang, C.Y.; Sutherland, G.B.B.M. *J. Chem. Phys.* **1956**, *25 (9)*, 549

28) Painter, P.C.; Coleman, M.M.; Koenig, J.L. *The Theory of Vibrational Spectroscopy and its Application to Polymeric Materials* ; Wiley : New York, 1982, p.358

29) Andrews, D.L. in: *Perspectives in Modern Chemical Spectroscopy*; Andrews, D.L. Ed.; Springer : Berlin, 1990, pp.77-78

30) Reilley, C.N.; Everhart, D.S. in: *Applied Electron Spectroscopy for Chemical Analysis*, Windawi, H.; Ho, F.F.-L., Eds., Wiley Interscience : New York, 1982, pp.106-107

31) Wesson, J.P.; Williams, T.C. *J. Pol. Sci. A - Pol. Chem. Ed.* **1981**, *19*, 65

32) Colthup, N.B.; Daly, L.H.; Wiberly, S.E. *Introduction to Infrared and Raman Spectroscopy* , 3rd ed., Academic Press : Boston, 1990, pp.358-361

33) Zhang, X.H.; West, R. *J. Pol. Sci. A - Pol. Chem. Ed* **1984**, *22*, 225

34) Bellamy, L.J *The Infrared Spectra of Complex Molecules*, 3rd ed., Vol. 1, Chapman and Hall : London, 1975, pp.374-384

35) Lisovskii, I.P.; Litovchenko, V.G.; Lozinskii, V.B.; Frolov, S.I.; Flietner, H.; Fussel, W.; Schmidt, E.G. *Journal of Non-Crystalline Solids* **1995**, *187*, 91

36) Labrenz, M. *Elektrische Gasentladungen zur Ozonerzeugung*, PhD Thesis, TU Braunschweig, 1983

37) Spialter, L.; Austin, J.D. *Inorg. Chem.* **1966**, *5*, 1975

Chapter 4:
Study on the reactions of poly(phenylmethylsilane) upon irradiation in the presence of CCl_4

4.1 Introduction

While chapter 3 was concerned with the reaction behaviour of polysilanes in a plasma the present chapter is focussed on a photochemical aspect, namely, the reactions of irradiated polysilane films in the presence of CCl_4 vapour. Only the reactions of poly (phenylmethylsilane), PPMS, are studied.

4.2 Background on the photochemistry of polysilanes

Due to a σ conjugation of the polymer backbone enabling σ-σ^* electronic transitions to occur [1-3] polysilanes show an absorption maximum in the UV region despite being formally saturated [4]. The position of the absorption maximum is dependent on the nature of the substituents as well as on the length and the conformation of the polymer chain [1, 3-5]. The relaxation from the excited state can proceed both via radiative and nonradiative transitions, the latter of which cause the scission of the Si-Si bonds [6] thus resulting in a reduction of the polymer chain length [1,5,7]. Concurrently, the absorption maximum is shifted towards lower wavelengths (bleaching) as soon as the chain contains less than about 50 monomer units [4,5,8].

The reduction in molecular weight suggests that the degradation of polysilanes mainly results in chain scission, simultaneous crosslinking occurs to a much lower extent and is relatively more important in polysilanes with pendant aromatic substituents [4,5,9] Photodegradation is observed both in polysilane solutions and solid films [1,4,5,9]. The photoefficiency for scission and crosslinking, however, is considerably lower for solid films of a particular polysilane than in the respective solutions of similar optical density [1,4]. This was ascribed to the reduced mobility of the chain ends due to solid-state cage effects [1,5] in the films. Furthermore, crosslinking was found to be more pronounced in solid state samples compared to solutions. This is shown by a smaller scission-to-crosslinking ratio in the solid films [7].

Most information about the reactive intermediates involved in the photolysis of polysilanes has been obtained from the analysis of product mixtures formed in exhaustively irradiated solutions in the presence of suitable trapping reagents (MeOH, triethylsilane, chlorinated hydrocarbons) [1,2,9,10]. Three possible reaction pathways were discussed on the basis of those mechanistic studies:

1) substituted silylene extrusion and chain abridgement:

$$\text{- Si R R'- Si R R'- Si-R R'-} \xrightarrow{h\nu} \text{:Si R R' + -Si R R'- SiR R'-}$$

2) Si-Si bond homolysis and formation of polysilyl radicals:

$$\text{- Si R R'- Si R R'- Si-R-R'-} \xrightarrow{h\nu} \text{-R R' Si}\bullet + \bullet\text{Si R R'- Si R R'-}$$

3) formation of persistent silicon radicals via 1,1 reductive elimination and production of chain silylenes:

$$\text{- Si R R'- Si R R'- Si-R-R'-} \xrightarrow{h\nu} \text{-Si R}_2\text{ R' + :Si R'- Si R R'-} \quad \text{(a)}$$

$$\text{or -Si R R'}_2\text{ + :Si R- Si R R'-}$$

$$\text{:Si R- Si R R'-Si R R'-} \rightarrow \text{Si R R' = SiR -Si R R'-} \quad \text{(b)}$$

$$\text{Si R R' = Si R -Si R R'-} + \bullet\text{Si R R'- Si R R'-} \rightarrow \text{- Si R R'-}\overset{\bullet}{\text{S}}\text{iR - (Si R R')}_3\text{-} \quad \text{(c)}$$

The first two reactions are well known pathways in the degradation of both acyclic and alicyclic low molecular weight oligosilanes. Silylenes and silyl radicals are formed in independent and competing reactions [2,4,10]. The third reaction is regarded to be of minor importance. It is taken as the possible formation route of a persistent silyl radical the structure of which corresponds formally to one formed by simple cleavage of the Si-C bond. The experimental evidence, however, precludes this reaction pathway. The detection of a trialkylsilyl product on the other hand supports the reaction sequence 3 (a)-(c) [10].

Photodegradation is observed in the whole absorption range of a polysilane under consideration [2]. Further studies revealed, however, a wavelength dependence for the formation of reactive intermediates. Evidence for the formation of both silylenes and silyl radicals was found upon irradiation at wavelengths of about 250 nm. The amount of silylene trapping product decreased gradually with increasing wavelength and was not observed at irradiation wavelengths > 300 nm such that under these conditions radicals are the only intermediates during photodegradation [2].

The intermediates undergo further reactions to form stable products. Silyl radicals can recombine or disproportionate whereas silylenes undergo intramolecular insertion reactions [2].

The products of disproportionation are a silane and a silene:

$$2\text{ -R R'Si}\bullet \rightarrow \text{ -R R' Si - H} + \text{R R' Si = C R''}_2$$

(the radical bears CHR_2''; the silane bears CHR_2'')

The latter being an unstable molecule goes on to react further, for example, by adding solvent molecules or forming dimers [11].

Little is known about the intermediates involved in the photodegradation of solid films and it is unclear whether the mechanism found for solutions applies in this case. Siloxane, silane, silanol and carbonyl bands identified in IR spectra of polysilane films irradiated in air were interpreted as evidence for radical intermediates. A rapid oxidation of silylenes in air was suggested to lead to cyclic siloxanes which were detected by mass spectrometry [8]. The same report found silylenes to be the major volatile product of vacuum irradiations, a finding that could not be confirmed in a later similar study [12].

It is known that silyl radicals abstract chlorine from chlorinated alkanes in solution [5]. A similar reaction of silyl radicals formed from solid polysilane films upon irradiation has not been mentioned yet in the literature. It was the aim of the following study to investigate the reactions occurring on solid polysilane surfaces upon irradiation in CCl_4 containing vapour.

4.3 Experimental

Carbon tetrachloride, CCl_4, (BDH, chromatography grade) and poly (phenylmethyl)silane, PPMS (ABCR), were used for the study. Thin PPMS films were spin coated onto strips of LDPE (ICI) from a 2% w/v solution in toluene. Prior to use the PE substrates were ultrasonically cleaned for 30 seconds in IPA (Isopropyl alcohol) and dried in air. CCl_4 was degassed in repeated freeze and thaw cycles.

4.3.1 Experimental set - up

PPMS films were placed into a glass sample holder and transferred into a glass reactor fitted with a quartz window, a needle valve gas inlet (Edwards LV 10K), a Pirani Pressure gauge (Edwards PR 10K) and a rotary pump (Edwards Speedivac) attached to a liquid nitrogen cold trap, figure 1. All joints in the set - up were grease free. The pump exhaust was placed into the fume cupboard to avoid possible dangers with accidental phosgene production.

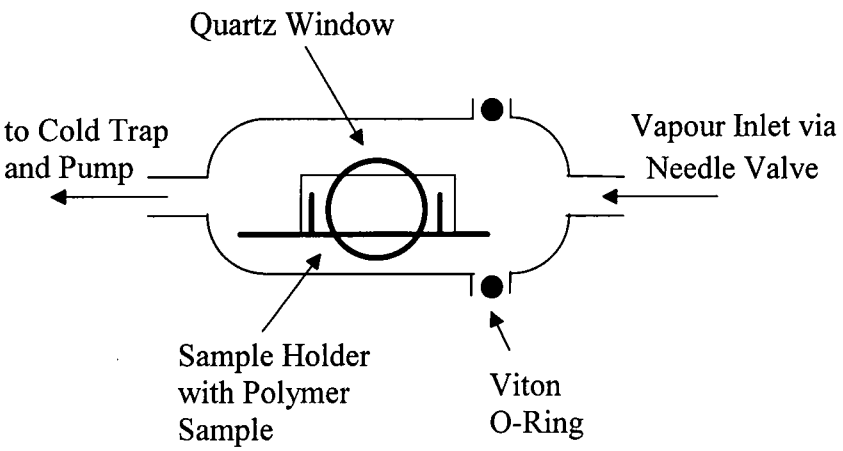

Fig. 1 Schematic representation of the glass reactor

The radiation was provided from an Oriel 200 W high pressure Hg (Xe) lamp operated at 100 W. This lamp emits intense emission lines in the near UV, VIS and IR region on an otherwise continuous spectrum.

4.3.2 Leak Rate

Leak rate and flow rate were determined assuming ideal gas behaviour and thus the ideal gas law was employed:

$$p \times V = n \times R \times T$$

where p = gas pressure, V = volume of the reactor, n = number of moles, R = universal gas constant and T = absolute temperature.

If a reactor fed by a continuous flow of gas is isolated from the pump and the pressure increase Δp and the time interval required for the observed change in pressure Δt are measured the leak rate can be approximately calculated according to [13,14]:

$$Fv \approx \frac{V}{RT} \times \frac{\Delta p}{\Delta t}$$

with p in atm, t in min, V in cm^3 and T in K, R= 82.06 atm cm^3 mol^{-1} K^{-1} and using Avogadro's Law according to which a mole of gas at standard conditions (T = 273K, P = 1atm) occupies a volume of 22414 cm^3 ;[15] the above equation can be rewritten as:

$$Fv \approx \frac{V}{RT} \times \frac{\Delta p}{\Delta t} \times 22414 \qquad [cm^3/min]$$

After placing the sample in front of the window of the reactor the set-up was evacuated to base pressure (4×10^{-3} torr) and the leak rate was determined. This was achieved by sealing the reactor off from the pump and measuring the time that elapsed until a certain pressure increase had taken place. If the value was acceptable (better than 1.5×10^{-3} cm^3/min) CCl_4 vapour was admitted to the reactor such that a pressure of 2×10^{-1} torr was attained. The flow rate was estimated to be 1.1 cm^3/min. During this time the light of the lamp was kept out of the set-up by a shutter placed in front of the window. Treatment time was started by the removal of the shutter and finished by placing the shutter back in the optical path. The monomer supply was then stopped and the apparatus evacuated. After bringing the set-up back to atmospheric pressure with nitrogen, and flushing the reactor with the gas for about 2

minutes to allow possible radicals which were not saturated to react in the absence of oxygen, the sample was removed from the reactor and immediately transferred into the XP spectrometer. The respective measurements were carried out under the conditions described in section 3.3.2.

In order to find out about the ageing of treated films selected samples were stored for 3 and 28 days respectively in an ambient atmosphere in the dark before being evaluated.

4.4 Results

4.4.1 XPS of fresh samples

The spectra of PPMS films exposed to CCl_4 vapour for 30 minutes without simultaneous irradiation were essentially like those of untreated PPMS films. A chlorine uptake was not observed.

A time study was carried out for the irradiation of PPMS films in the presence of CCl_4 vapour keeping all other experimental parameters constant. Figure 2 shows the elemental composition of the treated films plotted against irradiation time. The incorporation of chlorine into the surface is accompanied by a loss in carbon content; whereas the silicon content remains nearly unchanged. Besides chlorine there is also an increasing amount of oxygen present in the analysed films. The surface composition reaches a saturation value after a treatment time of about 450 seconds.

The main features of the PPMS XP spectra were already described in section 3.4.1. Treated samples show a slight reduction in the C (1s) shake-up intensity with increasing treatment time. No additional component is observed in the C (1s) spectra within the sensitivity range of the instrument. This excludes the presence of significant amounts of oxidized carbon moieties or chlorinated carbon environments which both would appear towards higher BE of the hydrocarbon component, figure 3.

The Si (2p) spectra of the treated films show the most obvious change in the photoelectron peak shape, figure 4. Initially, additional contributions on the high BE side of the original peak appear, these gain intensity at higher treatment times. The whole signal appears broadened and is shifted towards higher binding energy as the treatment time becomes longer. This observation suggests that the changes induced

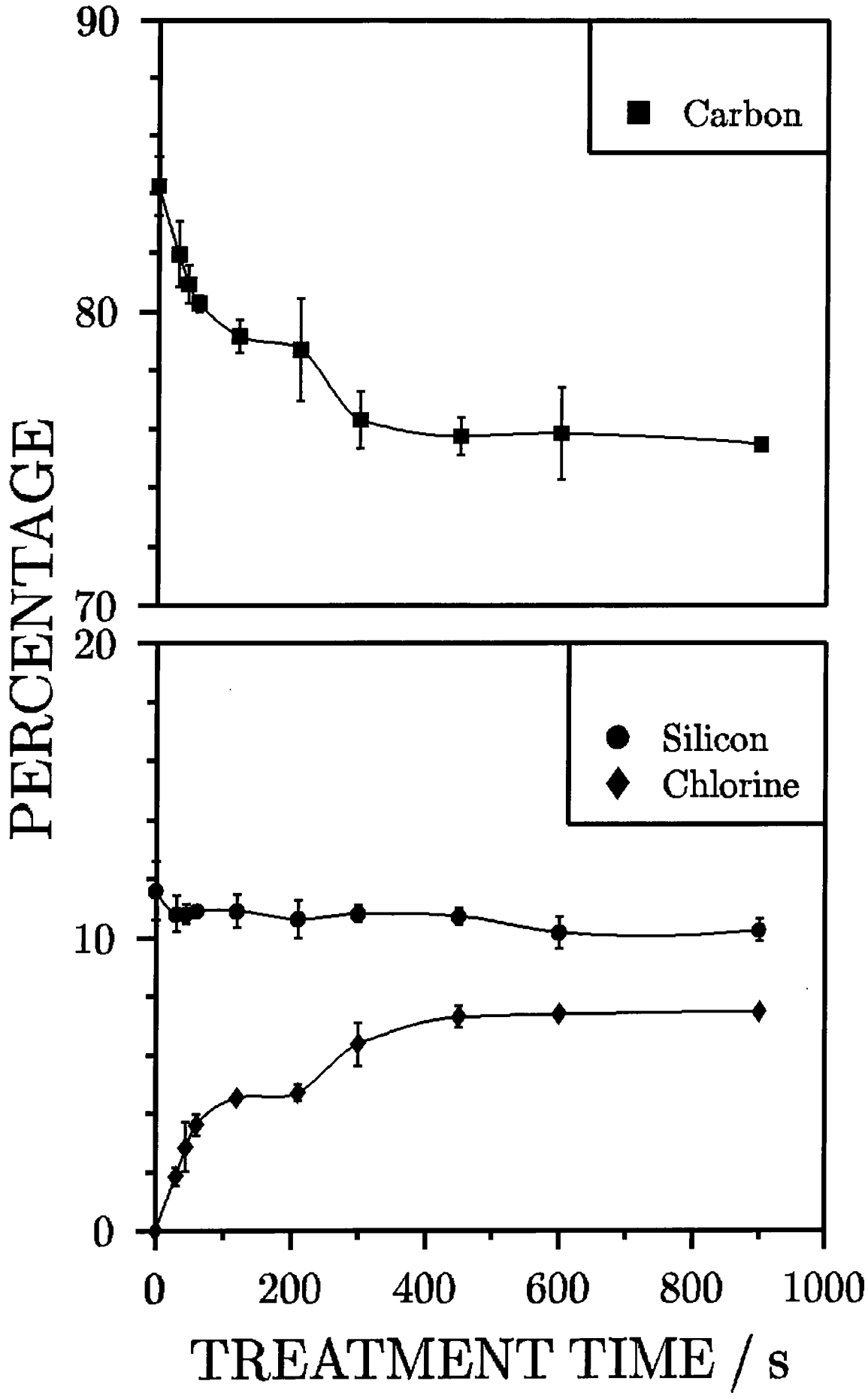

Fig. 2 Elemental composition (C, Si, Cl) of PPMS films as a function of irradiation time in CCl_4

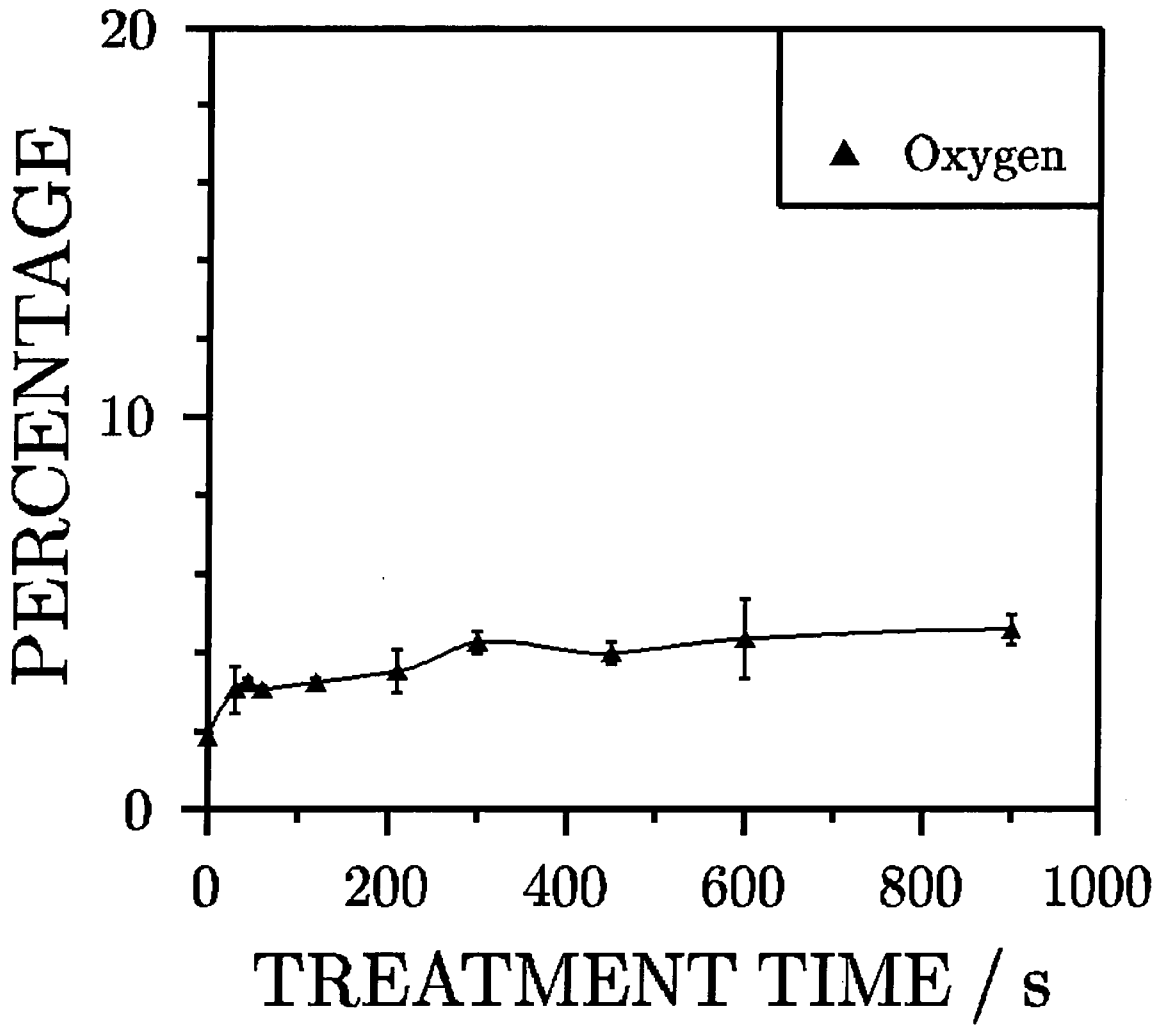

Fig. 2 Elemental composition (O) of PPMS films as a function of irradiation time in CCl_4

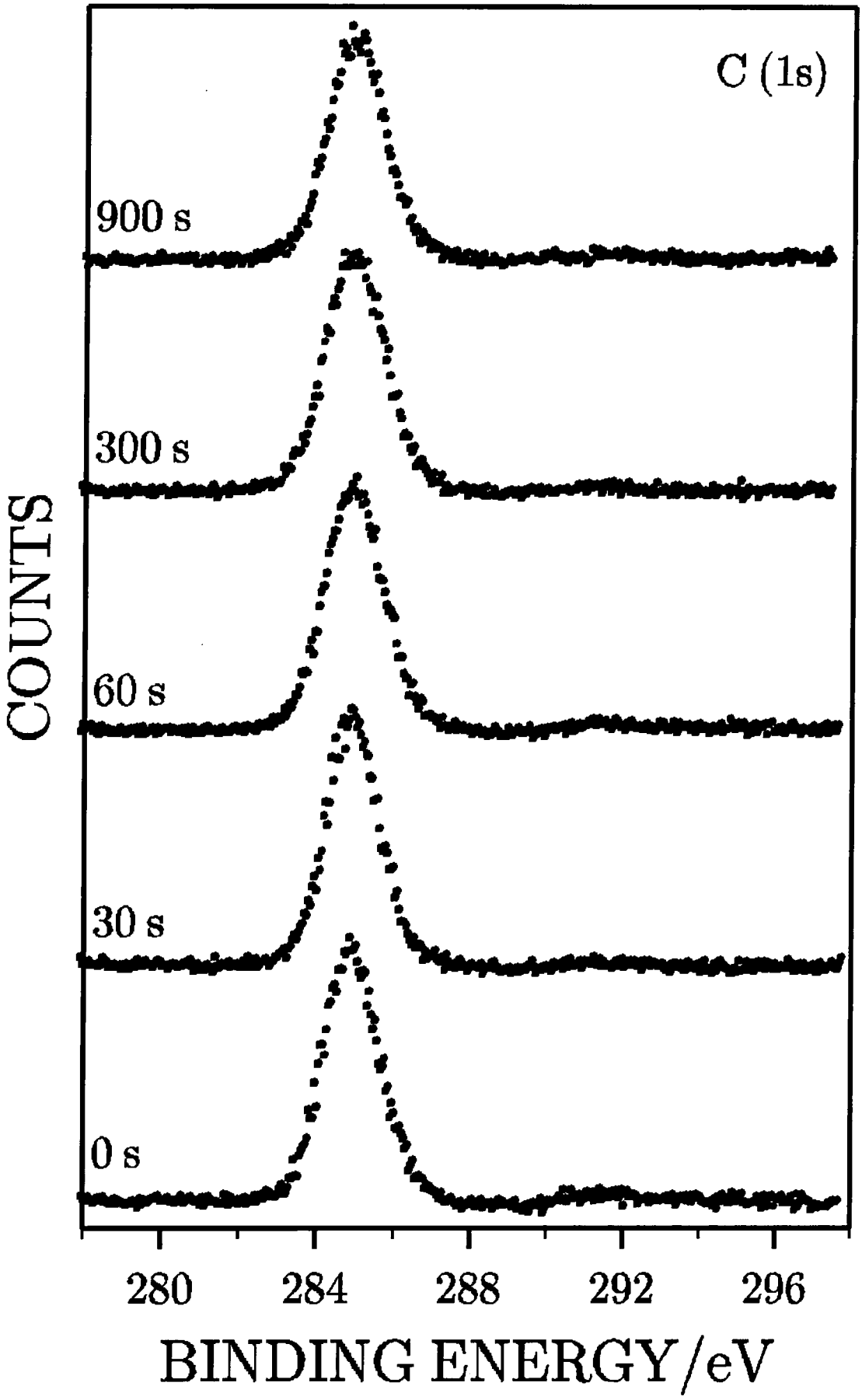

Fig. 3 C (1s) XP spectra of PPMS films as a function of irradiation time in CCl_4

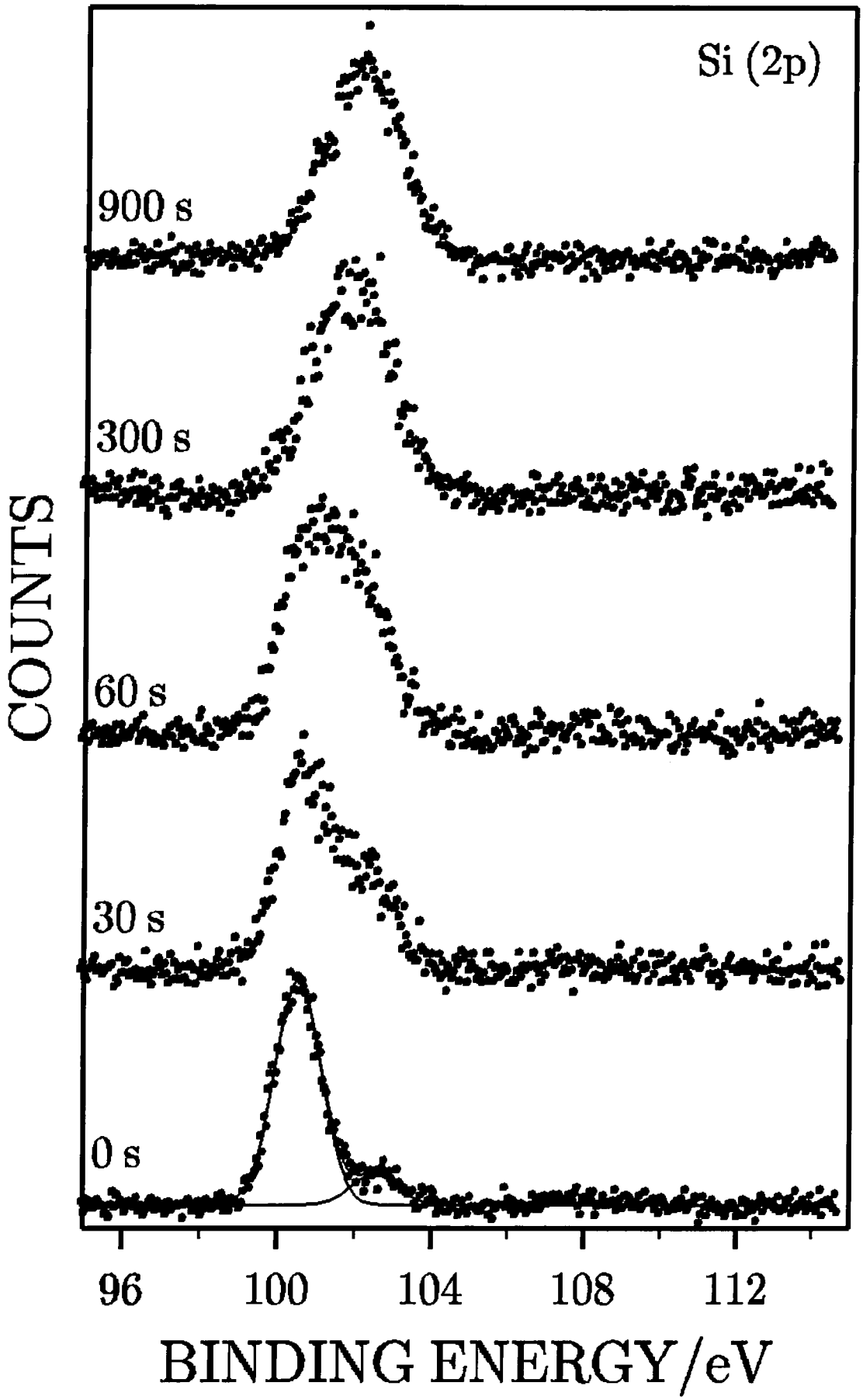

Fig. 4 Si (2p) XP spectra of PPMS films as a function of irradiation time in CCl_4

by the treatment occur on silicon centres. Since the Si (2p) signal is still broad even after the longest exposure time it can be concluded that the treatment does not result in the formation of a uniform silicon environment. Two elements are incorporated into the films, chlorine and oxygen. It can therefore be assumed that both silicon-chlorine and silicon-oxygen environments are present on the surface and contribute to the Si envelope. Both elements cause a shift towards higher BE which increases with increasing number of atoms attached to Si [16]. Additionally, the overall range of BE shifts is not very large in both cases. Therefore, the particular contributions to the Si (2p) spectra cannot be attributed unambiguously and so the signals are presented as unfitted spectra.

Cl (2p) XP spectra were fitted as Gaussian peaks with fixed FWHM (full width at half maximum) using a Marquardt minimisation computer programme, figure 5. The Cl ($2p_{3/2}$) component of the appearing chlorine signal is centred at a binding energy of 200.4 eV. Since the untreated film does not show a chlorine signal the spectra of the treated samples only are included in the figure.

The O (1s) environment appears at a binding energy of 532.5 eV which is characteristic of a siloxane environment [17].

4.4.2 XPS of aged samples

	% Cl	% Si	% C	% O
directly after treatment	8.0 ± 0.1	11.0 ± 0.6	76.3 ± 1.7	4.7 ± 1.1
after ageing in moist air for 3 days	3.4 ± 0.4	11.6 ± 1.1	74.8 ± 0.8	10.3 ± 0.1
after ageing in moist air for 28 days	1.3 ± 0.1	11.25 ± 1.2	70.9 ± 2.3	16.6 ± 1.1

Tab. 1 Change in composition of a 10 min treated sample with time exposed to moist air

In table 1 the composition of samples each treated for 10 minutes but measured immediately after treatment and after ageing for 3 and 28 days respectively are compared. The aged samples show a loss of chlorine and a strong uptake in oxygen which suggests that the chlorine species which were present initially are not

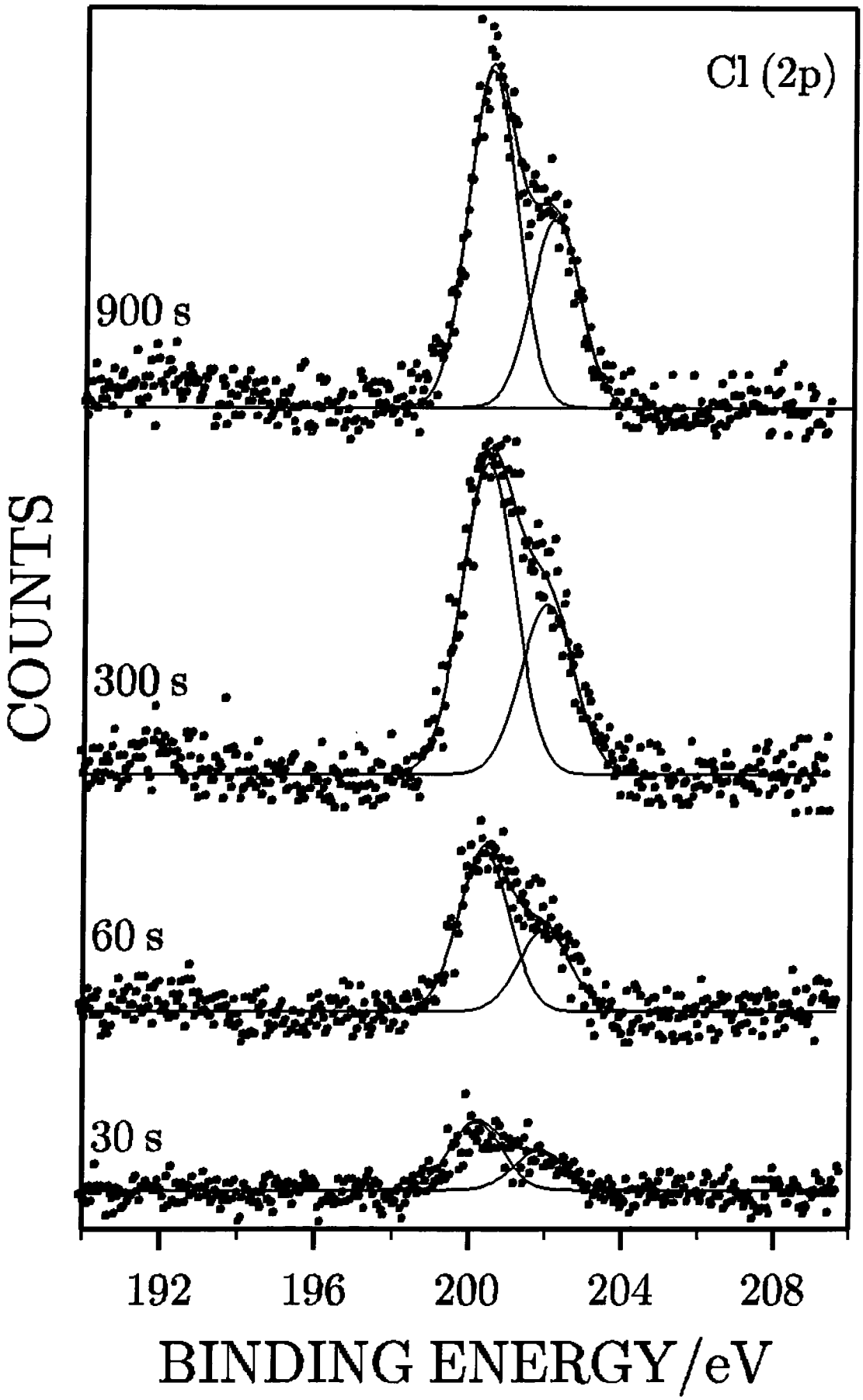

Fig. 5 Cl (2p) XP spectra of PPMS films as a function of irradiation time in CCl_4

stable in ambient air. Apart from the C (1s) spectrum of the sample aged for 28 days which shows a slight shoulder on the high binding energy side due to oxidized carbon moieties the other XP signals in the aged samples do not show a difference with respect to their shape and their position compared to the fresh sample, figures 6-9.

4.5 Discussion

Since there is only a small amount of information about the intermediates [5] formed upon the irradiation of solid polysilane films no definitive explanation can be given for the observations made in the study; however, the following tentative explanation is proposed:

The exposure of polysilanes to UV radiation is known to lead to silicon-silicon bond homolysis resulting in the formation of silyl radicals [5]. Under the present conditions those radicals can undergo four reactions:

1) recombination due to the cage effect
2) reaction with the chlorine species present in the vapour.
3) disproportionation
4) attack of aromatic substituents leading to crosslinking

Recombination leads to the 'repair' of the polymer chain. It cannot be detected and therefore the extent of this process cannot be estimated. Since the reaction takes place in the solid state where the mobility of the chain ends is restricted it is, however, likely to occur.

There are two possible pathways which might lead to the formation of the chlorinated species: the reaction with photodissociation products of CCl_4 and abstraction of chlorine atoms from CCl_4 molecules. CCl_4 is photosensitive and absorbs continuously in the near UV starting below about 250 nm [18]. A study by Davis et al. of the gas phase photochemistry of CCl_4 vapour upon UV irradiation revealed a dependence of the species generated on the wavelength where the degree of fragmentation of the molecule increases with the energy content of the radiation [19]. These observations were confirmed by trapping experiments [20]. Under the

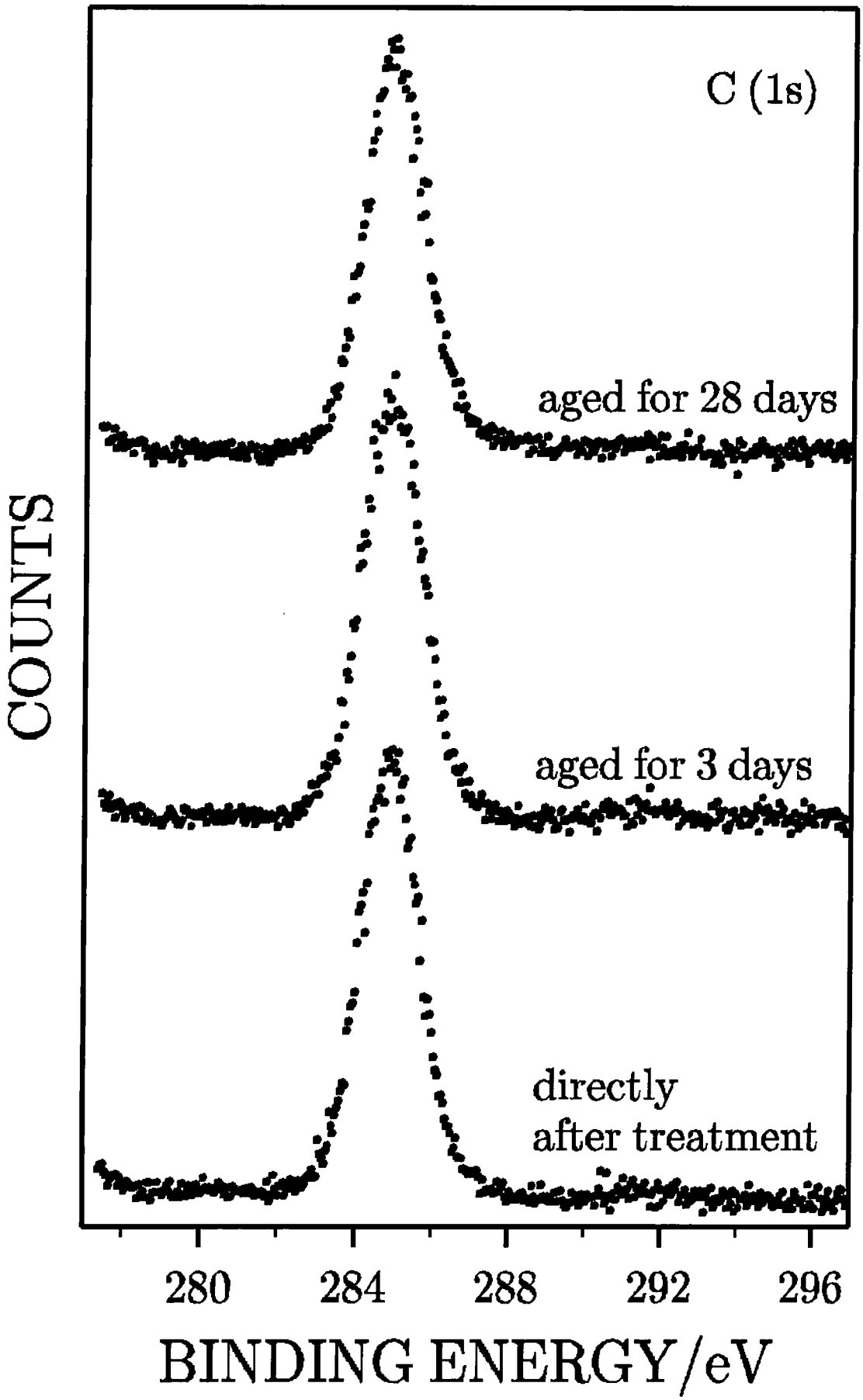

Fig. 6 C (1s) XP spectra of chlorinated PPMS films directly after CCl_4 treatment and after ageing

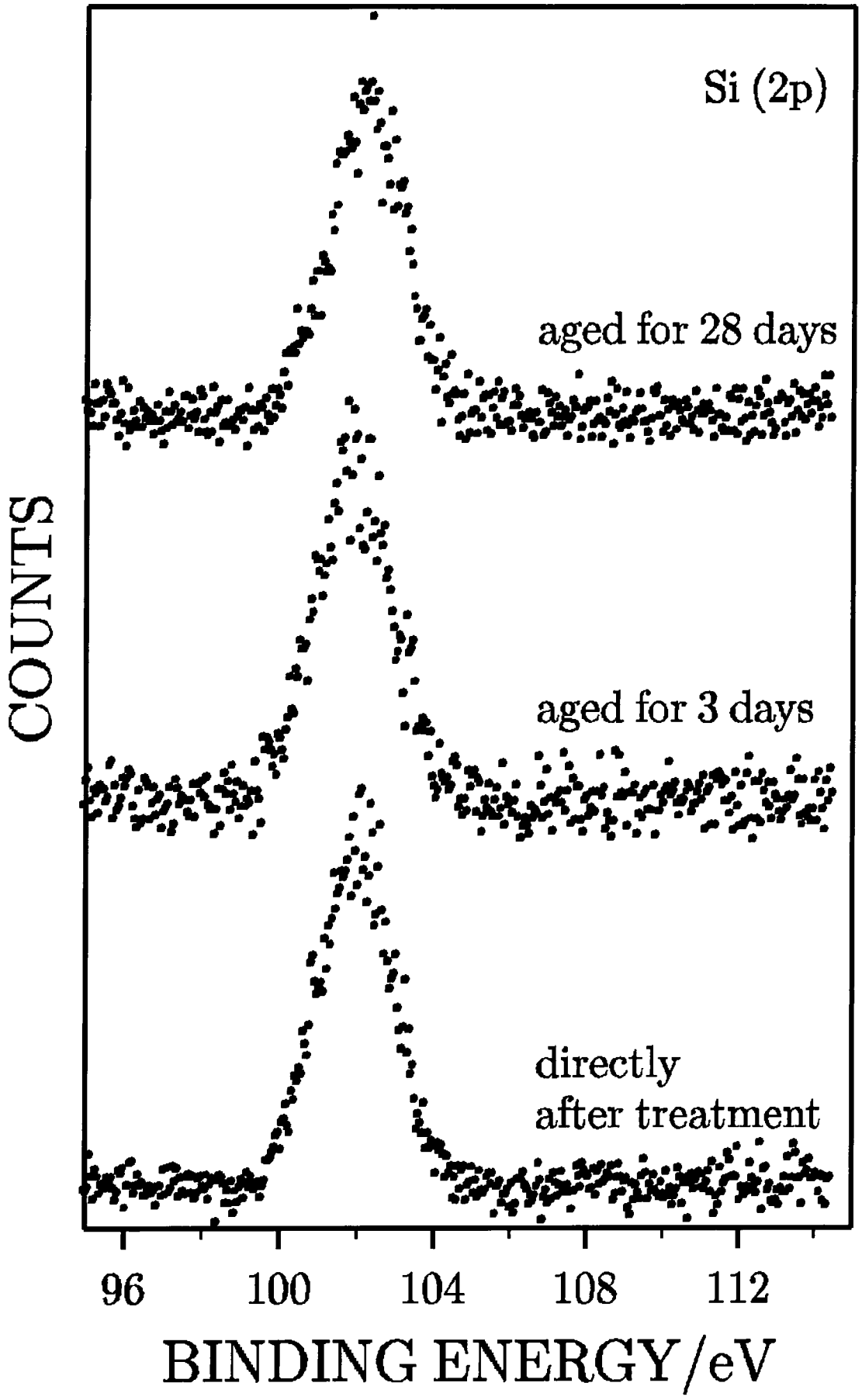

Fig. 7 Si (2p) XP spectra of chlorinated PPMS films directly after CCl_4 treatment and after ageing

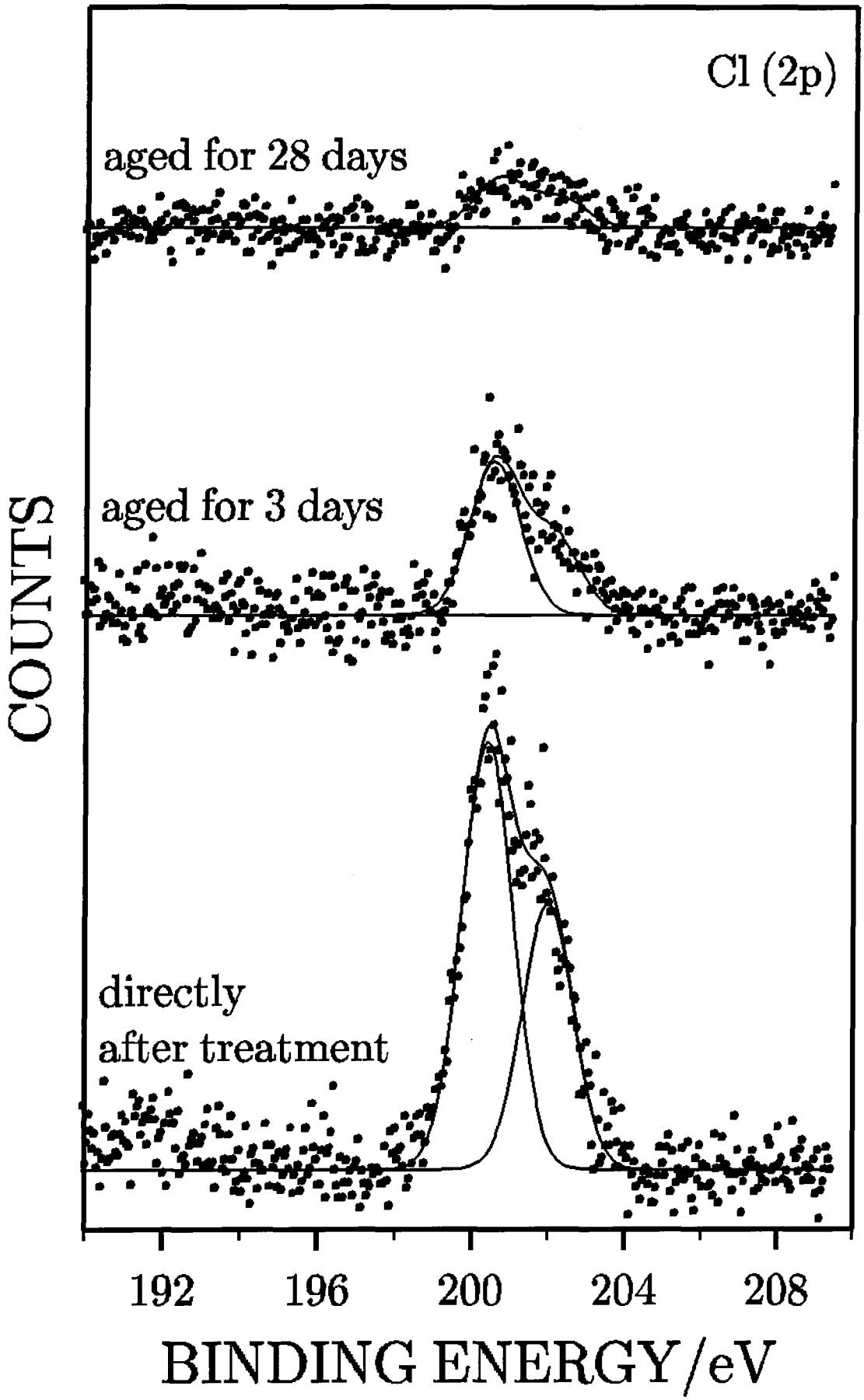

Fig. 8 Cl (2p) XP spectra of chlorinated PPMS films directly after CCl_4 treatment and after ageing

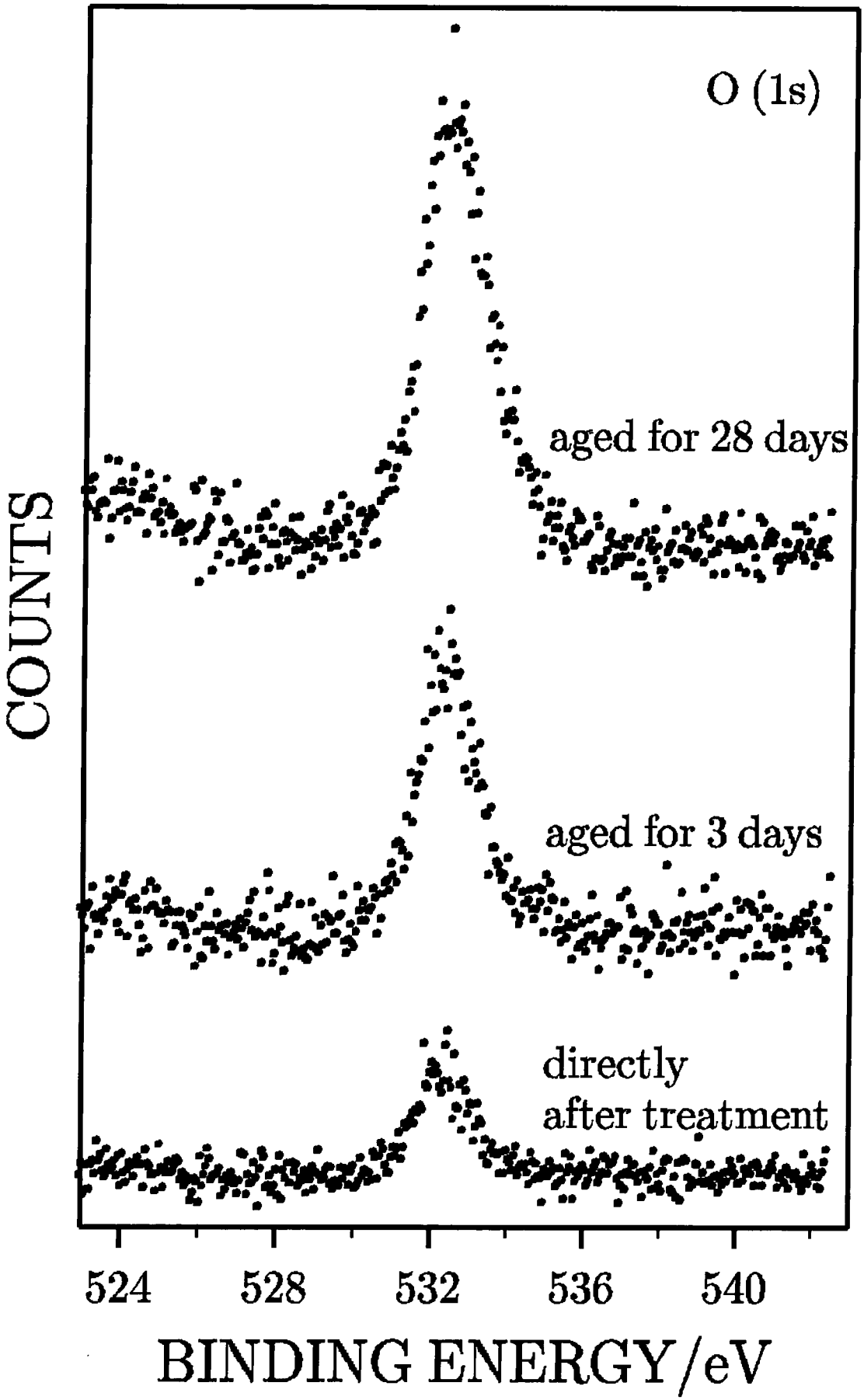

Fig. 9 O (1s) XP spectra of chlorinated PPMS films directly after CCl_4 treatment and after ageing

experimental conditions of the present study only one of three processes found in the studies mentioned above could be relevant. This reaction is:

$$CCl_4 \rightarrow CCl_3\bullet + Cl\bullet \qquad (1)$$

The other fragmentation processes would require radiation of higher energy. Stable products formed from the intermediates in (1) are Cl_2 and C_2Cl_6. Since the present experiments were carried out at shorter irradiation times and considerably lower pressure than the photodissociations in the literature a significant contribution of process (1) seems to be unlikely although it cannot be entirely ruled out. The initially formed silyl radicals therefore most probably abstract a chlorine atom from CCl_4 molecules similar to the reaction in solutions. The product of this reaction are chlorosilanes with lower molecular weight compared to the starting material. The XP spectra lend support to the formation of chlorinated silicon functionalities.

Disproportionation leads to the formation of Si-H functionalities and initially to silenes which subsequently react, for example, by dimerisation. XPS cannot detect changes caused by the formation of these products because they are not associated with easily discernible BE shifts, therefore, the role of this process cannot be assessed with the information available. The same is true for possible crosslinking reactions.

The ageing observed in the films after storage in moist air can be explained as follows: Small chlorosilanes are known to be susceptible to hydrolysis, the initial product being a silanol which subsequently condensates under formation of a siloxane bond [21] according to:

$$\rangle Si\text{-}Cl + H_2O \rightarrow \rangle Si\text{-}OH + HCl$$

$$2\ \rangle Si\text{-}OH \rightarrow \rangle Si\text{-}O\text{-}Si\langle + H_2O$$

The Si-O bond thus formed is thermodynamically more stable than the original Si-Cl bond, the binding energies being 112 kcal/mol (469 kJ/mol) and 93 kcal/mol (389 kJ/mol), respectively [22]. The reactivity of a chlorosilane towards hydrolysis decreases with increasing bulk of its substituents [22]. The loss in chlorine and the

simultaneous uptake of oxygen suggests that a similar process is taking place in the samples when stored in moist air. The condensation step is only likely in cases where 2 chain ends carrying hydroxyl groups meet. Comparing the loss of chlorine and the gain of oxygen in the ageing samples the oxygen uptake is larger than can be expected from the reaction sequence described above. In the samples aged for three days the additional amount of oxygen can probably be explained by a steric hindrance of the condensation step. The oxygen content of the samples aged for 28 days is that high that there must be an additional oxidation process. The reduction in the shake-up intensity and the appearance of a slight shoulder on the high BE side of the respective C (1s) XP spectra suggest that there is also a certain degree of oxidation in the carbon species which is not immediately obvious in the freshly treated samples. This reaction could possibly account for the discrepancy in the oxygen uptake.

It is conceivable that the oxygen detected in freshly treated films is due to the hydrolysis of easily accessible Si-Cl bonds during transfer of the sample into the spectrometer. This undesired reaction could be avoided by handling of the samples in an inert atmosphere or by carrying out the reaction in-situ which could probably lead to more conclusive results. Furthermore, complementary measurements with other experimental techniques could provide more information about the reaction pathways of the intermediates involved in the treatment, like disproportionation (IR) or crosslinking (GPC).

4.6 Conclusions

The irradiation of PPMS films in the presence of CCl_4 vapour leads initially to the formation of chlorinated silanes. They are sensitive to moist air and degrade upon exposure to this atmosphere. The hydrolysis is characterised by a loss of chlorine and an uptake of oxygen. The appearance of small amounts of oxidized carbon species is observed after long ageing intervals.

4.7 References

1) Miller, R.D.; Hofer, D.; Rabolt, J.; Sooriyakumaran, R.; Willson, C.G.; Fickes, G.N.; Guillet, J.E.; Moore, J. In: *Polymers for High Technology - Electronics*

and Photonics; Bowden, M.J.; Turner, S.R., Eds.; ACS Symposium Series 346; American Chemical Society : Washington, DC, 1987, pp.170-187

2) Michl, J.; Downing, J.W.; Karatsu, T.; Mc Kinley, A.J.; Poggi, G.; Wallraff, G.M.; Sooriyakumaran, R.; Miller, R.D. *Pure & Appl. Chem.*, **1988**, *60*, 959

3) Mark, J.E.; Allcock, H.R.; West, R. *Inorganic Polymers*, Prentice Hall : New Jersey, 1992, pp.186-235

4) Miller, R.D. *Adv. Mater.* **1989**, *1(12)*, 433

5) Miller, R.D. in : *Silicon Based Polymer Science: A Comprehensive Resource*, Advances in Chemistry Series 224, American Chemical Society : Washington DC, 1990, pp.413-458

6) Kunz, R.R.; Horn, M.W.; Wallraff, G.M.; Bianconi, P.A.; Miller, R.D.; Goodman, R.W.; Smith, D.A.; Eshelman, J.R.; Ginsberg, E.J. *Jpn. J. Appl. Phys.*, **1992**, *31*, 4327

7) Miller, R.D.; Hofer, D.; McKean, D.R.; Willson, C.G.; West, R.; Trefonas III, P.T. In: *Materials for Microlithography*; Thompson, L.F.; Willson, C.G.; Frechet, J.M.J. Eds.; ACS Symposium Series 266; American Chemical Society : Washington, DC, 1984, pp.293-310

8) Zeigler, J.M.; Harrah, L.A.; Johnson, A.W. *SPIE Advances in Resist Technology and Processing*, **1985**, *539*, 166

9) Miller, R.D.; Michl, J. *Chem. Rev.* **1989**, *89*, 1359

10) Karatsu, T.; Miller, R.D.; Sooriyakumaran, R.; Michl, J. *J. Am. Chem. Soc.*, 111, **1989**, 1140

11) Barton, T.J.; Boudjouk, P. in: *Silicon Based Polymer Science: A Comprehensive Resource*, Advances in Chemistry Series 224, American Chemical Society : Washington DC, 1990, pp.24-27

12) Magnera, T.F.; Balaji, V.; Michl, J.; Miller, R.D.; Sooriyakumaran, R. *Macromolecules*, **1989**, *22 (4)*, 1989

13) Ehrlich, C.D.; Basford, J.A. *J. Vac. Sci. Technol.* **1992** *A 10*, 1

14) Wutz, M.; Adam, H.; Walcher, W *Theorie und Praxis der Vakuumtechnik*, Vieweg : Braunschweig, 1986, pp.457-470

15) Holleman-Wiberg, *Lehrbuch der Anorganischen Chemie*, 33rd edition, Walter de Gruyter : Berlin, 1985, p.31

16) Moulder, J.F.; Stickle, W.F.; Sobol, P.E.; Bomben, K.D. *Handbook of X-Ray Photoelectron Spectroscopy*, Perkin Elmer Corporation, 1992, p.238

17) Moulder, Stickle, Sobol, Bomben, p.45

18) Okabe H. *Photochemistry of Small Molecules*, Wiley Interscience, 1978, p.306

19) Davis, D.D.; Schmidt, J.F.; Neeley, C.M.; Hanrahan, R.J. *J. Phys .Chem.* **1975**, *79*, 11

20) Rebbert, R.E.; Ausloos, P.J. *Journal of Photochemistry* **1976/77**, *6*, 265

21) Holleman-Wiberg, p.742/p.449

22) S. Pawlenko In : *Methoden der Organischen Chemie (Houben-Weyl)* "Organo-Silicium-Verbindungen" Bayer, O.; Müller, E. Eds. Vol. 13,5, Thieme : Stuttgart, 1980, p.14

Chapter 5:

Studies on the silent discharge treatment of alkali halide discs

5.1 Introduction

It was already mentioned in chapter 3 that KBr discs are modified upon exposure to a silent discharge plasma. In the following chapter more detailed studies of this phenomenon are described. Apart from the reactions of KBr the behaviour of KCl and KI was studied as well.

5.2 Background

5.2.1 Plasma treatment of alkali halides

The reaction behaviour of alkali halides upon exposure to plasmas has not been widely researched.

The remote oxygen plasma treatment of NaCl crystals resulted in the formation of surface layers of $NaClO_3$ which was proved by the appearance of the product's characteristic IR band [1]. No reaction was observed upon exposure of NaCl crystals to remote nitrogen and helium plasmas and to ozonized oxygen. The formation of nitrate species when air was used as a feed gas in the experiments was mentioned but not further investigated.

An XPS study of in-situ oxygen glow discharge treated KCl did not show the formation of chlorate. In this case the formation of a higher oxide was observed. This compound was unstable at elevated temperature and in vacuum and decomposed into a stable oxide with time [2].

5.2.2 Reaction of alkali halides with nitrogen oxides

Reactions of alkali halide aerosols with HNO_3, N_2O_5 and NO_2 traces present in polluted air have met a great interest in atmospheric chemistry. Alkali halide aerosols mainly consist of NaCl but also contain a small proportion of NaBr. They are formed in the troposphere, the layer up to about 12 km above the earth's surface [3],

by the wavemotion of the ocean [4-9] and in the stratosphere, the layer comprising the altitudes between about 15 km and 50 km [3], as a result of volcanic eruptions [5,7-12]. Some of the volatile reaction products formed in the aerosol - nitrogen oxide reactions are potential photochemical chlorine and bromine sources respectively and might therefore have an influence on the ozone balance in the atmosphere [5,6,10,13,14].

A number of model studies employing different experimental techniques and conditions have been carried out in which the reactions of one of the nitrogen oxides mentioned above with a halide in the form of single crystals, dry or slightly wet powder or as an aerosol were examined [4-22]. Most of the studies concerned NaCl and NaBr, the most important constituents of natural halide aerosols. In some cases the reaction behaviour of the corresponding potassium salts was investigated as well. The reactions of the chlorides were found to follow equations (1) - (3):

$$MCl\,(s) + HNO_3\,(g) \rightarrow HCl\,(g) + MNO_3\,(s) \qquad (1)$$

$$MCl\,(s) + N_2O_5\,(g) \rightarrow ClNO_2\,(g) + MNO_3\,(s) \qquad (2)$$

$$MCl\,(s) + 2\,NO_2\,(g) \rightarrow ClNO\,(g) + MNO_3\,(s) \qquad (3)$$

The formation of nitrite was excluded in all three reactions [19]. Irrespective of whether NaCl, the halide used in this particular study, reacted with N_2O_5, HNO_3 or NO_2 [19] both the position and the appearance of the product IR bands were identical. This indicates the formation of an identical product as shown in the equations listed above. Contrary to the slowly reacting hydrogen chloride formed in reaction (1), nitrylchloride, $ClNO_2$, and nitrosylchloride, ClNO, formed in reactions (2) and (3), are examples of photochemically very active chlorine compounds [22]. Most studies were therefore focused on obtaining kinetic data for reactions (1) - (3) the comparison of which allows the importance of these reactions for atmospheric processes to be assessed.

Reactions (1) [7,11,21] and (3) [15] were reported to follow the stoichiometry given by their equations. With regards to reaction (2), Livingston et al. [10] observed a 1:1 ratio of N_2O_5 and $ClNO_2$ only in the presence of sufficient surface chloride and in the case of complete mixing of the reactants. Fenter et al. [9] found a less than unity yield

for the reaction. Since their investigations did not lead to the identification of an additional volatile product, the authors attribute this observation to a secondary process like the binding of N_2O_5 molecules to the salt surface in a state that does not immediately react [9].

Bromides partly follow the same reaction schemes as those described above for the chlorides. While NaBr undergoes a reaction with HNO_3 corresponding to equation (1) forming a stoichiometric amount of HBr [11], the reports about the equivalent of reaction (2) are controversial where the concentration of the reactants seems to play an important role. For the reaction of N_2O_5 with NaBr Finlayson-Pitts et al. [17] observed the formation of nitrylbromide, $BrNO_2$, only in the case of reaction times in the minute range followed by analysis of the gaseous products with IR. At shorter reaction times and mass spectroscopic detection only the decomposition products BrNO, Br_2 and NO could be identified. A similar study employing mass spectroscopy (MS) carried out later for both KBr and NaBr [9] confirmed the absence of $BrNO_2$ but found Br_2 as the only volatile bromine species together with nitrous acid, HNO_2. The formation of nitrosylbromide, BrNO, in the reaction of NaBr with NO_2 corresponding to pathway (3) was confirmed by a combination of FTIR and MS measurements [16].

Water vapour was found to exert an important influence on the morphology and chemical properties of the nitrate layer formed on the one hand and the reactivity of the salt on the other.

If dried halides react with nitrogen oxides in the absence of water vapour the nitrate is formed as a thin overlayer which covers the surface completely. As soon as a saturation of the surface is reached a further reaction is prevented [6,13]. This type of nitrate is metastable and is assumed to have a structure significantly different from the bulk nitrate. The exposure of the metastable nitrate to even small amounts of water vapour leads to the recrystallisation to the stable bulk nitrate structure. This process is thought to occur via a water induced surface dissolution of the nitrate in a "quasi-liquid layer" on the sample surface in which nitrate mobility is substantially enhanced and which is supersaturated with respect to the stable form of the nitrate. The bulk-type nitrate therefore starts to precipitate from the quasi-liquid layer. Isolated crystallites can be obtained by evacuating the adsorbed water from the sample surface [8,13]. Thereby new alkali halide is exposed which can possibly react

further. In cases where powders were not dried prior to the reaction the stable nitrate was formed immediately [19].

The differences in the structure of the two nitrate forms are reflected in their photochemical properties. While the metastable nitrate did not undergo a photoreduction to nitrite upon exposure to UV light, the recrystallised nitrate showed this reaction [12] thus reacting like bulk nitrate from which this reaction is well known.

Experimental evidence for the two nitrate forms and the transformation of the metastable into the stable form upon exposure to water vapour was obtained in studies employing DRIFTS (Diffuse Reflectance Infrared Fourier Transform Spectroscopy), XPS and TEM (Transmission Electron Microscopy). The phenomenon was observed independently of the sample preparation method [13]. In the first case the two forms of nitrate could be identified by their different band positions in the respective reflectance IR spectra [5,19]. TEM pictures provided the optical proof for both the smooth surface structure of the metastable surface nitrate formed under dry reaction conditions and the growth of nitrate crystallites accompanied by the simultaneous regeneration of unreacted halide upon exposure to water vapour [13]. The size of the microcrystallites was found to enlarge with increasing water vapour pressure [8]. With the help of XPS the saturation of the sample surface under dry reaction conditions could be confirmed [6,8]. The XP spectra recorded after the exposure of the metastable nitrate films to water vapour, revealed an increase in the chlorine content and a corresponding decrease in the nitrogen and oxygen percentage respectively on the sample surface. This observation is in accordance with the recrystallisation process [8]. A change in the peak shape of the O (1s) signal with exposure time to water led to the identification of hydroxyl functionalities in addition to the nitrate environment. The hydroxide ions were thought to be the product of dissociation processes of water molecules adsorbed at defect sites resulting from the surface roughening during the nitrate formation step. The hydroxide ions were assumed to enhance the water uptake during the course of the reaction [8].

Those hydroxide ions play an important role in an explanation given for the increase in reactivity observed when the powder used in the experiments was not heated prior to the reaction with HNO_3 [21]. A similar increase in reactivity was found in the reaction of NaCl with N_2O_5 [7]. Both observations suggest an influence of

adsorbed water. In the latter case the enhancement in reactivity was explained with the possible hydrolysis of N_2O_5 yielding HNO_3 as the product [7].

In a detailed study of the HNO_3 reaction with NaCl in a Knudsen cell [21] it was found that in the case of the reaction of „wet" halide powder there was an initial rapid reactant uptake followed by a slower, constant uptake. In dried powders, on the other hand, the initial HNO_3 uptake was significantly lower. Corresponding to the HNO_3 uptake there was a simultaneous development of HCl. These results suggested the existence of two kinds of sites holding surface water. The hydroxyl ions formed in the dissociation of water molecules at defect sites were thought to be the centre of the more reactive sites. The hydroxyl ions were believed to be surrounded by water molecules due to their polarity and the formation of hydrogen bonds [21]. If HNO_3 molecules are taken up into this water cluster the hydroxide is neutralised and the cluster acidifies. Once it is sufficiently acidified HCl starts to degas from the cluster. By the removal of the hydroxide the centre of the cluster is lost. As a consequence the binding of the water molecules to the surface is weakened and they finally desorb. The less reactive sites were not further specified. The water associated to these sites was thought to be sufficiently strongly adsorbed that it takes up HNO_3 and degasses HCl without desorbing [21].

Literature evidence for the reactions of nitrogen oxides with alkali iodides and for the reactions of dinitrogenmonoxide, N_2O, with alkali halides could not be found. The formation of oxidized halogen species was not reported in the studies of the reactions of nitrogen oxides with alkali halides [23].

The reaction of an alkali halide with a gas mixture was mentioned by Kogelschatz [24] who observed the deterioration of the NaCl windows of an IR cell upon contact with silent discharge treated air. The absorption peak at 7.4 μ (1351 cm^{-1}) which could not be attributed to one of the gaseous products (O_3, N_2O_5, N_2O) formed by the treatment of dry air was assumed to be due to $NaNO_3$. A further analysis of the product, however, was not carried out.

5.3 Experimental

Potassium bromide (SpectrosoL®, BDH), potassium chloride (SpectrosoL®, BDH) and potassium iodide (99.99+ %, Aldrich) were used in this study. The salts

were treated in the form of discs pressed from weighed amounts of dried alkali halide powder such that the thickness of the discs was 0.5 mm. For reasons of comparison with the literature values XP spectra of $KClO_3$, $KBrO_3$, KIO_3, KNO_3 and KNO_2 were recorded from analytical grade powders.

Two experimental set-ups were used: the standard set-up which was already described in chapter 3.3.1 and a flow cell, a schematic of which is shown in figure 1. Aluminium was the electrode material in both set-ups. The dielectric material, however, differed. The standard set-up used two layers of polyethylene foil whereas, in the case of the flow-cell, the bottom of the glass vessel represented the dielectric. The gap width in the standard treatments was 3 mm, in the cell treatments 4 mm. The same power supply was used for both set-ups. For the measurements in the standard set-up the discharge was supplied with a voltage of 7.7 kV whereas the cell set-up had to be operated with 11 kV in order to obtain a stable discharge. Due to these differences the results obtained with the two set-ups can only be compared qualitatively.

The discharge cell was integrated in a set-up as shown in figure 2. The advantage of this arrangement is that it offers the opportunity to study reactions in gas surroundings other than ambient air. Additionally, it is possible to investigate the influence of humidity in the feed gas on the reactions by using either dried or humidified feed gases. The feed gases for the cell in the present study were: oxygen, nitrogen, helium and artificial air (BTCA 74), all produced by BOC. The water bubbler contained deionized water and the drying column was filled with molecular sieve. The latter was dried in an oven prior to use. The bubbler at the cell outlet was filled with glycerol and served the purpose of controlling the flow speed of the gas. Nitrile O-rings, initially used instead of Viton O-Rings, were not found to be a suitable seal for the flow cell since they became brittle even after a short exposure to ozone containing gas.

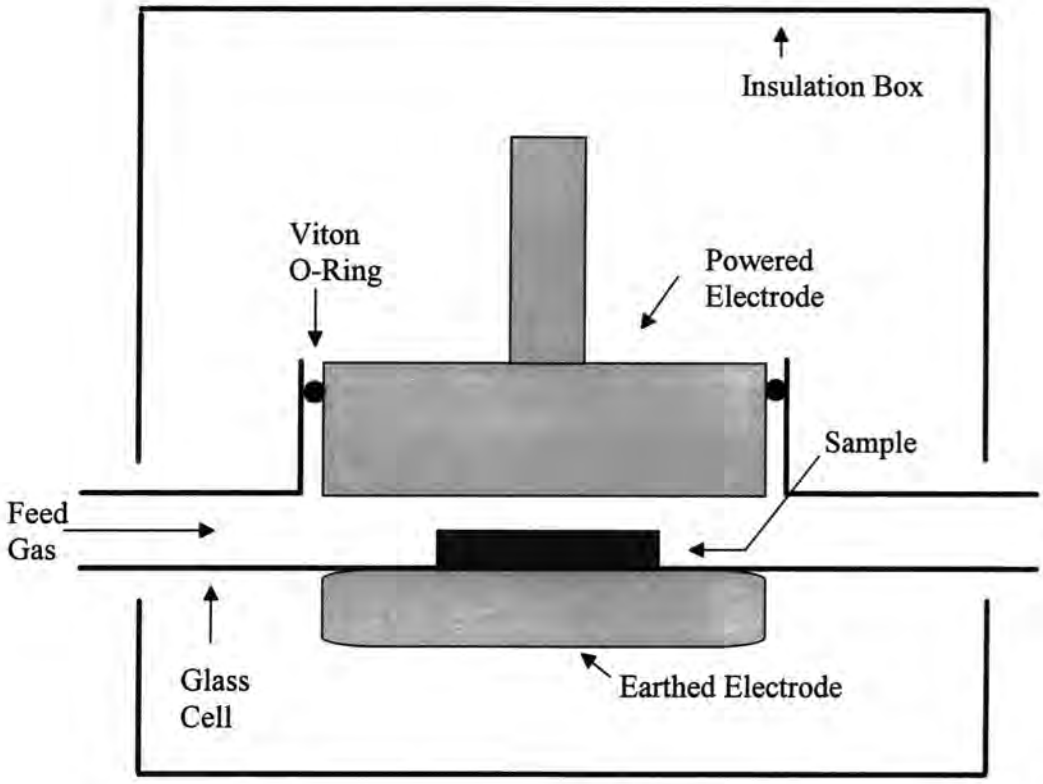

Fig. 1 Schematic of the flow cell

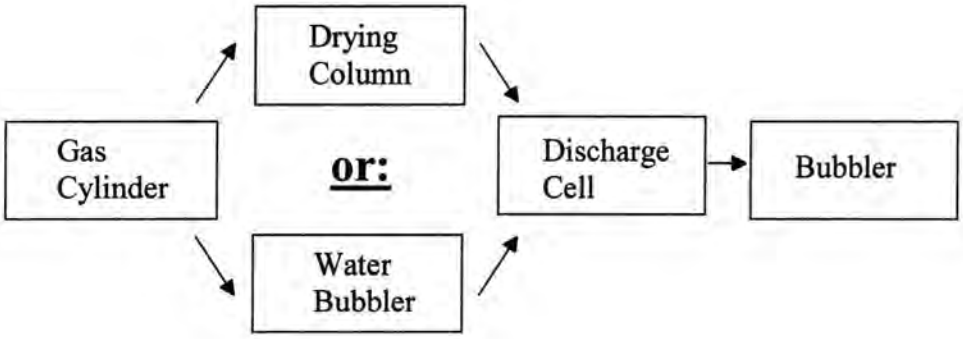

Fig. 2 Schematic of the flow cell set-up

Prior to each use the top electrode was cleaned with IPA. In cases of electrode corrosion the electrode was polished with Brasso®, rinsed with water, dried and degreased using IPA.

Treatments in the standard set-up were carried out by placing the disc on the dielectric and subsequently switching the discharge on for the time required. In the

second set-up the sample was placed on the bottom of the cell and the set-up was assembled. Prior to treatment, the set-up was purged with the respective feed gas for 12 minutes in order to provide defined reaction conditions.

The treated discs were analysed immediately after treatment by XPS or Transmission-IR measurements both under the conditions described in chapter 3.3.2. After being measured by IR some of the samples treated in the standard set-up were stored in a desiccator and the measurement was repeated after certain time intervals. Other samples were transferred into an oven in order to find out about the behaviour of the products upon their exposure to higher temperatures (145 and 192° C).

ATR - IR spectra of the deposited materials on the polyethylene dielectric were collected on a Mattson Polaris FTIR spectrometer equipped with a Golden Gate ™ Single Reflection Diamond ATR set-up (Greaseby-Specac). In a measurement, 64 scans were taken for the background and 32 scans were taken for the sample at a resolution of 4 cm^{-1}.

5.4. Results

5.4.1 Treatments in the standard set-up

5.4.1.1 General observations

Even during short treatment times in the standard set-up KI discs developed a brown colour which rapidly faded to light yellow when the discharge apparatus was switched off. In the case of the KBr discs a pale yellow colour and a bromine smell were observed only at high treatment times. No observation of this kind was made in the case of KCl. The surfaces of treated discs had an opaque appearance which suggests that surface roughening had taken place.

The appearance of the discharge in the gap was slightly inhomogeneous with strongly luminous discharge channels centred at the edges of the discs. These filaments burnt over extended times. The inhomogeneity became increasingly obvious with longer treatment times. Only moderate electrode corrosion was observed on the top electrode after the treatment.

5.4.1.2 IR

In figure 3 the IR spectra of a KCl, a KBr and a KI disc each treated for 600 seconds are compared. For reasons of clarity the spectra are focused on the wavelength range between 600 and 2000 cm^{-1}. All the three salts under consideration form two kinds of products: a nitrate species and an oxidized halogen species of the general formula XO_3^- (X = Cl, Br, I). Signals related to the nitrate species appear at ≈ 1377.3 (a'; shoulder)/1352.2 cm^{-1} (a; asymmetric stretching, strong), 833.3/825.6 cm^{-1} (b, b'; out of plane bending, medium) and 1766.9 cm^{-1} (c; combination band of symmetric stretching and in plane bending, very weak) which is in reasonable agreement with the literature values [25-27]. The strong and medium nitrate absorbances do not appear as a single sharp signal but in most cases as a broad envelope, separated less often into two distinct signals. This suggests that the nitrate is present in more than one form which absorb at slightly different wavenumbers. There is a general trend that in the asymmetric stretching region the contribution of the component at higher wavenumbers increases with increasing treatment time. In comparing the three halides, KI is the salt in which the contribution of the high wavenumber component is largest, followed by KBr and KCl. The 825.6 cm^{-1} contribution of the out of plane bending signal (b') gains intensity simultaneously with the high wavenumber component of the asymmetric stretch (a'). Irrespective of the treatment time the treated KI discs additionally show a nitrite signal centred at 1253.8 cm^{-1} (d). The absorbances of oxidized halogen species appear at 981.8/972.2 cm^{-1} (e) for chlorate, 792.8 cm^{-1} (f) for bromate and at 736.9 / 752.3 cm^{-1} (shoulder) / 798.6 (weak) cm^{-1} (g) for iodate [25,28]. The tendency to form oxidised halide species increases in the order $ClO_3^- < BrO_3^- << IO_3^-$. Furthermore, the treatment causes the loss of water from the sample surface which is obvious from negative water signals in the spectra.

5.4.1.3 Peak areas as a function of treatment time

The area of the asymmetric stretching vibration, the most intense absorbance in the IR spectrum of nitrate, was integrated and taken as a semiquantitative measure for the amount of nitrate formed. Figures 4 a-c show those nitrate peak areas

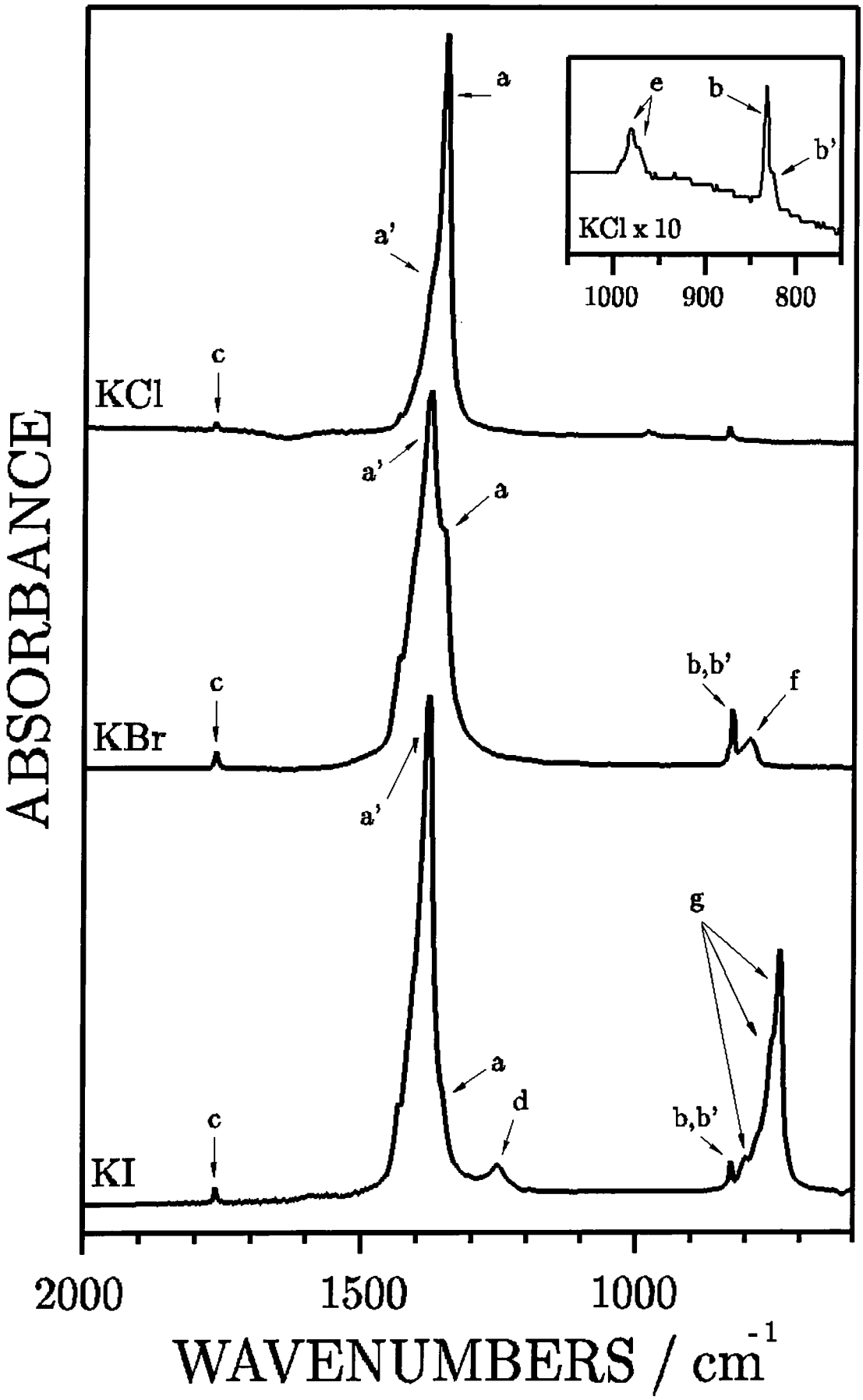

Fig. 3 IR spectra of alkali halide disks after 600 seconds silent discharge treatment in the standard set-up

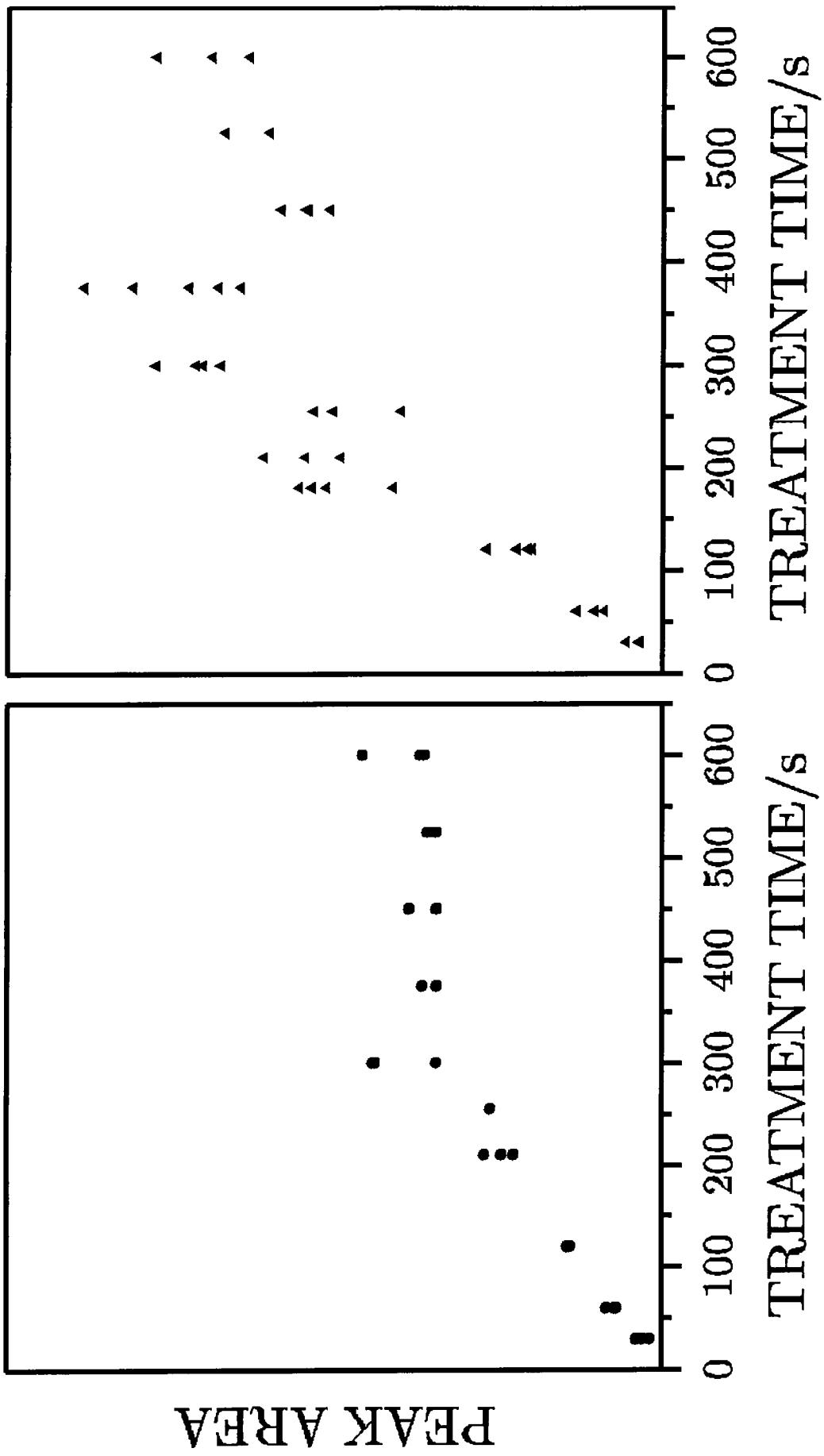

Fig. 4 a, b Peak areas of the asymmetric nitrate stretching vibration as a function of treatment time in the standard set-up (a: KCl, left; b: KBr, right)

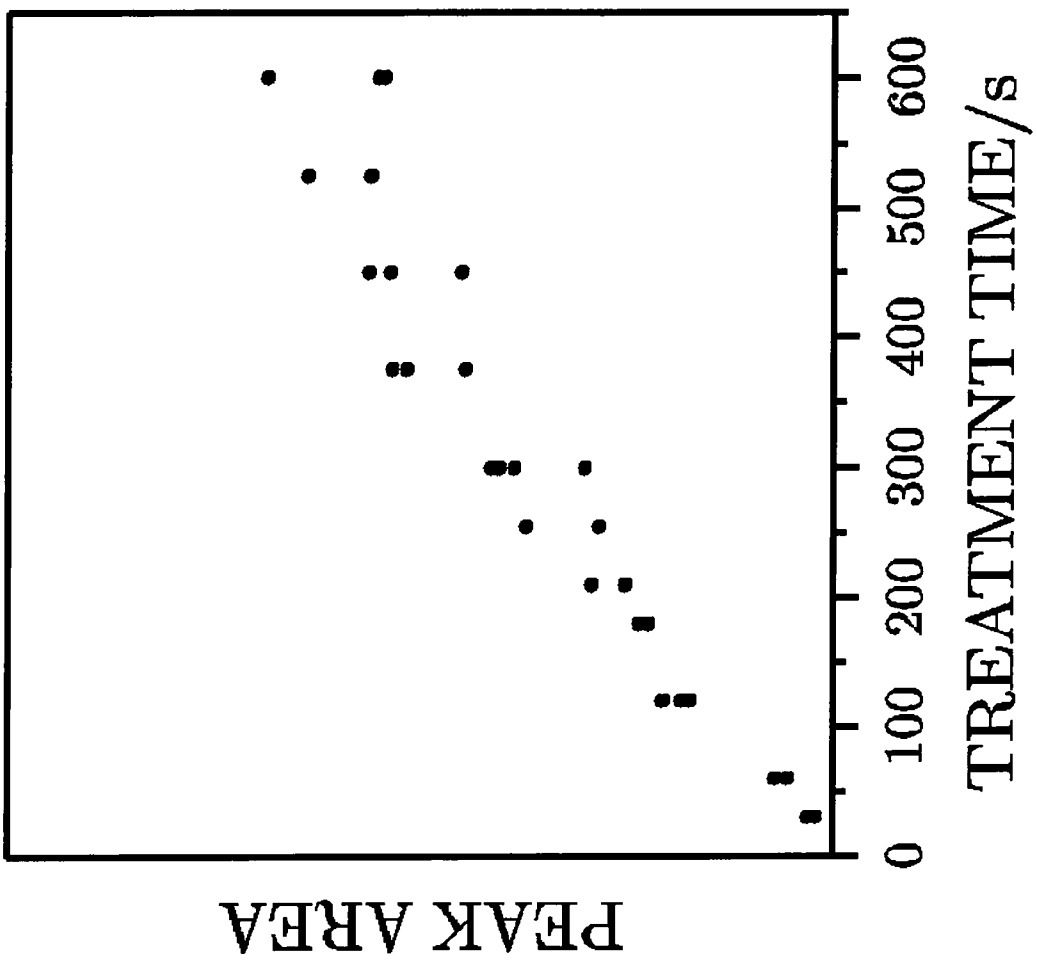

Fig. 4 c Peak areas of the asymmetric nitrate stretching vibration as a function of treatment time in the standard set-up (c: KI)

obtained in a time study of the three salts. The treatment time was varied between 30 and 600 seconds. Although there is a big scattering in the experimental data a saturation behaviour can be observed for KBr and KCl. For KI the saturation behaviour is not as obvious as in the case of the other salts.

A similar evaluation of the oxidised halogen species was not attempted because the transition of the bromate and iodate absorbance into the 825.6/833.3 cm^{-1} signal of nitrate would have rendered the integration too inaccurate. In the case of chlorate the peak areas were too small to obtain meaningful results from the integration of the respective areas. The optical appearance of the spectra, however, showed already that the amount of oxidised halogen species in samples treated for the same treatment times varied strongly. This observation is true for all the salts under consideration.

5.4.1.4 XPS

After being exposed to the X-radiation of the Mg K_α source samples of all three salts showed the formation of colour centres. KBr samples had a blue colour upon removal from the spectrometer, KCl had turned pink and KI faint blue-green. Table 1 summarizes the binding energies of the standards and the untreated halide salts. The BEs are in reasonable correspondence to the values reported in the literature. The BEs of Br ($3d_{5/2}$) in $KBrO_3$ and of iodine I ($3d_{5/2}$) in KI and KIO_3 appear, however, at slightly higher values (0.5-0.8 eV) in the present experiments. The oxygen signal observed in the untreated KI, KCl and KBr discs is most probably related to hydroxide ions formed by the hydrolysis of water molecules at defect sites [8].

A selection of treated samples (30, 60, 120, 600 seconds) of the three halides was measured by XPS but a complete time study using this analytical technique was not carried out. The XPS data provide more evidence for the formation of the nitrate and the oxidised halogen species. The N (1s) signal appears for all the salts studied at a BE of 407.6 ± 0.2 eV, figure 5. This value lies between that measured for the standard sample and the corresponding data of bulk nitrate reported in the literature [29] on the one hand and the value found by Laux et al. (407.2 eV) [6] for surface nitrate on the other. Although a small nitrite signal appears in the IR spectra of treated KI samples a nitrite signal cannot be detected in the corresponding XP spectra. It is possible that the amount of nitrite is not sufficient to give rise to a signal which can

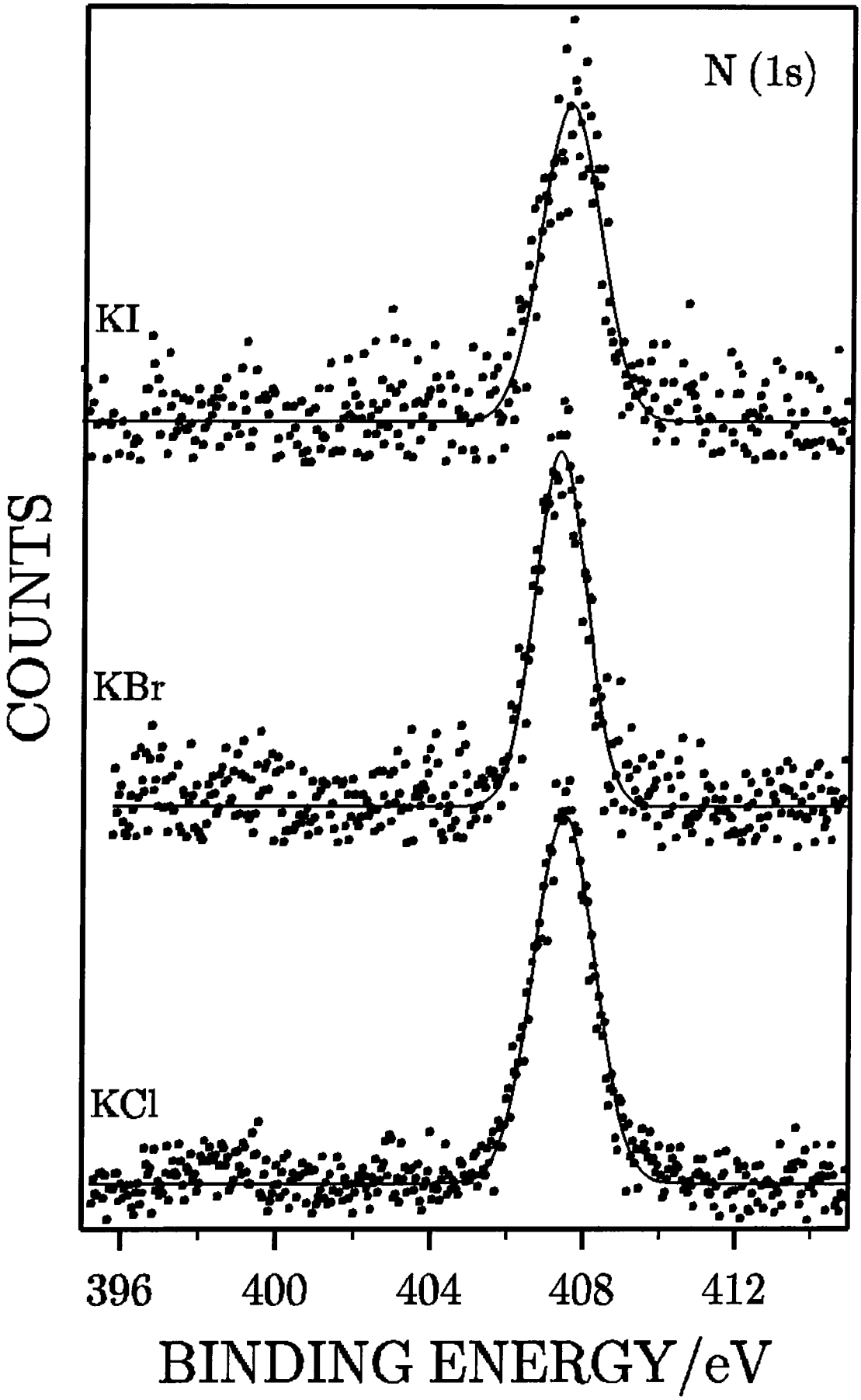

Fig. 5 N (1s) XP spectra of alkali halide disks after 120 seconds silent discharge treatment in the standard set-up

unambiguously be distinguished from the spectral background. The same explanation can be given for the absence of a chlorate signal in the Cl (2p) XP spectra of treated KCl discs. The bromate and the iodate signals of treated KBr and KI samples appear at the expected BE values of 75.3 ± 0.2 eV (Br ($3d_{5/2}$)) and 624.5 ± 0.1 eV (I ($3d_{5/2}$)), respectively, figure 6. The amount of halogenate formed increases in the order BrO_3^- << IO_3^- confirming the findings of the IR spectra. Concerning the amount of halogenate produced in samples of a particular halide treated for the same treatment time, the XPS measurements also confirm the scattering already found in the IR analysis.

Sample	K ($2p_{3/2}$)	N (1s)	O (1s)	Reference
KNO_3	293.5 ± 0.1	407.9 ± 0.1	533.4 ± 0.1	29
KNO_2	293.4 ± 0.1	404.0 ± 0.1	532.9 ± 0.1**	30

Sample	K ($2p_{3/2}$)	Cl ($2p_{3/2}$)	O (1s)	Reference
KCl	293.2 ± 0.1	198.7 ± 0.05	531.7 ± 0.2*	29
$KClO_3$	293. 4 ± 0.05	206.7 ± 0.05	532.8 ± 0.05	31
	K ($2p_{3/2}$)	Br ($3d_{5/2}$)	O (1s)	
KBr	293.2 ± 0.1	69.1 ± 0.1	531.9 ± 0.05 *	31
$KBrO_3$	293.3 ± 0.1	75.5 ± 0.1	531.7 ± 0.2	32
	K ($2p_{3/2}$)	I ($3d_{5/2}$)	O (1s)	
KI	293.3 ± 0.1	619.8 ± 0.1	531.7 ± 0.05*	31
KIO_3	293.0 ± 0.2	624.7 ± 0.2	530.9 ± 0.3	30

* hydroxide component [8]
** water component

Tab. 1 Binding Energies of the standards

The O (1s) envelope of the treated samples falls into two distinct regions, figure 7. No attempt was made to fit the spectra with all the possible components. The contribution on the high BE side which appears at a binding energy of 533.1 ± 0.2 eV represents that of the nitrate oxygen. An additional contribution to this signal

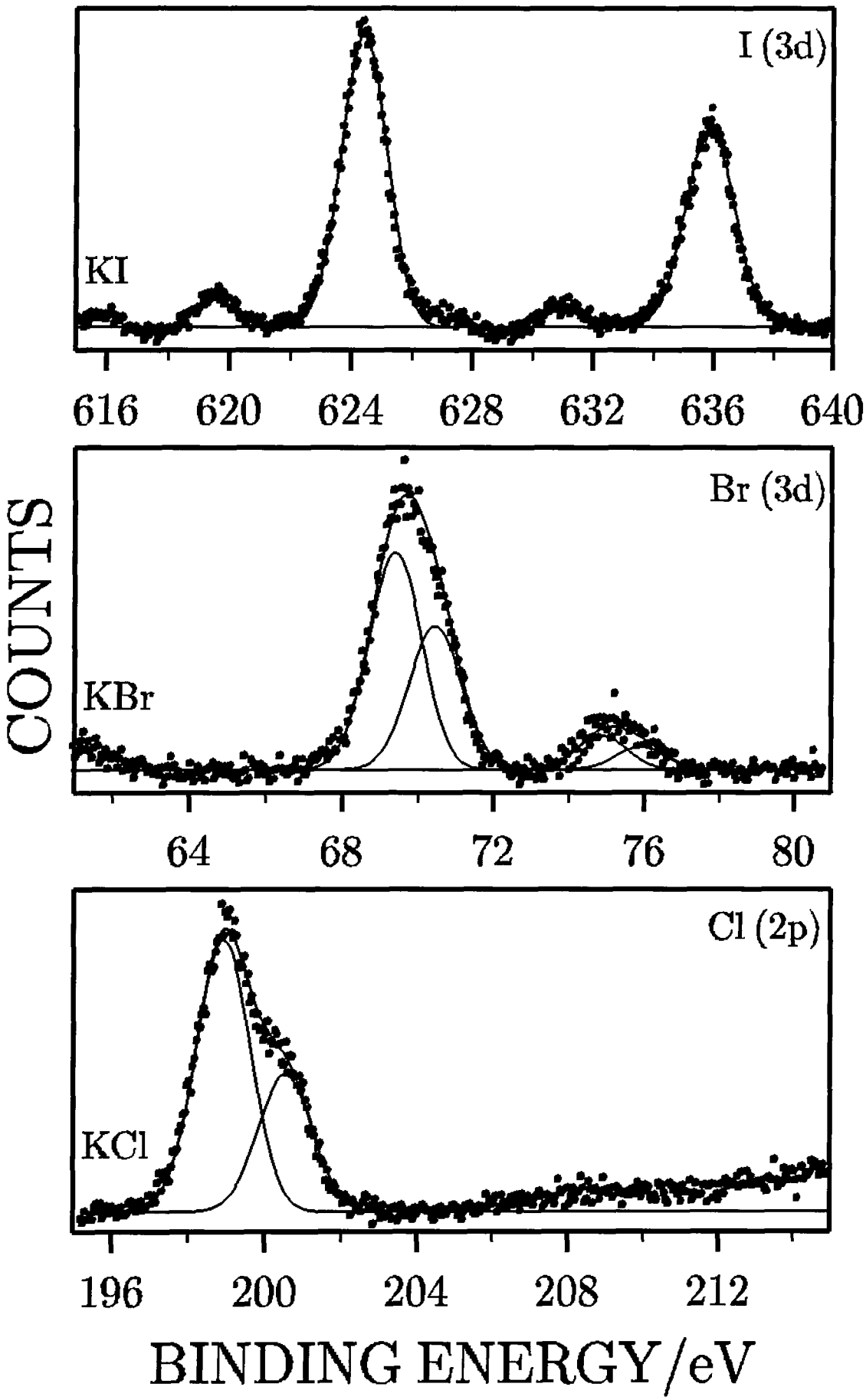

Fig. 6 Halogen XP spectra of alkali halide disks after 120 seconds silent discharge treatment in the standard set-up

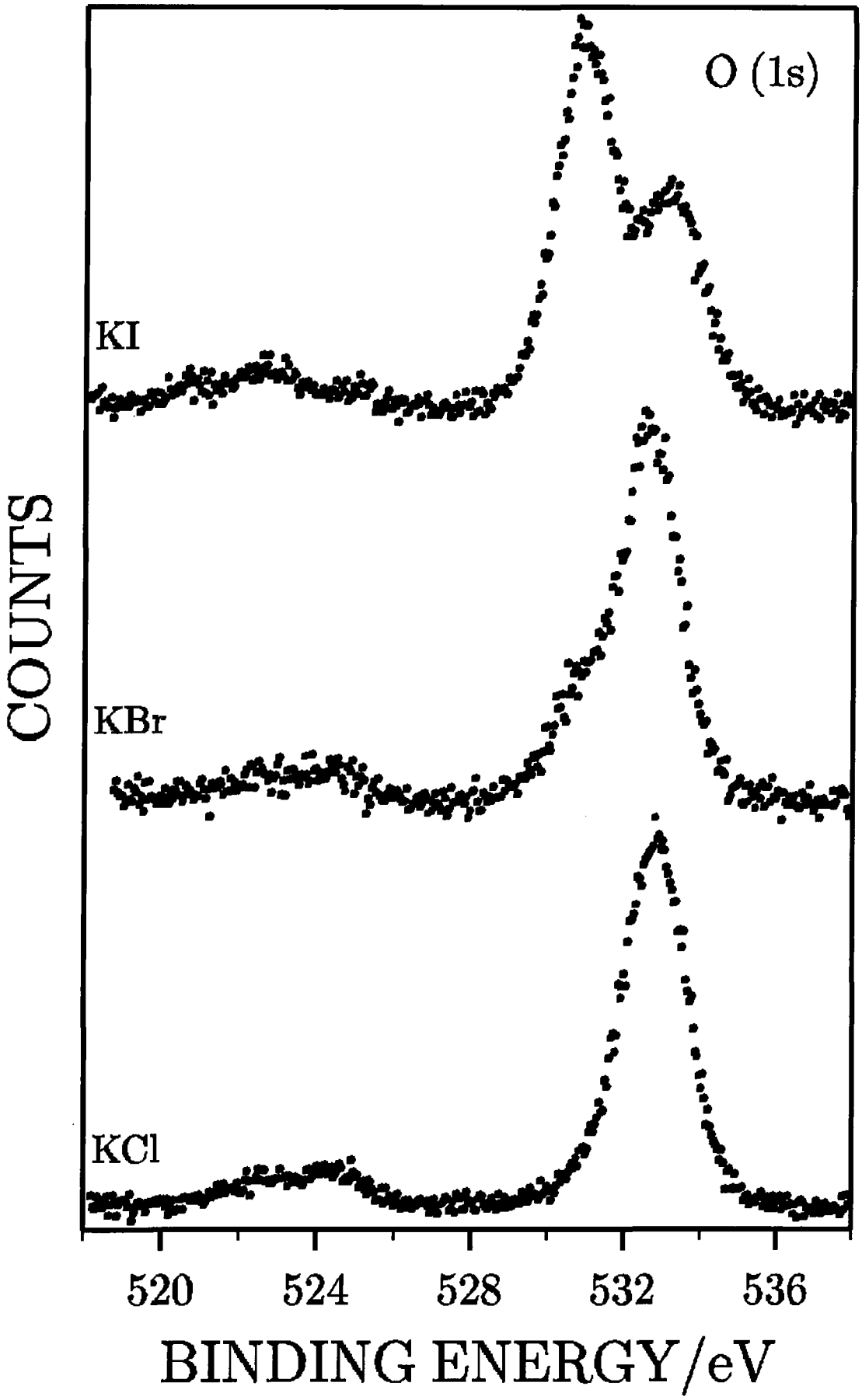

Fig. 7 O (1s) XP spectra of alkali halide disks after 120 seconds silent discharge treatment in the standard set-up

due to adsorbed water cannot be excluded [8]. Apart from the oxygen of the $\underline{X}O_3^-$ group, the low BE component can contain contributions of hydroxide ions formed in the dissociation of water molecules at defect sites on the sample surface [8]. Due to their small BE difference these two components of the oxygen photoelectron signal are likely to overlap.

The halogenate component $\underline{X}O_3^-$ in the Cl (2p) spectra of treated KCl discs was too small to be detected. Therefore, the small shoulder centred at a BE of about 531.5 eV in the corresponding O (1s) spectra can be attributed to hydroxide. In treated KI and KBr discs the signal of the halogenate, $X\underline{O}_3^-$, has to be taken into account as a second contribution. The comparison with the respective halogen spectra, figure 6, which show a large contribution of halogenate, suggests that in the case of KBr and KI the major component of the low BE oxygen peak is that due to $X\underline{O}_3^-$. In accordance with the halogen spectra the intensity of this environment is larger in the case of treated KI discs than in the case of treated KBr samples.

Within the measuring accuracy both the BE and the peak shape of the K (2p) XP spectra are not affected by the modification on the sample surface. The presence of aluminium on the sample surfaces could not be detected.

While IR measurements only allow the determination of the sum of the products, the two sides of the discs can be analysed separately using XPS. Measuring the side which had not faced the discharge, the same products as those detected on the top side, were identified on KBr discs silent discharge treated for 120 seconds. These findings show that the modification takes place on either side of the discs.

5.4.1.5 Change of the nitrate IR signals upon storage in a desiccator

In a further experiment a KCl sample treated for 120 seconds was measured using IR directly after treatment and the analysis of the same sample was then repeated after certain storage intervals in a desiccator, figure 8. Figures 9 and 10 show the corresponding spectra for KBr and KI. In order to illustrate the changes more clearly the spectra are shown on an expanded scale for the asymmetric stretch region of the nitrate ion. In all three cases a change of the peak shape as a function of storage time becomes obvious, a contribution at the high wavenumber side (a') either

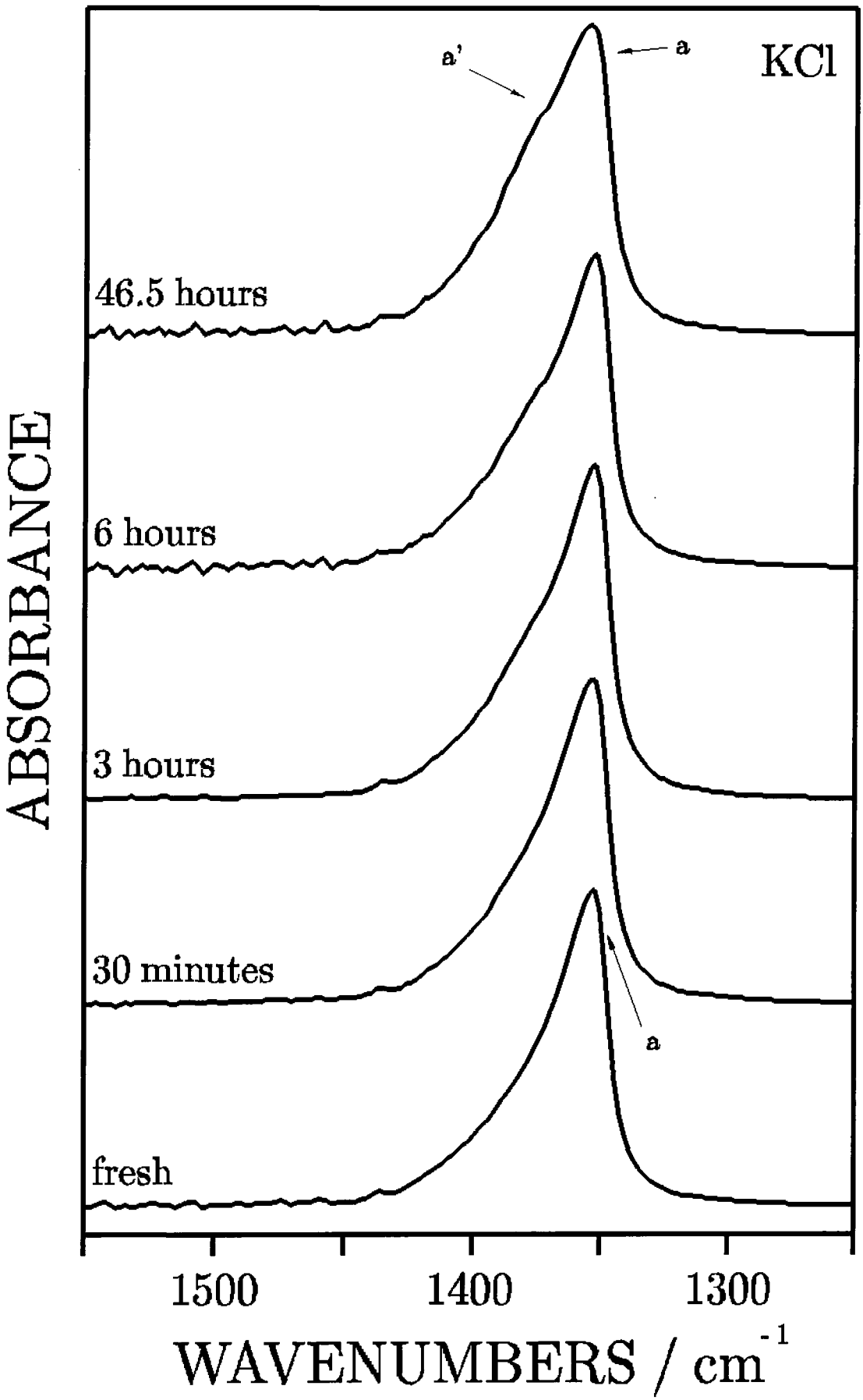

Fig. 8 IR spectra of a KCl disk silent discharge treated for 120 seconds in the standard set-up as a function of storage time in a desiccator

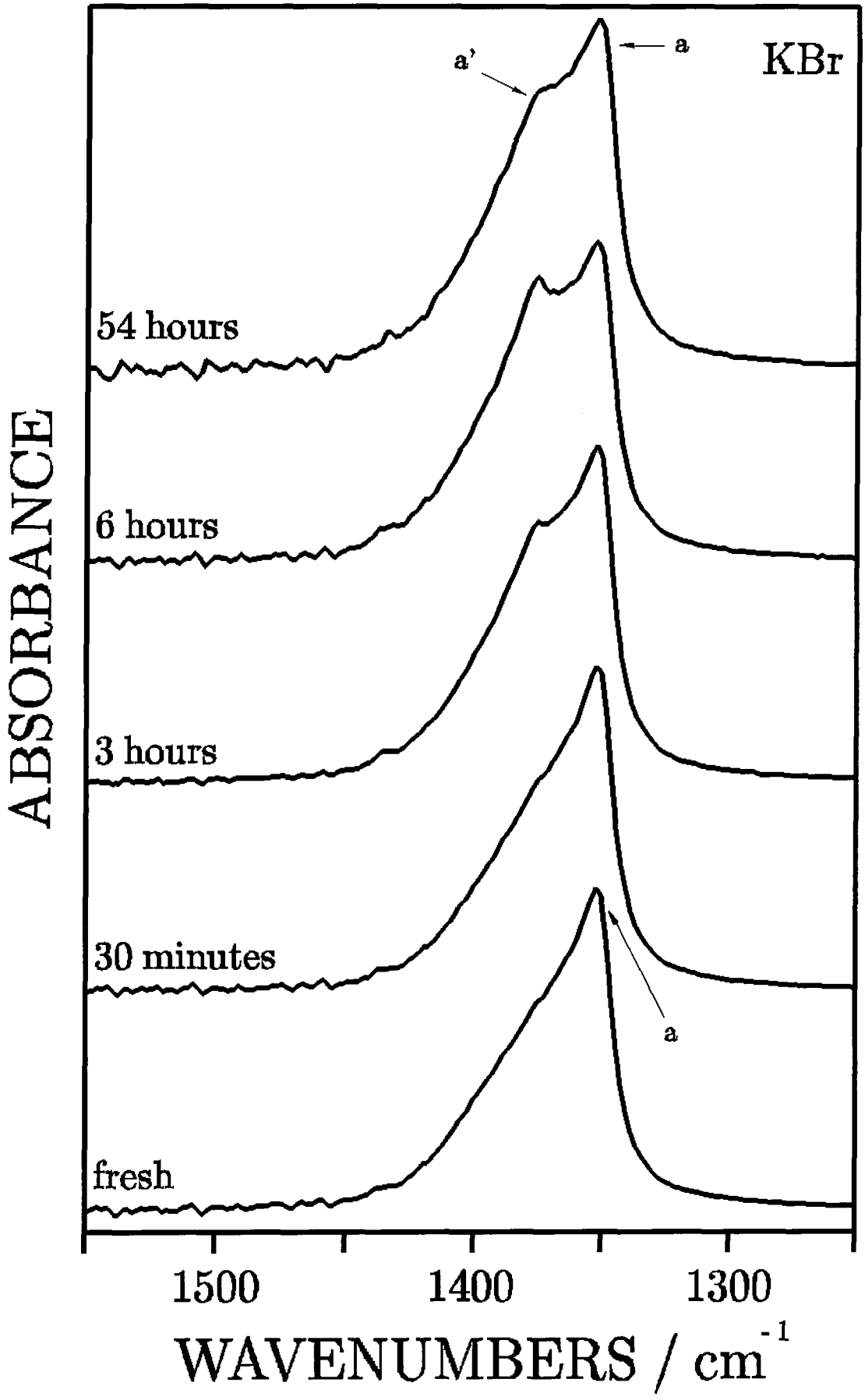

Fig. 9 IR spectra of a KBr disk silent discharge treated for 120 seconds in the standard set-up as a function of storage time in a desiccator

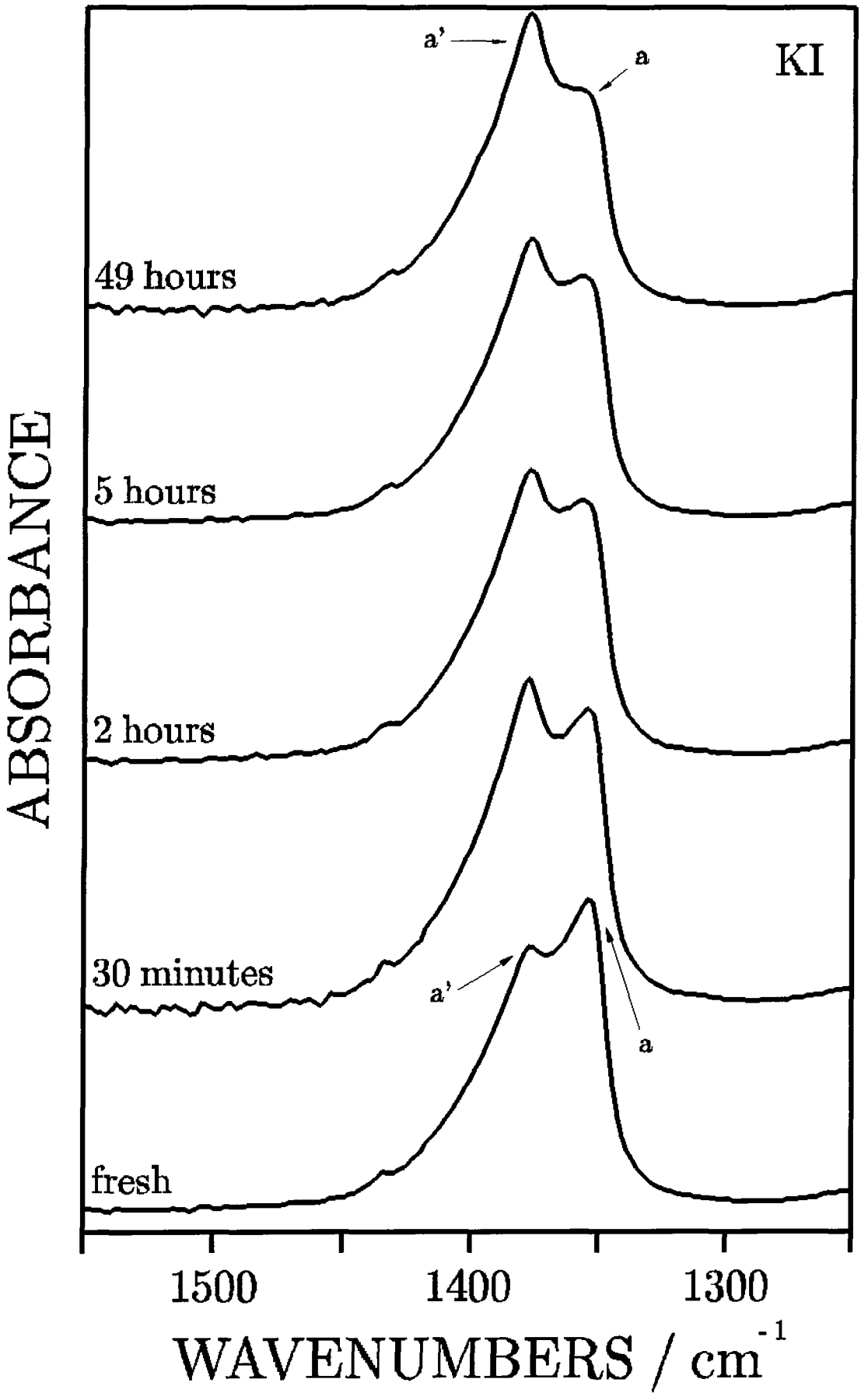

Fig. 10 IR spectra of a KI disk silent discharge treated for 120 seconds in the standard set-up as a function of storage time in a desiccator

appears (KCl) or intensifies (KBr and KI). Difference spectra reveal an increase of a component at 1377.3 cm^{-1} (a') and a decrease of a contribution at 1352.2 cm^{-1} (a) for all the salts studied. Within the measuring accuracy, the area of the envelope remains constant during the experiment which suggests that one species on the sample surface is transformed into another.

The nitrate absorption at 833.3/825.6 cm^{-1} follows a similar pattern as the asymmetric stretching vibration, though in this case it is the lower wavelength component that gains intensity with increasing storage time. The peak positions of the oxidised halogen species remain unchanged. The same applies to the location of the nitrite signal present only on treated KI discs. Since the peak shifts are accompanied by a loss of water, water seems to play an important role for the explanation of this phenomenon.

5.4.1.6 Change of the nitrate IR signals upon exposure to higher temperatures

In order to find out about the changes introduced on the sample surfaces when the water is completely removed the treated discs were exposed to a temperature of 192 °C. This treatment resulted in changes in the peak position and the shape of the nitrate asymmetric stretching and out of plane bending signal as well. The changes induced by this treatment, however, are not uniform as in the case of the storage in the desiccator described in the preceding section. Figures 11 a-c each show the spectrum of a 10 minute silent discharge treated disc before and after heat treatment (1 hour). Figure 11 a contains an additional spectrum of a treated KCl disc exposed to heat for 2 days. The IR spectra are again focused on the wavenumber range of the asymmetric nitrate stretching vibration.

After exposure to heat the main nitrate signal of treated KCl discs appears as a broad envelope consisting of a large contribution on the low wavenumber side and an additional, remarkably sharp peak at 1394.6 cm^{-1} (ax), figure 11 a. In addition to this new signal, difference spectra show a decrease of the initially pronounced component at 1352.2 cm^{-1} (a) and an increase in a contribution at 1369.5 cm^{-1}. The absorbance located at 833.3 cm^{-1} is initially not shifted. A drying time of 1 hour does not cause a change in the nitrate peak areas. After storing the same sample for a further two days in the oven the sharp absorbance at 1394.6 cm^{-1} (ax) is the largest

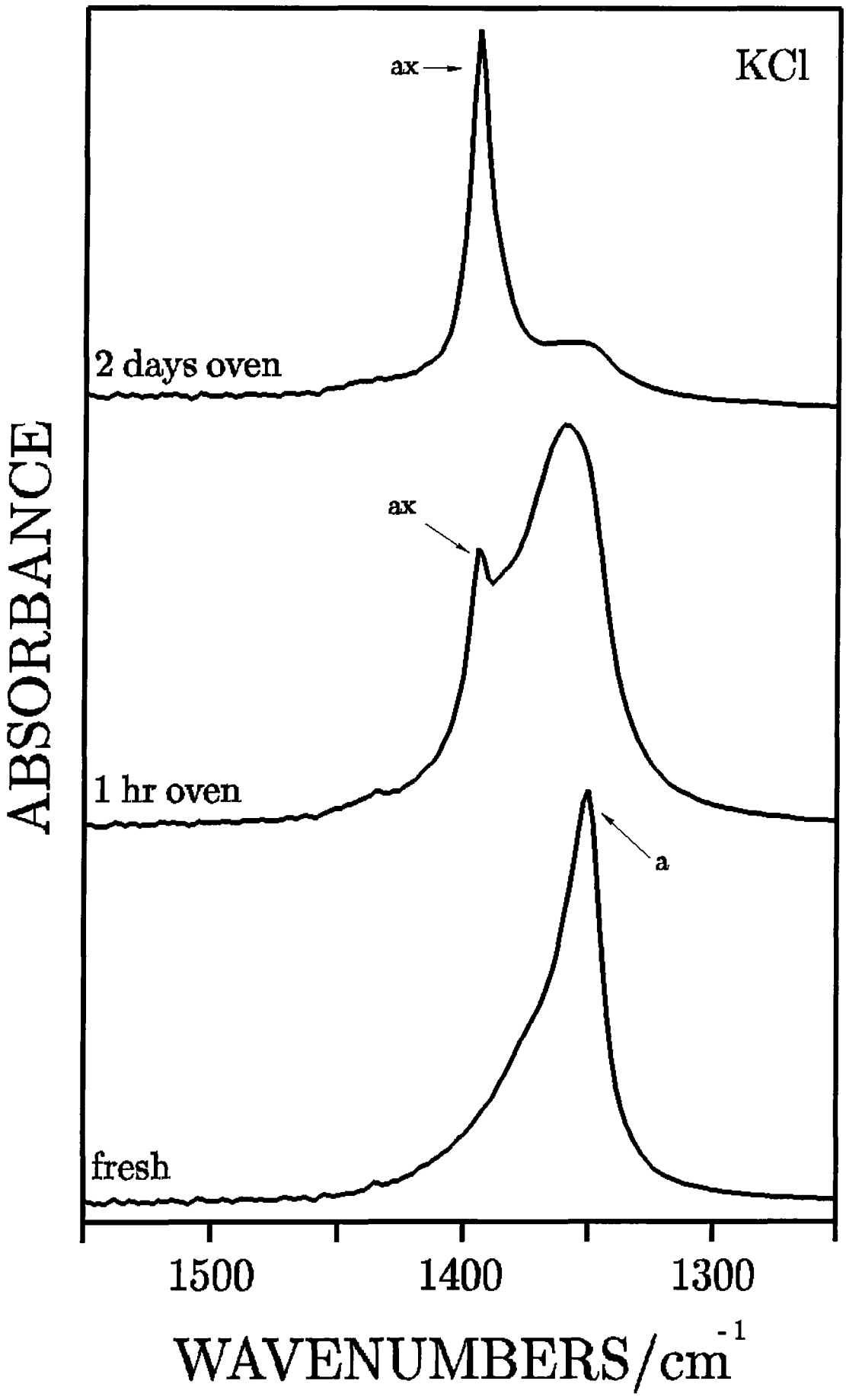

Fig. 11 a IR spectra of a KCl disk silent discharge treated for 600 seconds in the standard set-up before and after heat treatment at 192° C

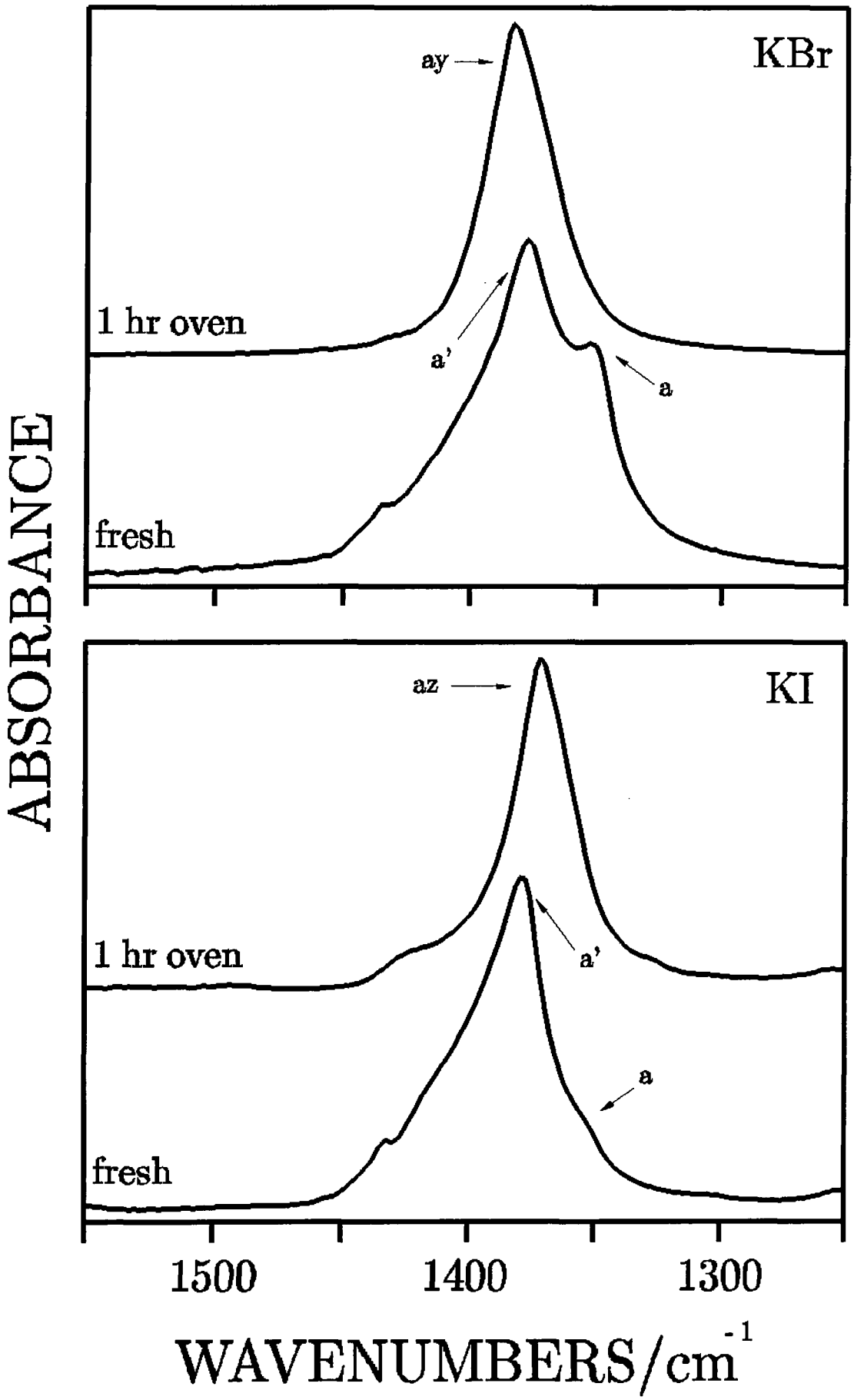

Fig. 11 b,c IR spectra of a KBr (top) and a KI (bottom) disk silent discharge treated for 600 seconds in the standard set-up before and after heat treatment at 192° C

signal in the spectrum and only a small contribution of the original absorbances at lower wavenumbers remains. The out of plane bending vibration now appears as a doublet with contributions at 833.3 and 841.0 cm^{-1}. At the same time, the area of the nitrate asymmetric stretching signal is reduced with respect to its initial area but not to such an extent that the loss can be explained with the volatilisation of the lower wavenumber component. Thus, it seems that at least some of the nitrate species originally contributing to the low wavenumber absorbances must have been transformed into the nitrate species absorbing at higher wavenumbers.

Contrary to treated KCl discs which require a long storage time in the oven for the transition of the nitrate species to occur, the corresponding nitrate species on KBr and KI samples are transformed within one hour. The asymmetric stretching vibration of treated KBr samples shows a complete shift to a single sharp signal centred at 1383.0 cm^{-1} (ay), figure 11 b, and the out of plane bending absorbance appears at 837.2 cm^{-1}. In contrast to the other two halides studied, the nitrate asymmetric stretching signal of treated KI samples appears shifted to a lower wavenumber after heat treatment, the peak initially located at 1379.2 cm^{-1} (a') being shifted to 1371.5 cm^{-1} (az), figure 11 c. There is a simultaneous shift of the out of plane bending absorbance initially centred at 825.6 cm^{-1} towards the opposite direction of a wavenumber of 837.2 cm^{-1}. The position of the nitrite signal at 1253.8 cm^{-1} is not affected by the heat treatment.

The halogenate peak positions are not shifted in the case of chlorate and iodate; bromate appears as a signal with a sharp maximum at 794.2 cm^{-1}. While the areas of iodate remain unchanged within the accuracy of the integration procedure, those of bromate and chlorate are reduced after the treatment.

The exposure of a 120 second silent discharge treated KBr disc to 145 °C did not lead to considerable changes in the nitrate peak shape in time intervals during which the treatment at 192 °C had caused the signals to shift completely.

5.4.1.7 Deposits on the PE surface

After the treatment of the KI discs the surface of the PE foil of the standard set-up was covered with a brown deposit at the location where the disc had been placed. This deposit could be easily wiped off with a tissue sprayed with IPA. Both

the PE film covered with deposit and the surface of the wiped PE foil were measured employing ATR-IR and XPS. For reasons of comparison PE foils on which KBr and KCl discs had been placed during treatment were also analysed although they did not show a visible change on their surface when the treated discs were removed. In all cases the treatment time was 600 seconds.

Figure 12 shows the ATR-IR spectra of the deposit on PE after KI treatment and after wiping the foil with IPA. In addition to the characteristic absorbances of PE (see section 3.4.3) the IR spectrum of the deposit contains signals at 3420.0, 1709.0 and 1643.5 cm^{-1} (x) as well as a conspicuous broad signal at 781.2 cm^{-1} (*). Despite the absence of potassium, the XP spectrum of the deposit reveals the presence of iodine in a high oxidation state, the I ($3d_{5/2}$) component appearing at a binding energy of 625.5 eV. The small additional component located about 3.5 eV towards the lower binding energy side of the main signal is most probably due to iodine. It is not possible to establish whether iodine is already present on the sample surface or whether it is formed in a decomposition process from the primary iodine compound under x-ray exposure, a difficulty reported to be often encountered in XP spectroscopy of iodine compounds [33]. Since an alternative metal cation could not be detected in a XPS widescan, only H^+ which cannot be identified by this technique remains as a possible counterion. This observation suggests the presence of iodic acid (HIO_3) on the surface of the PE foil. The broad and unresolved IR signal at 781.2 cm^{-1} is in the region of the iodate absorbance. There are, however, no further similarities to the spectra of treated KI discs in which the absorbances are sharp and correspond well to the KIO_3 reference spectrum in the literature [28]. Although the main absorbances of HIO_3 are located within the wavelength range of the broad signal [34,35] an unambiguous identification of HIO_3 from the IR spectra is not possible. The spectrum does, however, also not represent a contradiction to this attribution.

The C (1s) XP spectrum consists of an envelope with contributions at higher BE of the main C-H peak at 285.0 eV due to the presence of oxidised carbon species. Since iodic acid has no IR absorbances in the area of the three remaining signals [34,35] and since these absorbances are located in an area typical for carbonyl and hydroxyl groups, these signals are attributed to oxidised carbon species [36]. Furthermore, the presence of unsaturated products is also possible [36,37]. The products absorb,

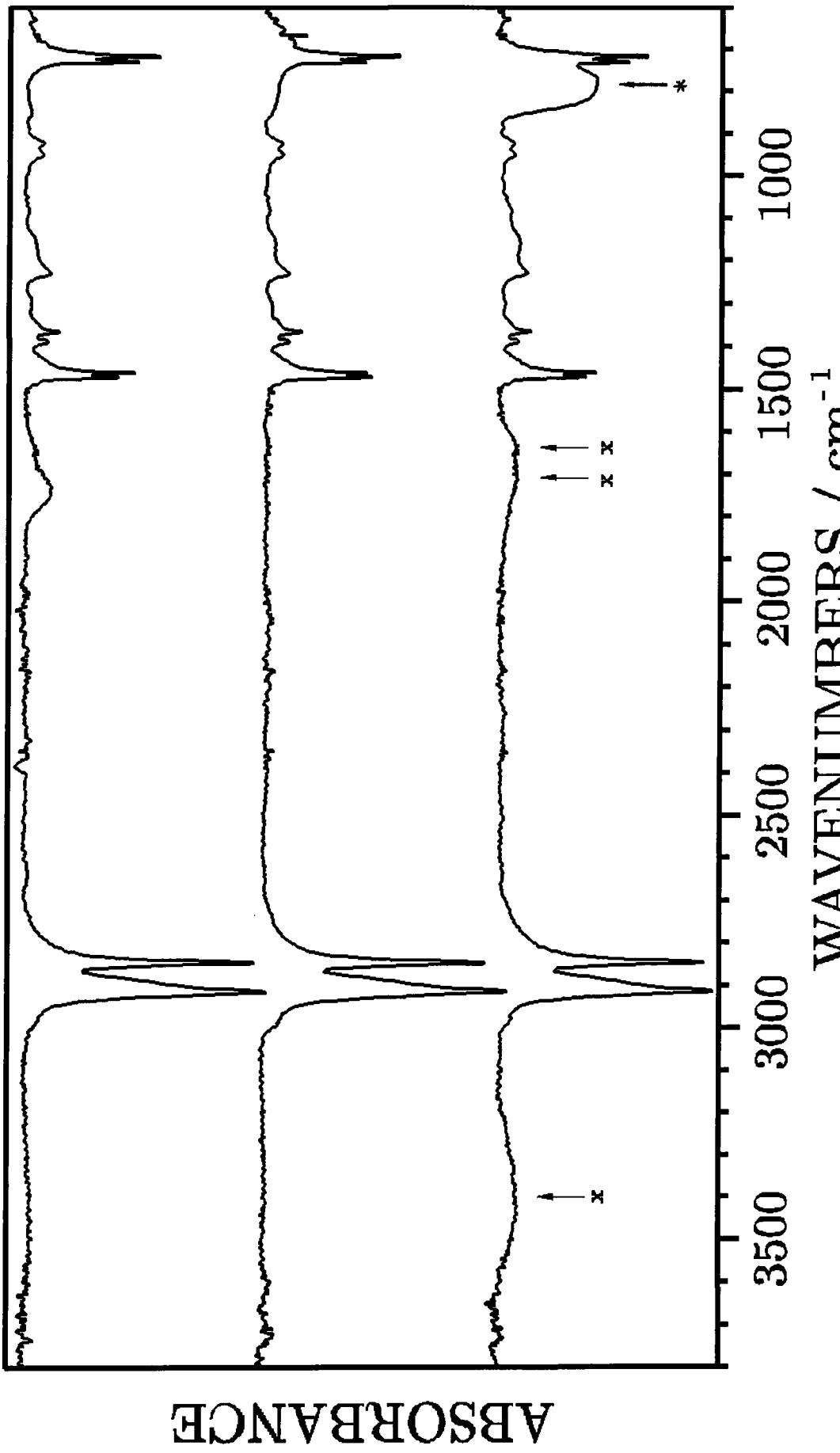

Fig.12 IR spectra of the deposit on PE after KI treatment (bottom), the wiped PE foil (middle) and 10 minute silent discharge treated PE (top)

however, at slightly different wavelengths than those obtained by direct silent discharge treatment of a PE sample, which is shown as the top spectrum in figure 12.

Both the IR (figure 12, middle) and the XP spectra of the wiped PE foil correspond to those of the untreated polymer. Thus, the deposit is removed in the wiping step. A spectrum of untreated PE is not included in figure 12 in order to keep its information content clear.

Apart from the XP signals already mentioned a small nitrogen signal which could be due to traces of nitric acid was detected as a further component of the deposit on PE after KI disc treatment.

The ATR-IR spectra of the PE foils after KBr and KCl treatment show no additional signals except those of oxidised carbon species. In both cases there are no deviations in the peak positions from those of silent discharge treated PE. Wiping with IPA leads to the removal of the oxidised species. Apart from the presence of the high BE shoulder of the oxidised carbon moieties, only small amounts of bromine together with traces of nitrogen are detected in the XP spectra of PE foil on which the treatment of KBr had taken place. PE films which had served as the dielectric for KCl treatment show only oxidised carbon species but neither a chlorine nor a nitrogen signal when analysed with XPS.

5.4.2 Treatments in the flow cell

Ambient air, the feed gas of the standard set-up, is a complex mixture with varying amounts of water vapour. In order to provide more defined reaction conditions for the treatments in air and to study the reaction behaviour of the potassium halides in gases other than air experiments were carried out in the cell set-up.

5.4.2.1 General observations

In the flow cell the discharge consisted of a homogeneous glow as long as dried feed gas was used. As soon as the feed gas was passed through the water bubbler the discharge changed its appearance and became similar to that described for the standard set-up. The extent of discharge concentration to the edges of the

discs, however, was considerably stronger in this instance, leading to pronounced electrode corrosion. It became obvious on the top electrode in form of a more or less complete white ring of the disc diameter. This white material is most probably due to aluminium oxide [38]. The changes in the discharge appearance were observed independent of the type of feed gas.

Since the set-up is closed colour changes of the samples during the treatment could not be seen.

5.4.2.2 IR and XPS

If not mentioned otherwise, the treatment time in the cell experiments was 600 seconds at a "flow speed" of the feed gas of 80 gas bubbles/minute. The analysis of the treated samples was carried out with transmission IR. Samples treated in humidified oxygen and humidified air atmospheres were additionally analysed with XPS. Table 2 summarizes the most important qualitative results obtained in the measurements.

Gas	Nitrate	Nitrite	Oxidized halogen species
Dried air	+ *	–	+ *
Dried oxygen	–	–	+ *
Humidified air : KCl, KBr	+	–	+**
KI	trace	+	+
Humidified nitrogen	trace	–	–
Humidified oxygen	–	–	+
Humidified helium	–	–	–

* small amount

** detected only by IR

Tab. 2 Qualitative overview over the products formed in the cell experiments (+ denotes the presence, – the absence of a component)

Irrespective of the type of feed gas used, water was lost from the sample surfaces in treatments with dried feed gas, whereas an uptake of water was found in the case of experiments carried out in the presence of humidified feed gas (signal h in figures 13 and 15). As far as the products are concerned there are some differences between the results obtained in the standard set-up and in the cell set-up when air is used as the feed gas. In most cases nitrate and the oxidised halogen species are formed on the KCl and KBr discs as a consequence of the plasma exposure. Sometimes the halogenate is, however, not detected by IR following treatments in dried feed gas. Different results are obtained in the IR and XPS analysis of KCl and KBr samples treated in humidified air. While the IR spectra show the presence of the halogenate in both salts where the amount of chlorate formed is smaller than that of bromate, the halogenate signals are missing in the corresponding XP spectra. KBr thus shows a different behaviour compared to the treatments in the standard set-up.

The peak positions in the IR spectra of the products obtained in the cell are comparable to those of the products obtained in the standard set-up. Figure 13 shows a comparison of the IR spectra of the three salts after silent discharge treatment in the cell set-up using humidified air as the feed gas. Cell treatments in humidified air result in the formation of a considerably larger amount of both products than cell treatments in dried air. This observation suggests a strong influence of water vapour on the modification of the discs.

In KCl and KBr samples treated in humidified air, the N (1s) XP signals, figure 14, and the O (1s) envelopes appear at a slightly lower BE than the equivalent signals of samples treated in the standard set-up.

KI shows the largest differences of the three halides in comparison to its behaviour in the standard set-up. A comparison of the IR spectra of a KI sample treated in dried air and a KI sample treated in humidified air is shown in the lower half of figure 13. Using dried air, nitrate is the only nitrogen containing product detected, whereas the treatment in humidified air results predominantly in the formation of nitrite. Since the nitrate asymmetric stretching signal is likely to overlap with a broad nitrite signal [25,28] the nitrate out of plane bending signal at 833.3/825.6 cm^{-1} is taken as the band indicative of nitrate on these samples. Since this signal is hardly discernible from the spectral background it can be assumed that only traces of nitrate are present in KI discs treated in humidified air. The

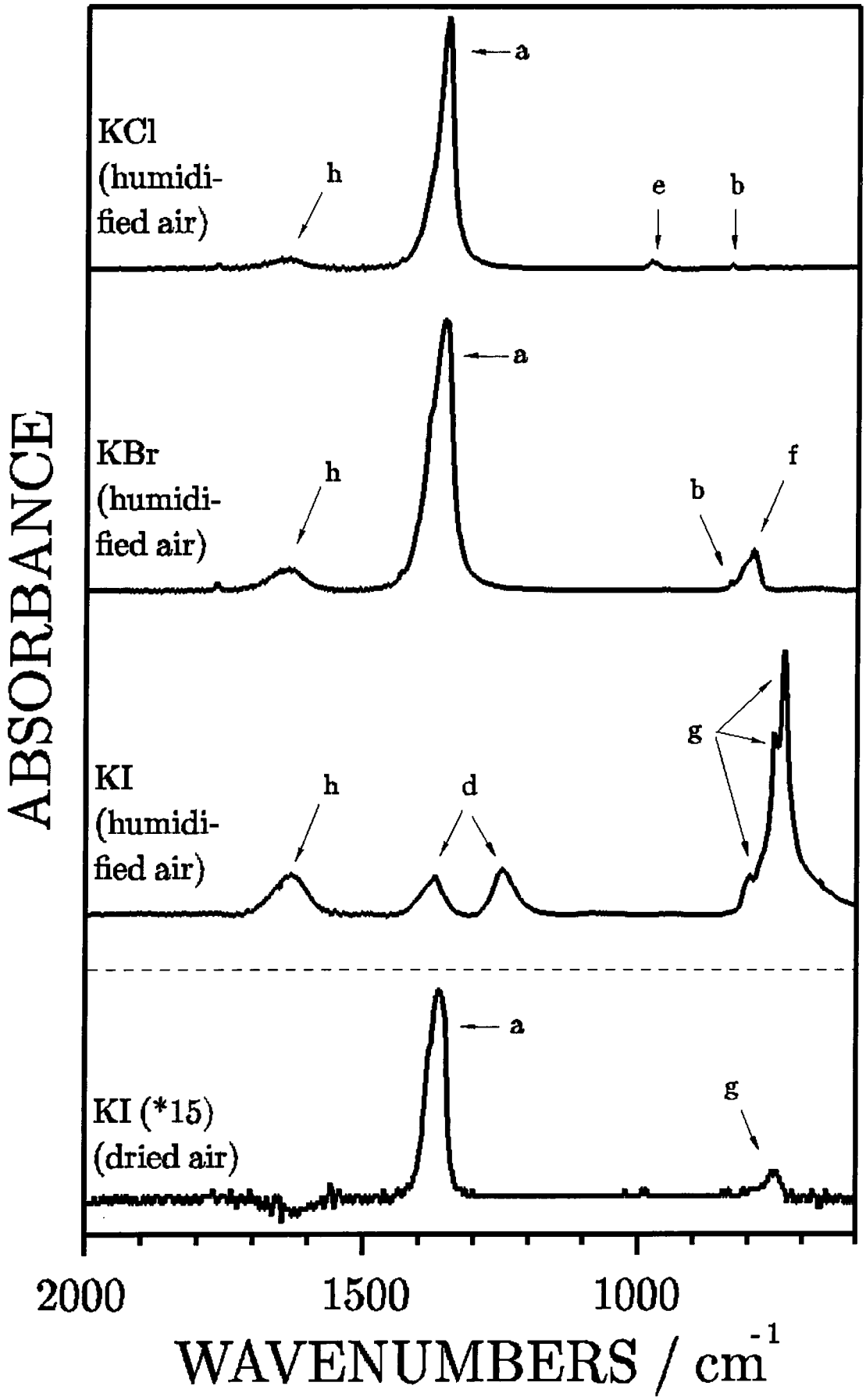

Fig. 13 IR spectra of alkali halide disks after 600 seconds silent discharge treatment in the cell set-up using air as the feed gas

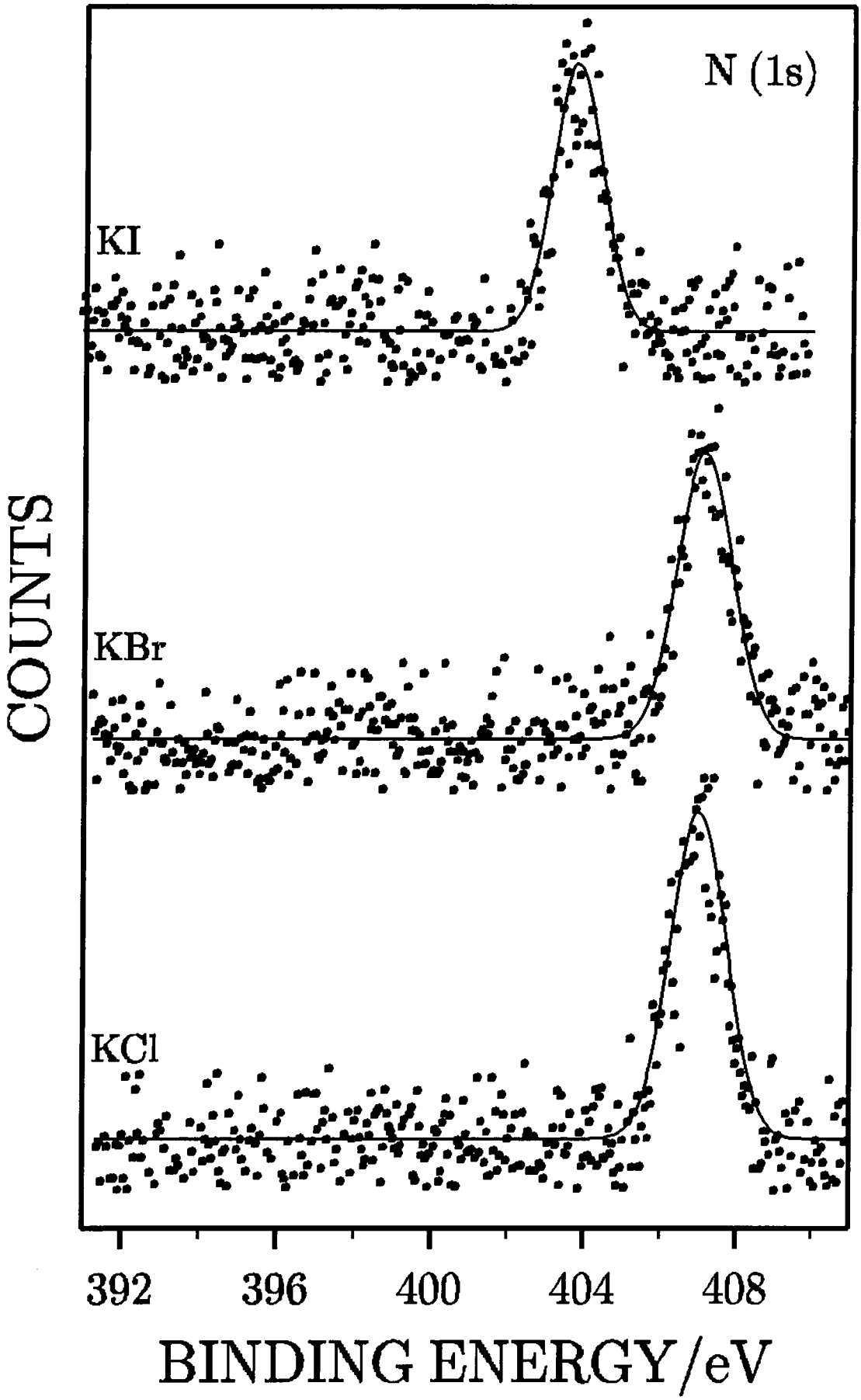

Fig. 14 N (1s) XP spectra of alkali halide disks after 600 seconds silent discharge treatment in the cell set-up using humidified air as the feed gas

corresponding XP spectra confirm this suggestion. Using this technique only nitrite is detected, the N (1s) signal appearing at a BE of 403.7 ± 0.08 eV, figure 14. In addition to the nitrogen species the formation of iodate is observed after treatments in dried and humidified air. As in the case of the other two halides studied, the amount of the products increases when the treatment is carried out in humidified feed gas.

A time study in which KBr discs were treated in dried air for treatment times between 5 and 15 minutes while keeping the flow speed of the gas constant (80 bubbles/minute) did not lead to reproducible amounts of both products. In another row of experiments in which KBr discs were treated for 10 minutes while the flow speed of humidified air was varied from static conditions (0 bubbles/minute) to a flow speed of 200 bubbles/minute, the scattering of the data obtained was also too strong to derive a meaningful trend.

Treatments in an oxygen atmosphere result in the exclusive production of the oxidized halogen component. Figure 15 compares the IR spectra of the three halides obtained after treatments in humidified oxygen. As in the case of air, the product yield is considerably enhanced when the treatment is carried out in humidified feed gas, which shows that the influence of water vapour is not limited to the treatments in air. An example of the treatment of KI in dried and humidified oxygen is shown in the lower half of figure 15. The order in the amount of halogenate formed in the three halides corresponds to that found in air: $IO_3^- > BrO_3^- > ClO_3^-$. The same conclusion can be drawn from the halogen XP spectra of samples treated in humidified oxygen, figure 16. In contrast to the experiments in air the treatment of KCl samples in humidified oxygen causes the formation of sufficient chlorate to give rise to a small XP signal. It appears as a weak shoulder at a BE of about 206.7 eV on the high BE side of the main Cl (2p) environment which is due to chloride. A nitrogen signal is absent in the XP spectra of samples of all three halides treated under those conditions.

In order to find out whether water vapour in the presence of an inert gas leads to the production of the halogenates, the salts were treated in humidified helium. The only change observed after this treatment consists in the uptake of water. Treatments in humidified nitrogen lead to the formation of very small amounts of nitrate on the

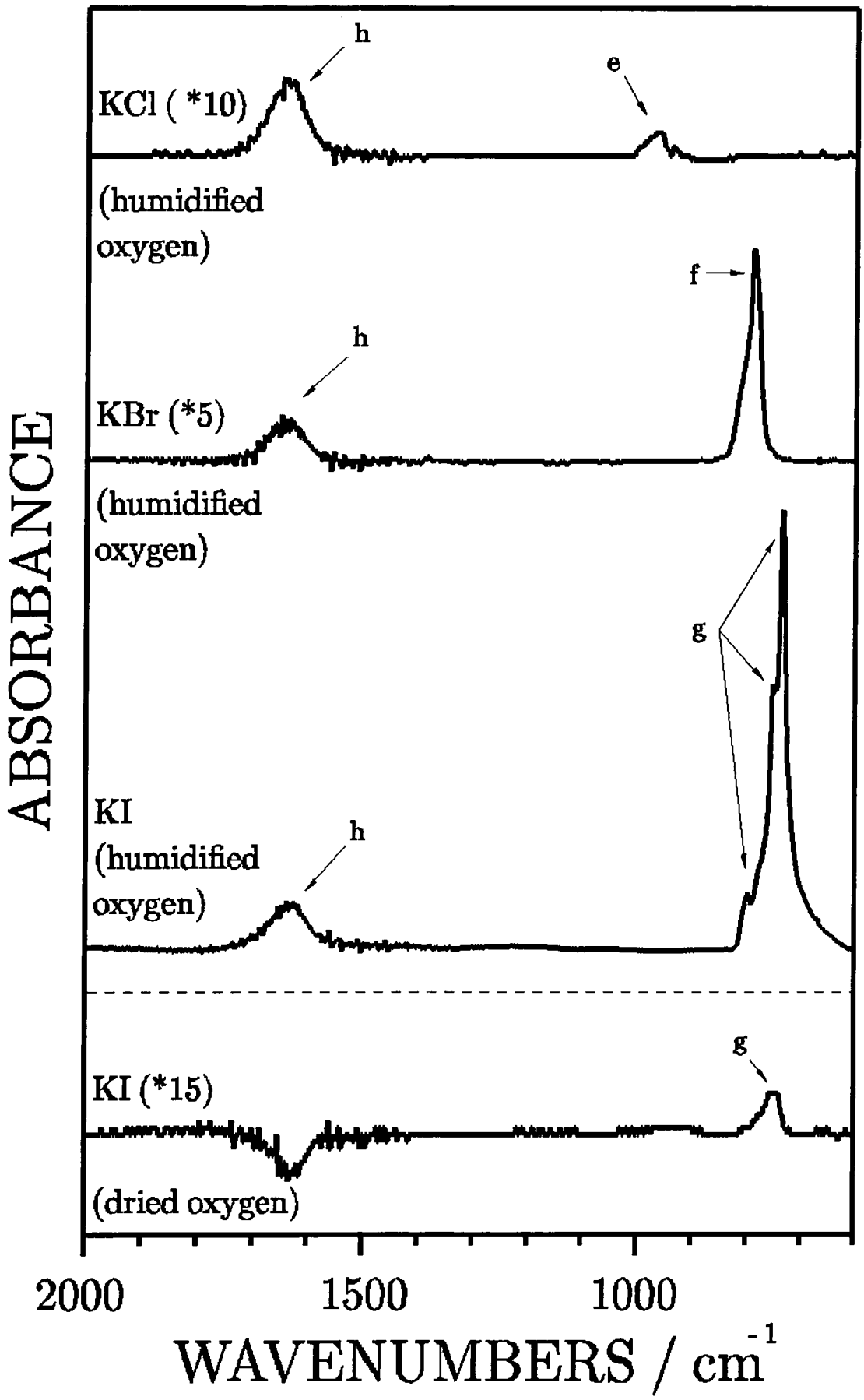

Fig. 15 IR spectra of alkali halide disks after 600 seconds silent discharge treatment in the cell set-up using oxygen as the feed gas

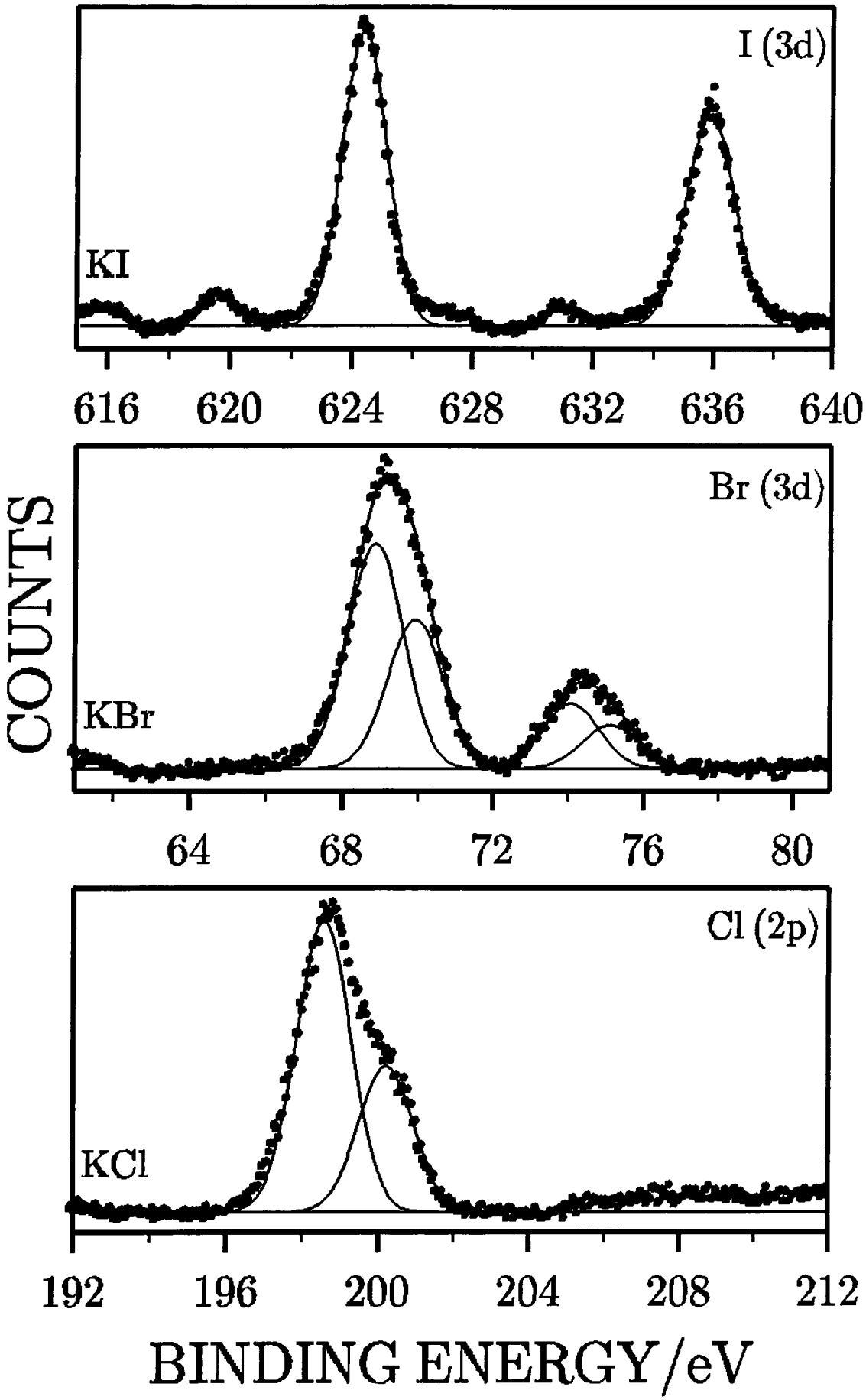

Fig. 16 Halogen XP spectra of alkali halide disks after 600 seconds silent discharge treatment in the cell set-up using humidified oxygen as the feed gas

three salts under consideration. This finding suggests that water is not a significant oxygen source for the formation of N-oxides.

5.5 Discussion

In comparison to the model reactions in 5.2.2 which describe the reactions of an alkali halide with a single nitrogen oxide, the conditions of the silent discharge treatments are much more complex because both the reactions with a gas mixture and the influence of the plasma on the sample surface have to be taken into account. The findings of the model reactions can therefore only be taken as a guideline for the interpretation of the results obtained in the silent discharge treatments.

Combining the information of chapters 1.5.1.2 and 5.2.2 the nitrate species formed during the silent discharge treatment of alkali halide discs in air can be explained with the reaction of the salts with the nitrogen oxide mixture produced in the plasma. During the experiments a discharge poisoning which would have been obvious in a colour change of the processed gas to brown was not observed. The low nitrogen oxides which are produced in considerable amounts only under these conditions are therefore unlikely to play an important role in the formation of the nitrate species. N_2O and N_2O_5, the latter being transformed into HNO_3 in the presence of humidity, are the predominant N-O products formed under normal operation conditions in the silent discharge. Since a reaction of N_2O with alkali halides seems to be unlikely HNO_3 remains as the most likely reactant to form the nitrate species. It is difficult to establish which nitrogen species reacts in the case of the cell treatments in dried air. N_2O_5 is produced in the gas volume. Since the discs are prepared in ambient air and are not dried prior to the treatment their surface is covered with a layer of adsorbed water (see below). It is therefore possible that N_2O_5 is transformed into HNO_3 upon contact with this layer before reacting with the halide.

The possibility that the volatile products of the reactions take part in the discharge chemistry cannot be excluded but it is difficult to assess their influence on the overall plasma process. Information concerning this question could probably be obtained by including the products in question and their elementary reactions into existing computer simulation programs for the N_2/ O_2/ H_2O system. Such an analysis

would be especially interesting in the case of the KI discs which show the strongest modification after the treatment. It is also the only halide on which nitrite is detected as an additional product and its formation could possibly be related to a change in the discharge chemistry.

Since the presence of HNO_3 has not been mentioned to cause the formation of halogenates despite it being a powerful oxidant, oxygen species must be responsible for halogenate formation. Possible candidates are ozone, atomic oxygen, hydroxyl radicals and hydrogen peroxide. The latter two species are only formed in gas environments containing water vapour. A contribution of all species together cannot be completely excluded.

It has been reported that the ozone yield is drastically reduced in cases where ozonisers are fed with humid feed gas (section 1.5.1.3). Since more oxidised halogen species is, however, produced in experiments carried out in the presence of water vapour, ozone is very unlikely to be the key oxidant in these experiments. This assumption can also be made for the reactions in the absence of water vapour because ozone was found not to react with dried NaCl [1,39].

The decrease in the amount of halogenate products from iodate to chlorate reflects the electronegativities of the halogens which follow the order EN (Cl) < EN (Br) < EN (I) where the difference is larger between bromine and iodine than between chlorine and bromine [40]. Iodine as the most electropositive of the three elements has therefore the strongest tendency to form bonds with the electronegative oxygen and hence produces the largest amount of XO_3^-.

Irrespective of the experimental conditions, reproducibility in the amount of the products could not be achieved except for the amounts of nitrate formed in the standard set-up which allowed at least a trend to be determined. There are two possible reasons for the scattering of the data in the experiments using the standard set-up. These are the varying humidity of ambient air and varying amounts of defects on the discs. The humidity influences the discharge chemistry and thus the composition of the reacting gas mixture which might lead to the formation of varying amounts of products. Defects are centres of high reactivity in the reactions of the halides with nitrogen oxides [21]. N-oxides are therefore very likely to react at those sites. Since the chemical reaction is accompanied by the formation of new surface

defects [13] it is conceivable that variations in the number of defect sites initially present on the sample surface finally lead to variations in the amount of products obtained. Defect sites may be introduced to the discs during sample preparation. It is not possible to give a statement concerning their number. The literature only provides the information that the pressure exerted on the alkali halide powder during disc preparation causes the formation of "single crystal like" discs via cold flow. The similarities and differences between the discs and single crystals, however, are not further described [36,37].

In the cell experiments with dried feed gas the variations in the amount of defects on the sample surface are likely to play the key role in the development of irreproducible results. In this case the small amount of products has also to be taken into account which causes a comparatively large error in the evaluation. In the cell experiments in which humidified feed gas was used, an extreme discharge concentration on the edges of the discs was observed. It is therefore possible that the inhomogeneity of the discharge led to variations in the composition of the treated gas and thus to the variations in the amount of the products formed.

Both longer treatment times in the standard set-up and the storage in the desiccator represent experimental conditions which cause an increase in the intensities of the 1377.3 cm^{-1} (a') component of the asymmetric stretching and the 825.6 cm^{-1} (b') component of the out of plane bending vibration in the IR spectra. This observation suggests that there is an increase in the same product in the two processes. A tentative explanation can be given in terms of the model developed by Beichert and Finlayson-Pitts for the reaction of HNO_3 with NaCl [21]. It assumes that the adsorption of water molecules from humid air leads to the formation of a surface adsorbed water layer on the salt surface. As a first approximation this layer is considered to possess the characteristics of a saturated solution of the respective halide [21]. Nitric acid is taken up in this layer. The more HNO_3 molecules are dissolved the lower the pH and the higher the concentration of the nitrate ions. Once the layer is sufficiently acidified HCl, one product of the reaction, degasses from the layer. $NaNO_3$, the other product of the reaction, is precipitated onto the salt surface as soon as its solubility in the layer is exceeded. Applying this model to the present experiments the absorbances at 1377.3 cm^{-1} (a') and 825.6 cm^{-1} (b') can be attributed

to crystalline KNO_3 while those appearing at 1352.2 cm^{-1} (a) and 833.3 cm^{-1} (b) are due to dissolved nitrate. It can be assumed that supersaturation of the adsorbed water layer and the ensuing crystallisation of KNO_3 occurs in both cases named above. The reason for the supersaturation is, however, different. As the treatment time increases more nitrate is dissolved in the the surface layer. Once the saturation is reached precipitation of potassium nitrate starts and nitrate subsequently introduced to the layer is also precipitated. This explains the increasing contribution of the absorbances related to the crystalline nitrate form to the IR spectra with increasing treatment times. Vogt and Finlayson-Pitts [5] have made a similar observation in the reaction of NaCl with NO_2. With increasing extent of the reaction the authors found the development of a signal which they attributed to growing $NaNO_3$ microcrystallites.

Comparing the asymmetric stretching signals in the IR spectra of samples of the three halides treated for the same treatment time, the contributions of the crystalline nitrate form increases in the order: KCl < KBr < KI. This could be explained by the influence of the halide dissolved in the water layer on the precipitation of the nitrate. Generally, the solubility of a salt in an aqueous solution is reduced in the presence of another salt which contains ions of the salt to be precipitated [41]. This is due to a shift of equilibrium towards the insoluble compound. In the present case the equilibrium to be considered is:

$$K^+(aq) + NO_3^-(aq) \leftrightarrow KNO_3$$

The solubilities of KI, KBr, KCl and KNO_3 in cold water are 7.7; 4.5; 3.7 and 1.3 mol/l (127.5; 53.5; 27.6 and 13.3 g/100 cm^3) respectively [42]. KI therefore forms the most concentrated solutions and is able to provide most potassium ions to shift the equilibrium towards the formation of the precipitated nitrate, thus giving rise to a large proportion of the high wavenumber component in the asymmetric stretching signal. This is, however, only valid assuming that KI exerts the major influence on the precipitation and the other products, KIO_3 and KNO_2 only play a minor role. In the case of the desiccator experiments the loss of water leads to a concentration of the solution and thereby causes the formation of crystals which manifests itself in the spectra as a shift towards the absorbances at 1377.3 and 825.6 cm^{-1}.

There is a remarkable match between the nitrate peak positions observed after heating the treated discs and the literature values reported for the absorbances of nitrate in solid solutions of the respective alkali halides [26]. This suggests that the heat treatment does not cause a separation of nitrate crystals from the halide host as has been observed in the literature for a drying process without the application of heat [8,13] but rather an incorporation of the nitrate in the lattice.

The analysis of the deposit on the PE dielectric suggests the presence of iodic acid, HIO_3. The formation of this oxyacid in the reaction of elemental iodine with ozone in the presence of water vapour has been described in the literature [43]. This study does not, however, suggest a reaction mechanism according to which the product is formed. In the absence of humidity the reaction of iodine and ozone using oxygen as the carrier gas results in the formation of an iodine oxide, the stoichiometry of which was determined as I_4O_9 [44-46]. Iodine oxides were also suggested to be formed as the anode deposit in the corona discharge treatment of iodine in dry air [47]. I_4O_9 is known to be sensitive towards moisture and to hydrolyse forming HIO_3 and I_2 [46]. The hydrolysis is accompanied by colour changes from yellow to brown or dark purple [44,47].

These results can be taken as the basis for an explanation of the observations made in the present experiments. The formation of iodine as an intermediate is obvious from the brown colour which the KI discs adopt during treatment. It is conceivable that some of these iodine molecules escape from the surface and react with the ozone produced in the discharge. Thus, I_4O_9 may be formed as a primary product which subsequently hydrolyses to the products mentioned above. The iodine formed in this process may account for the brown colour of the deposit, while the simultaneously formed HIO_3 is described in the literature as a colourless, crystalline solid [48].

Compared to the literature values [33] the I ($3d_{5/2}$) BEs determined for both iodine and for iodic acid in the XP spectra of the deposit are too high. The BE difference of the two signals corresponds, however, to the expected value. The possibility that periodic acid, H_5IO_6, which contains iodine in a higher oxidation state than HIO_3, is the product can be ruled out because the I ($3d_{5/2}$) BE of this compound is reported to be comparable to that of HIO_3 [33]. Additionally, the I-O stretches in the

IR spectra of this compound should appear at lower wavenumbers than those observed in the spectra of the deposit [49]. The deviation of the BEs is most probably due to referencing difficulties. The optical appearance of the deposit on the foil already suggests that the film might not cover the substrate evenly. It is therefore possible that the sample surface consists of different regions which acquire a different charge during the XPS measurement such that a steady state static charge which is required to accomplish a meaningful charge referencing is not built up [50].

The corresponding acids HXO_3 of chlorine and bromine cannot be isolated and are only stable in solutions [51] and could therefore not have been part of the respective deposits even if a halogen product had been detected.

It is known from the literature [52] that the exposure of carbon based polymers to corona discharge plasmas gives rise to simultaneous surface oxidation and chain scission of the polymer backbone. The so called Low Molecular Weight Oxidised Material (LMWOM) thus formed was furthermore reported to be soluble in alcohols [52]. It can therefore be assumed that the oxidised carbon species detected in the spectra of PE foils which had served as the dielectric during the salt treatment, are due to the formation of LMWOM. This product is removed in the subsequent wiping step with IPA which explains the observation that the spectra of wiped films only show the features of the untreated polymer.

5.6 Conclusions

The silent discharge treatment of KBr and KCl discs in air leads in most cases to the formation of nitrate and the respective halogenate. KI, the most reactive of the three halides studied, also forms small amounts of nitrite in addition to the other two products when the treatment is carried out in the standard set-up. Cell treatments of KI samples in humidified air lead to the production of nitrite as the major nitrogen containing product, whereas in dried air nitrate is formed. In an oxygen atmosphere the halogenate is formed exclusively. Both in air and in oxygen environments the amounts of halogenate decrease in the following order: $IO_3^- > BrO_3^- > ClO_3^-$. Treatments in humidified helium do not result in a modification of the samples while treatments in humidified nitrogen lead to the formation of traces of nitrate on the discs. Treatments in the presence of humidified gases generally give rise to the formation of larger amounts of products. Nitrate and nitrite are due to the reaction of

the salts with the nitrogen oxides produced in the discharge, whereas the halogenate species is a result of the reaction with oxygen species.

The reactivity of KI is also reflected in the formation of a brown deposit on the PE dielectric of the standard set-up during treatment. Apart from oxidised carbon species formed by the oxidation of the PE foil this deposit consists of a mixture of iodine and iodic acid, the decomposition products of an initially formed moisture-sensitive iodine oxide. In contrast, the corresponding PE foils after KCl and KBr treatments contain almost exclusively LMWOM due to the modification of the polymer.

For each of the salts under consideration the peak shapes of the nitrate asymmetric stretching and out of plane bending signal in the IR spectra of discs treated in the standard set-up change with treatment time. This change is related to the processes occurring in the water layer formed on the sample surface by adsorption of water molecules contained in humid air. The layer is assumed to have the properties of a saturated alkali halide solution. In the course of the reaction the layer becomes supersaturated with respect to potassium nitrate which leads to the precipitation of this compound. The contributions of the nitrate in the dissolved and in the crystalline form absorb at slightly different wavenumbers in the spectra. The proportion of the crystalline component inreases with increasing treatment time leading to the observed changes in the peak shape.

Comparing the spectra of samples of the three halides treated for the same treatment time, the amount of nitrate in the crystalline form decreases in the following order : KI > KBr > KCl. This observation is due to the differences in the solubilities of the salts, KI being the most soluble compound causes the largest shift of the precipitation equilibrium towards crystal formation.

Stepwise changes in the IR peak shapes due to an increase in the contribution of the crystalline form are observed when treated samples are stored for increasing time intervals in a desiccator. This can be explained with the concentration of the surface "solution" due to a gradual loss of water from the surface, which leads to the precipitation of nitrate crystals.

Heat treatment of silent discharge treated discs leads to the formation of a solid solution of KNO_3 in KX (X = Cl, Br, I). Contrary to the desiccator experiments different IR peak positions are observed for the three halides studied.

5.7 References

1) Shim, D.; Wittig, C. *Applied Optics* **1976,** *15 (8),*1896

2) Stoch, J.; Ladecka, M. *Appl. Surf. Sci* **1988,** *31(4),* 426

3) Finlayson-Pitts, B.J.; Pitts, J.N. Jr. *Atmospheric Chemistry - Fundamentals and Experimental Techniques*, Wiley : New York, 1986, pp.8-10

4) Finlayson-Pitts, B.J.; Ezell, M.J.; Pitts, J.N. Jr *Nature* **1989**, *337,* 241

5) Vogt, R.; Finlayson-Pitts, B.J. *J. Phys. Chem.* **1994**, *98,* 3747 and *J. Phys. Chem,* **1995**, *99*,13052

6) Laux, J.M., Hemminger, J.C.; Finlayson-Pitts, B.J. *Geophys. Res. Lett.* **1994**, *21 (15),* 1623

7) Leu, M.T.; Timonen, R.S.; Keyser, L.F., Yung, Y.L *J. Phys. Chem.* **1995**, *99,* 13203

8) Laux, J.M.; Fister, T.F.; Finlayson-Pitts, B.J.; Hemminger, J.C. *J. Phys. Chem.* **1996**, *100*, 19891

9) Fenter, F.F.; Caloz, F.; Rossi, M.J. *J. Phys. Chem* **1996**, *100,* 1008

10) Livingston, F.E.; Finlayson-Pitts, B.J. *Geophys. Res. Lett.* **1991**, *18 (1),* 17

11) Fenter, F.F; Caloz, F.; Rossi, M.J . *J. Phys. Chem* **1994**, *98,* 9801

12) Vogt, R.; Finlayson-Pitts, B.J. *J. Phys. Chem.* **1995**, *99,* 17269

13) Allen, H.C.; Laux, J.M.; Vogt, R.; Finlayson-Pitts, B.J.; Hemminger, J.C. *J. Phys. Chem.* **1996**, *100,* 6371

14) Finlayson-Pitts, B.J.; Livingston, F.E.; Berko, H.N. *Nature* **1990**, *343,* 622

15) Finlayson-Pitts, B.J. *Nature* **1983** , *306,* 676

16) Finlayson-Pitts, B.J.; Johnson, S.N. *Atmospheric Environment* **1988**, *22 (6),* 1107

17) Finlayson-Pitts, B.J.; Livingston, F.E.; Berko, H.N. *J. Phys. Chem.* **1989**, *93,* 4397

18) Timonen, R.S.; Chu, L.T.; Leu, M.T.; Keyser, L.F. *J. Phys. Chem.* **1994**, *98,* 9509

19) Vogt, R.; Finlayson-Pitts, B.J.; *Geophys. Res. Lett.* **1994**, *21 (21),* 2291

20) George, C.; Ponche, J.L.; Mirabel, P.; Behnke, W.; Scheer, V.; Zetzsch, C. *J. Phys. Chem.* **1994**, *98*, 8780-8784

21) Beichert, P.; Finlayson-Pitts, B.J. *J. Phys. Chem.* **1996**, *100*, 15218

22) Langer, S.; Pemberton, R.S.; Finlayson-Pitts, B.J. *J. Phys. Chem. A* **1997**, *101*, 1277

23) Vogt, R., personal communication

24) Kogelschatz, U. in: *Process Technologies for Water Treatment*, Brown Boveri Symposium on Process Technologies for Water Treatment, Stucki, S. Ed., Plenum Press: New York, 1987, p.113

25) Miller, F.A.; Wilkins, C.H. *Anal. Chem.* **1952**, *24*, 1253

26) Narayanamurti, V.; Seward, W.D.; Pohl, R.O. *Physical Review* **1966**, *148 (1)*, 481

27) Kato, R.; Rolfe, J. *J. Chem. Phys.* **1967**, *47 (6)*, 1901

28) *The Sadtler Standard Spectra - Inorganics and Related Compounds*, Sadtler Research Laboratories : Philadelphia, PA, 1965, Y110K ($KClO_3$), Y107K ($KBrO_3$), Y115K (KIO_3), Y62K (KNO_2)

29) Nefedov, V.I.; Salyn, Y.V.; Leonhardt, G.; Scheibe, R. *J. Electron. Spectrosc. Rel. Phenom.* **1977**, *10*, 121

30) Moulder, J.F.; Stickle, W.F.; Sobol, P.E.; Bomben, K.D. *Handbook of X-Ray Photoelectron Spectroscopy*, Perkin Elmer Corporation, 1992

31) Morgan, W.E.; Van Wazer, J.R.; Stec, W.J. *J. Am. Chem. Soc.* **1973**, *95(3)*, 751

32) Wagner, C.D.; Riggs, W.M.; Davis, L.E.; Moulder, J.F.; Muilenberg, G.E. *Handbook of Photoelectron Spectroscopy,* Perkin Elmer Corporation, 1979

33) Sherwood, P.M.A. *J. Chem. Soc. Faraday Trans.II* **1976**, *72*, 1805

34) Dasent, W.E.; Waddington,T.C. *Journal of the Chemical Society* **1960**, 2429

35) Sherwood, P.M.A.; Turner, J.J. *Spectrochim. Acta* **1970**, *26 A*,1975

36) Hesse, M.; Meier, H.; Zeeh, B. *Spektroskopische Methoden in der Organischen Chemie*, Georg Thieme: Stuttgart, 1987, pp.27-50

37) Günzler, H.; Böck, H. *IR Spektroskopie*, 2nd ed., VCH : Weinheim, 1983, p.116

38) Esrom, H., personal communication

39) Alebic-Juretic, A.; Cvitas, T.; Klasinc, L. *Ber. Bunsenges. Phys. Chem.* **1992**, *96 (3)*, 493

40) *Ullmanns Encyclopädie der Technischen Chemie* (4th ed.), VCH : Weinheim, 1977, p.422

41) Seel, F. *Grundlagen der analytischen Chemie*, 7th ed., Verlag Chemie: Weinheim, 1979, pp.73-75

42) *Handbook of Chemistry*,10th edition, Lange, N.A. (Ed.), Forker, G.M. McGraw Hill : New York, 1967, pp.304-309

43) Sunder, S.; Vikis; A.C. *Canadian Journal of Spectroscopy* **1987**, *32(2)*, 45

44) Vikis, A.C.; Mac Farlane, R. *J. Phys. Chem.* **1985**, *89*, 812

45) Sunder, S.; Wren, J.C.; Vikis; A.C. *Journal of Raman Spectroscopy* **1985**, *16(6)*, 424

46) Schmeisser, M.; Brändle, K. *Advances in Inorganic Chemistry and Radiochemistry Vol. 5*, Emeleus, H.J.; Sharpe, A.G. Eds., Academic Press : New York, 1963, pp.78-79

47) Sano, N.; Tamon, H.; Okazaki, M. *Journal of Chemical Engineering of Japan* **1997**, *30 (5)*, 944

48) *Kirk-Othmer Encylopedia of Chemical Technology* (3rd ed.), Wiley Interscience : New York, 1981, p.665

49) Siebert, H. *Anwendungen der Schwingungsspektroskopie in der Anorganischen Chemie,* Springer: Berlin, 1966, pp.105-106

50) Wagner, C.D. *J. Electron. Spectrosc. Rel. Phenom.* **1980**, *18*, 345

51) Hollemann-Wiberg *Lehrbuch der Anorganischen Chemie*, 33rd ed., Walter de Gruyter: Berlin, 1985, pp.419-437

52) Briggs, D; Kendall, C.R.; Blythe, A.R.; Wootton, A.B. *Polymer* **1983**, *24*, 47

Chapter 6:
Investigation of the suitability of pentafluoropropionic anhydride as a reagent for the chemical derivatisation of hydroxyl groups on polymer surfaces

6.1 Introduction

In XPS analysis the presence of hydroxyl groups on multifunctional surfaces is often proved by derivatisation with trifluoroacetic anhydride (TFAA) [1-7]. This is achieved by exposing the sample to TFAA vapour prior to the XPS measurement. In the spectra subsequently recorded the hydroxyl groups initially present are replaced by the reaction product, a fluorinated ester. The aim of this chapter is to investigate the suitability of the higher homologue of TFAA, pentafluoropropionic anhydride (PFPA), for the labelling of hydroxyl groups. Since PFPA has a higher fluorine content than TFAA its use would promise a higher sensitivity of the labelling reaction.

6.2 Background

The range of core level chemical shifts caused by different functional groups on polymer surfaces is not always sufficient to distinguish the functionalities present. This is especially true for multifunctional surfaces, for example, for samples containing several carbon-oxygen or carbon-nitrogen species. The spectra of such samples consist of a broad unresolved envelope rather than distinct signals [4].

A popular way to gain information about the species contributing to a photoelectron envelope is the application of mathematical peakfitting procedures. These suffer from the disadvantage that their result can be ambiguous [1-4]. Using this method it is also difficult to separate the contributions of functionalities which give rise to very similar chemical shifts like hydroxyl, ether, peroxide and epoxide groups [4].

Another approach consists of chemical derivatisation also called labelling or tagging of functional groups [3]. In this case the specific reactivity of a functionality towards a suitable reagent which contains an element or a molecular species not present in the original surface is used to identify and quantify this particular moiety [4].

Ideally, a new element introduced to the surface should have a high cross section for XPS such that even small amounts of the functionality of interest can be easily detected [1,2]. Fluorinated compounds are often used for this purpose. The sensitivity of the reaction can be further increased by using reagents which replace the original functional group in a ratio higher than 1:1 [2]. Compared to liquid phase labelling, vapour phase derivatisations have a number of advantages [5-7]. In vapour phase derivatisations low molecular weight components possibly formed by a treatment like exposure to a plasma are prevented from being washed off. Moreover, the reaction of the labelling product with a solvent is avoided and the reorganisation of the surface species is minimised. This, however, requires both the labelling reagent and possible undesired side products of the reaction to be sufficiently volatile which is not always the case [4]. The reaction itself should not only be fast, quantitative and homogeneous throughout the XPS sampling depth but also selective for the functional group under consideration [2-4]. In cases where a washing step is involved in the procedure stability of the derivatisation product against the solvent in question is an additional requirement [1]. Finally, the product of the labelling rection should be stable towards vacuum and x-radiation and if the sample has to be exposed to air prior to transfer to the spectrometer it should be reasonably stable against atmospheric gases as well. A number of reagents have been employed for the derivatisation of different functional groups [1-3]. Most of them do not fulfill all the requirements listed above but rather represent a compromise between the conditions [4].

Generally, not all reactions which proceed stoichiometrically in solution are automatically found to be appropriate surface labelling reactions [3]. Steric and thermodynamic factors were made responsible for this finding [4]. For halogen containing reagents it was also discussed that the reactivity of the labelling molecules towards reaction sites in partially derivatised samples may be disturbed in the presence of already formed reaction products [8].

6.3 Experimental

Pentafluoropropionic anhydride (PFPA) (99.9%, Fluorochem, Aldrich) was used as the main reagent in the labelling experiments. Trifluoroacetic anhydride (TFAA, Aldrich) and Heptafluorobutyric anhydride (HFBA, Aldrich) were employed

as additional labelling reagents for nylon 6,6. The anhydrides were used without further purification. The purity of the reagents was controlled with ^{19}F NMR; TFAA contained a minor amount of trifluoroacetic acid.

For the measurements in which the reaction of the model polymer with PFPA was studied (6.4.1) thin films of Polyvinylalcohol (PVA, M_w 115000, Aldrich) were spin coated onto glass slides from a 1 % w/v solution in deionised water. For the sensitivity measurements, in which the covering of both sides of the substrate was more practical, films of the following polymers were dip coated from solutions onto glass slides: Polystyrene (PS, M_w 280000, Aldrich, 2 % w/v in toluene), polymethylmethacrylate (PMMA, medium molecular weight, Aldrich, 4 % w/v in toluene), polyethylene oxide (PEO, M_w 200000, Polymer Laboratories, 1 % w/v in chloroform), Polyacrylic Acid (Aldrich, M_v = 450.000, 1.5 % w/v in methanol). Spin coated or dip coated PVA samples were dried for at least 3 hours, dip coated samples of the remaining polymers were dried for at least 1 hour in a vacuum oven at 45 °C before measurement or derivatisation.

In order to avoid a contribution of the substrate to the ATR-IR spectra, PVA granules were pressed into a disk which was subsequently treated and measured.

Samples of Polysulfone (Westlake Plastics Company), Polyethylene (LDPE, ICI), nylon 6,6 (Goodfellows) and Polyetheretherketone (PEEK, ICI) were cut from polymer sheets. The sample strips were ultrasonically cleaned in cyclohexane for 30 seconds and dried in air. Both polymer films on glass slides and cleaned polymer strips were transferred to the sample tube of the labelling apparatus. A schematic of this apparatus is shown in figure 1. The set-up was fitted with a rotary pump (Edwards Speedivac ED 50) attached to a liquid nitrogen cold trap; pressure measurements were carried out with a Pirani gauge (Edwards). The labelling reagents were degassed by subjecting them to repeated freeze and thaw cycles prior to use.

Diethylether (99,5%, especially dried, BDH), n-hexane (AnalaR, BDH) and chloroform (AnalaR, BDH) were used in the solvent washing experiments of treated films.

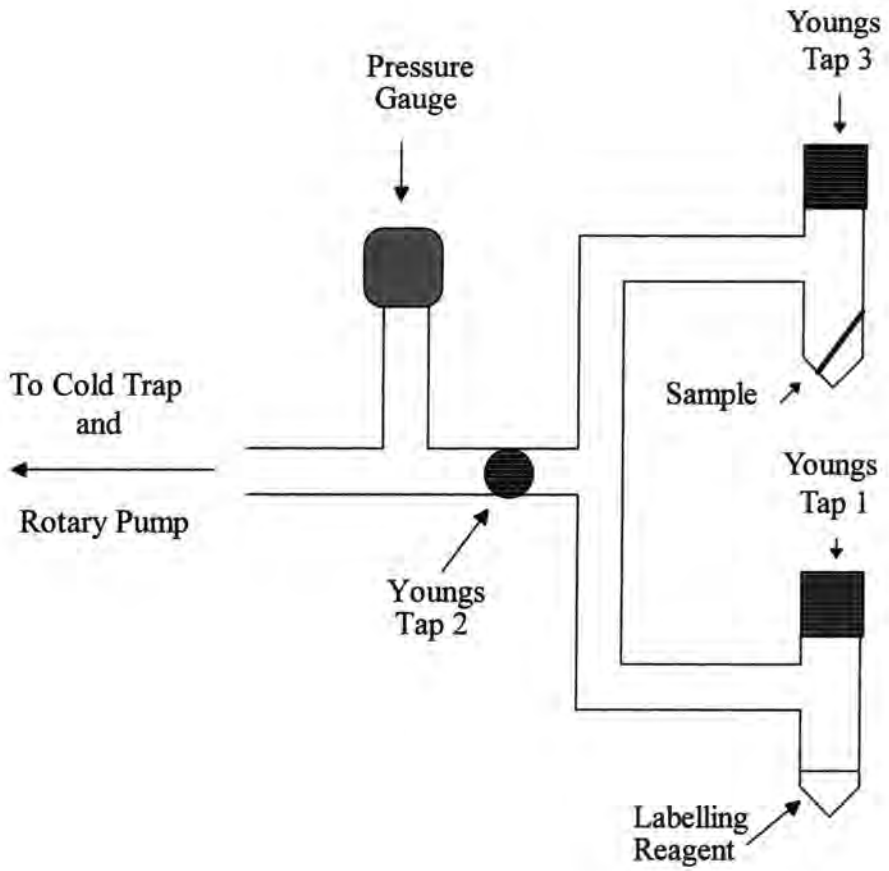

Fig. 1 Schematic of the labelling rig

In a typical experiment the apparatus was first evacuated keeping Youngs tap 1 of the monomer tube containing the labelling reagent shut. After the base pressure (3×10^{-3} torr, leak rate < 3×10^{-3} cm ^{3}/min, see chapter 4.2.2) was reached, Youngs tap 2 was closed and the monomer tube was opened allowing the vapour of the reagent to expand into the vacuum and to saturate whilst keeping Youngs tap 3 towards the sample closed. Control experiments showed that 2 minutes are sufficient to reach an equilibrium vapour pressure. After that the sample was exposed to the reactant vapour by opening Youngs tap 3. The time of the reaction was measured from when this tap was opened. After a set reaction time, the monomer tube (Youngs tap 1) was closed and the apparatus was pumped out again to base pressure by opening Youngs tap 2. The sample tube was sealed and taken off the apparatus after venting the remaining set-up.

The samples were evaluated by XPS and ATR-IR either directly or after washing for 30 seconds in a beaker containing 25 ml of the respective solvent. For

the ageing studies of N-fluoroacylated nylon 6,6, treated samples were stored for a set time in moist air prior to ATR-IR analysis.

XPS measurements were carried out as described in chapter 3.3.2. Instrumentally determined sensitivity factors are 0.62 for O (1s), 0.74 for N (1s) and 0.46 for F (1s) with respect to a value of 1.00 for C (1s). Peak fits for the XP spectra were obtained using a Marquardt minimisation computer programme. The components are assumed to have a Gaussian peak shape with fixed FWHM (full width at half maximum). ATR-IR spectra were collected according to the procedure given in section 5.3.

6.4 Results

6.4.1 Esterification of hydroxyl groups

The first step in the study was to check whether the labelling reagent undergoes the desired reaction which is the esterification proceeding according to scheme 1:

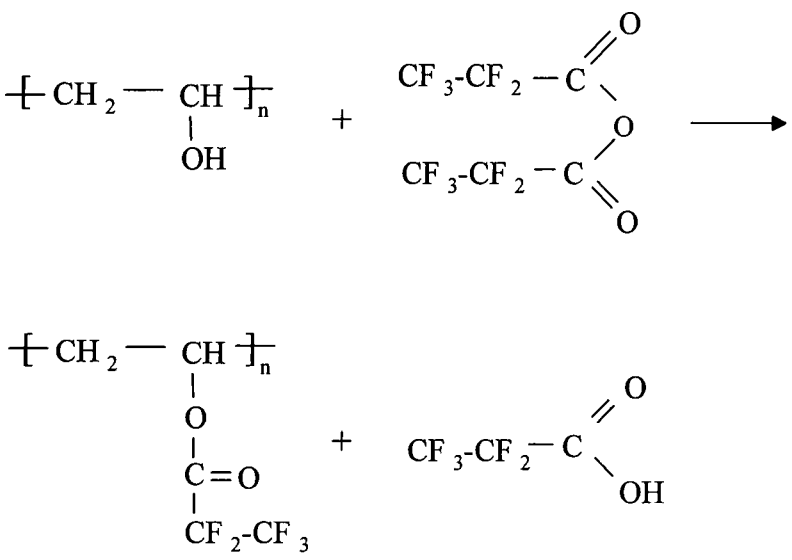

Scheme 1 Equation of the labelling reaction of PVA with PFPA

Polyvinylalcohol (PVA) which contains hydroxyl groups bound to a saturated carbon backbone was chosen as a model polymer.

6.4.1.1 XPS

The XP spectra of the underivatized PVA samples are in agreement with those reported in the literature [9], figure 2. Two environments contribute to the C (1s) spectrum; these are the -$\underline{C}H_2$- groups appearing at a binding energy of 285.0 eV and the >$\underline{C}$H-OH signal centred at 286.6 eV. A small additional component observed at higher binding energy is probably due to carboxyl groups [9]. The ratio between the two main carbon moieties is not exactly 1:1, the hydrocarbon environment is always observed with a slightly higher intensity compared to the hydroxyl environment. The reason for this finding is most probably the accumulation of adventitious hydrocarbon on the sample surface. The O (1s) signal is sharp and located at a binding energy of 532.6 eV. Fluorine is not present in the surface of untreated PVA samples. Due to the presence of the carboxyl impurity the elemental composition of the films shows a higher oxygen content than expected, table 1.

	% C	% O
theoretical value	66.6	33.3
experimental value	63.9 ± 0.4	36.1 ± 0.4

Tab. 1 Elemental compositions of untreated PVA film

After the PFPA treatment the C (1s) envelope appears very complex due to the introduction of carbon fluorine linkages and the ester carbonyl functionality, figure 2. Since the envelope is broad there is a transition of the low BE -$\underline{C}F_2$- and -$\underline{C}F_3$ Mg $K_{\alpha\,3,4}$ satellites into the main photoelectron signal. Only the high BE components are presented as fitted data in the figure because it is difficult to fit the contributions to the remaining part of the spectrum unambiguously especially in the case of partly derivatized surfaces. In this case, there are contributions of the satellites, adventitious hydrocarbon / the -$\underline{C}H_2$-CHOH group of unlabelled PVA, the β - shifted -$\underline{C}H_2$-CH-$OCOC_2F_5$ environment of the product ester, the >$\underline{C}$H-OH group of unlabelled PVA and the >$\underline{C}$H-$OCOC_2F_5$ moiety of the ester (in order of increasing BE). The difficulty in separating the adventitious hydrocarbon / -$\underline{C}H_2$-CHOH (if present) component from the -$\underline{C}H_2$-CH-$OCOC_2F_5$ environment in a unique

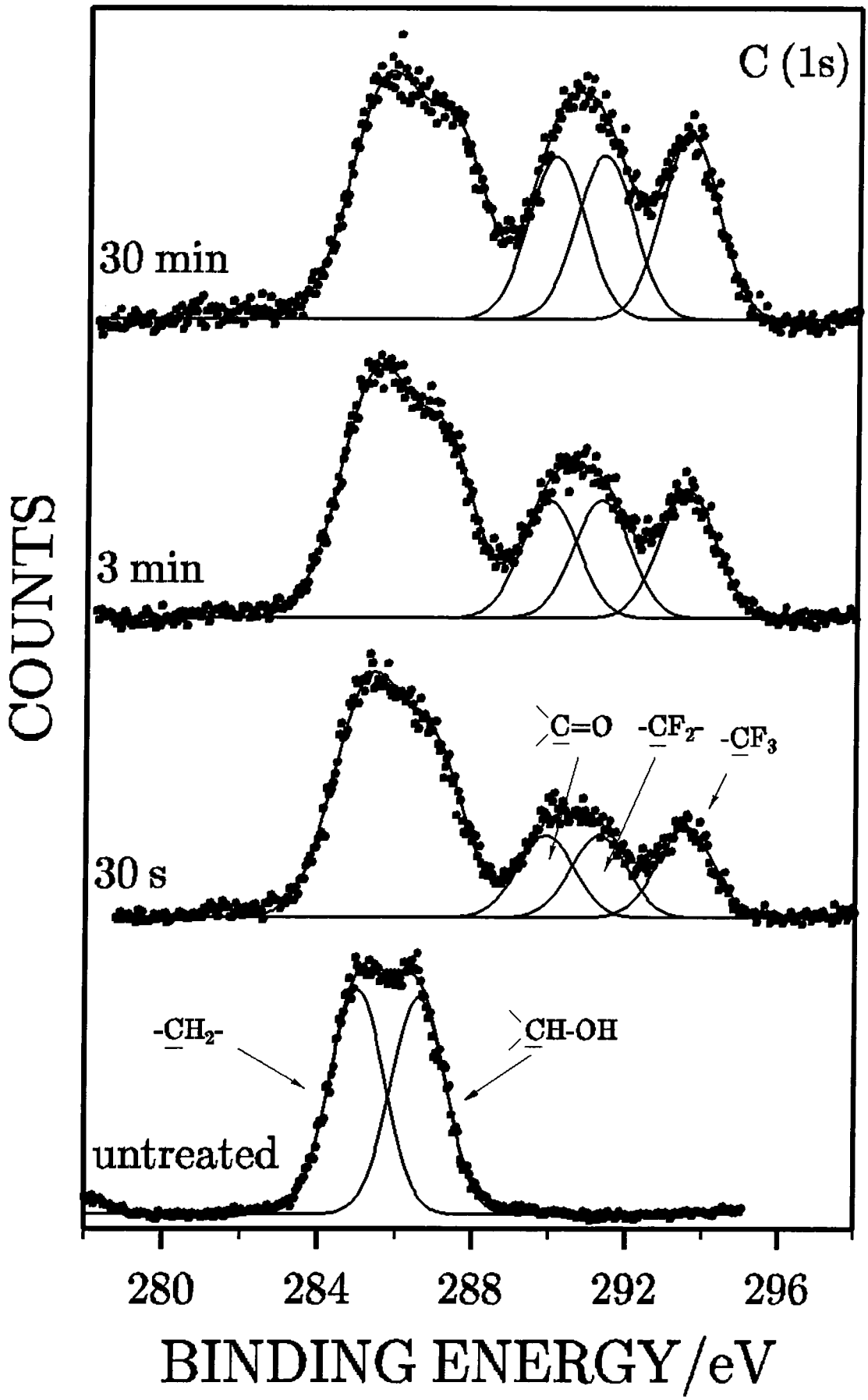

Fig. 2 C (1s) XP spectra of PVA films as a function of exposure time to PFPA vapour

meaningful fit could additionally lead to erroneous results in binding energy referencing. Therefore, the C (1s) binding energy of the -$\underline{C}F_3$ component was taken as the reference point assuming its value to be 293.5 eV as found in the case of the corresponding TFAA ester [10]. With respect to this point the -$\underline{C}F_2$- and >$\underline{C}$=O environment appear at binding energies of about 291.3 and 290.0 eV respectively. The high binding energy part of the envelope gains intensity with increasing treatment time.

Changes are also observed in the appearance of the O (1s) signal which is broadened due to an additional oxygen environment. The F (1s) peak is centred at a binding energy of 688.8 eV.

Figure 3 shows the elemental composition of PVA films as a function of exposure time to PFPA vapour. The sample surfaces are derivatized quickly and a plateau is reached after a treatment time of about 5 minutes. Table 2 compares the elemental composition of PVA samples treated for 30 minutes with the theoretical value which can be expected from the ester structure.

	% C	% O	% F
theoretical value	41.7	16.7	41.7
experimental value	40.8 ± 0.6	19.4 ± 0.1	39.8 ± 0.4

Tab. 2 Elemental composition of the ester

The saturation value obtained for the product ester does not correspond exactly to the theoretically expected value. This is most probably due to the presence of the carboxyl groups in the untreated polymer which disturb the stoichiometry and are not labelled in the reaction. They are responsible for the lowering of the fluorine percentage and the relatively increased amount of oxygen.

6.4.1.2 ATR-IR

The ATR-IR spectra of untreated and PFPA treated PVA samples also show the transformation of PVA into the ester, figure 4. The respective assignments for the signals are given in tables 3 and 4.

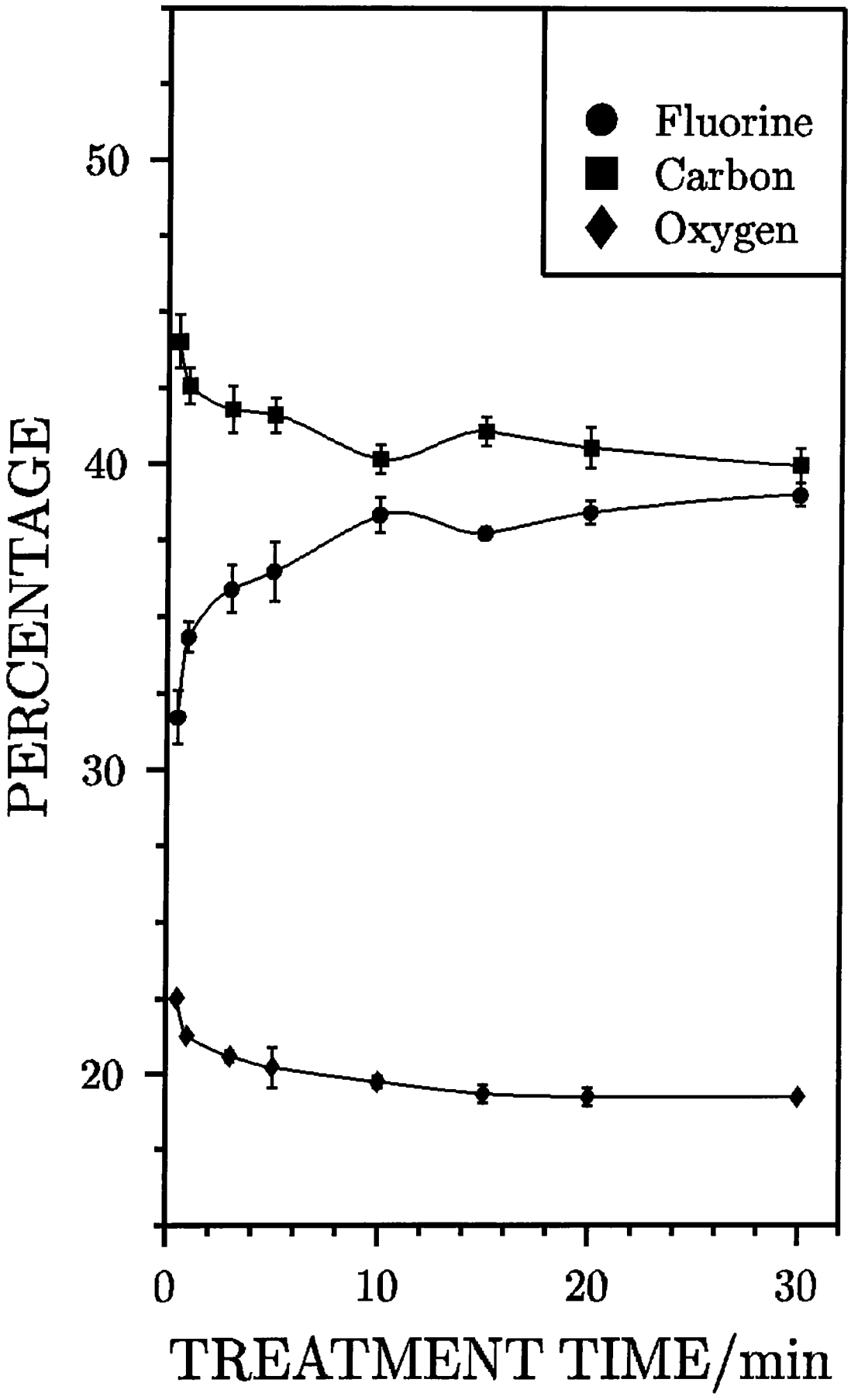

Fig. 3 Elemental composition of PVA films as a function of exposure time to PFPA vapour

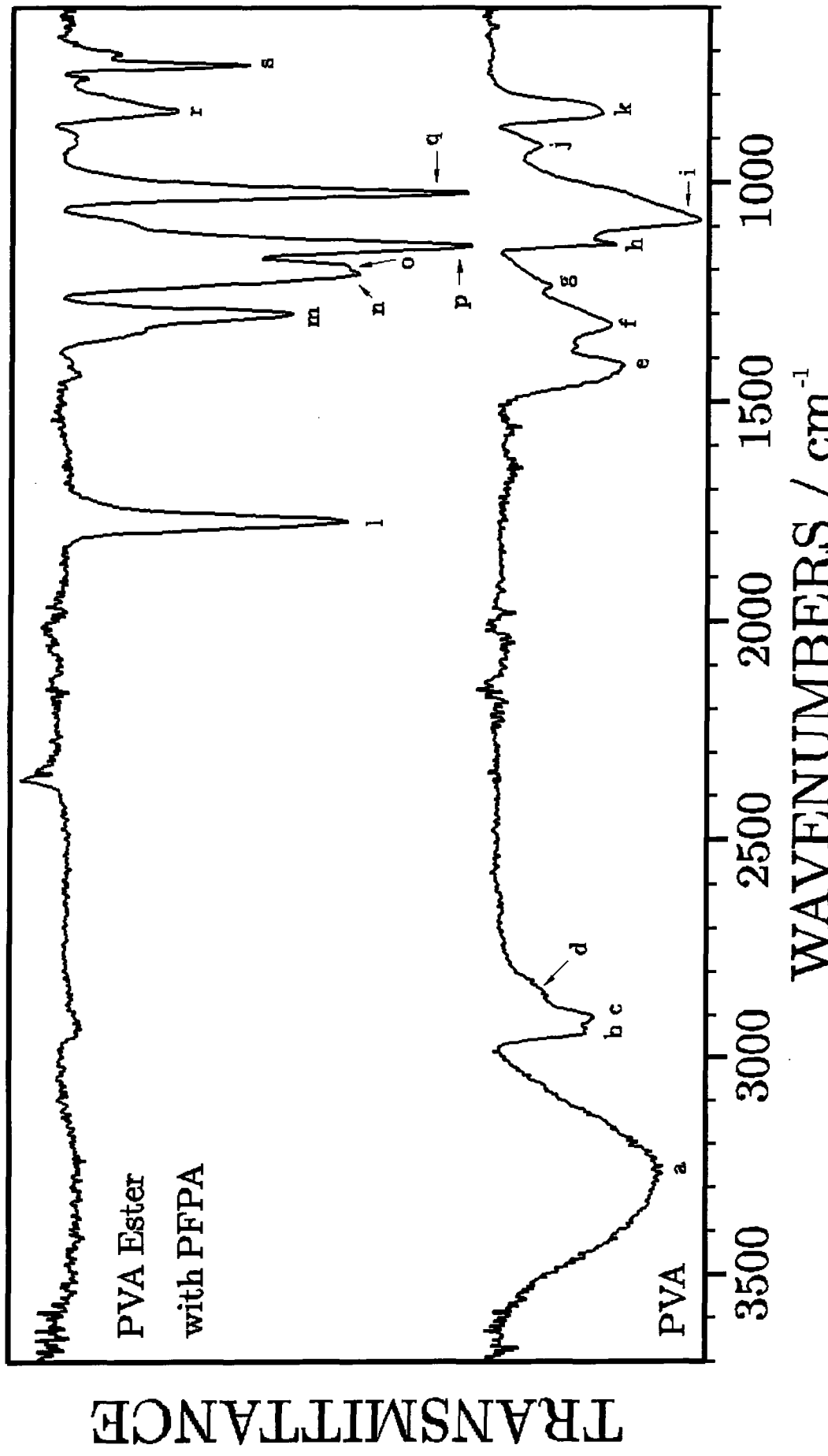

Fig. 4 ATR - IR spectra of PVA (bottom) and the PVA ester formed with PFPA (top)

Peak	Wavenumber [cm^{-1}]	Assignment
a	3290.8	O-H stretching
b	2939.7	asymmetric stretching in CH_2
c	2905.0	symmetric stretching in CH_2
d	2839 (shoulder)	C-H stretching
e	1419.7	CH_2 bending
f	1323.3	combination C-H and OH bending
g	1236.6	C-H wagging
h	1141.9	symmetric C-C stretching
i	1086.0	C-O stretching
j	918.2	CH_2 rocking
k	833.3	C-C stretching

Tab. 3 Characteristic absorbances of PVA [11-13]

Peak	Wavenumber [cm^{-1}]	Assignment
l	1776.6	C=O stretching
m, n, o, p	1302.0, 1211.4, 1194.0, 1147.7	C-F stretching
q, r	1026.2, 839.1	C-C stretching
s	733.0	C-F deformation

Tab. 4 Absorbances of the PVA ester with PFPA [14]

Washing of the treated samples with diethylether resulted in the partial removal of the product, whereas no change in the IR spectra was observed after washing with n - hexane. Halving a treated sample and measuring one half directly after treatment and the other half after being stored for 42 hours in moist air did not result in significantly different spectra which suggests that the ester is sufficiently stable in a normal atmosphere.

6.4.1.3 Selectivity of the labelling reaction

In order to examine the selectivity of PFPA for the labelling reaction of hydroxyl groups, polymer samples containing functionalities other than hydroxyl were treated in the same manner as the PVA samples. Their structures are listed in figure 5. The reaction of nylon 6,6 will be treated seperately in chapter 6.4.2. Within the detection limits of XPS a widescan of the untreated polymers did not reveal the presence of other elements than those expected from the respective polymer structure. A treatment time of 15 minutes was chosen for these experiments. The standard treatment led to the adsorption of varying amounts of fluorine moieties. Since the exposure to heat at 45°C and reduced pressure could not establish reproducible results a washing procedure of the samples had to be carried out. The solvent chosen for this purpose was n-hexane. It neither dissolves the product ester nor the polymers concerned. The results are listed in table 5.

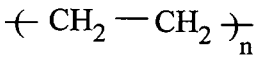

Polyethylene (PE)

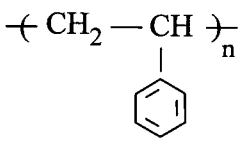

Polystyrene (PS)

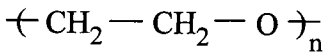

Polyethyleneoxide (PEO)

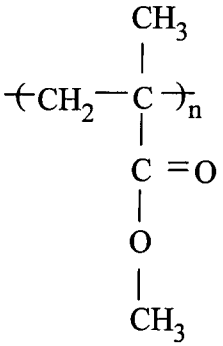

Polymethylmethacrylate (PMMA)

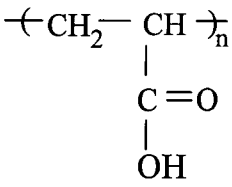

Polyacrylic Acid (PAA)

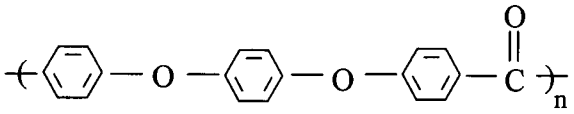

Polyetheretherketone (PEEK)

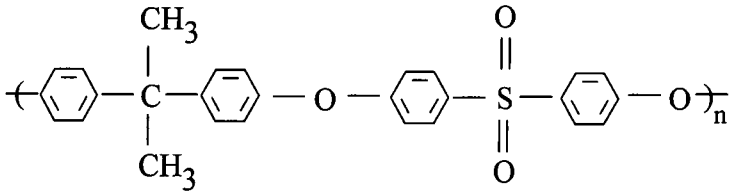

Polysulfone (PSF)

Fig. 5 Structures of the polymers used in the sensitivity experiments

Polymer	% C	% O	% S	% F
PE (theor.)	100	-	-	-
PE (exp.)	99.2 ± 0.2	0.8 ± 0.2	-	-
PE - PFPA	99.1 ± 0.4	0.9 ± 0.4	-	-
PS (theor.)	100	-	-	-
PS (exp.)	99.4 ± 0.1	0.6 ± 0.1	-	-
PS - PFPA	98.3 ± 0.8	1.4 ± 0.5	-	0.3 ± 0.3
PEO (theor.)	66.6	33.3	-	-
PEO (exp.)	63.5 ± 0.8	36.5 ± 0.8	-	-
PEO - PFPA	55.6 ± 0.7	33.9 ± 0.1	-	10.7 ± 0.8
PMMA (theor.)	66.7	33.3	-	-
PMMA (exp.)	69.4 ± 0.6	30.6 ± 0.6	-	-
PMMA - PFPA	70.9 ± 0.7	28.5 ± 0.6	-	0.8 ± 0.1
PAA (theor.)	60	40	-	-
PAA (exp.)	64.9 ± 0.6	35.1 ± 0.6	-	-
PAA - PFPA	62.1 ± 0.9	37.4 ± 0.8	-	0.6 ± 0.1
PEEK (theor.)	86.4	13.6	-	-
PEEK (exp.)	86.7 ± 0.4	13.3 ± 0.4	-	-
PEEK - PFPA	83.9 ± 0.6	13.4 ± 0.9	-	2.8 ± 0.3
PSF (theor.)	84.4	12.5	3.1	-
PSF (exp.)	82.6 ± 0.5	14.1 ± 0.4	3.3 ± 0.1	-
PSF - PFPA	72.8 ± 3.5	16.7 ± 2.4	2.4 ± 0.3	8.2 ± 1.4

Tab. 5 Results of the selectivity experiments

Since PFPA is a higher homologue of TFAA it can be expected that both compounds show a similar reaction behaviour. Therefore, a selectivity study of TFAA [4] is taken as a rough guide for the discussion of the results.

Contrary to the TFAA study where only PAA and Polyvinylmethylketone (PVMK) showed a small degree of cross-reaction, a trace of fluorine is detected in the present study in all the samples except PE even after the washing procedure. For PS, PMMA and PAA the amount of fluorine observed is low compared to that found

for the PVA ester. The surfaces of the other polymers studied, however, are enriched with fluorine. In the selectivity study of the TFAA reaction carbonyl groups were found to show the highest rate of cross reaction. In this case polyvinylmethylketone was used as the model polymer. Despite this observation the amount of fluorine detected for PEEK in the present study seems to be too high considering the low number of carbonyl groups present in this polymer.

Since the behaviour of PSF was not studied in the TFAA investigation a comparison is not possible. A chemical reaction of polysulfone with PFPA can be considered to be unlikely [15]. Although the contribution of a reaction with an impurity cannot be ruled out, physisorption could be predominant in this case because the polymer sheet had a surface structure which might have faciliated adsorption. A support for this assumption can be the observation that ATR-IR spectra of both treated and untreated PSF samples show a weak signal at 1776 cm^{-1}. This is most probably due to a combination band of the p-substituted aromatic rings [16] rather than a reaction product with possibly present hydroxyl groups.

In contrast, the ATR-IR spectra of treated PEO samples contain signals due to the >C=O and C-F stretches of the ester as well as an additional signal at 1689.7 cm^{-1}. The >C=O and C-F stretches are an indication for the presence of hydroxyl groups in the untreated polymer. Since PEO has only a very low concentration of reactive hydroxy end groups [17] there must be another source of this functionality.

6.4.2 The reaction with Nylon

The reaction of nylon 6,6 with TFAA in XPS labelling experiments has been mentioned previously but this was not further investigated and no spectra were reported [18]. The respective bulk organic reaction has been described in the literature [19], the product of the process being the N-trifluoroacetylated polyamide formed according to reaction scheme 2 ($X = CF_3$):

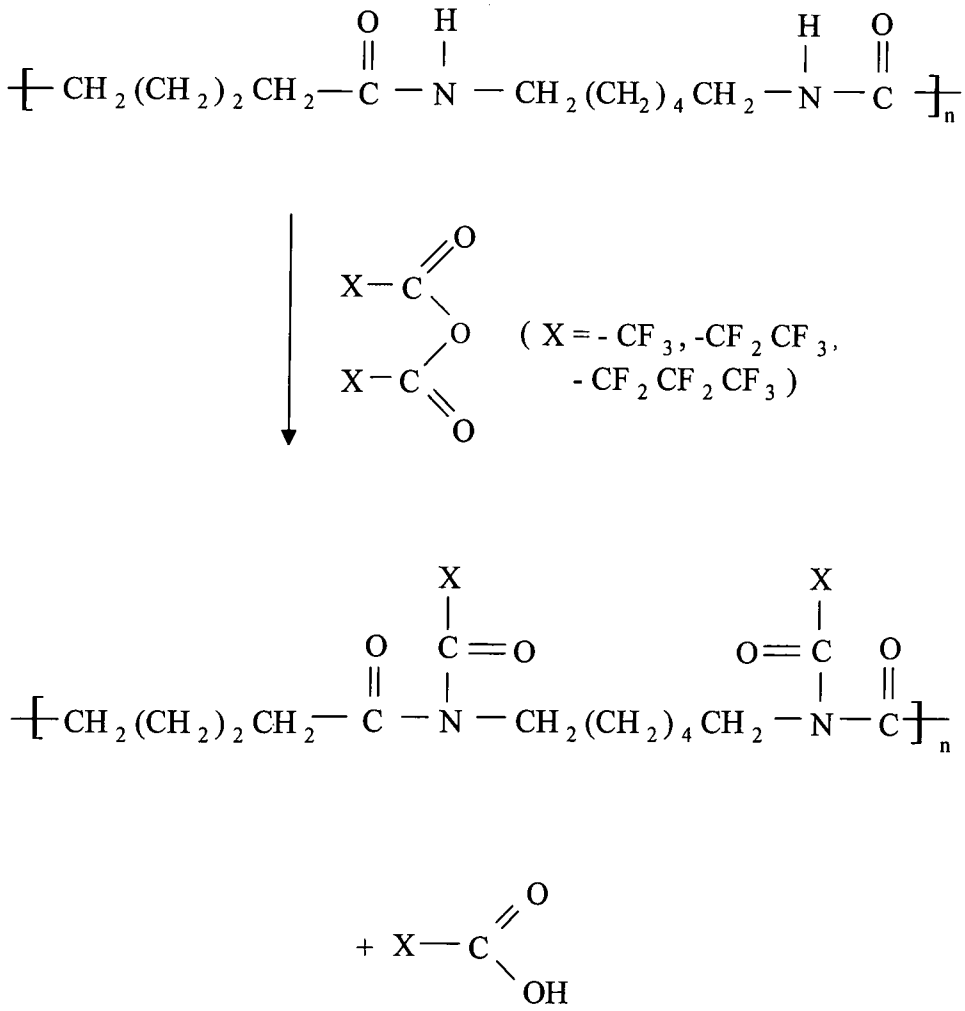

Scheme 2. Equation of the fluoroacylation of nylon 6,6

The product was reported to be sensitive towards the attack of nucleophiles like amines, alcohols and water. Most polyamides undergo this reaction. Apart from being quantitative and proceeding without degradation of the polymer chain the reaction yields a product which is in contrast to the original polyamides soluble in many common organic solvents. The combination of these properties makes the reaction a convenient method to determine the molecular weights of polyamides with Gel Permeation Chromatography (GPC) [20-22].

The interesting reaction of nylon 6,6 was studied in detail with three anhydrides containing fluorine substituents with increasing chain length: trifluoroacetic anhydride (TFAA), pentafluoropropionic anhydride (PFPA) and heptafluorobutyric anhydride (HFBA).

6.4.2.1 General observations

Upon treatment with all three anhydrides the nylon 6,6 films changed their appearance from opaque to transparent and were considerably softened tending to stick to the glass walls of the sample tube. Washing of the samples with diethylether changed the colour of the treated films from transparent to white, whereas washing with chloroform resulted in opaque films similar to the starting material. The products of all three reactions have in common that they are insoluble in ether and soluble in chloroform.

6.4.2.2 XPS

Figure 6 shows the C (1s) spectra of untreated nylon 6,6 and of nylon 6,6 films after 15 minutes exposure to the vapour of the respective labelling reagent. The C (1s) envelope of untreated nylon 6,6 contains contributions of the following environments [9]: 285.0 eV (-$\underline{C}H_2$-), 285.6 eV (-$\underline{C}H_2$-CO-NH-), 286.2 eV (-CO-NH-$\underline{C}H_2$-) and 288.1 eV (-CH_2-$\underline{C}$O-NH-). The N (1s) and O (1s) signals appear at binding energies of 399.9 eV and 531.5 eV, respectively. The elemental composition of the untreated nylon 6,6 is given in table 6. A wide scan showed the presence of carbon, oxygen and nitrogen only, no other elements were detected.

	% C	% O	% N
theoretical value	75.0	12.5	12.5
experimental value	77.4 ± 0.4	12.7 ± 0.3	9.8 ± 0.3

Tab. 6 Elemental composition of untreated nylon 6,6

The most obvious change in the C (1s) XP spectra of the treated nylon 6,6 samples are the new signals on the high BE side. Due to the presence of -$\underline{C}H_2$- groups which remain unaffected by the presence of the strongly electron withdrawing substituent referencing to the hydrocarbon component is possible. For all three samples the >$\underline{C}$=O component is centred at a binding energy of 289.0 eV. The -$\underline{C}F_2$- component appears at 291.3 eV (PFPA) and 291.4 eV (HFBA) respectively. The

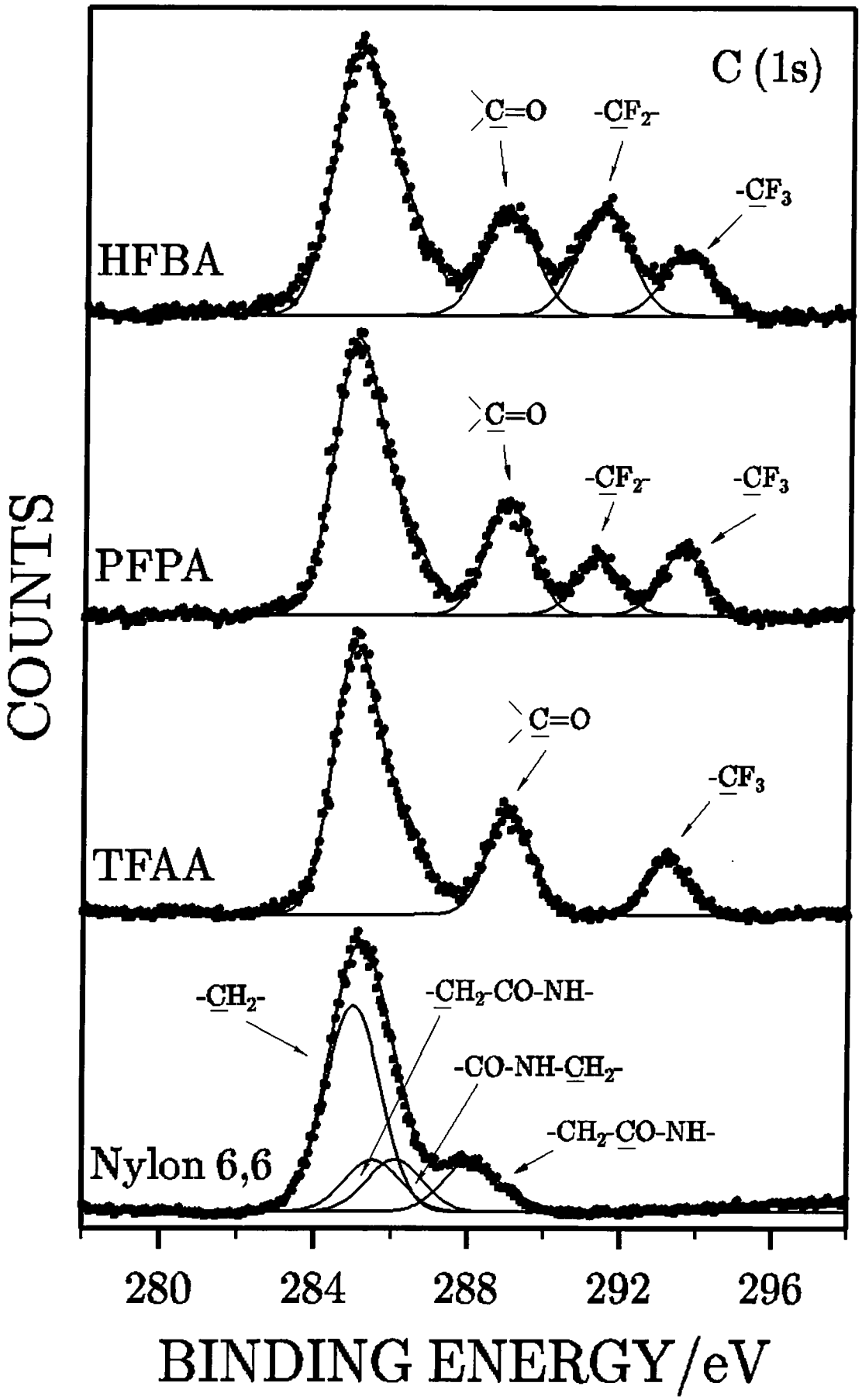

Fig. 6 C (1s) XP spectra of nylon 6,6 films before and after treatment with TFAA, PFPA and HFBA

binding energies of the -$\underline{C}F_3$ groups are observed at values of 293.3 eV (TFAA), 293.5 eV (PFPA) and 293.6 eV (HFBA). The experimentally determined intensity ratio of the >$\underline{C}$=O and -$\underline{C}F_3$ environments in TFAA treated nylon 6,6 is 2 : 1.1 (theor. 2 : 1), the corresponding ratio >$\underline{C}$=O : -$\underline{C}F_2$-: -$\underline{C}F_3$ in PFPA and HFBA is 2 : 1 : 1.1 (theor. 2 : 1: 1) and 2 : 2 : 1.1 (theor. 2 : 2 :1) respectively.

The elemental compositions of the modified films, table 7, correspond well to the theoretically expected values for the N-fluoroacylated products shown in scheme 2. Within the range of the experimental error the composition of treated films does not change upon ether washing. Chloroform washed samples, in contrast, show a loss in fluorine due to product removal.

	% F	% C	% O	% N
TFAA (theor.)	21.4	57.1	14.3	7.1
TFAA (exp.)	21.6 ± 0.4	56.1 ± 0.3	14.7 ± 0.1	7.8 ± 0.1
PFPA (theor.)	29.4	52.9	11.8	5.9
PFPA (exp.)	30.0 ± 0.3	52.2 ± 0.6	11.8 ± 0.3	6.1 ± 0.1
HFBA (theor.)	35	50	10	5
HFBA (exp.)	35.2 ± 0.8	49.0 ± 0.6	10.4 ± 0.1	5.5 ± 0.2

Tab. 7 Calculated and experimentally determined elemental composition of the N-fluoroacylated nylon 6,6 films

6.4.2.3 ATR-IR

Figure 7 shows the ATR-IR spectra obtained for samples treated under the same conditions as those measured with XPS. The spectrum of untreated nylon is in agreement with the literature [23] showing bands characteristic of a secondary amide [24,25], table 8.

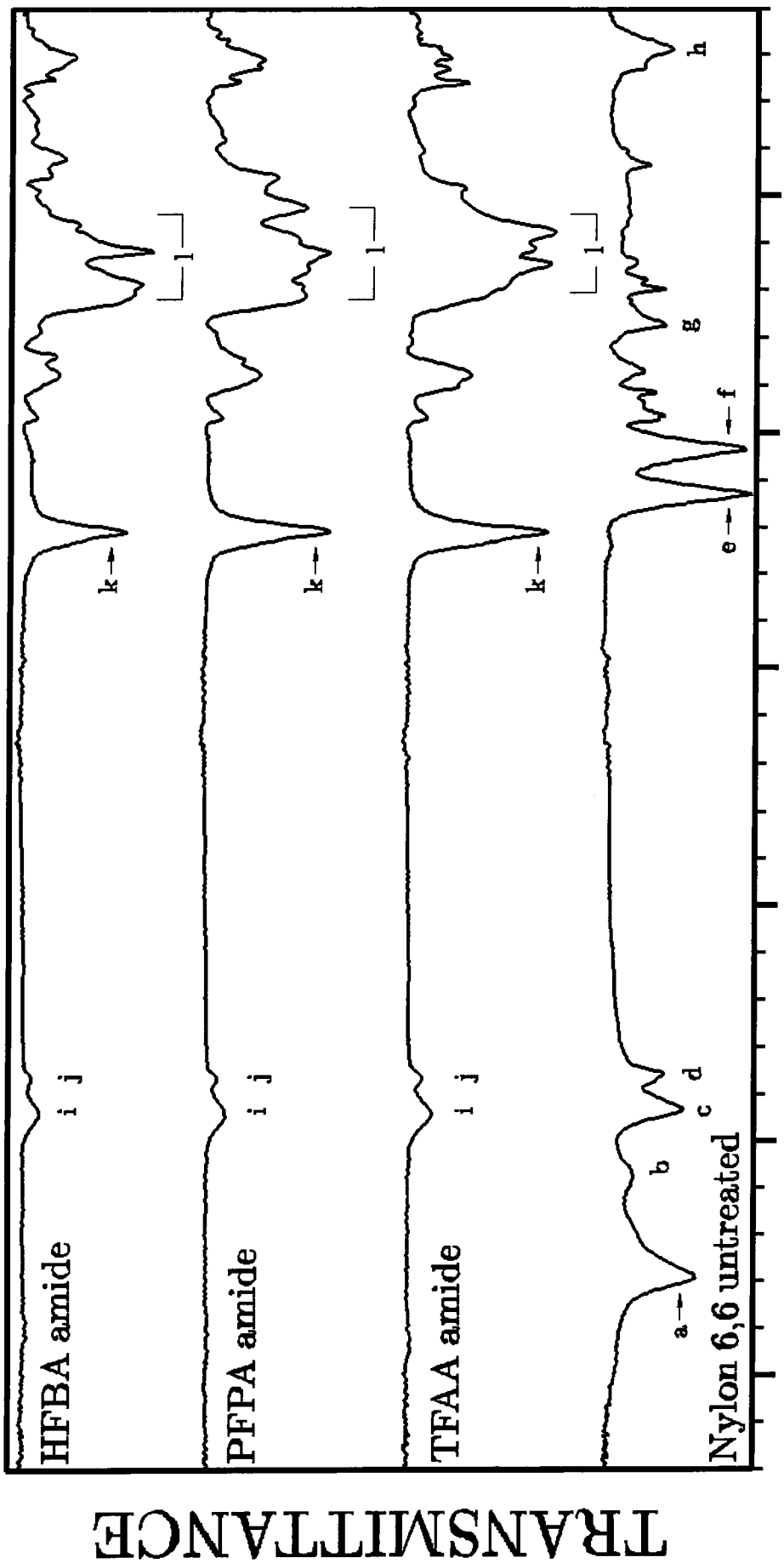

Fig. 7 ATR - IR spectra of nylon 6,6 films before and after treatment with TFAA, PFPA and HFBA

Peak	Wavenumber [cm^{-1}]	Assignment
a	3292.7	N-H stretch
b	3074.7	overtone amide II absorption
c	2933.9	asymmetric C-H stretch
d	2860.6	symmetric C-H stretch
e	1631.9	amide I band involving C=O and C-N stretch and N-H bending
f	1535.4	amide II band involving C-N stretch and N-H bending
g	1273.1	amide III band with contibutions of C-N stretch and N-H bending
h	686.7	N-H deformation out of plane

Tab. 8 Characteristic absorbances of nylon 6,6

The spectrum of the treated samples is entirely different from that of the starting material suggesting that the modification takes place up to the sampling depth of the ATR technique. The signals related to the secondary amides have disappeared following the treatment with the reagents. The products of all three anhydrides show spectra which are similar in the region of the group frequencies but show different patterns in the fingerprint region, figure 6 and table 9. The C-F stretches of samples containing both $-CF_3$ and $-CF_2-$ groups appear as a series of intense bands in the region of 1250 - 1000 cm^{-1} and cannot be assigned in detail because they are difficult to separate and no correlation rules can be set up [24,25].

Peak	TFAA	PFPA	HFBA	Assignment
i	2945.5	2943.6	2941.6	asymmetric C-H stretching
j	2864.5	2868.3	2868.3	symmetric C-H stretching
k	1712.9	1712.9	1711.0	C=O stretching
l	1080.2, 1147.7, 1114.9	1213.3, 1195.9, 1159.3, 1122.6, 1095.6, 1028.1	1209.4, 1190.2, 1120.7, 1062.8	C-F stretching modes

Tab. 9 Absorbances of the modified nylon 6,6 spectra [19,24,25]

Although washing with diethylether causes a change in the colour of the treated nylon 6,6 samples, the ATR-IR spectra of the films show no difference compared to the spectra of unwashed samples. The product formed in the labelling reaction therefore seems to be insoluble in diethylether. The spectra of chloroform washed samples, on the other hand, contain contributions of both the product and the untreated polymer which means that parts of the product must have been dissolved. This assumption was confirmed by the observation that after evaporation of the chloroform used in the washing procedure a white solid was obtained. The IR analysis of this material carried out a day later revealed that it was pure nylon which indicates the instability of the initially formed product towards moist air. Both the solubility of the product in chlorinated hydrocarbons and its reaction with moisture are in line with the properties reported for the N-fluoroacetylated nylon by Schuttenberg and Schulz [19].

The decomposition behaviour of the N-fluoroacylated nylon 6,6 samples in ambient air was subsequently studied in detail. Figures 8, 9 and 10 show ATR-IR spectra of TFAA, PFPA and HFBA treated nylon 6,6 films (treatment time: 15 minutes) after varying storage times in air. In all cases the >C=O band at about 1713 cm^{-1} disappears gradually and the carbon-fluorine stretches change their appearance and decrease in intensity. At the same time, the features characteristic of nylon 6,6 (the amide I and II doublet and the N-H stretch) appear again. A shoulder on the >C=O signal is observed at 1782.3 cm^{-1} in the case of TFAA and at 1776.6 cm^{-1} in the case of PFPA and HFBA. These signals can be attributed to trifluoroacetic acid [26,27], pentafluoropropionic acid [28] and heptafluorobutyric acid [29], respectively suggesting that these compounds are formed in the decomposition process and remain trapped in the polymer matrix. It is most obvious from the respective spectra taken after 9 hours storage in air that there is a difference in the decomposition speed of the three products. The TFAA product is almost completely transformed into nylon. The spectrum only contains a small >C=O contribution of the fluoroacetylated product. It appears as a weak shoulder on the low wavenumber side of the signal of trifluoroacetic acid. The spectrum of the PFPA product shows an intermediate behaviour. The >C=O signal of the fluoroacylated product is still clearly visible together with a small acid peak on its high wavenumber side and intense amide I and amide II contributions of nylon on its low wavenumber side. The slowest progress in

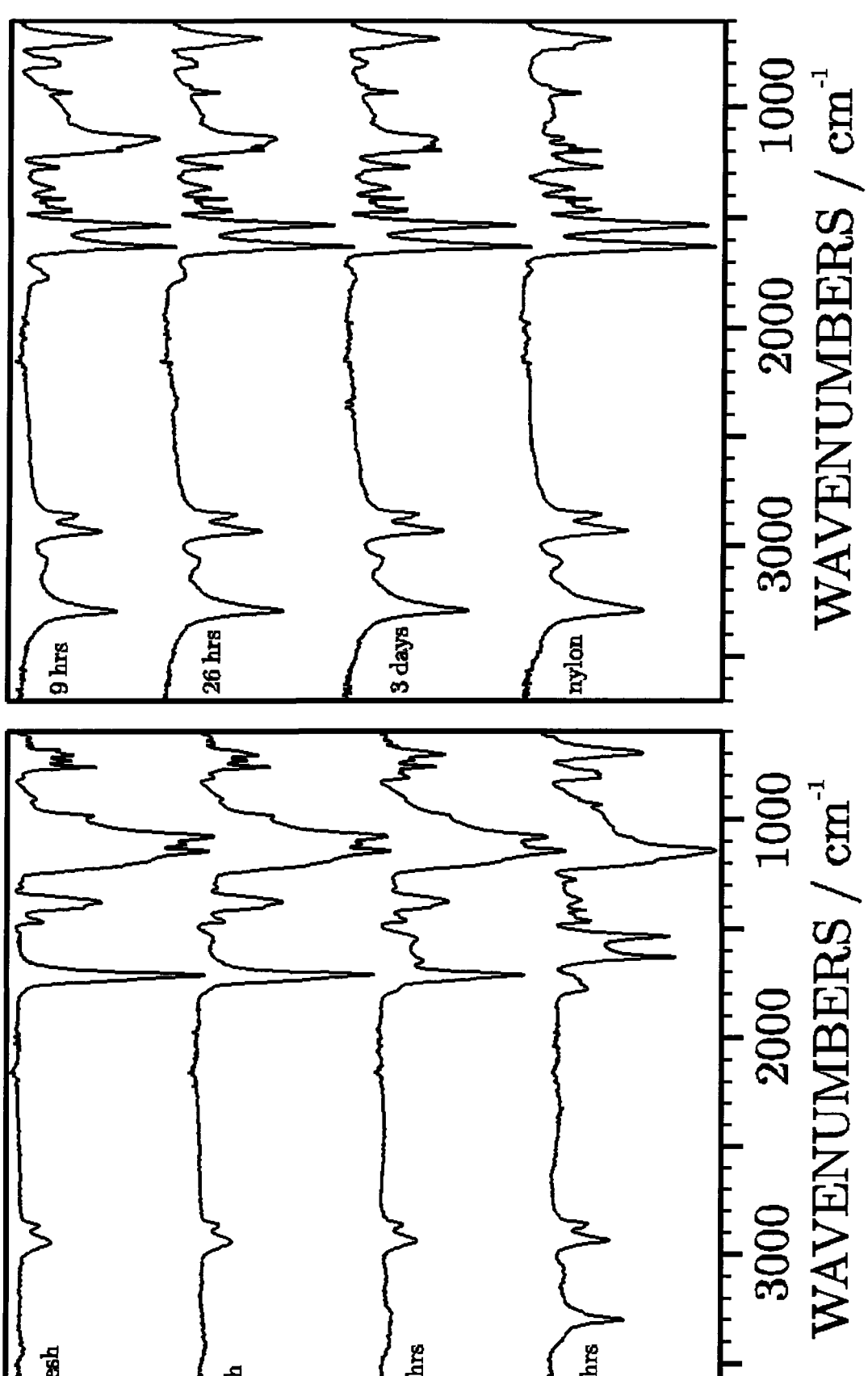

Fig. 8 Changes in the ATR - IR spectra of TFAA treated nylon 6,6 films as a function of storage time in ambient air

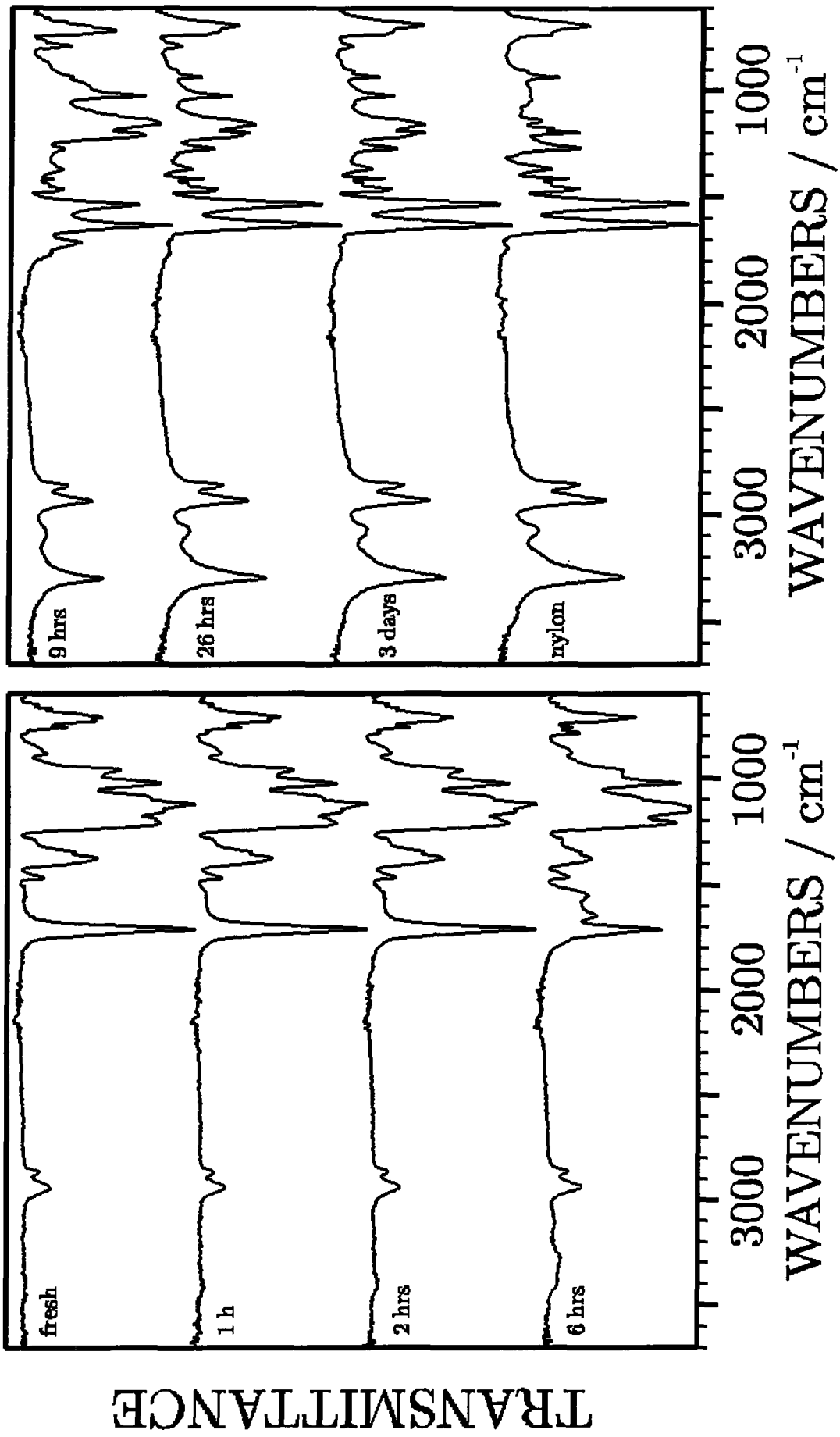

Fig. 9 Changes in the ATR - IR spectra of PFPA treated nylon 6,6 films as a function of storage time in ambient air

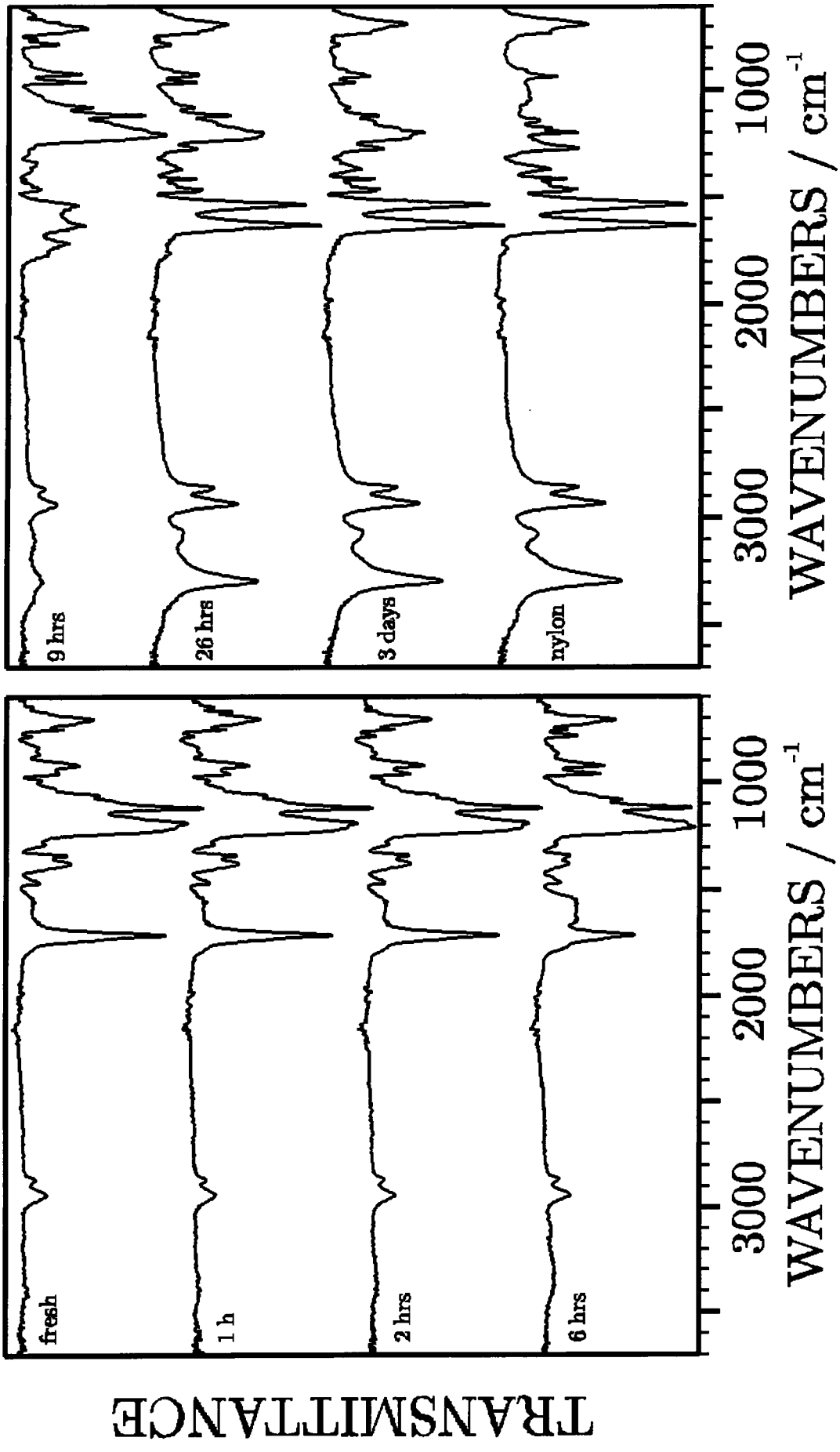

Fig. 10 Changes in the ATR - IR spectra of HFBA treated nylon 6,6 films as a function of storage time in ambient air

the decomposition is found for the HFBA product. While the amide I and amide II signals in the spectra of the other two products have a higher intensity than the products' >C=O peak, these signals have an almost equal intensity in the corresponding spectrum of the HFBA product. The attachment of fluorine containing substituents with increasing chain length to nylon 6,6 surfaces therefore leads to an increasing stabilisation of the product against hydrolysis. It is conceivable that this is due to the accumulation of carbon-fluorine species which renders the attack of water molecules more and more difficult.

6.5 Discussion

Although the carboxyl species present in the model polymer renders the exact measurement difficult the results suggest that the expected esterification takes place quantitatively. As far as the reaction with PVA is concerned the reaction proceeds quickly. The derivatisation of other samples containing hydroxyl functionalities might take longer depending on their respective structure. Although XPS measurements at varied take-off angles were not carried out the ATR-IR spectra of the ester suggest that homogeneous labelling takes place even to a larger depth than accessible with XPS. Furthermore, the product ester was found to be sufficiently stable in ambient air.

In the selectivity experiments it is difficult to distinguish the contributions of physisorption, reaction of impurities possibly present in the commercial polymers and true cross-reaction. This applies especially to PSF, PEO and PEEK. Therefore it is not possible to come to a conclusion concerning the selectivity of PFPA towards the functionalities contained in these polymers. It is conceivable that n-hexane used as the solvent in the present study was not suited to remove all the material adsorbed. The use of other washing solvents perhaps with a slightly higher polarity and the use of defined polymer standards could provide a more complete picture about the selectivity of PFPA in labelling reactions.

With respect to the practical application of PFPA derivatisation the requirement of a washing procedure is a big disadvantage. As already mentioned in 6.2 the use of a solvent can cause changes on the sample surfaces. Those include the removal of low molecular weight material which might be present on the sample

surface, reorganisation at the surface and undesired reactions with the solvent. All these changes are sources for erroneous results. Additionally, the solvent cannot be used in the case of polymers which dissolve in the washing reagent.

In the present study only the reaction of PFPA with a polyamide was studied. TFAA, the lower homologue, was not only found to react with polyamides but also with amine groups [18] and polyurethanes [20,22]. Polyurethanes reacted much slower than polyamides [20,22]. It can be assumed that PFPA undergoes similar reactions. In the presence of nitrogen species PFPA is therefore most probably not sufficiently specific as a labelling reagent because it reacts with too many funtionalities. As a consequence PFPA derivatisation is only suited for surfaces composed of carbon and oxygen. This finding represents a further limitation to the labelling method in addition to the washing step.

6.6 Conclusions

PFPA effectively undergoes the desired reaction with hydroxyl functionalities in the model polymer. It is selective towards ester and carboxylic acid groups. No firm conclusions can be drawn regarding the cross-reaction with the functionalities contained in PSF, PEO and PEEK. Further studies with defined polymer standards are required to elucidate this question.

Due to the tendency of PFPA to adsorb, solvent washing of the samples is required. The washing procedure represents a drawback of the method because it can lead to changes in the sample and thus to errors in the results.

A cross-reaction with a polyamide, nylon 6,6, takes place. The polymer reacts quantitatively with TFAA, PFPA and HFBA to give a N-fluoroacylated product which is unstable towards moist air. The stability of the product increases with the length of the fluorinated chain attached. Due to the likely reaction with a number of nitrogen containing functionalities PFPA labelling can only be applied in the derivatisation of surfaces containing carbon - oxygen species.

6.7 References

1) Reilley, C.N.; Everhart, D.S.; Ho, F.-L. In: *Applied Electron Spectroscopy For Chemical Analysis*, Windawi, H.; Ho, F.-L., Eds., John Wiley and Sons : New York, 1982, pp.105-133

2) Everhart, D.S.; Reilley, C.N. *Anal. Chem.* **1982**, *53*, 665

3) Batich, C.D. *Appl. Surf. Science* **1988**, *32*, 57

4) Chilkoti, A.; Ratner, B. In: *Surface Characterizsation of Advanced Polymers* Sabbatini, L.; Zambonin, P.G. Eds., VCH : Weilheim, 1993, pp.221-256

5) Dickie, R.A.; Hammond, J.S., de Vries, J.E. Holubka, J.W. *Anal. Chem.* **1982**, *54*, 2045

6) Gerenser, L.J.; Elman, J.F.; Mason, M.G.; Pochan, J.M. *Polymer* **1985**, *26*, 1162

7) Pochan, J.M.; Gerenser, L.J.; Elman, J.F. *Polymer* **1986**, *27*, 1058

8) Briggs, D.; Munro, H.S. *Polymer Communications*, **1987**, *28*, 307

9) Beamson G., Briggs, D., *High Resolution XPS of Organic Polymers - The Scienta ESCA 300 Database*, John Wiley & Sons : Chichester, 1992, p.97

10) Ameen, A.P.; Ward, R.J.; Short, R.D.; Beamson, G.; Briggs, D. *Polymer* **1993**, *34*, 1795

11) Krimm, S. Liang, C.Y., Sutherland G.B.B.M. *J. Pol. Sci.* **1956**, *22*, 227

12) Tadokoro, H.; Seki, S.; Nitta, I. *J. Pol. Sci.* **1956**, *22*, 563

13) Haas, H.C.; *J. Pol. Sci.* **1957**, *23* 391

14) Crowder, G.A. *J. Fluorine Chem.* **1972**, *2*, 217

15) Prof. D.Parker, University of Durham, personal communication

16) Colthup, N.B.; Daly, L.H.; Wiberley, S.E. *Introduction to Infrared and Raman Spectroscopy*, 3rd edition, Academic Press : Boston, 1990, pp.275-276

17) *Römpps Chemielexikon* Vol.5 Falbe, J.; Regitz, M. Eds., Thieme : Stuttgart, New York, 1992, p.3532

18) Nakayama, Y.; Takahagi, T.; Soeda, F.; Hatada, K.; Nagaoka, S.; Suzuki, J.; Ishitani, A., *J. Pol. Sci.: Part A: Pol. Chem*, **1988**, *26*, 559

19) Schuttenberg, H.; Schulz, R.C. *Angew. Chem. Int. Ed. Engl.* **1976**, *15 (12)*, 777

20) Jacobi, E.; Schuttenberg, H.; Schulz, R.C. Makromolek. Chem. Rapid Comm. **1980**, *1(6)*, 397

21) Weiskopf, K.; Meyerhoff, G. *Polymer* **1983**, *24*, 72

22) Biagini, E.; Gattiglia, E.; Pedemonte, E.; Russo, S. *Makromol. Chem.* **1983**, *184*, 1213

23) Siesler, H.W.; Holland-Moritz, K., *Infrared and Raman Spectroscopy of Polymers,* Marcel Dekker Inc. : NewYork, 1980

24) Bellamy, L.J. *The Infrared Spectra of Complex Molecules*, Vol.1, 3rd edition, Chapman and Hall : London, 1975, p.369

25) Lin-Vien, D.; Colthup, N.B.; Fateley, W.G., Graselli, J.G. *The Handbook of Infrared and Raman Characteristic Frequencies of Organic Molecules*, Academic Press Inc. : Boston, 1991, p.41

26) Fuson, N.; Josien, M.L.; Jones, E.A.; Lawson, J.R. *J. Chem. Phys.* **1952**, *20 (10)*, 1627

27) Kagarise, R.E. *J. Chem. Phys* **1957**, *27 (2)*, 519

28) Crowder, G.A. *J. Fluorine Chem.* **1971/72**, *1*, 385

29) Crowder, G.A. *J. Fluorine Chem.* **1973/74**, *3*, 133

Chapter 7:
In-situ mass spectrometric study on the vacuum photodegradation of Polyethersulfone

7.1 Introduction

Polyethersulfone (PESF, figure 1) is a representative of the polysulfones, a group of polymers containing the sulfone group. Polysulfones possess a number of favourable properties [1-3] including high transparency, high toughness and rigidity over a broad range of temperatures (from -100 to +180 °C), high resistance against thermal oxidation, flame resistance, good electrical isolation properties and resistance towards mineral acids, alkalis, lubricants, detergents and alcohols. They can, however, be attacked by chlorinated and aromatic solvents as well as by ketones. Their properties make polysulfones candidates for demanding engineering purposes in the electronic, car and plane industries.

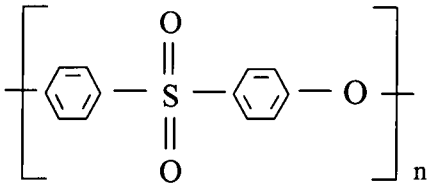

Fig. 1 Chemical Structure of Polyethersulfone (PESF)

7.2 Background

The most common polysulfones are bisphenol A polysulfone (PSF) and polyethersulfone (PESF). Despite their thermal stablity these polymers are known to suffer rapid degradation by exposure to sunlight [4] leading to yellowing and a deterioration of the mechanical properties. In solutions both polysulfones show an absorption maximum at about 270 nm [5] whereas their respective films absorb at wavelengths below 320 nm [6,7]. In contrast to other polymers whose absorbance is due to impurities introduced into the polymer during preparation or processing, the

two polysulfones possess a chromophore, the diphenylsulfone moiety [4]. Upon irradiation the absorbance of the film gradually shifts towards higher wavelengths up to the VIS region. This shift is held to be responsible for the discoloration of irradiated films to yellow-brown [2,4] and is thought to be due to the formation of a conjugated π-electron system [4]. Yellowing is found both in air and in inert atmosphere [5]. In practice, this behaviour can be used as an intensity monitor for UV radiation from both the sun and artificial light sources [6]. This is achieved by relating the degree of degradation of the polymer film to the incident dose of radiation by measuring the change in its spectroscopic properties.

The degradation of polysulfones both in air [4-9] or oxygen [8,10,11] and in inert atmosphere (nitrogen) [9,12,13] as well as in vacuum [7,9,13] has been investigated with a number of techniques. Most of the studies were carried out using bisphenol A polysulfone (PSF) as the model polymer. Although slightly different in chemical structure (see chapter 5, figure 5) and reactivity [9] its reaction behaviour can give valuable hints for that of PESF, the subject of the present study. In addition, it is difficult to compare the individual studies because the experimental conditions vary considerably. An overall degradation mechanism was not established in any of the studies. The following paragraphs will be limited to the review of the photodegradation studies.

In their investigation of PSF and PESF degradation at wavelengths > 290 nm employing gel permeation chromatography (GPC) Kuroda et al. [5] found that the degradation of both polymers proceeds via simultaneous chain scission and crosslinking. Later studies showed the dependence of the scission to crosslinking ratio on the reaction temperature where crosslinking was the predominant reaction at higher temperatures [9,12]. The deceleration of the degradation observed in the later stages of the irradiation was linked to the formation of a phenol moiety by a photorearrangement process. The appearance of O-H stretches in the IR spectra of PESF films irradiated in nitrogen which became more intense with increasing treatment time was taken as evidence for the presence of these stabilizing species [5]. The authors summarized their results for both polymers in a mechanism which relies on the scission of the C-S bond as the initial step, scheme 1. The breakage of the ether linkage was regarded to be much less likely [5]. Since the number of SO_2 molecules formed per crosslinking point was found to be small, SO_2 formation was

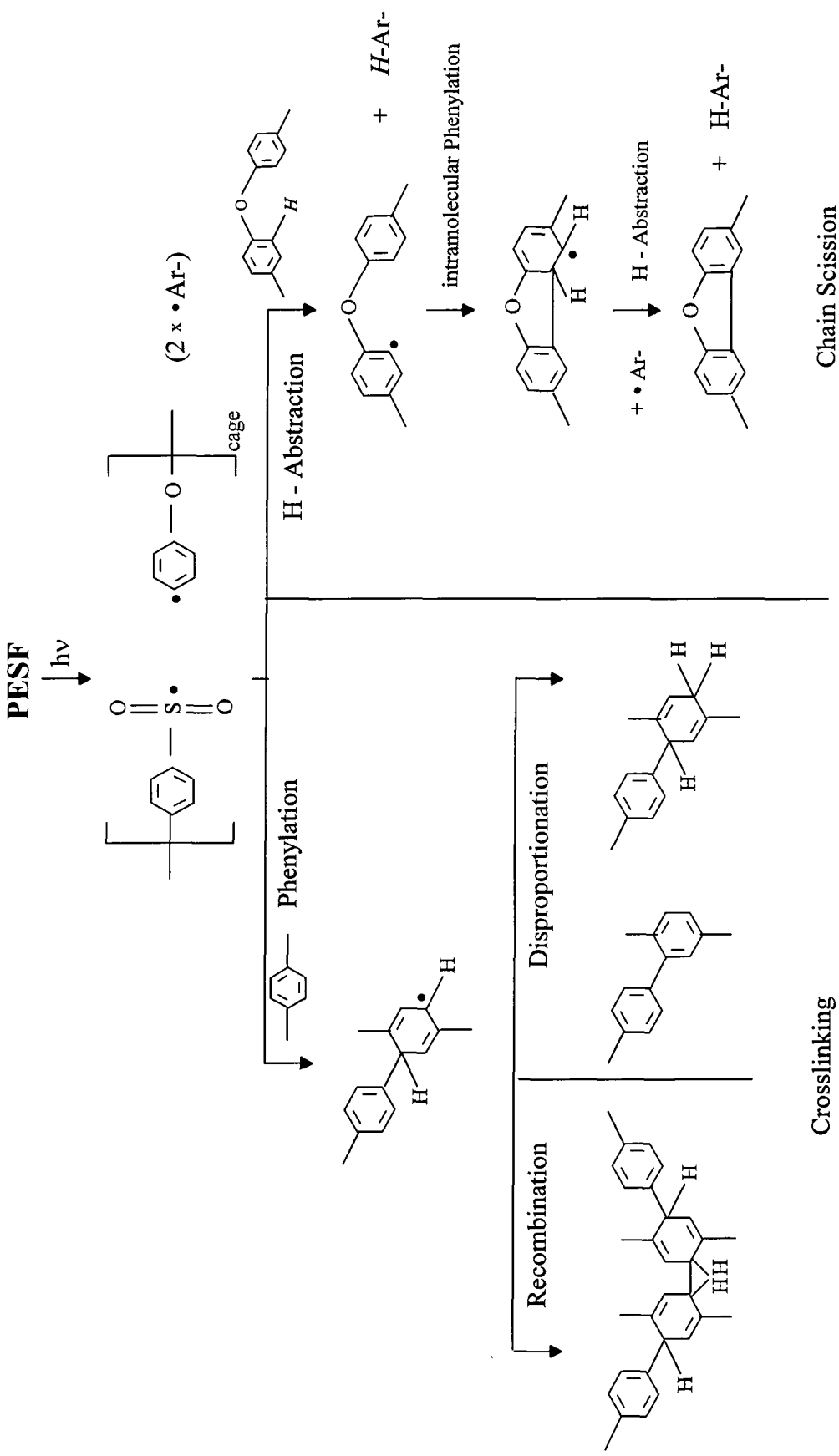

Scheme 1 Degradation mechanism for polysulfones suggested by Kuroda et al [5]

considered to be only a secondary reaction. A mechanism for this process was not suggested [12].

Munro and Clark reported a XPS study on the degradation of PSF in a nitrogen atmosphere and in vacuum at wavelengths > 290 nm [13]. The irradiation resulted in an overall reduction of the sulfur content. The most striking change observed in the irradiated films in both atmospheres, however, was the appearance of a reduced sulfur environment which was attributed to the presence of an organic sulfide. Further experiments suggested that the sulfide species was only formed in polymers containing aromatic rings. Additionally, the XP spectra of irradiated films showed a reduced contribution of the ether component to the C (1s) envelope which signifies that scission of the ether linkages had occurred. Allen and Mc Kellar presented other spectroscopic evidence for the scission of the phenyl-oxygen bond [4,14].

There is only scarce information about gaseous degradation products of polysulfones. Kuroda et al. who investigated the degradation behaviour of both PSF and PESF only mention the formation of gaseous products stating that SO_2 is their main component; a detailed analysis, however, is not given [5,12].

Mass spectral data are available for the sum of the gaseous products evolved during 500 hours of irradiation with a sun lamp from a PSF sample sealed in an evacuated quartz tube [7]. The products obtained were then expanded into a mass spectrometer. Hydrogen, carbon monoxide and carbon dioxide were detected along with methane, benzene, oxygen, carbonyl sulfide and sulfur dioxide in the product mixture. The carbon oxides were thought to arise from aldehydes and carboxylic acids already present in the polymer as impurities as it was thought to be unlikely that these were due to oxygen developed from the polymer during irradiation. The authors assume a mechanism in which random chain scission of all bonds occurs except the breaking of the aromatic C-C and C-H bonds.

The aim of this chapter was to study the volatile photodegradation products in the mass range m/z > 50 in order to obtain further information about the mechanism and temporal aspects of the degradation process. The in-situ detection used in the mass spectrometry experiments offers the advantage that the gaseous degradation products are detected as they are evolved. The probability for secondary reactions of the products between their development and their detection is therefore reduced.

Furthermore, it is less likely that solid products escape detection by deposition on the walls of the vessel.

7.3 Experimental

The photodegradation experiments were carried out in a UHV chamber, a schematic of which is shown in figure 2. The base pressure of the apparatus was 3×10^{-9} torr.

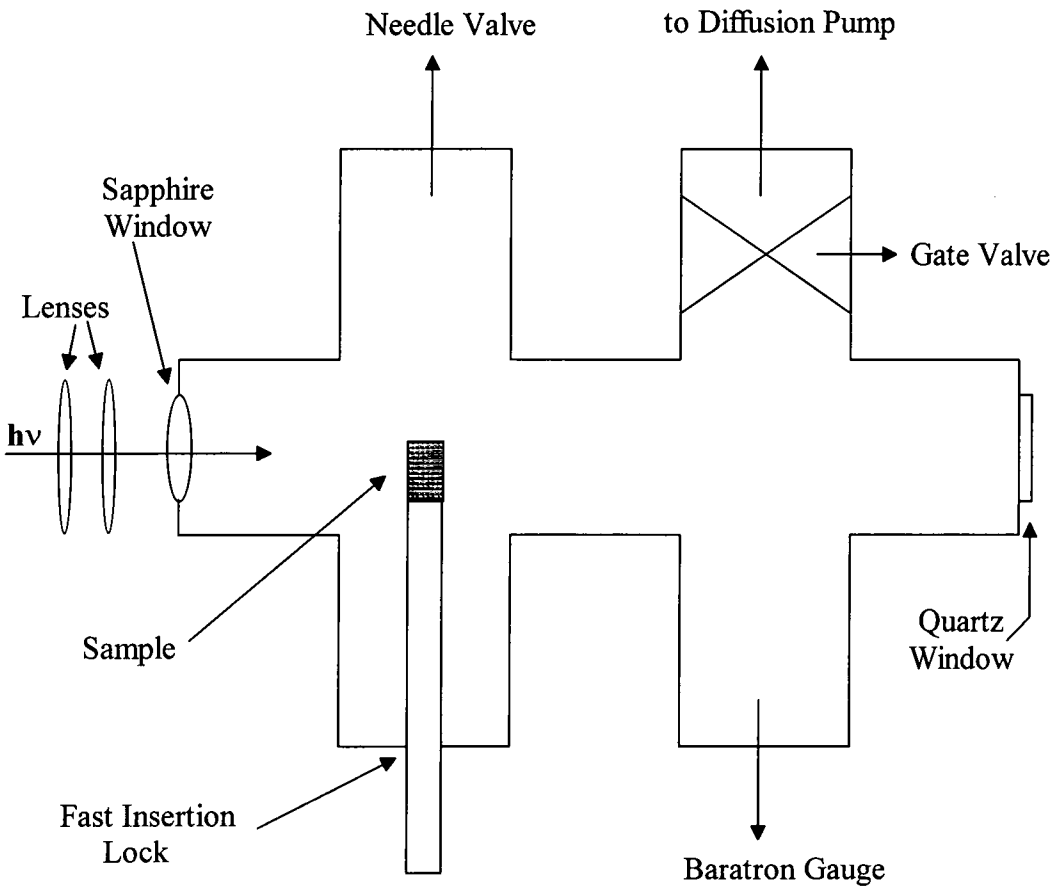

Fig. 2 Schematic representation of the in-situ MS set-up (QMS head situated out of plane of paper)

Volatile degradation products evolved during irradiation were detected using a VG SX 200 quadrupole mass spectrometer. The ions were created by electron impact, 70 eV. The instrument was interfaced with a PC; experimental data were registered and analysed employing in-house software.

The radiation source was the Oriel high pressure Hg (Xe) lamp described in chapter 4.3.1. In the present experiments it was operated at 200 W. The sample was irradiated through a sapphire window with a cut-off wavelength between 141-161 nm. In some experiments, a Czerny-Turner type monochromator (Model 7300 grating monochromator, Applied Photophysics) was placed between the lamp and the window to filter out undesired components of the lamp spectrum. The radiation passing the monochromator was then focussed onto the sample using two planoconvex fused silica lenses (f =10.2 cm, Ealing Electrooptics and f = 10 cm Comar). The chosen wavelength on the monochromator was 307 nm, an intensity maximum of the lamp, the bandwidth of the transmitted radiation was 46,5 nm [15].

Thin stripes of polyethersulfone (Westlake Plastics Company) were ultrasonically cleaned for 30 seconds in cyclohexane and dried prior to insertion into the spectrometer. The samples were attached to a stainless steel sample holder using stainless steel screws in order to avoid the use of double sided adhesive tape which could have possibly caused unwanted contributions to the spectra by outgassing.

A calibration of the instrument's mass scale was carried out prior to each experiment using the signals of the residual gases (water, carbon monoxide, carbon dioxide) in the mass range < m/z = 50 whereas for the higher mass range signals of Perfluoro tri n-butylamine appearing at m/z = 50, 69, 100, 119, 131, 150, 169, 176 and 181 were employed as mass markers. The mass scale in the range between two signals of the mass marker was extrapolated linearly by the computer programme.

After the base pressure was reached the experiment started with a 30 minute irradiation phase of the chamber walls in order to remove adsorbed species. Light admission to the chamber was achieved by removing a shutter otherwise placed in front of the window. During the cleaning procedure the sample was held back from the light. After finishing the irradiation and pumping away the products of the cleaning step the sample was positioned in the centre of the chamber and turned to an angle as shown in figure 3.

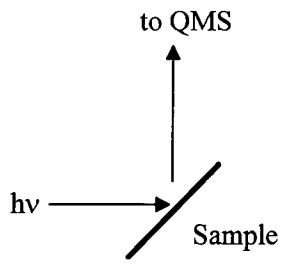

Fig. 3 Arrangement of the sample with respect to the light source and the QMS entrance

The pump had to be throttled in order to increase the residence time of the products and allowing them to be detected. This was done by closing the gate valve between pump and chamber and subsequently opening it again by 5 full turns. Then data acquisition started.

Qualitative and quantitative information were obtained in separate experiments each requiring an undegraded sample. In both cases the experimental conditions were approximately the same but a different kind of information was registered with the computer programme. The first step consisted of the irradiation of samples while scanning the mass spectra in the mass range available. Relevant signals were chosen on the basis of these initially recorded mass spectra. In the second step the amounts of those masses developed from a PESF sample in consecutive irradiation phases were monitored. This was achieved by recording a profile composed of 270 data points for each particular mass during each irradiation phase. A data point corresponding to the intensity of the mass under consideration was recorded every 10 seconds such that one profile describes an overall time of 45 minutes. In a profile the actual irradiation time which lasts 10 minutes (60 scans) is sandwiched between two phases in which the sample is not exposed to light. Those phases last 10 minutes at the beginning and 25 minutes at the end and constitute the baseline for the subsequent evaluation by integration of the area. The duration of the second phase was chosen to be longer because in some cases a tailing off of the signal intensity was observed after the irradiation time was finished. Light admission and exclusion were achieved by using the shutter as described above.

After the removal from the mass spectrometer some of the degraded samples were transferred to a different sample holder and inserted into the XP spectrometer so as to find out about possible changes in their surface composition. The XP spectra were recorded under the conditions described in section 3.3.2 and peakfitted as

described in section 6.3. In this case the sensitivity factors for unit stoichiometry were taken as being: C (1s) : O (1s) : S (2p) = 1.00 : 0.62 : 0.55.

7.4 Results

7.4.1 Qualitative information from the mass spectra

The irradiation of the samples while recording the mass spectra provides qualitative information about the volatile products. Since a product mixture is obtained the spectra contain many contributions which are difficult to assign. In the low m/z region particularly several fragmentation processes may contribute to a single signal.

From the polymer structure and the reports in the literature, certain products are likely to be formed. These include sulfur dioxide, diphenylsulphone and diphenylether which represent structural units in the polymer. Biphenyl and dibenzofurane are further possible products. The former is the product of the recombination of two phenyl radicals after the extrusion of SO_2 and the formation of the latter can be assumed from the degradation mechanism suggested by Kuroda et al.[5]. The fragmentation patterns of those compounds, except SO_2, are given in table 1. The main signals only are listed here.

m/z	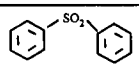 *) ***) [16]	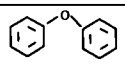 **) [17]	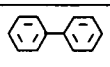 **) [17]	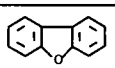 **) [17-19]
218	100 %			
188				
187				
186				
185				
184				
171		36.0		
170		**266**		
169		9.7		63.9

168		5.1		**482**
155			50.2	
154	6.5 %		**386**	
153	14.5 %		**106.1**	
152	17.3 %		76.3	
151			21.2	
142		69		
141	4.55 %	104		
140				18
139	1.88 %			121
128			10.1	
125	**384 %**			
115		27.7	14.1	
114				13.7
113				13.7
109				
94		11.8		
93	3.1 %			
92				
87				10.6
84				45.1
77	**190 %**	114.5	39	
76			72.3	
75				9.2
74				9.4
71		15.1		
70		12.4		11.1
69				13.8
65		15.1		
64			28.1	
63		11.5	20.7	19.4
62				10

51		96.5	20.6	
50		20.6		
39		30.3		10.8

Tab. 1 Fragmentation Patterns of important degradation products

* intensity definition: "scale of relative intensities is defined by assigning a value of 100% to the parent peak" [16]

** intensity definition: "peak heights are expressed as parts per 1000 of total ion beam without isotope correction"[17]

*** no information available for m/z < 77

The most conspicuous signal that appears as soon as the radiation reaches the PESF sample is that at m/z = 64. Together with another signal at m/z = 48 this signal is related to SO_2 [20], a volatile degradation product mentioned by others [5,7,12]. A signal at m/z = 60 is due to COS which has also been identified in an earlier polysulfone degradation study [7]. It is formed in a reaction between CO and SO_2 according to [7,14]:

$$CO + SO_2 \rightarrow COS + O_2$$

Furthermore, there is evidence for all the compounds listed in table 1. Other signals are observed in addition to those the fragments, the attribution of these is not straightforward. Comparing the peak intensities obtained at the same gain for m/z = 125 and 170 taken as representatives for diphenylsulfone and diphenylether respectively it can be seen that diphenylsulfone is only formed in minor amounts. This observation together with the detection of SO_2 as the main volatile product suggests that the sulfone bond is the favourite site for bond breaking rather than the ether linkage. This is in agreement with the findings reported by Kuroda et al. [5].

The overlap of its most important signals at m/z = 154 and 153 with fragments of diphenylsulfone as well as a lack of other intense peaks characteristic of the compound renders the identification of biphenyl difficult. Considering the fragmentation pattern of diphenylsulfone in table 1 and taking the decrease in sensitivity of the quadrupole filter towards higher masses into account the peak

intensity of m/z = 154 should be much smaller than that of m/z = 125 if only this compound were present. In the irradiation experiments, however, the signal intensity at m/z = 154 is considerably larger than that of m/z = 125 when both signals are recorded at the same gain. This observation suggests that biphenyl is formed as a reaction product and that it constitutes the largest contribution of the signal at m/z = 154.

During the time of a typical experiment ($h\nu_{max}$ = 90 minutes) a delayed appearance of a further compound in the mass range accessible with the present set-up was not observed.

7.4.2 Quantitative information from the profiles

7.4.2.1 Profiles obtained with the full lamp spectrum

After chosing intense, characteristic m/z values for the compounds of interest found in the first step, profiles of these masses were recorded by subjecting a sample to a row of consecutive irradiation phases. The areas of the profiles representing the amount of the respective volatile product were integrated and plotted against treatment time. Examples are given in figures 4 - 6 for m/z = 60, 64, 125, 154, 168 and 170 representative of COS, SO_2, diphenylsulfone, biphenyl, dibenzofurane and diphenylether respectively. The profile areas of all the products monitored decrease with increasing exposure time to light. The largest decrease in profile area is observed between the first and the second irradiation phase; the decrease in peak area becomes slower in later stages of the degradation. In an experiment in which 9 instead of 7 irradiation phases were monitored a continuation of this trend was observed. The corresponding pressure increase, Δp, accompanying product desorption during irradiation is in line with the findings for the profile areas. In the first irradiation period an increase in pressure from 3×10^{-9} torr to 1.5×10^{-8} torr was observed upon light admission to the sample. During later irradation phases, the pressure difference became gradually smaller signifying that less products were being evolved. In the last irradiation phase the pressure only increased from 3×10^{-9} to 7×10^{-9} torr.

Within the set time intervals none of the monitored masses showed a delayed increase in peak area. Such behaviour would have been conceivable for biphenyl and

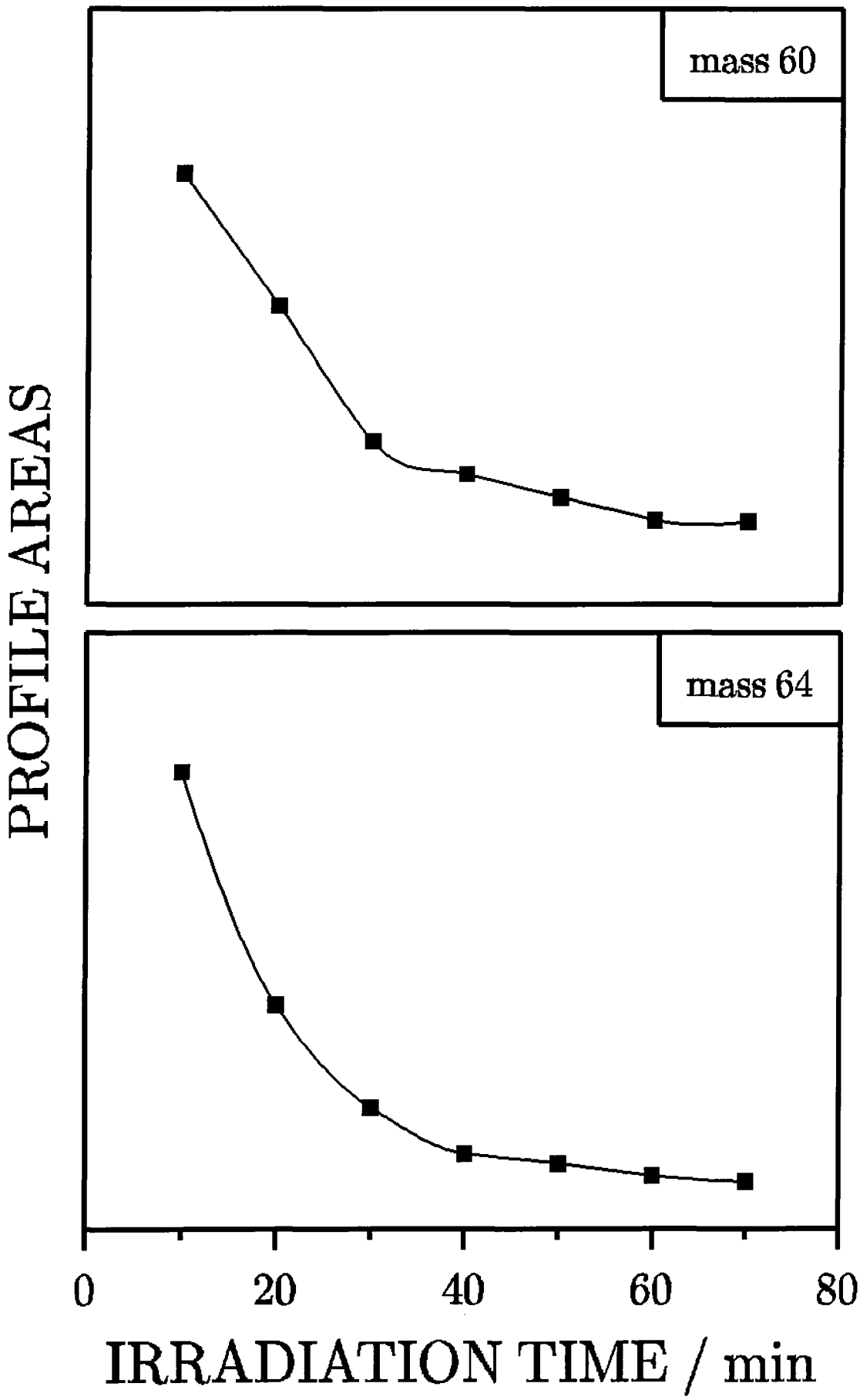

Fig. 4 Profile areas of masses 60 and 64 as a function of irradiation time ($h\nu_{unmonochr.}$)

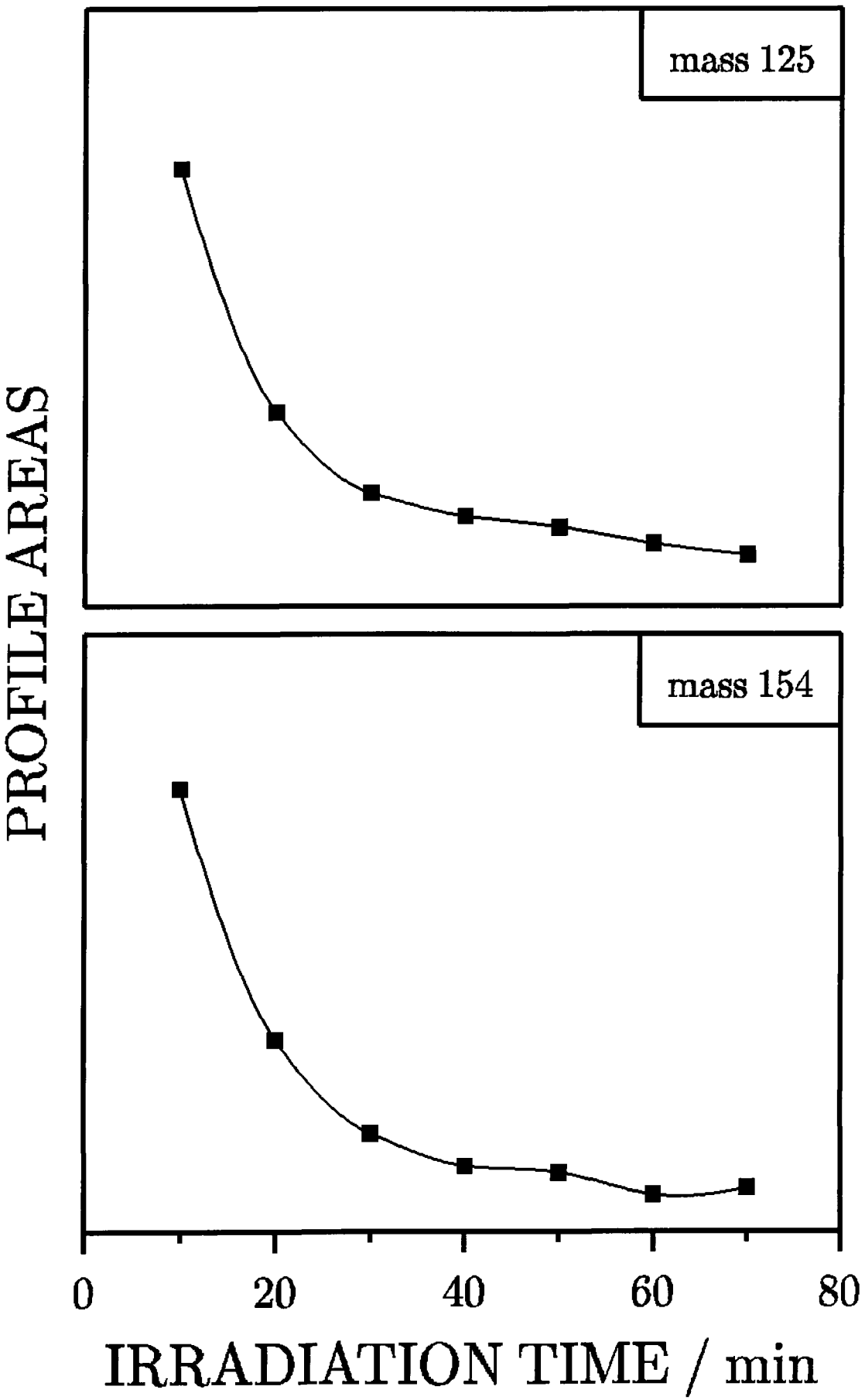

Fig. 5 Profile areas of masses 125 and 154 as a function of irradiation time ($h\nu_{unmonochr.}$)

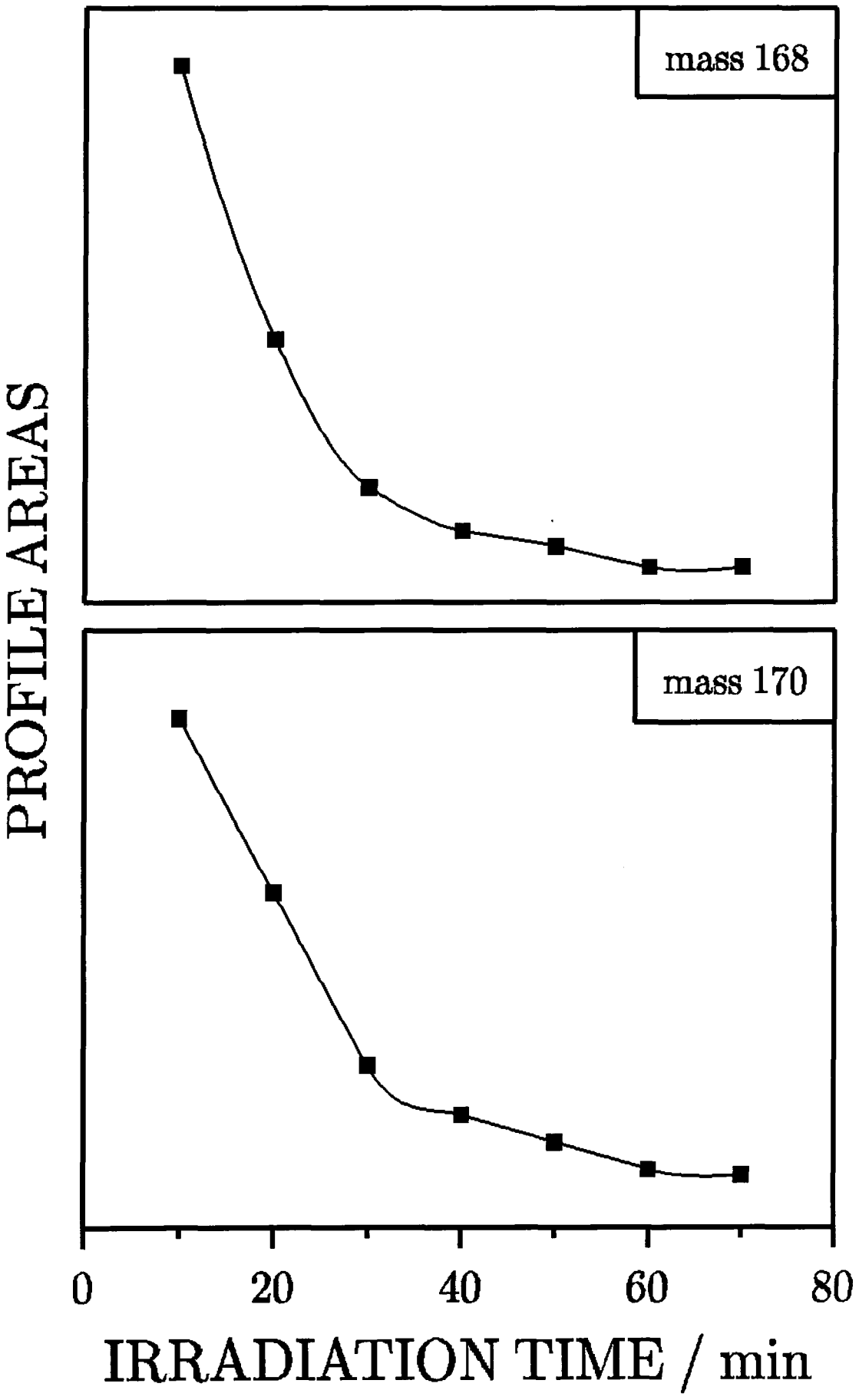

Fig. 6 Profile areas of masses 168 and 170 as a function of irradiation time ($h\nu_{unmonochr.}$)

dibenzofurane which are both primary products. After their formation they could have initially remained on the sample surface before being desorbed.

Comparing the profiles obtained at the beginning and at later stages of the degradation a reversal of the profile shape can be observed for masses 60 and 64. Figure 7 shows this behaviour taking m/z = 64 as an example. In contrast, no reversal in the profile shape is observed for masses 125, 168 and 170, figure 8 shows the profiles of mass 168. Mass 154 has an intermediate behaviour, the top of the profile recorded during the first irradiation phase is almost linear. This change probably reflects a fast crosslinking process occurring on the sample surface which allows small fragments to escape easier. The differences in the tailing-off of the profiles of masses 64 and 168 are due to the dependence of pumping speed on the mass of the products.

In the irradiation experiments where the whole lamp spectrum was used the beam hit both the sample surface and the chamber walls. During irradiation product species adsorbed to the chamber walls were therefore desorbed in addition to the products evolved from the sample. Profiles obtained by irradiating the empty chamber after finishing the experiment reveal a desorption tendency of adsorbed compounds for all the masses monitored except 64 and 60. The proportion of the desorbed product with respect to the amount measured in the irradiation experiment varies for the different products and is found to increase in the order 154 < 168 < 170 < 125. In the case of mass 125 the desorbed amount could be as much as 50% of the total amount of product measured. Therefore a direct comparison of the temporal behaviour of the different products is not possible. In order to avoid this problem experiments in which the lamp radiation was passed through a monochromator were carried out. Using this set-up the beam could be focussed directly onto the sample.

7.4.2.2 Profiles obtained with monochromatised light

Compared to the irradiation of PESF with the unfiltered spectrum the use of monochromatised light led to the development of considerably less volatile products. The signals in the m/z range > 150 were very weak. Within the instrument's sensitivity no other masses than those found in the experiments using unmonochromatised light could be detected. Due to the small amount of the

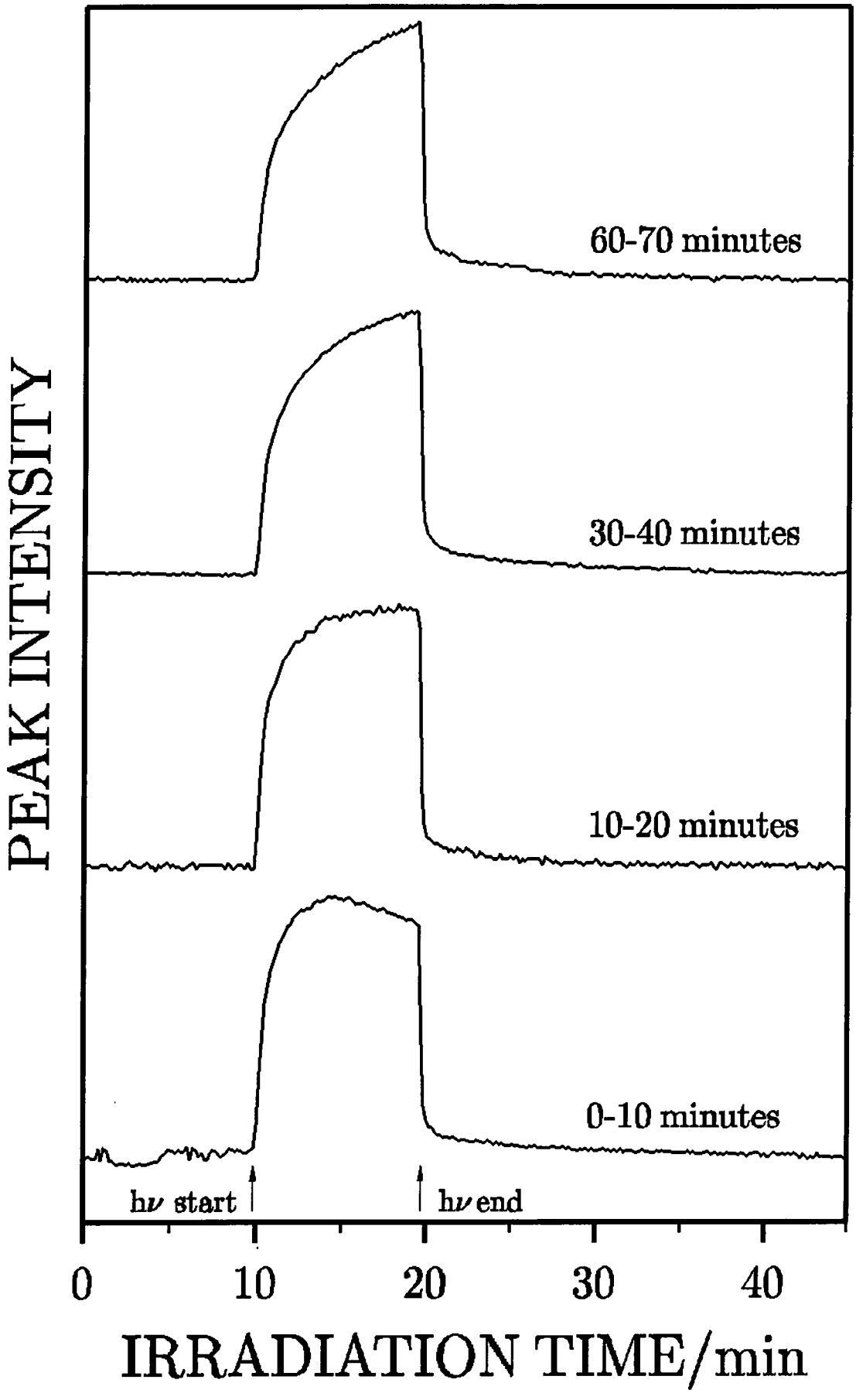

Fig. 7 Change of the profile shape of mass 64 as a function of irradiation time ($h\nu_{unmonochr.}$)

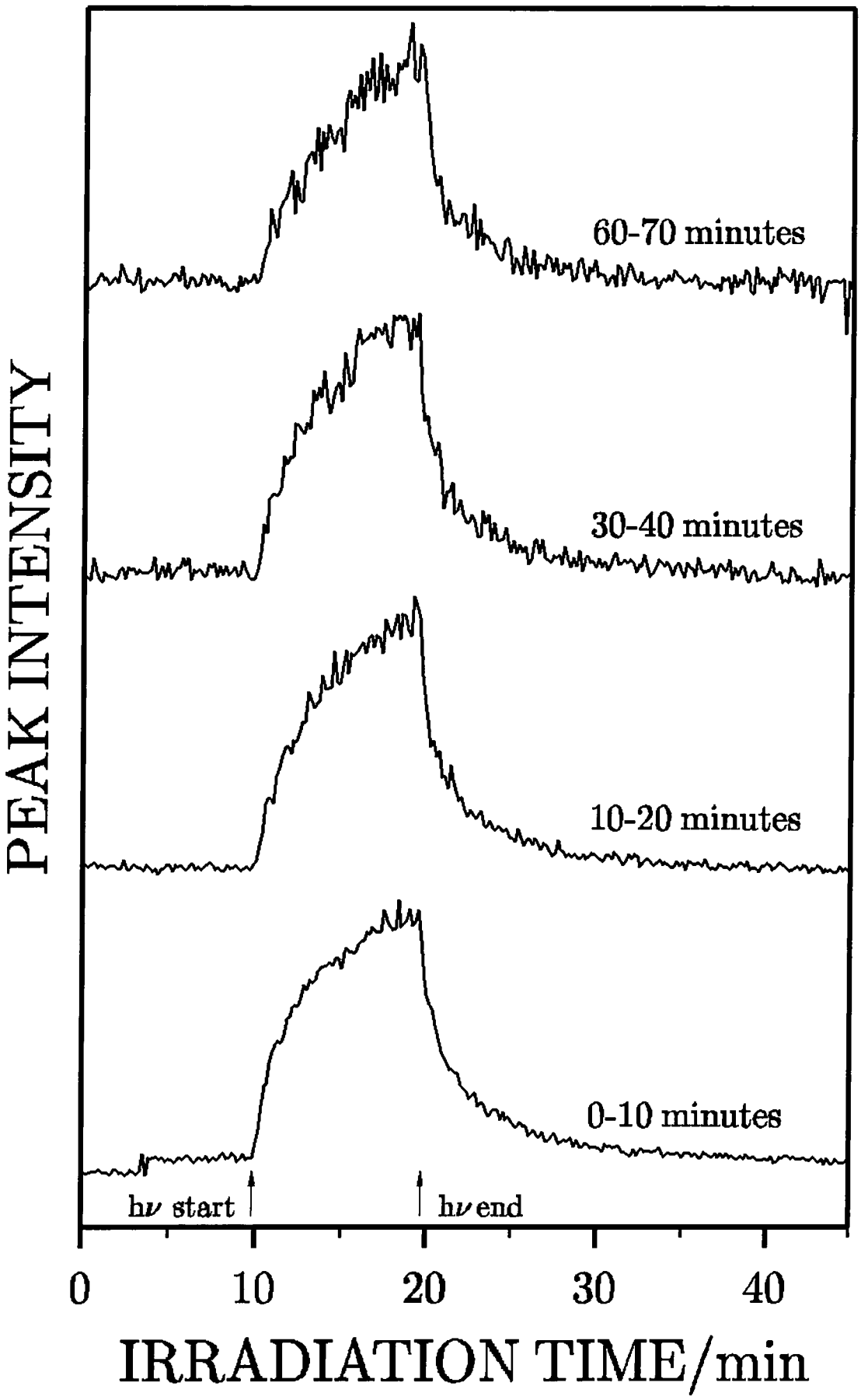

Fig. 8 Change of the profile shape of mass 168 as a function of irradiation time ($h\nu_{unmonochr.}$)

products profiles of masses 168 and 170 could only be recorded during the initial irradiation phases, in later stages of the degradation the reduced amount of product did not allow the registration of further profiles. Profiles of the less intense signals 125 and 154 could not be recorded at all. In contrast, the development of products with smaller m/z values could be monitored for all the irradiation steps, figure 9 showing the corresponding plots for masses 60 and 64. The difference in pressure caused by the irradiation of the polymer was also low, during the first irradiation phase only an increase from 5.5×10^{-9} to 6.5×10^{-9} torr was observed.

The observations concerning the development of SO_2 do not change drastically when changing from irradiation with the full lamp spectrum to that with a small band of wavelengths. The area of the profiles gradually decreases in both cases, the decrease in the first case being, however, stronger than in the second case. Additionally, the changes in the shape of the profiles are not as pronounced as in the case of the sample exposure to the full lamp spectrum, figure 10. A reversal of the profile shape is not observed. This could be related to a slower build-up of the crosslinked layer which may be due to the lower overall irradiance that the sample is exposed to under these conditions. Lower temperatures due to the filtering out of the IR component of the lamp spectrum may play an additional role in this process. The nearly linear profile obtained for COS might be related to a corresponding change in CO development. Using the monochromatised light the irradiation of the empty chamber before and after treatment of the films led only to the detection of a small signal at m/z = 94.

7.4.3 XPS

The elemental composition of untreated polyethersulfone films is in good agreement with the theoretical value, table 2. Independent of the type of radiation used in the experiments irradiated films generally show a reduction in sulfur and oxygen content whereas the carbon content is increased. These findings suggest that irradiation gives rise to a loss of sulfur and oxygen from the sample surface. The degree of modification observed in the films irradiated with unmonochromatised radiation is, however, much larger than in films exposed to monochromatised light. This result could have already been expected from the the optical appearance of the

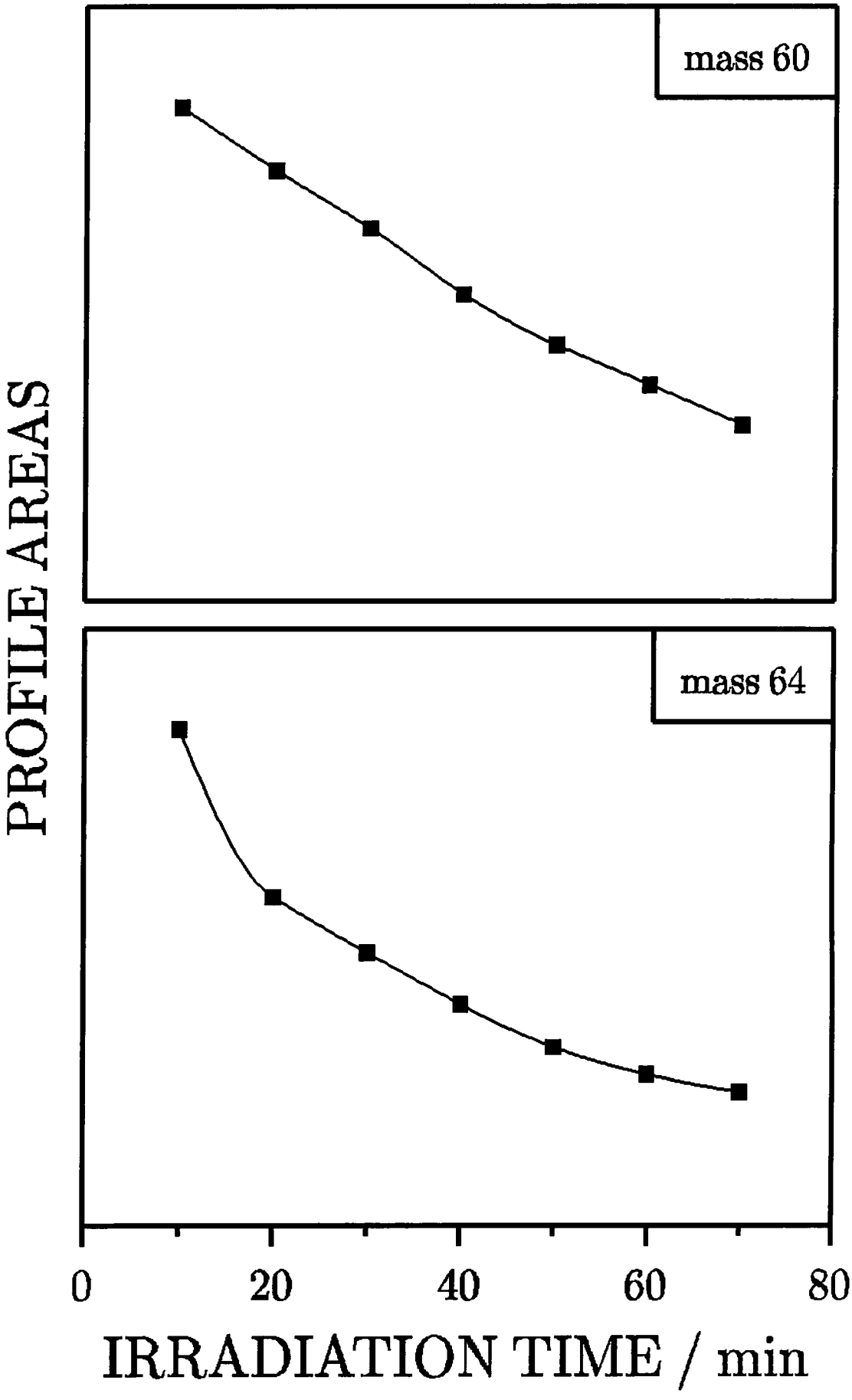

Fig. 9 Profile areas of masses 60 and 64 as a function of irradiation time ($h\nu_{monochr.}$)

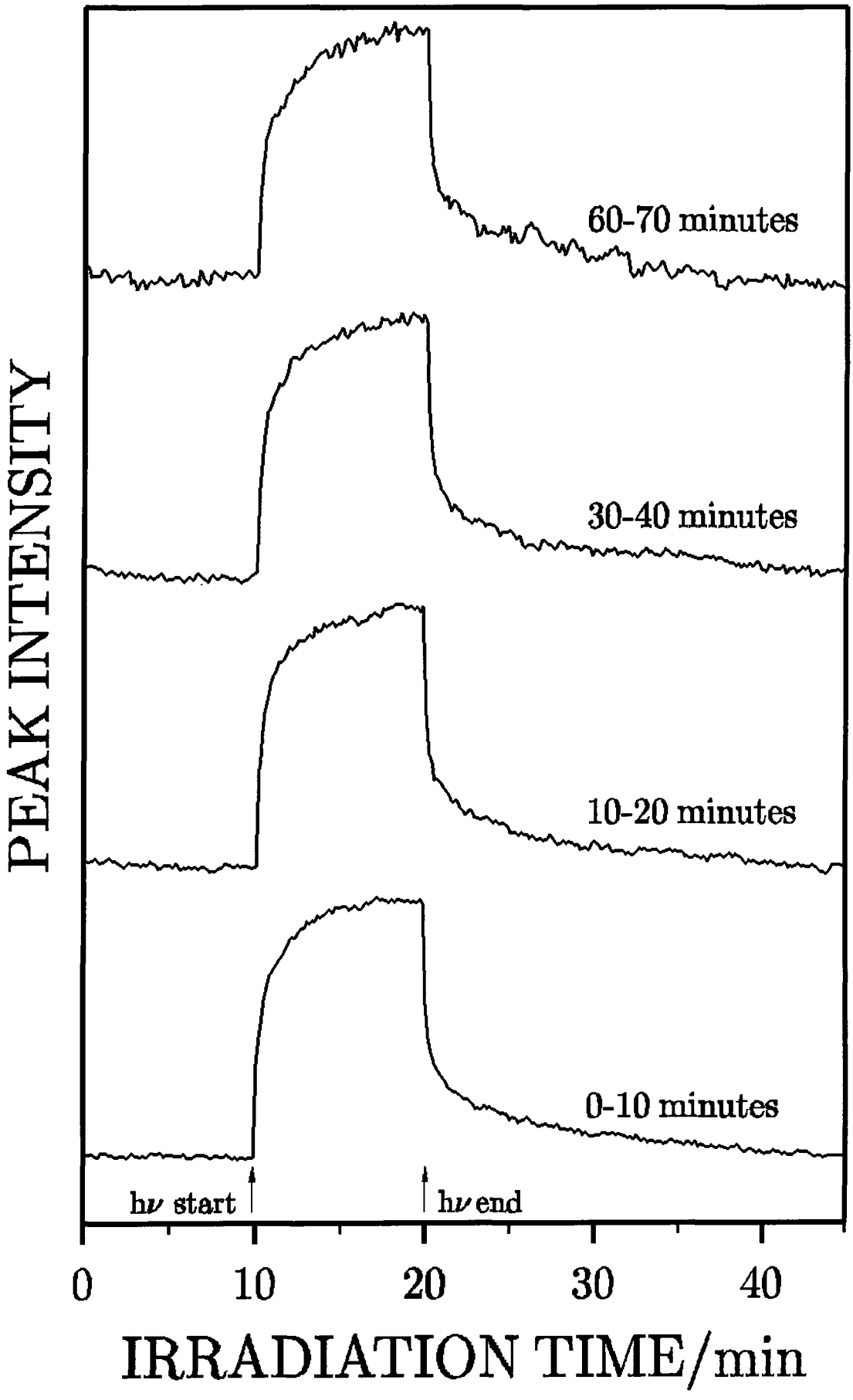

Fig. 10 Change of the profile shape of mass 64 as a function of irradiation time ($h\nu_{monochr.}$)

films: PESF samples irradiated with unmonochromatised light showed an intense discoloration to yellow-brown, whereas, films degraded with monochromatised radiation only had a slight yellow colour.

	% C	% S	% O
untreated PESF (theoretical)	75.0	6.2	18.8
untreated PESF (experimental)	74.5 ± 0.3	6.0 ± 0.1	19.6 ± 0.3
$h\nu_{\text{unmonochromatised}}$ 70minutes	79.7 ± 1.1	5.1 ± 0.2	15.3 ± 0.9
$h\nu_{\text{monochromatised}}$ 70 minutes	76.1 ± 0.6	5.4 ± 0.1	18.5 ± 0.8

Tab. 2 Elemental composition of untreated and treated PESF films

The XP spectra of untreated and treated polyethersulfone, figures 11-13, provide more information about the changes occurring on the sample surface. There are three contributions to the envelope of the C (1s) spectrum of untreated PESF: firstly, C-H at a binding energy of 285.0 eV, secondly the C-S environment at 285.6 eV and finally the C-O contribution of the ether linkage at 286.7 eV [21,22]. The π-π^* shake-up typical for the presence of the aromatic ring is observed at a BE of 291.9 eV and exhibits a different FWHM compared to the other components of the main carbon signal.

The O (1s) peak appears as a doublet with contributions from the oxygen atoms contained in the sulfone group and those contained in the ether moiety at a binding energy of 532.3 eV and 534.0 eV respectively [21]. Since there are twice as many oxygen atoms attached to sulfur atoms in the sulfone groups than are sandwiched between two aromatic rings in the ether groups of the polymer backbone the ratio of the peak areas should be 2:1. The experimentally determined ratio of 1.84 ± 0.02 : 1 is, however, slightly lower than this theoretical value.

The S (2p) signal can be resolved by peakfitting to a 2:1 doublet, the S ($2p_{3/2}$) contribution being centred at 167.8 eV which is typical for the sulfone environment [21,23].

While the shape and the position of the XP signals in PESF samples irradiated with monochromatised light remain nearly unchanged, the appearance of the corresponding signals of films exposed to unmonochromatised radiation is considerably altered: The shoulder, initially present on the high BE side of the C (1s)

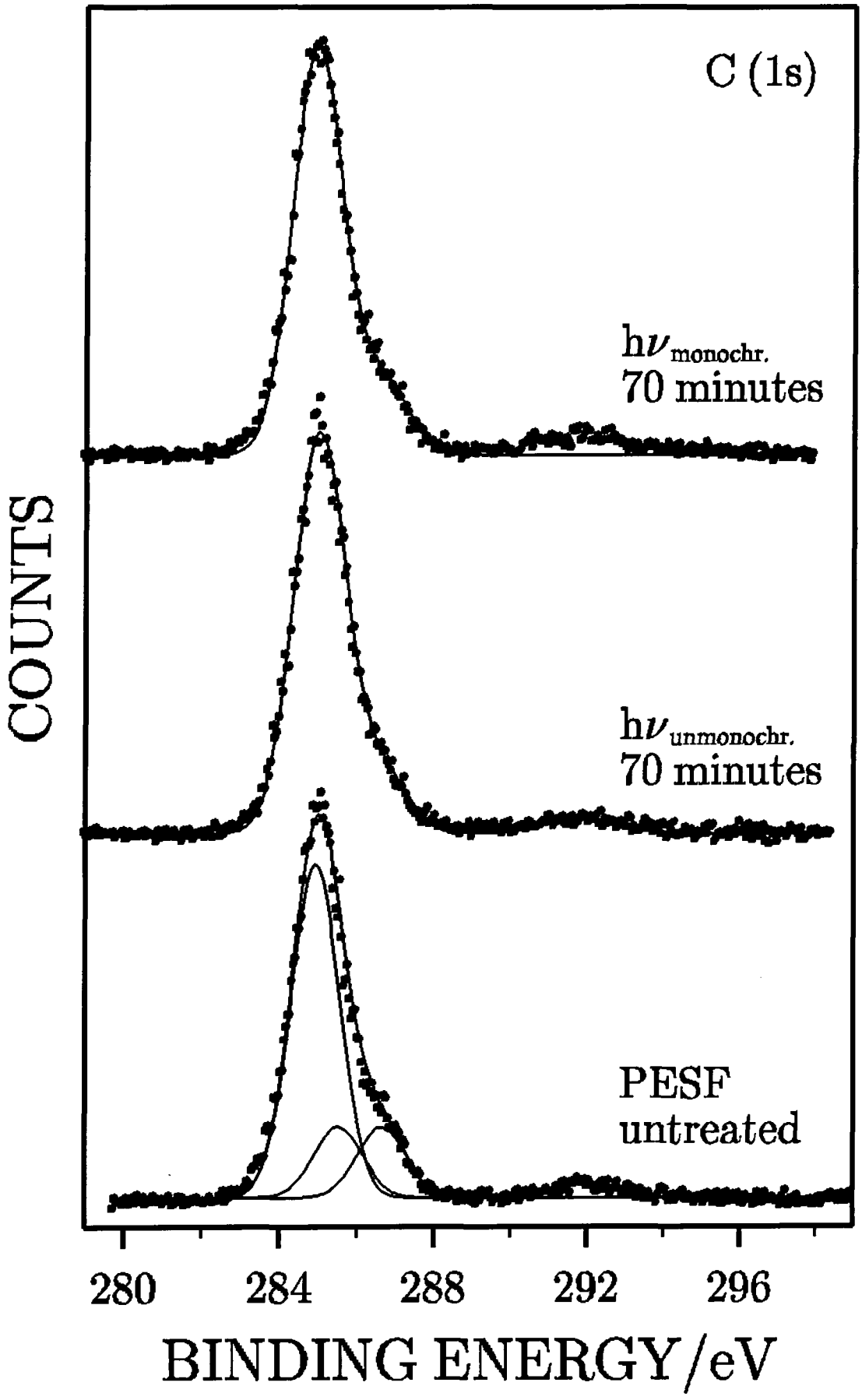

Fig. 11 C (1s) XP spectra of untreated and irradiated PESF films

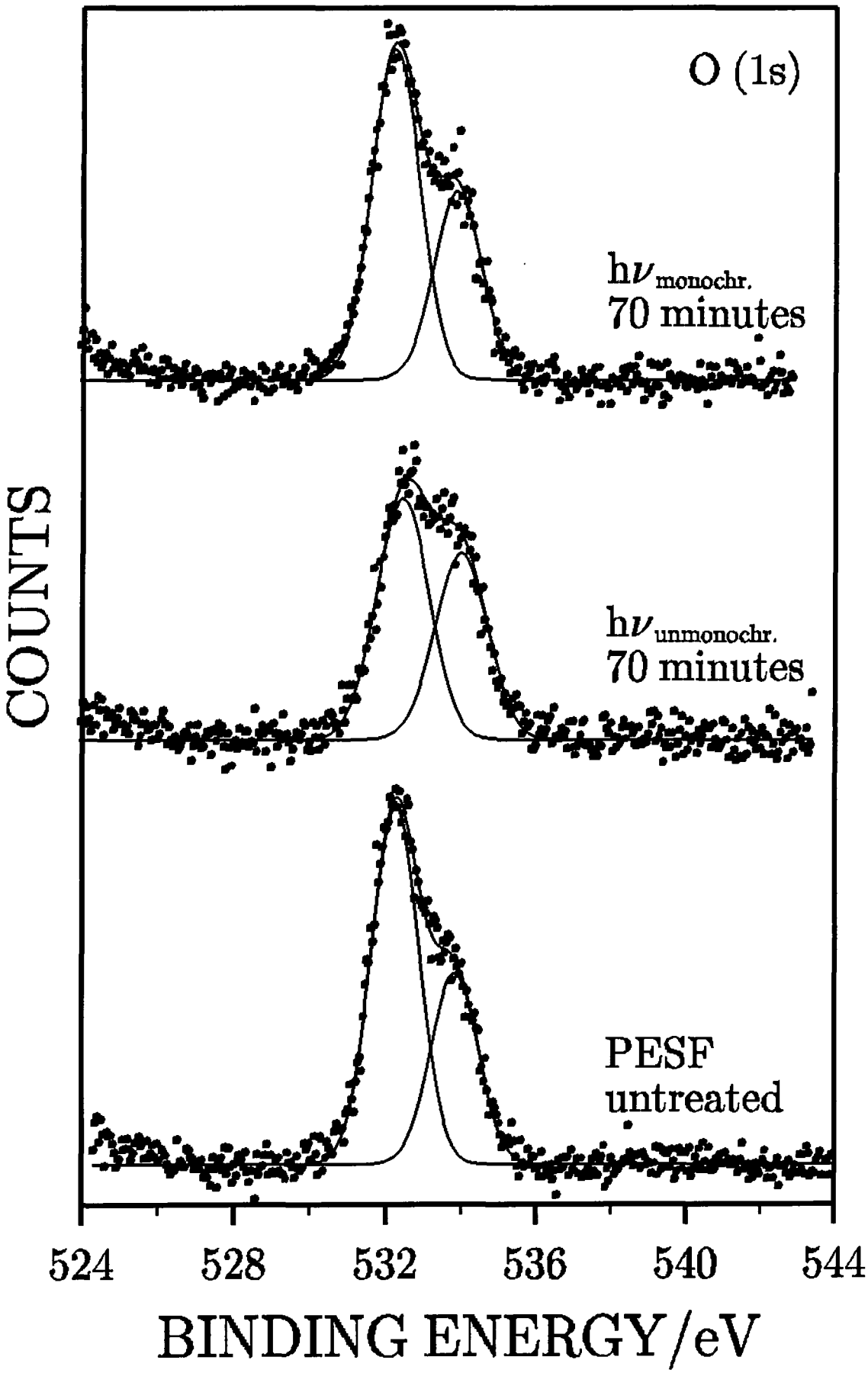

Fig. 12 O (1s) XP spectra of untreated and irradiated PESF films

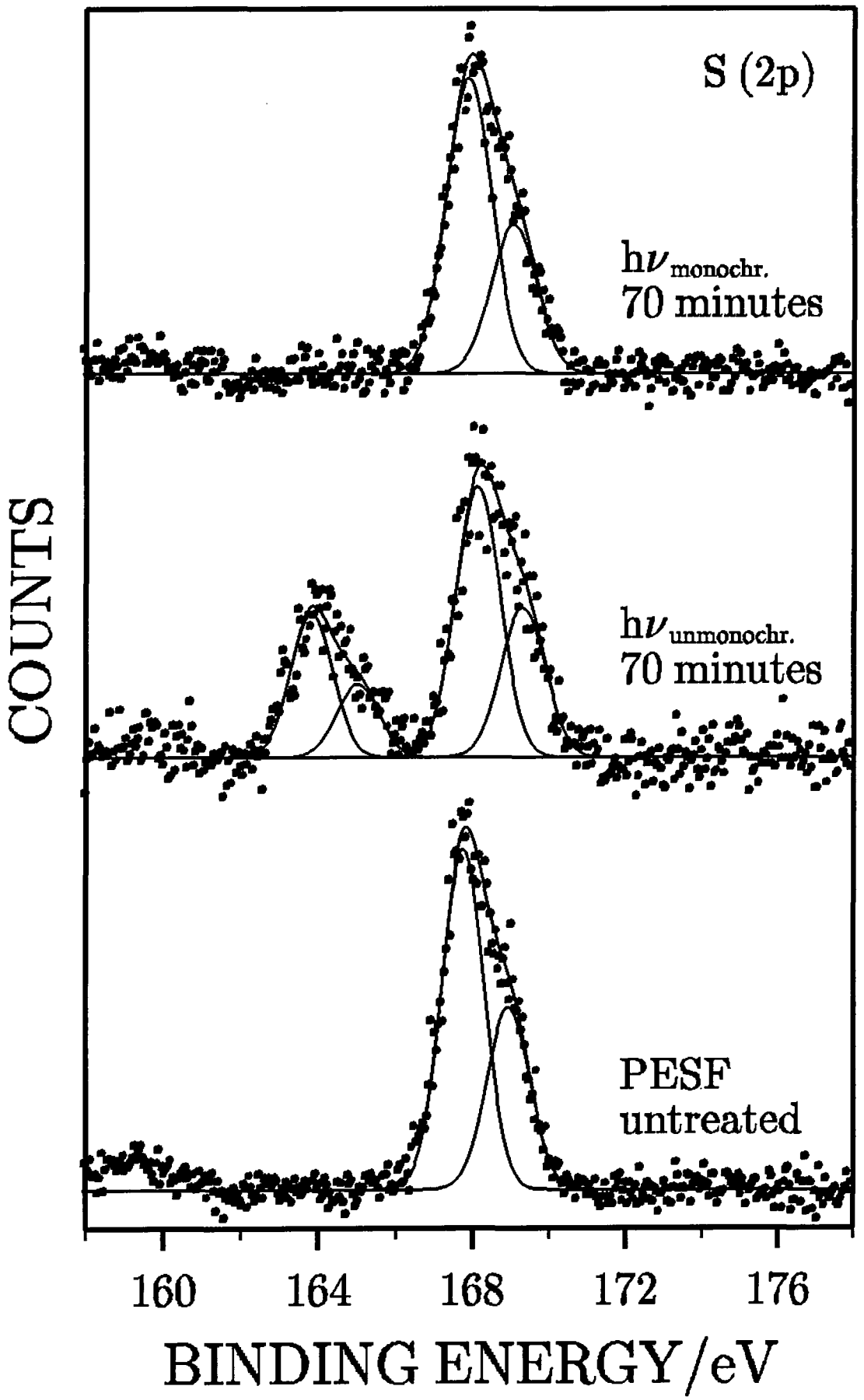

Fig. 13 S (2p) XP spectra of untreated and irradiated PESF films

envelope, appears less pronounced and reduced in intensity which suggests a reduction in the amount of ether groups. Additionally, there are further contributions of low intensity on the high BE side of the main carbon signal. These might be due to a slight surface oxidation which is probably caused by the short exposure of the samples to ambient atmosphere during the transfer from the MS to the XP spectrometer. The small binding energy difference of the environments contributing to the C (1s) signal with respect to the resolution of the spectrometer does not allow the spectra of the treated samples to be fitted unambiguously. Therefore these are presented as unfitted data.

The positions of the O (1s) peaks in both kinds of treated samples remain constant. The O (1s) envelope of PESF films irradiated with unmonochromatised light appears slightly broadened signifying a less homogeneous surface composition. The intensity ratio of the oxygen atoms contained in a sulfone environment with respect to those contained in an ether environment in the O (1s) envelope is reduced from 1.84 : 1 in the untreated samples to 1.76 : 1 and 1.29 : 1 in samples exposed for 70 minutes to monochromatised and unmonochromatised light, respectively. A sample measured after 90 minutes irradiation time with unmonochromatised light showed an even lower ratio. This reduction reflects the loss of SO_2 from the irradiated PESF surfaces.

The most striking change in the S (2p) XP spectra of samples degraded with unmonochromatised light is the appearance of a reduced sulfur environment. A similar species has been observed in a previous investigation on the photodegradation of PSF [13]. The complete sulfur envelope consists of two well separated parts, one at a slightly higher (approximately + 0.4 eV) and one at a lower BE of the original sulfone environment. Fitting the low BE environment as one component with a doublet structure the S ($2p_{3/2}$) contribution is centred at a BE of 163.9 eV. The FWHM values of the spectra of the untreated and treated samples are not significantly different. This suggests that in both parts of the envelope there can be only contributions of species with a very similar or even identical chemical shift. Thus, an overlap of a multitude of species as found in the case of the thermal degradation of polyethersulfone HTA in the presence of oxygen [24] is not observed. The sulfur envelope of PESF samples irradiated with monochromatised light is slightly broadened; the formation of the reduced sulfur species is not observed.

7.5 Discussion

The irradiation of PESF films leads to a complex degradation process. Not all the details of this process could be probed with the equipment available for the present study. This is the case with the volatile products in the m/z range less than 50 and greater than 180. Within the accessible mass range products already known (COS, SO_2) as well as new products (diphenylsulfone, biphenyl, diphenylether, dibenzofurane) can be identified. These higher molecular weight products, which are solids, show a strong tendency to be adsorbed at the chamber walls. This behaviour probably explains why these compounds escaped detection in the earlier gas analysis [7]. Contributions of fragments of two or more different compounds to one signal cannot be excluded. There is also a possibility that parts of the products detected are formed in fragmentation processes of initially larger degradation products. It would therefore be interesting to study PESF degradation employing a mass spectrometer offering a larger mass range and which ideally also allows the separation of the volatile products prior to analysis.

The gradually decreasing amount of products obvious from the temporal development of the profile areas could be due to two processes. The first is a chemical reaction leading to the formation of a product which possesses stabilizing properties and thus decelerates the degradation as it has been suggested by Kuroda et al. [5]. The second possibility is a crosslinking process at the sample surface which increasingly hinders the escape of volatile components as the mesh size of the network becomes smaller. A combination of these two factors is conceivable as well. The observation that the bulkier products do not show a reversal in profile shape as a function of irradiation time like the smaller masses suggests, however, that a fast crosslinking process is the more likely factor responsible for the decrease of the products, although the other pathway cannot be entirely ruled out.

Differences in the irradiance on the one hand and thermal effects on the other are likely to be the two most important factors accounting for the differences observed in the experiments with monochromatised and unmonochromatised radiation. Passing the lamp spectrum through the monochromator and the two lenses has two effects: the irradiance of the transmitted radiation is reduced and the contributions of the lamp spectrum other than the chosen wavelengths (including

those in the IR region) are filtered out. The reduction of the irradiance causes the initiation of less reaction steps while the lack of thermal energy precludes an increase of the mobility of the chain ends. This means that in the experiments using monochromatised radiation not only are less radicals formed on the sample surface, but these radicals are more likely to recombine due to a cage effect. This might explain the smaller crosslinking speed observed in the experiments using monochromatised light.

A straightforward explanation for the formation of the solid products remaining on the sample surface cannot be given because several reaction pathways are possible [25] some of which are outlined in scheme 2. Additionally, some of the primary products are likely to take part in further photoreactions upon prolonged irradiation [25, 26]. No literature evidence could be found for the direct photoreduction of sulfones.

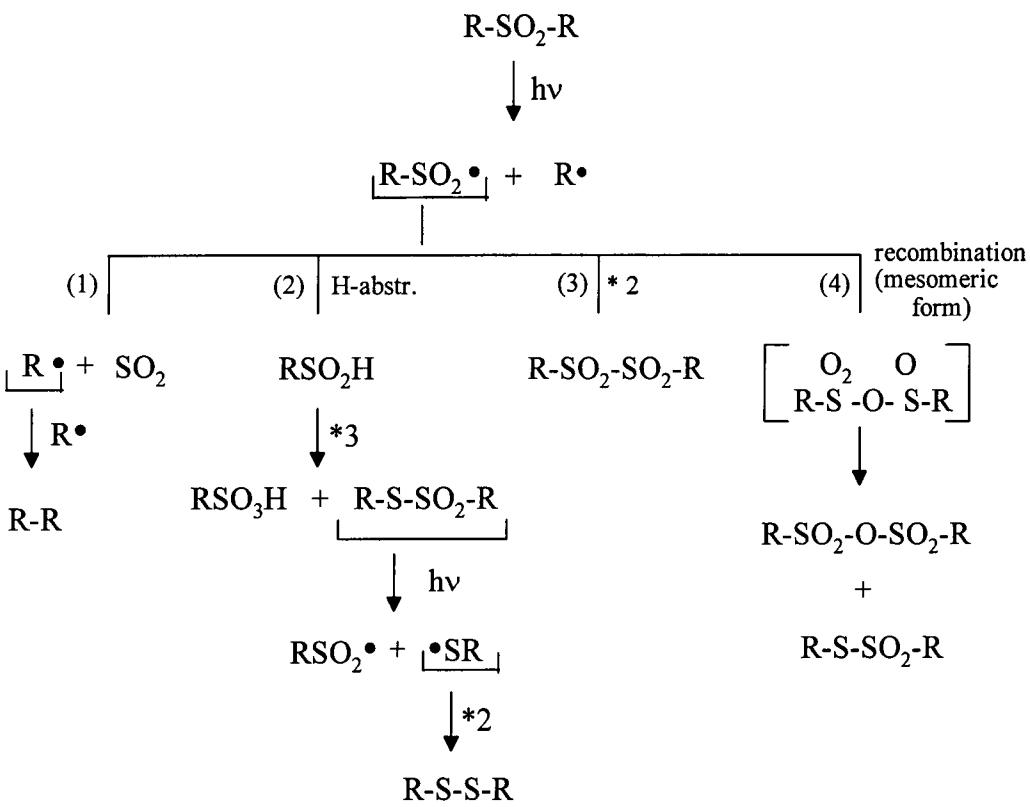

Scheme 2 Possible reactions on the sample surface

Extrusion reactions of sulfur dioxide from sulfones (1) are well known. Practically this reaction is a popular synthetic route for the formation of C-C bonds [26].

The energy required for this process can be provided thermally [27] or photochemically [26]. The detection of sulfur dioxide in the mass spectra and the reduction in the intensity of the sulfone contribution to the O (1s) XP spectrum of degraded films show that SO_2 extrusion is an important process in the photodegradation of PESF as well. The observation of Yamashita et al.[9] that the amount of SO_2 evolved per crosslinking point in PESF degradation is very small, however, suggests the occurrence of at least one additional degradation pathway.

Sulfonyl radicals can also recombine to form bis-sulfones (3) [26] or abstract hydrogen atoms to form sulfinic acids (2) [28-30]. Sulfinic acids especially aliphatic ones are unstable and disproportionate even under exclusion of air [31]. Simple aromatic sulfinic acids disproportionate faster than those protected by bulky substituents. The process can be accelerated by an increase in reaction temperature [32]. The products are a thiolsulfonate and the corresponding sulfonic acid (2). Pathway (4) describes the formation of a sulfonic anhydride and a thiolsulfonate via an unstable sulfinyl sulfonate intermediate [26].

Sulfur environment	BE range
R-S-SO_2-R	164.0 - 164.2 eV
R-S-S-R	163.5 - 164.2 eV
R-S-H	163.2 - 164.1 eV
R-S-R	163.4 - 164.2 eV
R-S-SO_2-R	168.2 - 168.8 eV
R-SO_2-O-SO_2-R	169.0 eV

Tab. 3 BE ranges for sulfur environments according to Lindberg et al. [23]

Table 3 lists the BE ranges for some of the sulfur environments in question. They were obtained from the measurement of model compounds. In the corresponding study the S (2p) doublet was not resolved but it was fitted as one peak [23]. Applying the same procedure, the high and the low BE environments in the spectra of the PESF films degraded with unmonochromatised light are found at BE values of 168.5 eV and 164.2 eV, respectively. From the reported values the -S-SO_2- environment of the thiolsulfonate could contribute to the high BE component of the

S (2p) spectrum. In the case of the -$\underline{S}O_2$-O- environment the study only reports the BE of one compound. A range of compounds could possibly include smaller values such that the anhydride cannot be excluded as a possible product. According to pathway (2), sulfonic acids could also contribute to the envelope at higher BE with respect to the original sulfone environment. Free sulfonic acids degrade rapidly upon storage [25] which might be the reason why XP spectra of these compounds are not reported in the comprehensive study of organic sulfur compounds mentioned above [23]. Therefore the contribution of the sulfonic acid to the present spectra cannot be estimated. Reports about BE values for bissulfones, the fourth possible contribution to the high BE environment could not be found in the literature.

The BE range reported for the -$\underline{S}$-SO_2- environment agrees with the experimental data of the low BE component of the present study. The same applies to the sulfur environments in R-$\underline{S}$-S-R which is a possible degradation product of the thiolsulfonate. These compounds are thus two possible contributions to the low BE component of the S (2p) XP spectrum of PESF samples irradiated with unmonochromatised radiation.

From the photochemistry point of view, the product gases COS and SO_2 could theoretically also play a role in the formation of the reduced sulfur environment. COS has an absorption maximum at 223 nm [33,34] and dissociates upon irradiation into CO and sulfur atoms which can insert into olefinic double bonds forming thiiranes, cyclic thioethers, and thiols [34,35]. Typical binding energies observed for these compounds are included in table 3. Assuming the mechanism in scheme 1 to be valid, the olefinic moieties required for this reaction would have been present on the sample surface. This pathway can be considered unlikely because of the low partial pressure of COS and the comparatively low irradiance of the lamp in the required wavelength region. The same applies to SO_2 which has three absorption bands in the near UV [36]. A triplet species is thought to be the species that causes the chemical reactions [37]. The reaction product with olefins are sulfinic acids, aromatic compounds react as well, but the product was not identified [37]. Considering the low partial pressure of SO_2 developed in the experiments and the low quantum yield reported for sulfinic acid formation [37], this reaction is also unlikely to contribute to a large degree to the formation of the reduced sulfur species.

The possible overlap of the XP signals does not allow an unambiguous identification of the products formed in the reactions of the sulfur species on the surface of PESF films irradiated with unmonochromatised radiation. Since a whole reaction sequence is likely to occur the peak intensities cannot be used to support a reaction stoichiometry. In order to find out more details about the products and the processes involved in their formation further studies including the application of other analytical methods would be required. This is also true for the samples irradiated with monochromatised radiation where one S (2p) environment is found at a BE of 168.3 eV.

Differences in irradiance and thermal energy were already suggested to be the reason for the different crosslinking velocity observed for samples irradiated with monochromatised and unmonochromatised light. The same factors might also be the reason why the reduced sulfur species is only observed in PESF films irradiated with unmonochromatised radiation. Due to the change in the reaction conditions, the rate of the reaction is probably so much reduced in the case of the irradiation with monochromatised light that the reduced sulfur species cannot be formed within the reaction time monitored. The observation of Munro and Clark [13], who obtained the reduced S-species in the irradiation of PESF films with light of wavelengths > 290 nm (Hg medium pressure lamp, pyrex filter), rules out the alternative explanation that the formation of the reduced sulfur species requires radiation wavelengths < 290 nm.

7.6 Conclusions

Irradiation of PESF samples in vacuum leads to complex chemical processes which are reflected in the development of volatile products and in the modification of the solid films. Degradation is observed both upon exposure to the full and to a selected part of the Hg (Xe) lamp spectrum. SO_2, COS, dibenzofurane and diphenylether are the main volatile products of the reaction; biphenyl and diphenylsulfone are also identified. These findings provide experimental evidence for the breakage of the C-O as well as of the C-S bonds. The respective product intensities show that bond breaking occurs more often at the sulfone groups than at the ether linkage. For both types of radiation used the rate of the degradation decreases with increasing treatment time which mainly reflects a crosslinking

process. The differences observed in the experiments with monochromatised and unmonochromatised light are probably due to different irradiances and thermal conditions. Irradiation with unmonochromatised radiation leads to the development of larger quantities of volatile products and a stronger modification of the polymer film. The corresponding XP spectra show the presence of a reduced sulfur species which is not detected upon irradiation with monochromatised radiation. The processes which occur on the sample surfaces are complex and further studies are required to identify the reaction products unambiguously and to elucidate the pathways involved in their formation.

7.7 References

1) Stoeckhert, K. *Kunststofflexikon*, 7.ed, Hanser : München, 1976, p.398
2) Davis, A.; Sims, D. *Weathering of Polymers*, Elsevier Applied Science Publishers: London, 1983, pp.173-179
3) *Römpps Chemielexikon* Vol.5, Falbe, J.; Regitz, M. Eds., Thieme : Stuttgart, New York, 1992, p.3572
4) Allen, N.S.; Mc Kellar, J.F.; *J. Appl. Pol. Sci.* **1977,** *21*, 1129
5) Kuroda, S.I.; Nagura, A.; Horie, K.; Mita, *I. Europ. Pol. J.* **1989**, *25(6)*, 621
6) Davis, A.; Gardiner, D. *Polymer Degradation and Stability* **1982**, *4*, 145
7) Gesner, B.D.; Kelleher, P.G. *J. Appl. Pol. Sci* **1968**, *12*, 1199-1208
8) Peeling, J.; Clark, D.T.; *J. Appl. Pol. Sci.* **1981**, *26*, 3761
9) Yamashita,T.; Tomitaka, H.; Kudo, T.; Horie, K.; Mita I. *Polymer Degradation and Stability* **1993**, *39*, 47
10) Munro, H.S.; Clark, D.T. *Polymer Degradation and Stability* **1985**, *11*, 211
11) Clark, D.T.; Munro, H.S. *Polymer Degradation and Stability* **1985**, *11*, 225
12) Kuroda, S.I.; Mita, I.; Obata, K; Tanaka, S. *Polymer Degradation and Stability* **1990**, *27*, 257
13) Clark, D.T.; Munro, H.S. *Polymer Degradation and Stability* **1987**, *17*, 319
14) McKellar, J.F.; Allen, N.S. *Photochemistry of Man-Made Polymers* Applied Science Publishers : London, 1979, pp.156-160
15) Operation Manual, grating monochromator model 7300, Applied Photophysics
16) Meyerson, S.; Drews, H.; Fields, E.K. Anal. Chem. **1964**, *6 (7)*, 1294

17) Eland, J.H.D.; Danby, C.J. *J. Chem. Soc.* **1965**, 5935

18) Pring, B.G.; Stjernström, N.E. *Acta Chem. Scand.* **1968**, *22 (2)*, 12

19) Porter, Q.M. *Mass Spectrometry of Heterocyclic Compounds*, 2nd ed., Wiley Interscience, 1985, p.191

20) Cornu, A. Massot, R. *Compilation of Mass Spectral Data* 2nd edition, Vol.1, Heyden : London, 1975, p.A-6

21) Dilks, A.; Clark, D.T. *J. Pol. Sci : Pol. Chem. Ed.* **1981**, *19*, 2847

22) Beamson, G.; Briggs, D. *High Resolution XPS of Organic Polymers : The Scienta ESCA 300 Database*, John Wiley & Sons : Chichester, 1992, pp.264-265

23) Lindberg, B.J.; Hamrin, K.; Johansson, G.; Gelius, U.; Fahlman, A.; Nordling, C.; Siegbahn, K. *Physica Scripta* **1970**, *1*, 286

24) Brauman, S.K. *J. Pol. Sci. A: Pol. Chem.* **1992**, *30*,1247

25) Schank, K., private communication

26) Schank, K. in: *Houben-Weyl: Methoden der Organischen Chemie*, 4th edition Vol. E11 Organische Schwefelverbindungen, Klamann, D. Ed , Thieme : Stuttgart, 1985, pp.1272-1273

27) Vögtle, F.; Rossa, L. Angew. Chem. **1979**, *91*,534-549

28) Still, I.W.J. In *The Chemistry of Sulphones and Sulphoxides*, Patai, S.; Rappoport, Z.; Stirling, C.M.J. John Wiley & Sons: Chichester 1988, pp.879-880

29) Horspool, W. M. In *The Chemistry of Sulphonic Acids, Esters and their Derivatives*, Patai, S; Rappoport, Z. Eds., Wiley & Sons: Chichester, 1991, pp.505-506

30) Dürr, H. in: *Houben-Weyl: Methoden der Organischen Chemie*, 4th edition, Photochemie, Teilband II , Müller, E. Ed., Thieme : Stuttgart, 1975, pp.1008-1058

31) Krauthausen, E. in: *Houben-Weyl: Methoden der Organischen Chemie*, 4th edition Vol. E11,1 Organische Schwefelverbindungen, Klamann, D. Ed , Thieme : Stuttgart, 1985, p.619

32) Muth, F. in: Houben- Weyl: *Methoden der Organischen Chemie*, 4th edition Vol. 9: Schwefel - Selen - Tellur - Verbindungen, Müller, E. Ed., Thieme : Stuttgart, 1955, pp.331-332

33) Reid, *Organic Chemistry of Bivalent Sulfur*, Vol.4, New York, 1962, pp.389-394

34) Leppin, E. PhD thesis, Universität Bonn, 1969

35) Strausz, O.P. In *Organosulfur Chemistry*, Janssen, M.J. Ed., Interscience Publishers: New York, 1967, pp.11-32

36) Gmelin - Handbuch der Anorganischen Chemie, S-Schwefel, Ergänzungsband S, Schwefeloxide, Bitterer, H. Ed., 1980, p.128

37) Sidebottom, H.W.; Badcock, C.C.; Calvert, J.G.; Rabe, B.R.; Damon, E.K.; *J. Am. Chem. Soc.* **1971**, *93*, 3121

Appendix

UNIVERSITY OF DURHAM - BOARD OF STUDIES IN CHEMISTRY
COLLOQUIA, LECTURES AND SEMINARS

04.10.1993	Prof. F. J. Feher (University of California, Irvine, USA) Bridging the Gap between Surfaces and Solution with Sessilquioxanes
27.10.1993	Dr. R. A. L. Jones (Cavendish Laboratory, Cambridge) Perambulating Polymers
10.11.1993	Prof. M. N. R. Ashfold (University of Bristol) High Resolution Photofragment Translational Spectroscopy : A New Way to Watch Photodissociation
17.11.1993	Dr. A. Parker (Rutherford Appleton Laboratory, Didcot) Applications of Time Resolved Resonance Raman Spectroscopy to Chemical and Biochemical Problems
26.01.1994	Prof. J. Evans (University of Southhampton) Shining Light on Catalysts
02.02.1994	Dr. A. Masters (University of Manchester) Modelling Water Without Using Pair Potentials
16.02.1994	Dr. R. E. Mulvey (University of Strathclyde) Structural Patterns in Alkali Metal Chemistry
23.02.1994	Prof. P. M. Maitlis (University of Sheffield) Across the Border: From Homogeneous to Heterogeneous Catalysis
19.10.1994	Prof. N. Bartlett (University of California) Some Aspects of Ag(II) and Ag(III) Chemistry
07.12.1994	Prof. D. Briggs (ICI and University of Durham) Surface Mass Spectrometry

18.01.1995	Dr. G. Rumbles (Imperial College) Real or Imaginary 3rd Order Non-Linear Optical Materials
01.02.1995	Dr. T. Cosgrove (Bristol University) Polymers do it at Interfaces
01.03.1995	Dr. M. Rosseinsky (Oxford University) Fullerene Intercalation Chemistry
11.10.1995	Prof. P. Lugar (Freie Universität Berlin): Low Temperature Crystallography
17.11.1995	Prof. D. Bergbreiter (Texas A&M, USA) Design of Smart Catalysts, Substrates and Surfaces from Simple Polymers
22.11.1995	Prof. I. Soutar (Lancaster University) A water of Glass? Luminescence Studies of Water - Soluble Polymers
29.11.1995	Prof. D. Tuck (University of Windsor, Ontario, Canada) New Indium Coordination Chemistry
17.01.1996	Prof. J.W. Emsley (Southhampton University) Liquid Crystals: More than Meets the Eye
31.01.1996	J. Penfold (ISIS Facility) Soft Soap and Surfaces
06.03.1996	Dr. R.Whitby (University of Southampton) Tandem Reactions on the Zr Template
12.03.1996	Prof. V. Balzani (University of Bologna) Supramolecular Photochemistry